



Fisheries New Zealand

Tini a Tangaroa

Spatial distribution modelling of at-risk seabirds in New Zealand commercial fisheries

New Zealand Aquatic Environment and Biodiversity Report No. 298

J.O. Roberts, D.N. Webber, D.W. Goad, J.P.Y. Arnould, E.A. Bell, P. Crowe, L. Deppe, G.P. Elliott, T.J. Landers, A.N.D. Freeman, T. Mattern, P.J. Moore, D.G. Nicholls, G.P. Parker, K. Rexer-Huber, G.A. Taylor, D.R. Thompson, K.J. Walker, S.M. Waugh, M.J. Young

ISSN 1179-6480 (online)

ISBN 978-1-99-106235-2 (online)

November 2022



Te Kāwanatanga o Aotearoa
New Zealand Government

Disclaimer

This document is published by Fisheries New Zealand, a business unit of the Ministry for Primary Industries (MPI). The information in this publication is not government policy. While every effort has been made to ensure the information is accurate, the Ministry for Primary Industries does not accept any responsibility or liability for error of fact, omission, interpretation, or opinion that may be present, nor for the consequence of any decisions based on this information. Any view or opinion expressed does not necessarily represent the view of Fisheries New Zealand or the Ministry for Primary Industries.

Requests for further copies should be directed to:

Fisheries Science Editor
Fisheries New Zealand
Ministry for Primary Industries
PO Box 2526
Wellington 6140
NEW ZEALAND

Email: Fisheries-Science.Editor@mpi.govt.nz
Telephone: 0800 00 83 33

This publication is also available on the Ministry for Primary Industries websites at:
<http://www.mpi.govt.nz/news-and-resources/publications>
<http://fs.fish.govt.nz> go to Document library/Research reports

© Crown Copyright – Fisheries New Zealand

Please cite this report as:

Roberts, J.O.; Webber, D.N.; Goad, D.W.; Arnould, J.P.Y.; Bell, E.A.; Crowe, P.; Deppe, L.; Elliott, G.P.; Landers T.J.; Freeman, A.N.D.; Mattern, T.; Moore, P.J.; Nicholls, D.G.; Parker, G.P.; Rexer-Huber, K.; Taylor, G.A.; Thompson, D.R.; Walker, K.J.; Waugh, S.M.; Young, M.J. (2022). Spatial distribution modelling of at-risk seabirds in New Zealand commercial fisheries. *New Zealand Aquatic Environment and Biodiversity Report No. 298*. 167 p.

TABLE OF CONTENTS

EXECUTIVE SUMMARY	1
1 INTRODUCTION	2
1.1 Background	2
1.2 Research objectives	3
1.3 At-risk species	4
1.4 Report structure	4
2 METHODS	6
2.1 Spatial information	6
2.1.1 Tracking data	6
2.1.2 Scientific fisheries observer sightings	7
2.1.3 Public sightings	8
2.1.4 Te Papa Tongarewa sightings	8
2.2 Spatial models	8
2.2.1 Seabird distribution information	8
2.2.2 Candidate covariates	9
2.2.3 Pre-processing of seabird observations	9
2.2.4 Model development	10
2.2.5 Model prediction	12
2.3 Proportion of seabirds in zone	13
3 RESULTS	13
3.1 Summary of spatial information	13
3.2 Seabird distribution modelling	15
3.2.1 Flesh-footed shearwater	18
3.2.2 Black petrel	20
3.2.3 Westland petrel	22
3.2.4 White-chinned Petrel	24
3.2.5 Northern and Southern Buller's albatross	26
3.2.6 Chatham Island albatross	30
3.2.7 Salvin's albatross	32
3.2.8 White-capped albatross	34
3.2.9 Antipodean albatross	36
3.2.10 Gibson's albatross	38
3.2.11 Yellow-eyed penguin	40
3.3 Proportion of seabirds in zone	44
4 DISCUSSION	46
4.1 Spatial and seasonal coverage	46
4.2 Integrating sources of spatial information	46
4.3 Environmental covariates of seabird distribution	47
4.4 Changes to assumed spatial distributions	48

4.5	Changes to proportion in zone	48
4.6	Future research	49
5	ACKNOWLEDGEMENTS	49
6	REFERENCES	51
Appendix A.	PREVIOUS SEABIRD DISTRIBUTION LAYERS	55
Appendix B.	CANDIDATE SPATIAL COVARIATES OF SEABIRD DISTRIBUTION	62
Appendix C.	SEABIRD TRACKING DATA SUMMARIES	76
Appendix D.	FINAL SEABIRD DATA SUMMARIES	87
Appendix E.	SEABIRD DISTRIBUTION MODEL DIAGNOSTIC PLOTS	96
Appendix F.	NEW SEABIRD DISTRIBUTION LAYERS	127

EXECUTIVE SUMMARY

Roberts, J.O.¹; Webber, D.N.²; Goad, D.W.³; Arnould, J.P.Y.; Bell, E.A.; Crowe, P.; Deppe, L.; Elliott, G.P.; Landers T.J.; Freeman, A.N.D.; Mattern, T.; Moore, P.J.; Nicholls, D.G.; Parker, G.P.; Rexer-Huber, K.; Taylor, G.A.; Thompson, D.R.; Walker, K.J.; Waugh, S.M.; Young, M.J. (2022). Spatial distribution modelling of at-risk seabirds in New Zealand commercial fisheries.

New Zealand Aquatic Environment and Biodiversity Report No. 298. 167 p.

This project estimated the at-sea distribution within the New Zealand Exclusive Economic Zone (EEZ) of eleven seabird species/taxa considered to be most at risk from captures by commercial fishing operations around New Zealand. The assessed seabirds included flesh-footed shearwater / toanui (*Puffinus carneipes*), black petrel / tāiko (*Procellaria parkinsoni*), Westland petrel / tāiko (*Procellaria westlandica*), white-chinned petrel / karetaī kauae mā (*Procellaria aequinoctialis*), Northern Buller's albatross / toroa (*Thalassarche bulleri platei*), Southern Buller's albatross / toroa (*T. bulleri bulleri*), Chatham Island albatross / toroa (*Thalassarche eremita*), Salvin's albatross / toroa (*Thalassarche salvini*), white-capped albatross / toroa (*Thalassarche steadi*), Antipodean albatross / toroa (*Diomedea antipodensis antipodensis*), Gibson's albatross / toroa (*Diomedea antipodensis gibsoni*), and yellow-eyed penguin / hoiho (*Megadyptes antipodes*). Except for yellow-eyed penguin, this assessment focused on the distribution of adults.

Predictive habitat models were fitted to the best-quality spatial abundance information that was available for each species, including tracking data of individual birds (making no distinction between individuals based on reported breeding status) and boat-based sightings data from multiple sources (i.e., Fisheries New Zealand commercial fisheries observer sightings, public sightings, and sightings from merchant vessels). Spatial smooths were included in most models, which were seasonal for some species to allow for changes in foraging patterns during chick-rearing. Environmental covariates were also offered to all models. Sea surface turbidity was the most frequently selected environmental model term (six species, all of which appear to avoid turbid waters), followed by distance to colony (four species), and sea surface temperature (three species).

The optimal models were then used to predict the expected at-sea distribution of each species/taxon for each month of the year. For some species, the predicted distributions resembled those used by the most recent spatial risk assessment for New Zealand seabirds (e.g., black petrel, Westland petrel, Chatham Island albatross, and Antipodean albatross), although were quite different for other species (e.g., flesh-footed shearwater, white-capped albatross, Gibson's albatross, and yellow-eyed penguin).

In addition, tracking data were used to empirically calculate the monthly proportion of birds in-zone (i.e., inside the New Zealand EEZ). For all species, the derived monthly proportions in-zone were nearly always lower than those used in the most recent multispecies seabird spatial risk assessment. Excluding yellow-eyed penguin, no seabird species were found to forage entirely in-zone in any month (as was previously assumed for many species). However, for some species there were months where all birds were predicted to be out of zone.

This research highlights the value of integrating seabird spatial information from multiple sources. While some promising environmental covariates of seabird distribution were identified (particularly turbidity), it is likely that future research will identify new and improved environmental predictors for each species that may yield improved species distributions.

¹ Anemone, Wellington, New Zealand.

² Quantifish Limited, Tauranga, New Zealand.

³ Vita Maris, Papamoa, New Zealand.

1 INTRODUCTION

1.1 Background

More than 90 seabird taxa breed inside the New Zealand Exclusive Economic Zone (EEZ, Figure 1), including albatrosses, petrels, shearwaters, prions, gannets, skuas, shags, and penguins (Croxtall et al. 2012). Many of these species are known to be vulnerable to incidental mortality in commercial fishery operations, as confirmed by Fisheries New Zealand scientific observer records. Approximately 70 taxa are routinely included in a spatial multispecies risk assessment using a Bayesian implementation of the spatially-explicit fisheries risk assessment (SEFRA) method (Fisheries New Zealand 2020, Richard et al. 2020a).

Spatial seabird distribution layers are a key input for SEFRA models, which may vary throughout the year, reflecting changes in at-sea foraging patterns during the breeding cycle (Fisheries New Zealand 2020). These spatial layers are used to calculate commercial fishery overlap, which is used twice during SEFRA modelling:

1. observed overlap is used during model fitting; and
2. total overlap is used to make inference about seabird captures for all fishing effort.

Observed and total overlap are both functions of fishing effort by different fishing groups (g). A fishing group is a subjective group of similar fishing types (e.g., snapper bottom longline fleet, butterfish set net fleet). Fishing effort for each fishing group during each fishing event (i) is represented as a a_{gi} and takes the units of each fishing group (e.g., number of sets for bottom and surface longline, kilometres of net for set nets, or number of tows for trawl). Some fishing events are observed and represented using the prime symbol ($'$), thus observed effort is a a'_{gi} . Observed effort can be thought of as a subset of the total effort

$$a'_{gi} \subset a_{gi},$$

which means that a_{gi} contains the observed fishing events a'_{gi} and the unobserved fishing events. For display purposes, fishing effort can be aggregated within raster cells (c)

$$a_{gc} = \sum_{i \in c} a_{gi} \quad \text{and} \quad a'_{gc} = \sum_{i \in c} a'_{gi},$$

where $i \in c$ denotes that fishing event i occurred in cell c .

Species distribution layers, generally rasters or sometimes polygons, are represented as p_{sc} for each species (s) and cell (c). Each species distribution is rescaled to have the property

$$\sum_c p_{sc} x_{sc} = 1 \quad \forall s,$$

where x_{sc} is the area in square kilometres of each cell (note that the area of each cell is not necessarily the same depending on the type of spatial projection being used). If N_s is the total population size for species s , then the abundance in each cell is defined as

$$y_{sc} = p_{sc} x_{sc} N_s \quad \text{where} \quad \sum_c y_{sc} = N_s,$$

and the density (mean number of individuals per square kilometre) in each cell is

$$z_{sc} = \frac{p_{sc}x_{sc}N_s}{x_{sc}} = p_{sc}N_s.$$

Using species distribution layers, the species distribution for each species (s) at the location of each fishing event (i), where fishing event i occurs in cell c (i.e., $i \in c$), is extracted and denoted p_{si} (i.e., p_{si} is derived from p_{sc}).

Finally, overlap for species s , fishing group g , and fishing event i is defined as the product of fishing effort and species distribution

$$O_{sgi} = a_{gi}p_{si},$$

and density overlap is defined as

$$\mathbb{O}_{sgi} = O_{sgi}N_s\alpha_{si}$$

where α_{si} is the proportion of the breeding population inside the New Zealand EEZ at the time fishing event i occurred. Density overlap is important as it is used within the SEFRA framework to estimate the annual number of captures for each species, and therefore make inference about the risk of different fishing practices to different species. Therefore, it is imperative that spatial seabird distribution layers are as accurate as possible.

1.2 Research objectives

This document describes research under Fisheries New Zealand projects PRO2019-09 and PSB2020-04, which collectively estimated the at-sea spatial distribution of the eleven seabird taxa that were estimated to be at relatively high risk to commercial fishing operations by the most recent SEFRA (Richard et al. 2020a). The overall objective of PRO2019-09 was:

Using available data, estimate the spatial density of at-risk seabird species, including seasonal variation, estimated separately for breeding and non-breeding birds

The specific objectives of this project were:

1. *Secure access to existing satellite telemetry for New Zealand seabird populations, including via the Global Procellariiform Tracking Database.*
2. *Compile available data indicative of seabird distributions – including satellite telemetry, sightings data, fisheries captures, and colony-specific population estimates – for up to ten seabird species chosen in consultation with Fisheries New Zealand.*
3. *Apply spatial modelling techniques to estimate the spatial distribution and density of selected seabird species (including seasonal variation, and estimated separately for breeding and non-breeding birds), using seabird data from Objective 2 and spatially comprehensive environmental data layers available from other Fisheries New Zealand funded projects.*

Although not stated in the above objectives, this project was focused on the distribution of adults. This was because the spatial layers produced by these projects were intended to be used by the updated New Zealand seabird SEFRA model produced under PRO2019-10, which is an adult-only model, as per previous iterations of this assessment (e.g., Richard et al. 2020a).

The overall objective of PSB2020-04 was:

*Using available data, estimate the spatial density of **hoiho (yellow-eyed penguin)**, including seasonal variation, estimated separately for breeding and non-breeding birds.*

The specific objectives of this project were:

1. *Secure access to existing satellite telemetry data collected under government contract.*
2. *Compile available data indicative of hoiho distribution: Nomad sightings data, CSP sightings data, fisheries capture, and colony specific population estimates.*
3. *Apply spatial modelling techniques to estimate the spatial distribution and density of hoiho (including seasonal variation, and estimated separately for breeding and non-breeding birds), using data from Objective 2 and spatially comprehensive environmental data layers available from other Fisheries New Zealand funded projects.*

Although previous iterations of the New Zealand seabird SEFRA model provided adult-only assessments for yellow-eyed penguin, the scope of project PSB2020-04 was expanded to include sub-adults, because, unlike most of the species assessed under PRO2019-09, juveniles of this species will be present around New Zealand in all months.

1.3 At-risk species

In consultation with Fisheries New Zealand and the New Zealand Department of Conservation (DOC), spatial distribution layers were produced for a selection of seabird species that were considered most at-risk from commercial fishing around New Zealand, based on the most recent iteration of the SEFRA multispecies risk assessment (Richard et al. 2020a) and expert opinion. The selected species were as follows, arranged in the following format—‘common name, *scientific name*, Fisheries New Zealand species code’:

- Flesh-footed shearwater / toanui, *Puffinus carneipes*, XFS
- Black petrel / tāiko, *Procellaria parkinsoni*, XBP
- Westland petrel / tāiko, *Procellaria westlandica*, XWP
- White-chinned petrel / karetai kauae mā, *Procellaria aequinoctialis*, XWC
- Buller’s albatross / toroa, *Thalassarche bulleri*, XPB
 - Northern Buller’s albatross, *Thalassarche bulleri platei*, XNB
 - Southern Buller’s albatross, *Thalassarche bulleri bulleri*, XBM
- Chatham Island albatross / toroa, *Thalassarche eremita*, XCI
- Salvin’s albatross / toroa, *Thalassarche salvini*, XSA
- White-capped albatross / toroa, *Thalassarche cauta*, XWM
- Wandering albatross / toroa, *Diomedea antipodensis*, XRU
 - Antipodean albatross, *Diomedea antipodensis antipodensis*, XAN
 - Gibson’s albatross, *Diomedea antipodensis gibsoni*, XAU
- Yellow-eyed penguin / hoiho, *Megadyptes antipodes*, XYP

The at-sea spatial distribution was estimated for each taxon for each month of the year.

1.4 Report structure

Section 2 describes the methods used to achieve the research objectives specified in Section 1.2. This is followed by characterisations of the various spatial data sources (Section 3.1) and a description of the spatial analysis for each species (Section 3.2). Although not stated in the higher-level project objectives (above), this project updated estimates of the proportion of birds in-zone (i.e., inside the New Zealand EEZ) by month for each taxon, which was achieved using the tracking data (Section 3.3). The report

concludes with a discussion of the key outputs of this research, some limitations, and recommendations for future research (Section 4).

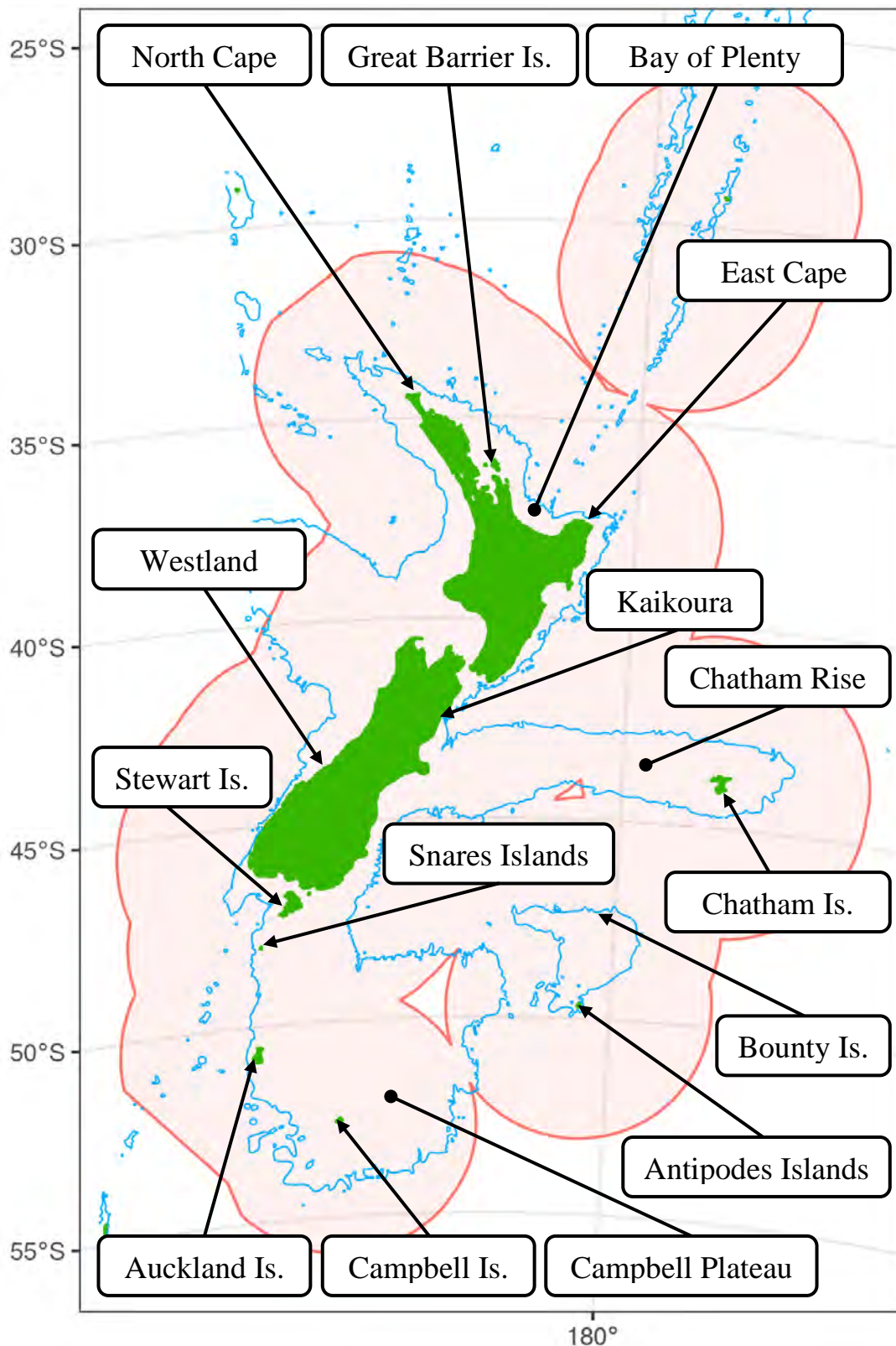


Figure 1: The New Zealand EEZ (red shaded region), the 1000 m depth contour (blue line), and the locations referred to in this document.

Given the large number of assessed species, many of the key tables and figures are in appendices in order to avoid repetition in the main text. These include: the previous seabird distribution layers used for spatial risk assessment (Appendix A), candidate spatial covariates of seabird distribution (Appendix B), summaries of spatial information for each of the study species/taxa (Appendix C and Appendix D), the diagnostic plots of the models used to predict the distribution of each seabird (Appendix E), and the new predicted distributions of each seabird by month (Appendix F).

2 METHODS

2.1 Spatial information

A project workshop was held on 17–18 March 2021 with Fisheries New Zealand and DOC, which identified the various sources of tracking and sightings-based spatial information that would be available to this project for each species. Tracking data and sightings data provided different types of spatial information.

Tracking data represent the recorded spatial locations of individuals on to which tracking instruments have been attached. Since these data are collected from certain individuals and may have patchy coverage with respect to age and breeding stage, they may not be representative of the wider population. Furthermore, because they are presence only data (rather than presence-absence or counts), locations without tracking data cannot be considered as true absences. However, these data are informative of the distributions of birds in locations where sighting effort is minimal or absent, and they do not suffer from species identification issues.

By contrast, **sightings count data** provide information about the relative abundance of a seabird taxon where there is spatial coverage of sighting effort. These data are more representative of the wider population than tracking data and sighting events where a species was not recorded as observed can be regarded as a true absence. However, species misidentifications will be a factor for all species to some extent and, for some taxa that cannot be separately identified during sightings, may entirely prevent the use of sightings data for estimating spatial distributions. The relative sighting rate by species may also be sensitive to the platform used to make an observation (i.e., commercial fishing vessel compared with merchant ship or wildlife tour boat).

From a statistical perspective, presence only data (i.e., tracking data) are the most problematic type of data for estimating species distributions, followed by presence-absence data, and then count-based data (e.g., observer sightings data), which are the best type of spatial information, assuming species identifications are accurate.

Fisheries observer capture data were not fitted to in any spatial models. This was done because the spatial layers produced by this analysis are intended to be used by SEFRA models, and this would have resulted in a ‘double-dipping’ of these data.

2.1.1 Tracking data

Tracking data have been collected for New Zealand seabirds using different tag types, including:

- Global Positioning System (GPS) tags;
- Platform Transmitter Terminal (PTT) tags;
- Global Location Sensor (GLS) tags; and
- Very High Frequency (VHF) tags.

The spatial accuracy of tracking data is known to vary considerably by tag type, ranging from most precise (GPS and best-quality PTT fixes) to least precise (raw GLS and lowest-quality PTT fixes) (e.g., Phillips et al. 2004). While GLS data often lack precision, the devices used to collect these data are smaller and more

energy efficient and, so, may collect data over longer periods or for smaller species. Hence, GLS data can be particularly useful for elucidating seasonal changes in foraging patterns over broad spatial and temporal scales. Methods also exist for filtering GLS data to remove inaccurate locations (Rakhimberdiev et al. 2017). Based on visual inspection of the data, the VHF data appeared to be of intermediate precision relative to the other tracking data types.

Requests were issued in December 2019 to all lead researchers, asking for all tracking data including any associated metadata and raw files for GLS tags. Any data held by BirdLife International on the seabird tracking database were also requested through that platform. Copies of some data sets from the BirdLife International database were sourced from DOC, rather than through the BirdLife International platform.

Tracking data were received in several formats, including BirdLife International database extracts, groomed data sets directly from researchers, and individual tag records aggregated at a data set level representing one research organisation, one tag type, one colony, and one season or more of field work. All original data fields have been retained and extra fields were added, where necessary and possible, to describe the following attributes: species, colony, track identifier, band number, tag type, sex, breeding status, year, month, day, hour, minute, second, order in which the data were supplied, and a data set name. In some cases, doubled-up data or data from the earlier studies were removed from individual tag files.

Each data set was summarised to provide an indication of coverage. To account for the different tag reporting rates, the number of bird-days of tracking data were tabulated by month and year, for each data set.

The track of every tagged bird was plotted and a histogram of the speed (kilometre/hour) between each recorded point that the bird travelled (assuming a straight line between points) was generated. The histogram of speed for each bird was compared with the density of the speed travelled for all birds of the same species to allow rapid identification of unusual birds. Although we could not present the raw tracks for these birds in this document, this allowed us to make decisions about dropping tag types (e.g., dropping the GLS data for some species) or make informed decisions when processing the data. This processing varied by species:

- White-chinned petrel – only GLS tracking data were available for this species and, based on visual inspection, were deemed of insufficient accuracy for this assessment and, therefore, were not used.
- Westland petrel – dropped all GLS data. Kept all GPS data and applied no changes. Kept all PTT data with location class 3 (< 250 m error), 2 (< 500 m), 1 (< 1500 m), 0 (> 1500 m, but deemed acceptable based on visual inspection), or A (unbounded accuracy, but deemed acceptable based on visual inspection) (CLS 2011). Applied a speed filter of 100 km/hr.
- Flesh-footed shearwater – applied 100 km/hr speed filter (this was done for all birds), dropped all GLS data. No PTT.
- Black petrel – applied a 100 km/hr speed filter, no PTT, retained all GPS, hand picked some of the better looking GLS data.
- Yellow-eyed penguin – applied a 15 km/hr speed filter.

2.1.2 Scientific fisheries observer sightings

A groomed data set of observer sightings from commercial fishing vessels covering the fishing years 2007–08 to 2018–19 was supplied by Dragonfly Data Science (Richard et al. 2020b). This was split by observation method. ‘Nomad’ data were recorded onboard inshore fishing vessels using (Trimble Nomad) handheld electronic devices, typically at 15-minute intervals, and ‘paper form’ data were recorded from larger vessels, typically during the first daylight haul of the day.

2.1.3 Public sightings

Several online platforms are used to collate and share public sightings data of global seabird species. Of these, eBird is well-used for New Zealand species and has a major advantage over other platforms in that users can specify records collected during a complete checklist. As such, complete checklist sightings events in which a species was not observed can be considered a true negative sighting event. Users are also able to indicate whether sightings events included complete checklists of all observable species.

2.1.4 Te Papa Tongarewa sightings

Te Papa Tongarewa staff compiled a data set from the at-sea bird observations recorded in the logbooks of Captain John Arthur Francis Jenkins (1928–1989) and count cards held by the convenor of the Australasian Seabird Mapping Scheme. This is licensed by Te Papa Tongarewa for re-use under the Creative Commons BY 4.0 International licence and was downloaded from the Te Papa Tongarewa website (<https://www.tepapa.govt.nz/learn/research/datasets/sea-observations-seabirds-dataset>). Each observation record was categorised as either a full (F) or partial (P) observation. Only full observations were retained in the final data set.

2.2 Spatial models

Predictive models of seabird spatial distribution were developed for all of the focal species/sub-species, fitting to observations of seabird counts for each event, and including spatial covariates of count rate, determined by a model optimisation process. For all model fits, a variant of generalised additive models (GAMs) for large data sets (called BAMs) was implemented, using the *R* package *mgcv* (Wood et al. 2015).

2.2.1 Seabird distribution information

Up to six different sources of spatial seabird information were available for each species:

- Fisheries New Zealand observer sightings (non-anonymised data obtained from Dragonfly Data Science), including:
 - daily fisheries observer sightings recorded on paper forms (referred to in this summary as ‘**Paper form**’); and
 - more regular fisheries observer sightings recorded on Nomad GPS devices (‘**Nomad**’);
- Merchant ship crew sighting data, curated by Te Papa Tongarewa (‘**Te Papa**’) – including only “Full” census method events;
- Public sightings data submitted to eBird, including only complete checklists of species obtained from:
 - Checklists completed while stationary (‘**eBird stationary**’);
 - Checklists completed along transects of variable length (‘**eBird travelling**’).
- Tracking data (‘**Tracking**’), including ‘GPS’, ‘PTT’, and also ‘GLS’ data where the other two types were not available.

Tracking points (presence only) were converted into gridded counts so that they were in a comparable format to the sightings-based counts for the purposes of model fitting. Tracking data locations were aggregated into gridded counts across the New Zealand EEZ by species, month, and year. A 20 km grid cell resolution was used for the tracking data, which was found to result in an optimal trade-off between adequate spatial resolution and resulting computing time. Pseudo-zero values were obtained where no points were recorded in a particular grid cell. A unique dummy ‘observer ID’ and ‘vessel key’ was allocated across all cells in each grid, so that they could be modelled with the sightings-based count

data, and so that variability in the number of tracking data locations within each grid would not interfere with the estimation of month effects.

2.2.2 Candidate covariates

Several candidate environmental covariates of seabird count rate were offered to spatial models during the optimisation process, including temporally static variables, temporally dynamic variables (a separate value for each month and year), and quarterly climatologies. These covariates included:

- Bathymetric depth and slope
- Sea surface temperature (SST) and SST gradient
- Sea surface wind speed
- Sea level anomaly
- Sea surface turbidity (an ocean-colour based proxy)
- Sea surface chlorophyll-a concentration
- Distance to colony (excluding colonies with < 1% of total breeding pairs for each species)
- Benthic sediment type (yellow-eyed penguin only)
- Spatial presence of key prey species (yellow-eyed penguin only)

All of the spatial covariates, including their sources (Table B.1), are described and presented in Appendix B. Note that the spatial density of commercial fishing events was also explored as a covariate of seabird sighting rate, although this was not found to be influential when fitting to all data sources simultaneously. Benthic sediment type and spatial presence of key prey species (see Figure B.13) were only attempted for yellow-eyed penguin because they were deemed unlikely to be relevant to the other assessed species, and the spatial extent of these habitat layers did not include some offshore regions within the EEZ. The respective covariate value was extracted for each covariate at the location and time (year, month, and/or day) of every data point.

Other non-spatial variables offered to models included:

- Month
- Vessel key
- Observer ID
- Data source

Year was also trialled in a prior exploratory analysis, although was generally not found to be influential. Time-specific variables, such as time of day, sun altitude, and moon fraction were trialled early in the analysis when fitting to sightings data only. However, these were subsequently not offered for any species, once gridded tracking data were used, because the reporting rate of these tracking devices is not time dependent.

2.2.3 Pre-processing of seabird observations

The tracking-based counts were combined with the true sightings-based counts and candidate covariates, which were then all subjected to further pre-processing prior to model fitting.

1. A relatively small number of events prior to 1980 and in 2021 were excluded, for which temporally-dynamic environmental variables were not available.
2. Counts were capped at 1000 individuals for each species per fishing event, which was deemed by the Aquatic Environment Working Group (AEWG) the maximum plausible count for a single species.

3. Events were then linked to each candidate environmental covariate using event location and date (for temporally dynamic variables), removing any events that could not be linked to any of the candidate covariates in space.
4. Events lacking an observer ID were removed.
5. All events by observers recording fewer than 200 events were removed.
6. All events by vessels from which fewer than 200 events were recorded were removed.

No attempt was made to remove spatially anomalous and unlikely counts of some species (e.g., positive counts of black petrel in the sub-Antarctic region), which were typically attributed to individual observers. This was effectively dealt with by including an ‘Observer ID’ term in all models.

2.2.4 Model development

Not all data sets were used for all species, and the data sources were often assigned different relative weightings. The choice of relative weighting for each data set differed by species (justified for each species in Section 3.2).

Month and data source were included in the models for most species as fixed effects. Vessel key and observer ID were included in all models fitting to sightings data as random effects. Gaussian process (GP) spatial smooths were offered to all models, accounting for spatial auto-correlation between adjacent observations.

The model optimisation process followed a modification of the standard approach used in catch-per-unit-effort (CPUE) analyses for Fisheries New Zealand. Specifically, model terms that explained the greatest amount of residual model deviance were iteratively added, until the addition of any remaining term explained $< 0.2\%$ of model deviance. Note that this threshold is less stringent than the 1% explained deviance threshold typically used for CPUE analyses and was chosen on the basis that the foraging patterns of seabirds can be spatially complex and that the spatial predictions used by SEFRA models should ideally capture this complexity. The use of a 0.1% threshold was also explored although this resulted in overly complex models. Some model terms were forced, that were found to be universally influential by prior exploration.

Throughout this document, we represent a GP spatial smooth as $GP(k)$ or $GP(k|t)$ where k represents the dimension of the basis used to represent the smooth term and t represents a season. A one-dimensional smooth of variable x is represented as $s(x, k)$, a random effect as $(1|x)$, and a fixed effect as x . For example, a model structure may have the form

$$\mu = GP(k = 50) + s(\log(\text{turbidity}), k = 3) + (1|\text{observer}) + \text{month}$$

which specifies a model that includes: a GP with an initial basis dimension of 50; a spline of turbidity in log-space with an initial basis dimension of 3; observer ID as a random effect; and month as a fixed effect. The basis dimension value for GP smooth was selected by iteratively increasing this value in multiples of ten (i.e., $k = 10$, $k = 20$, $k = 30$, etc.) until an increase resulted in a less than 0.2% increase in model deviance explained relative to the null model.

For all model runs, the negative binomial distribution was assumed, parametrised in terms of its mean μ and variance σ^2

$$p = \frac{\sigma^2 - \mu}{\sigma^2},$$

and

$$r = \frac{\mu^2}{\sigma^2 - \mu},$$

where

$$\Pr(X = k) = \binom{k + \frac{\mu^2}{\sigma^2 - \mu} - 1}{k} \left(\frac{\sigma^2 - \mu}{\sigma^2} \right)^k \left(\frac{\mu}{\sigma^2} \right)^{\mu^2 / (\sigma^2 - \mu)}$$

Estimated parameters included the coefficients for each explanatory variable and the variance. The dimension of the basis used to represent the smooth terms for each explanatory variable were set to sensible initial values to allow non-linear relationships while avoiding over-parametrisation due to overly wiggly relationships.

Seasonal GP surface smooths were offered at the end of the model optimisation process. If this resulted in at least 0.2% additional deviance explained, then the model optimisation process was started from the beginning with a seasonal GP surface smooth. Up to two seasons were offered for each species, representing non-chick-rearing (Season = '1') and chick-rearing (Season = '2') periods for each respective species, based on the mean date of hatching and fledging inferred from summaries by New Zealand Birds Online (<http://nzbirdsonline.org.nz/>) (Table 1).

Note that the chick-rearing versus non-chick-rearing seasons used here differ from the breeding versus non-breeding seasons assumed by previous iterations of the New Zealand seabird SEFRA model (Richard et al. 2020a), which gave a coarse-level representation of the seasonal presence of each species around New Zealand driven by seasonal migrations. The updated SEFRA model (produced under project PRO2019-10) disaggregated the biological model inputs by month. For that assessment, the seasonal presence of seabirds around New Zealand would primarily be driven by the monthly proportions of birds within the New Zealand EEZ (as calculated by the analysis under Section 3.3), whereas the chick-rearing/non-chick-rearing periods used here were intended to represent finer-scale seasonal variability in their spatial distribution within the wider breeding period, as imposed by the requirement to regularly return to feed chicks. For most of these seabird taxa, so few seabirds will be present around New Zealand during the non-breeding period that very little value is added by estimating a separate spatial distribution in these months, and, in any case, the data to inform this were extremely limited.

Table 1: Seasonal periods offered for each focal seabird species/sub-species. Up to two seasons were offered for each species, representing non-chick-rearing (Season = '1') and chick-rearing (Season = '2') periods for each respective species, based on the mean date of hatching and fledging inferred from summaries by New Zealand Birds Online (<http://nzbirdsonline.org.nz/>).

Taxon	Non-chick-rearing season ('1')	Chick-rearing season ('2')	Accepted as model term?
Flesh-footed shearwater	Jun–Jan	Feb–May	Yes
Black petrel	Jun–Jan	Feb–May	No
Westland petrel	Dec–Jul	Aug–Nov	No
White-chinned petrel	May–Jan	Feb–Apr	No
Salvin's albatross	Mar–Oct	Nov–Feb	Yes
White-capped albatross	Jun–Jan	Feb–May	No
Chatham Island albatross	May–Nov	Dec–Apr	Yes
Buller's albatross spp.*	Jul–Jan	Feb–Jun	Yes
Antipodean albatross	Jan–Mar	Apr–Dec	Yes
Gibson's albatross	Dec–Feb	Mar–Nov	Yes
Yellow-eyed penguin	Mar–Oct	Nov–Feb	No

*Months approximating to the mid-point between the seasons for the northern and southern sub-species were used at the species level.

2.2.5 Model prediction

Monthly spatial distributions for each species were generated by predicting the expected count at a 1 km resolution using the optimal fitted model for each species. During the model fitting step, the closest covariate possible was used (e.g., sea surface temperature during the month/year of the observation). However, during the model prediction step, the monthly average value of each covariate was used (see Appendix B).

The monthly spatial distributions for Northern and Southern Buller's albatross were for both species combined. To split these two species into separate distributions for Northern and Southern Buller's required an additional step. The spatial probability of Northern Buller's albatross was estimated using a separate GAM fitted to spatially explicit necropsy data, obtained from Wold (2017) (see Figure 7). This GAM only included a single term, a 2-dimensional spline. A binomial distribution was used with probability defined as:

$$p = s(\text{east, north}, k = 10).$$

This model was used to derive a spatial prediction layer for Northern Buller's albatross which was standardised to sum to one (see Figure 7). This distribution was then used to split the total Buller's albatross distribution above into Northern and Southern Buller's distributions (where Southern Buller's is extracted using the inverse of the Northern Buller's probability layer).

The prediction step was also slightly different for adult yellow-eyed penguins. During model fitting, the distance to colony covariate layer was modified to include only those colonies for which we had tracking data. This was done to avoid the model attempting to predict the presence of seabirds in regions that were close to colonies and for which we had no data (i.e., fitting to pseudo-zero cells), and failing to do so because the observation and predictions are at odds with each other. However, during the predictive step, the distance to colony covariate layer included all breeding colonies. This step was important as it allowed inference to be made about the spatial distribution of colonies for which no data were available. The model predictions for each respective breeding colony were rescaled to account for variation in colony population size by first rescaling the spatial prediction for each colony to sum to one and then multiplying each by the latest colony-specific population size estimate (in order to protect the exact locations of breeding birds, the tabulation of population estimates was not permitted at the colony level, although the approximate locations of breeding colonies are shown in Figure B.11).

The output format of the final seabird distribution maps followed the format outlined by Wood et al. (2022) and Mormede et al. (2022):

- a 1×1 km raster based upon the standard grid specification that was defined by Fisheries New Zealand. The coordinate reference system (CRS) for this raster was therefore “+proj=aea +lat_0=-40 +lon_0=175 +lat_1=-30 +lat_2=-50 +x_0=0 +y_0=0 +datum=WGS84 +units=m +no_defs” or European Petroleum Survey Group (EPSG) 9191;
- the spatial extent of each raster is a rectangular box that bounds the New Zealand EEZ but conforms to the standard grid specification (i.e., a rectangle that touches the EEZ boundary). However, the spatial predictions do not always fill this entire extent of the raster because some of the covariate layers do not cover the entire extent; and
- for each species, monthly (i.e., twelve) distribution maps were generated. For one species (XCI), there were no data during the month of May in any year, so the map for this month was assumed to be the mean of the April and June distributions.

Extending the predictions beyond the New Zealand EEZ was attempted, but was clearly problematic. There are two major problems when trying to extend the predictions beyond the EEZ:

1. the spatial extent of the available data for several covariates included in the optimal models of some species does not extend much further beyond the EEZ (i.e., depth, currents); and
2. spurious predictions begin to manifest at the edges of the distribution when attempting to predict too far beyond the extent of the EEZ. Most of these models include a spatial smoothing term. However, when too far from the core data (i.e., the Nomad and paper form data) the spatial smooths begin to extrapolate high predictions at the fringes of the prediction area. These high predictions are not credible and can totally drown out the visible distribution of the impacted species within the core range of the species (e.g., > 99% of the predicted at-sea abundance would be at the edge for some species).

In short, attempting to make model predictions too far from the data results in the model interpolating poor model predictions. The goal of this project was to develop maps to be used for SEFRA modelling, and therefore any seabird distribution maps generated by this project should be as accurate as possible within the New Zealand EEZ and make use of the best available predictive layers. If a wider distribution is desired in the future, this should be developed separately (and potentially the spatial smooths should be dropped), rather than at the expense of the distributions intended for SEFRA modelling within the EEZ.

2.3 Proportion of seabirds in zone

The proportion of seabirds within the New Zealand EEZ by month was calculated empirically using the tracking data. The average daily location was derived for each tracked bird and each daily location was flagged as either inside or outside the EEZ. The proportion of days spent inside versus outside the EEZ was calculated for each species by month. Only those strata (a bird/month) with at least 28 average daily locations were considered, to avoid making inference about the proportions in zone for birds with observations that do not cover an entire month. This analysis produced estimates of the proportion in zone for each species by month.

3 RESULTS

3.1 Summary of spatial information

All of the available tracking data were collated for each seabird taxon, including different combinations of GPS, PTT, GLS, and VHF data. The temporal distributions of the tracking data for each species (in terms of birds with locations by year and month) are shown in Appendix C. The sources of raw tracking data for each species are summarised in Appendix D. Adult VHF data were sourced from Bruce McKinlay at DOC and methods have been published by Moore et al. (1995). Adult GPS data were sourced from Thomas Mattern and were collected under a project for DOC's Conservation Services Programme (POP2018-02) and are described by Mattern (2020) (Table C.12 in Appendix C).

In general, the GLS data (lowest accuracy of the various tracking data types) had the best seasonal coverage, providing almost as much spatial information outside each species' respective breeding season. By comparison, PTT and GPS data provided more information during the breeding season and, for some species, very little spatial information outside this period (e.g., flesh-footed shearwater; see Table C.1). The sightings data provided excellent monthly coverage of spatial information for those species that can be accurately identified to species level (Table 2 and Table 3). The sample size of sighting events was substantially reduced by pre-processing (see Section 2.2.3) and produced approximately equal numbers of events by source for paper form (19 119 sighting events), Nomad (24 658), eBird stationary (18 087), and eBird travelling (19 726), and a relatively smaller sample of container ship (Te Papa Tongarewa) sighting events (5843).

The different data sources were informative in different locations (e.g., see the bottom right-hand plot of Figure D.1 in Appendix D). The fisheries observer sightings data (paper form and Nomad) provide

best information in areas of high overlap with offshore and inshore fishing, respectively. Much of the eBird data were outside the New Zealand EEZ, and those within zone were generally concentrated closer to shore than the fisheries observer data. The merchant ship data were collected up until 1988 (earlier than most effort data for the other sources) and were more concentrated off the west of New Zealand, where sighting events from other sources were very sparse.

Table 2: Total count of seabird sightings events by data source and year for the full available data set from 1980 to 2020, and for the final data set used for spatial distribution model fitting. This table does not include the gridded counts obtained from tracking data.

Year	Prior to pre-processing					After pre-processing				
	Paper form	Nomad	eBird stationary	eBird travelling	Te Papa	Paper form	Nomad	eBird stationary	eBird travelling	Te Papa
1980	0	0	1	4	443	0	0	0	0	309
1981	0	0	3	1	456	0	0	1	1	435
1982	0	0	6	3	346	0	0	0	2	323
1983	0	0	57	1	217	0	0	0	0	210
1984	0	0	11	6	1 117	0	0	0	0	1 114
1985	0	0	25	10	983	0	0	1	1	977
1986	0	0	14	48	995	0	0	1	2	988
1987	0	0	152	12	1 278	0	0	137	3	1 278
1988	0	0	440	58	220	0	0	383	5	209
1989	0	0	295	46	0	0	0	278	4	0
1990	0	0	82	103	0	0	0	78	29	0
1991	0	0	468	48	0	0	0	438	1	0
1992	0	0	364	111	0	0	0	347	2	0
1993	0	0	380	54	0	0	0	352	3	0
1994	0	0	17	32	0	0	0	11	3	0
1995	0	0	23	24	0	0	0	16	13	0
1996	0	0	27	44	0	0	0	13	8	0
1997	0	0	57	83	0	0	0	19	9	0
1998	0	0	55	73	0	0	0	22	2	0
1999	0	0	23	59	0	0	0	10	5	0
2000	0	0	33	75	0	0	0	12	8	0
2001	0	0	33	45	0	0	0	16	2	0
2002	0	0	36	43	0	0	0	21	7	0
2003	0	0	60	72	0	0	0	29	6	0
2004	0	0	45	111	0	0	0	19	0	0
2005	0	0	145	54	0	0	0	12	3	0
2006	0	0	305	195	0	0	0	99	21	0
2007	0	0	395	703	0	0	0	177	549	0
2008	2 854	0	630	1 031	0	741	0	205	603	0
2009	3 967	7 835	1 091	1 445	0	1 792	3 311	464	862	0
2010	2 975	4 127	1 179	1 271	0	1 127	1 731	467	460	0
2011	3 578	1 343	1 192	1 097	0	1 001	338	440	253	0
2012	3 623	2 089	1 432	1 088	0	1 769	961	410	346	0
2013	4 415	3 352	2 543	1 484	0	1 810	2 079	743	318	0
2014	4 108	1 652	4 230	2 766	0	1 538	1 172	1 228	574	0
2015	4 478	3 609	5 006	4 726	0	2 145	3 513	1 248	1 333	0
2016	6 323	6 319	5 197	5 549	0	3 224	5 004	1 172	1 355	0
2017	5 403	5 910	6 035	7 793	0	2 699	4 315	1 726	1 728	0
2018	3 559	3 371	9 021	12 743	0	1 273	2 234	1 918	2 347	0
2019	0	0	19 088	24 951	0	0	0	2 884	4 002	0
2020	0	0	27 755	38 731	0	0	0	2 690	4 856	0

Table 3: Total count of seabird sightings events by data source and month for the full available data set from 1980 to 2020, and for the final data set used for spatial distribution model fitting. This table does not include the gridded counts obtained from tracking data.

Month	Prior to pre-processing					After pre-processing				
	Paper form	Nomad	eBird stationary	eBird travelling	Te Papa	Paper form	Nomad	eBird stationary	eBird travelling	Te Papa
Jan	3 249	7 204	8 215	10 432	200	1 620	4 279	1 394	1 897	184
Feb	4 255	7 097	5 656	9 395	460	1 971	4 073	808	1 551	454
Mar	4 613	3 502	5 805	7 562	574	2 203	2 346	1 761	1 833	540
Apr	3 916	2 820	5 650	6 611	341	1 724	1 591	1 247	1 382	320
May	3 653	2 122	5 490	6 584	382	1 393	1 035	1 155	1 481	369
Jun	3 842	1 313	6 090	6 865	296	1 425	801	1 485	1 582	277
Jul	3 336	1 230	6 355	6 956	624	1 145	943	1 478	1 369	596
Aug	3 862	1 305	5 697	7 791	554	1 566	920	1 168	1 521	533
Sep	3 851	1 241	6 750	8 082	447	1 706	928	1 752	1 634	414
Oct	3 579	2 271	8 866	11 000	572	1 541	1 454	2 078	2 374	563
Nov	3 270	5 006	11 831	12 925	1 080	1 350	3 139	1 862	1 667	1 080
Dec	3 857	4 496	11 546	12 590	525	1 475	3 149	1 899	1 435	513

For the purposes of model fitting, some of the data sources were not used for certain species (Table 4), e.g., lowest precision tracking data, or sightings data if not considered reliable for a species. Where relevant, the reasons for this are given with the modelling results for each species (Section 3.2.1 to Section 3.2.11).

The final seabird data sets used for spatial modelling are plotted spatially in Appendix D, including the spatial density of sightings from different sources and the gridded tracking data.

3.2 Seabird distribution modelling

A high-level summary of the optimal models for each species is given in Table 4, including optimal model structure, data sets used, relative data set weighting of tracking data, and the percentage of the model deviance explained by the optimal model. The percentage of deviance explained was high for most species (> 80% for all except for Antipodean albatross, Gibson's albatross, and fledgling yellow-eyed penguin). Environmental covariates were retained in the optimal models of all species except Chatham Island albatross. Turbidity was the most frequently selected environmental model term (6 out of 12 species models), followed by distance to colony (4 out of 10 species models, not including yellow-eyed penguin models for which this was a fixed term), and sea surface temperature (3 out of 12 species models).

Table 4: Summary of model terms (as specified in R), data sets included data set weights for tracking data, and percent deviance explained for each species. Non-fixed model terms (i.e., those selected by the optimisation routine) are bolded and are shown in the order in which they were selected. (Continued on next page)

Species	Model terms	Data sets included	Trackingweights	Deviance explained (%)
Flesh-footed shearwater	s(east, north, bs = "gp", k = 50, by = season) + s(observer, bs = "re) + s(vessel, bs = "re) + source + month + s(log(turbidity), k = 3)	Tracking (GLS, GPS) Nomad Paper form eBird Te Papa	0.5	80.6
Black petrel	s(east, north, bs = "gp", k = 50) + s(observer, bs = "re) + s(vessel, bs = "re) + source + month + s(sst, k = 3) + s(depth, k = 3)	Tracking (GLS, GPS) Nomad Paper form eBird Te Papa	0.5	88.3
Westland petrel	s(east, north, bs = "gp", k = 50) + s(observer, bs = "re) + s(vessel, bs = "re) + source + month + s(log(turbidity), k = 3) + s(distance_to_colony, k = 3)	Tracking (GLS, GPS, PTT) Nomad Paper form eBird Te Papa	0.5	88.0
White-chinned petrel	s(east, north, bs = "gp", k = 50) + s(observer, bs = "re) + s(vessel, bs = "re) + source + month + s(log(turbidity), k = 3)	Tracking (GLS) Nomad Paper form eBird Te Papa	0.1	90.6
Buller's albatross	s(east, north, bs = "gp", k = 50, by = season) + s(observer, bs = "re) + s(vessel, bs = "re) + source + month + s(log(turbidity), k = 3) + s(distance_to_colony, k = 3)	Tracking (GPS, GLS, PTT) Nomad Paper form eBird Te Papa	0.1 if Southern Buller's, or count = 0 and Northern Buller's	87.8
Chatham Island albatross	s(east, north, bs = "gp", k = 40) + s(observer, bs = "re) + s(vessel, bs = "re) + source + month	Tracking (GLS, GPS, PTT) Nomad Paper form eBird Te Papa	0.5	95.5

Species	Model terms	Data sets included	Trackingweights	Deviance explained (%)
Salvin's albatross	s(east, north, bs = "gp", k = 40, by = season) + s(observer, bs = "re) + s(vessel, bs = "re) + source + month + s(turbidity, k = 3) + s(distance_to_colony, k = 3)	Tracking (GPS, PTT) Nomad Paper form eBird Te Papa	0.5	88.7
White-capped albatross	s(east, north, bs = "gp", k = 50, by = season) + s(observer, bs = "re) + s(vessel, bs = "re) + source + month + s(log(turbidity, k = 3) + s(sst, k = 3) + s(currents, k = 3)	Tracking (GPS, PTT) Nomad Paper form eBird Te Papa	0.5	85.3
Antipodean albatross	s(east, north, bs = "gp", k = 50, by = season) + s(tag, bs = "re) + distance_to_colony + s(sst, k = 3)	Tracking (GLS, PTT)	1.0	58.5
Gibson's albatross	s(east, north, bs = "gp", k = 50, by = season) + s(tag, bs = "re) + s(sqrt(slope), k = 3) + s(sst, k = 3) + s(distance_to_colony, k = 3) + s(wind_speed, k = 3)	Tracking (PTT)	1.0	52.9
Yellow-eyed penguin – fledglings	s(sqrt(distance_to_colony), k = 5) + s(tag, bs = "re) + s(tag, distance_to_colony , bs = "re) + s(shore, k = 3) + s(sea level anomaly, k = 3) + s(sqrt(currents), k = 3) + s(log(chlorophyll), k = 3)	Tracking (PTT)	0.1 if count = 0	60.7
Yellow-eyed penguin – adults	s(sqrt(distance_to_colony), k = 5) + s(tag, bs = "re) + s(tag, distance_to_colony , bs = "re) + s(sqrt(shore), k = 3) + s(depth, k = 3)	Tracking (GPS, VHF)	0.1 if count = 0	91.1

3.2.1 Flesh-footed shearwater

The flesh-footed shearwater spatial data included paper form, Nomad, eBird, Te Papa, and tracking (GLS and GPS) data. The tracking data were deemed to be of good quality and, so, were given a weighting of 50% relative to the sightings data. There was good agreement in the spatial information among all data sources, in that most individuals were observed off the north coast of the North Island and in adjacent coastal regions of the North Island (Figure D.1).

The initial model for this species included a seasonal GP spatial smooth (one for each of the chick-rearing and non-chick rearing seasons), a random effect for each observer, a random effect for each vessel, and fixed effects for each data source and month (Table 5). The final model added a spline for sea surface turbidity (Table 5). This model explained 80.6% of the model deviance—a 0.5% improvement over the initial model. Expected counts were higher in regions of low surface turbidity, and lower during February–May (Figure 2), although note that the month effect was strongly confounded with the seasonal spatial smooths for this species and, therefore, seasonal patterns should be discerned from the model prediction only. Expected counts differed somewhat by data source, with greater uncertainty for the eBird, Te Papa, and tracking data sets relative to the fisheries observer sightings (Figure 2).

The mean spatially-explicit residuals were all relatively low, ranging from about -0.6 to 0.6 (Figure E1, Figure E.2 in Appendix E). The maximum spatially-explicit residuals were generally low, but were very high (over 7.5) in some cells (Figure E1, Figure E.3). However, these types of residual patterns are not surprising given that the model was predicting the expected number of flesh-footed shearwaters to a very high spatial resolution (by 1 km cell), and that the number of seabirds observed from the stern of a vessel can often be very high. The residuals by date, month, and data source were all centered about zero (Figure E.4).

Flesh-footed shearwaters were predicted by the model to be most abundant in New Zealand waters from October to April and were present in much lower numbers or absent from the EEZ for the remainder of the year (Figure F.1 in Appendix F). This seasonal pattern is supported by the proportion in zone analysis, which indicated that they are most abundant within the New Zealand EEZ from November to April (see Section 3.3).

The predicted distribution was reasonably consistent by month, discernable when a different scale is used for each month (Figure F.2 and Figure F.3), although flesh-footed shearwaters were predicted to be distributed closer to shore during the assumed chick-rearing period in February–May. The predicted monthly distributions indicate that flesh-footed shearwaters are most abundant off the north coast of the North Island, although they also occur as far south as Hawke Bay (Figure F.2 and Figure F.3). The predicted distribution is much more dispersed than was previously assumed in the breeding period and less dispersed than was assumed during the non-breeding period (compare Figure F.2 and Figure F.3 with Figure A.1).

Table 5: Degrees of freedom (DF) for each term in the final model for flesh-footed shearwater and percentage deviance explained/Akaike information criterion (AIC) for the fixed terms (above the second horizontal line) and with the addition of each selected term (below the line). The DF was derived from the number of levels for non-splined terms (i.e., without the ‘s’ prefix), and was the effective degrees of freedom reported using ‘summary.gam’ for splined terms.

Model terms	DF	Deviance explained (%)	AIC
s(easting, northing; non-chick-rearing season)	40.5		
+ s(easting, northing; chick-rearing season)	46.9		
+ s(observer)	155.8		
+ s(vessel)	63.4		
+ source	5.0		
+ month	11.0	80.1	110 211.6
+ s(log(turbidity))	2.0	80.6	109 202.3

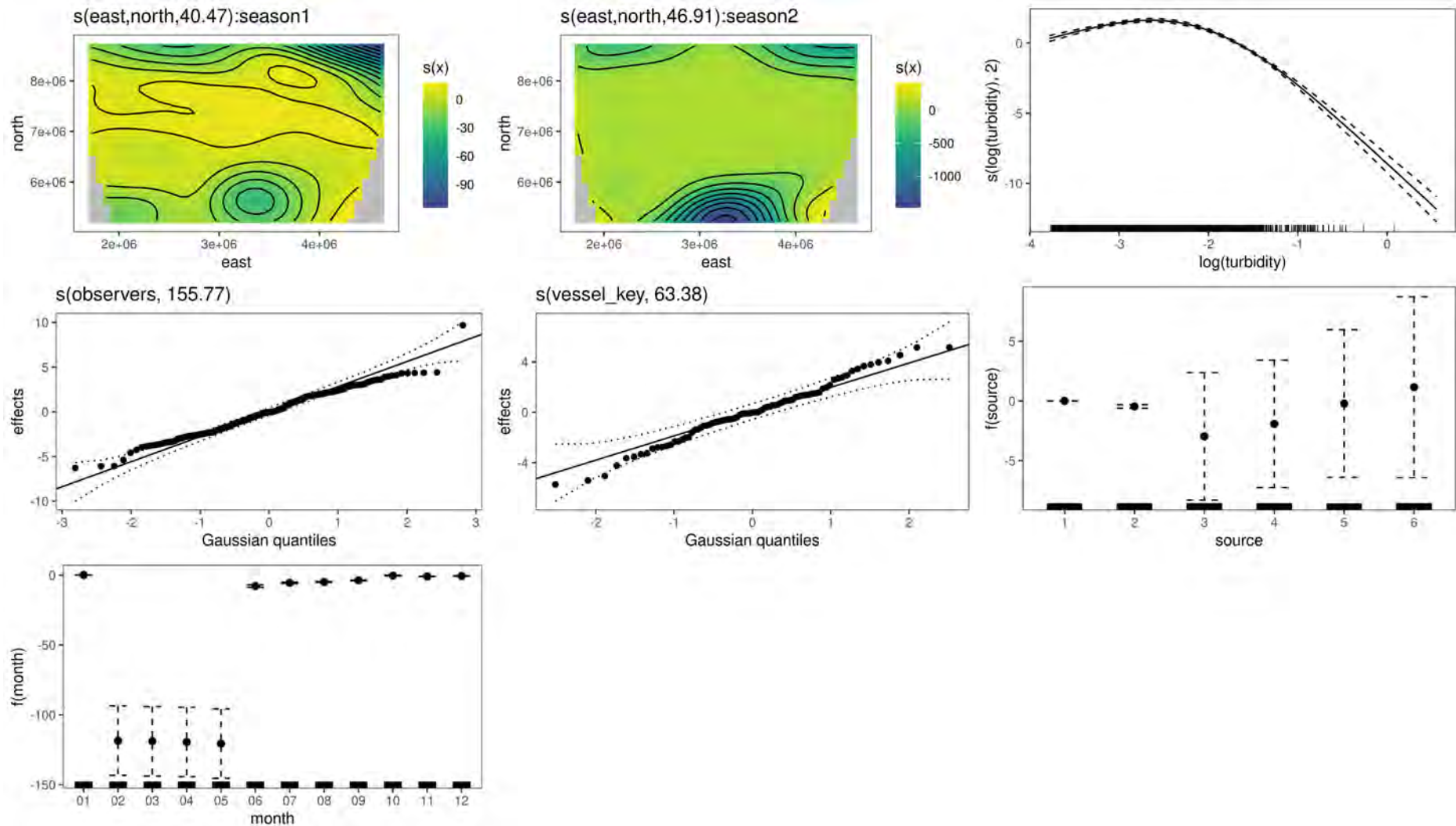


Figure 2: Model terms for the final model for flesh-footed shearwater including: the Gaussian process spatial smooths by season (season1 = non-chick-rearing, season2 = chick-rearing); turbidity spline; the observer ID and vessel key random effects; and the data source (1 = paper form, 2 = Nomad, 3 = eBird stationary, 4 = eBird travelling, 5 = Te Papa, 6 = tracking) and month fixed effects, where month 01 is January.

3.2.2 Black petrel

The black petrel spatial data used by this analysis included paper form, Nomad, eBird, Te Papa, and tracking (GLS and GPS) data. The tracking data were determined to be of relatively good quality, so these data were only downweighted by 50% relative to the sighting data. Generally, there was good agreement in the spatial information across the data sources, with greatest density in the Bay of Plenty and in the offshore region to the north of this (Figure D.2), near to the main breeding colonies of this species (top-right plot of Figure B.9).

The initial model for this species included a GP spatial smooth, a random effect for each observer, a random effect for each vessel, and fixed effects for each data source and month. The model optimisation process added splines for SST and then depth, and the final model explained 88.3% of the model deviance—a 3.3% improvement over the initial model (Table 6). The expected counts were greatest at SST values above 20 °C, and over shallow seafloor (Figure 3). Offering a seasonal surface smooth to account for potential variability in foraging patterns, a comparison of the chick-rearing and non-chick periods did not result in much increase in deviance explained.

There was no evident spatial pattern in the residuals across all data sources (Figure E.5), or when plotted separately by data source (Figure E.6 and Figure E.7). The residuals by date, month, and data source were all centered about zero (Figure E.8).

Black petrels were predicted to be almost entirely absent from the New Zealand EEZ during the assumed non-breeding period from June to September (Figure F.4), in agreement with the empirical analysis of tracking data only (see Section 3.3). When the colour scale was allowed to be different for each month, the predicted distribution was reasonably consistent across all months (Figure F.5 and Figure F.6).

The model predicted that black petrels are most abundant over regions of shallow seafloor to the north of the main breeding colony at Great Barrier Island (Figure F.5 and Figure F.6). At a regional scale, these predictions are similar to the previously assumed distributions (Figure A.2)

Table 6: Degrees of freedom (DF) for each term in the final model for black petrel and percentage deviance explained/Akaike information criterion (AIC) for the fixed terms (above the second horizontal line) and with the addition of each selected term (below the line). The DF was derived from the number of levels for non-splined terms (i.e., without the ‘s’ prefix), and was the effective degrees of freedom reported using ‘summary.gam’ for splined terms.

Model terms	DF	Deviance explained (%)	AIC
s(easting, northing)	45.3		
+ s(observer)	129.3		
+ s(vessel)	61.9		
+ source	5.0		
+ month	11.0	85.0	85 191.8
+ s(sst)	2.0	87.8	85 048.4
+ s(depth)	2.0	88.3	84 730.3

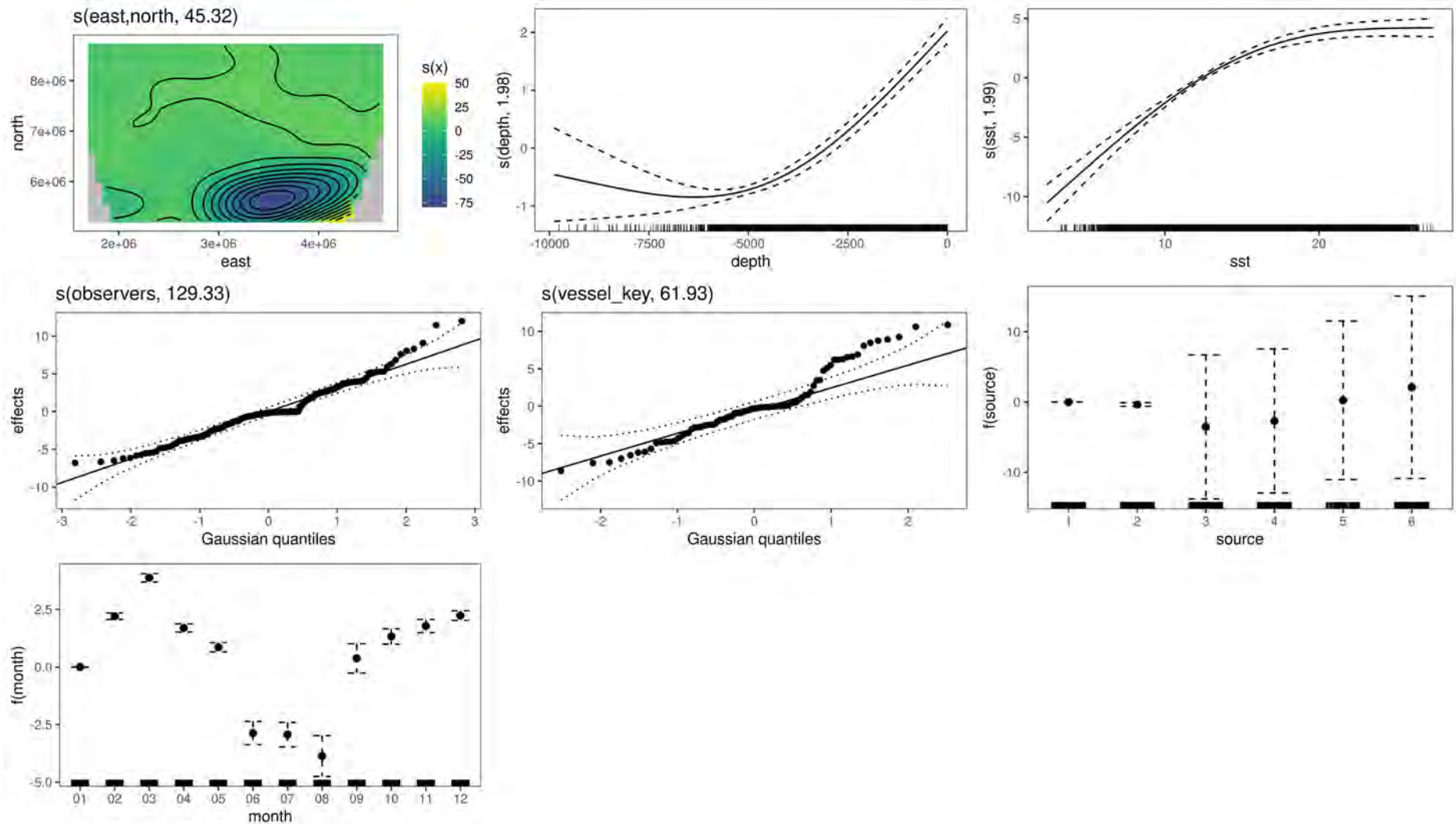


Figure 3: Model terms for the final model for black petrel including: the Gaussian process spatial smooth; the depth and sea surface temperature (sst) splines; the observer ID and vessel key random effects; and the data source (1 = paper form, 2 = Nomad, 3 = eBird stationary, 4 = eBird travelling, 5 = Te Papa, 6 = tracking) and month fixed effects, where month 01 is January.

3.2.3 Westland petrel

The Westland petrel spatial data included paper form, Nomad, eBird, Te Papa, and tracking (GLS, GPS, and PTT) data. The tracking data set was downweighted by 50% relative to the sightings data. Generally, there was good agreement in the spatial information across all data sources, with most individuals observed off the west coast South Island (Figure D.3), near to the main breeding colony in the West Coast Region (bottom-left plot of Figure B.9).

The initial model for this species included a non-seasonal GP spatial smooth, a random effect for each observer, a random effect for each vessel, and fixed effects for each data source and month. The model optimisation process added splines for turbidity and distance to colony (Table 7). The final model explained 88.0% of the model deviance, a 1.3% improvement on the initial model. Model expected counts of Westland petrel were greatest in regions of low surface turbidity and close proximity to the main breeding colony for this species (Figure 4).

There was no obvious spatial pattern in the model residuals across all sources (Figure E.9), or by data source (Figure E.10 and Figure E.11). The residuals by date, month, and data source were all centered about zero (Figure E.12).

The predicted monthly distributions indicated that Westland petrels were most abundant off the west coast South Island, near to their only known breeding colony in the West Coast Region (Figure F.7). The predicted distributions are slightly more spatially constrained than the layer previously used for the breeding period, and considerably more spatially constrained than the old non-breeding layer (compare Figure F.7 with Figure A.3). Furthermore, the predicted density was low in turbid nearshore waters, compared with the old layers.

The seasonal pattern of Westland petrel presence within the EEZ was not well-defined by this spatial model (Figure F.7), although it broadly agreed with the empirical analysis of tracking data only, which indicated that they are almost totally absent from the EEZ from December to March (see Section 3.3). Spatial model predictions indicated minimal variability in the spatial distribution of birds remaining within the EEZ, which was evident when the colour scales used for monthly predictions were allowed to vary by month (Figure F.8, Figure F.9).

Table 7: Degrees of freedom (DF) for each term in the final model for Westland petrel and percentage deviance explained/Akaike information criterion (AIC) for the fixed terms (above the second horizontal line) and with the addition of each selected term (below the line). The DF was derived from the number of levels for non-splined terms (i.e., without the ‘s’ prefix), and was the effective degrees of freedom reported using ‘summary.gam’ for splined terms.

Model terms	DF	Deviance explained (%)	AIC
s(easting, northing)	44.3		
+ s(observer)	149.7		
+ s(vessel)	62.7		
+ source	5.0		
+ month	11.0	86.7	73 301.4
+ s(log(turbidity))	2.0	87.7	71 902.7
+ s(distance_to_colony)	1.8	88.0	71 601.8

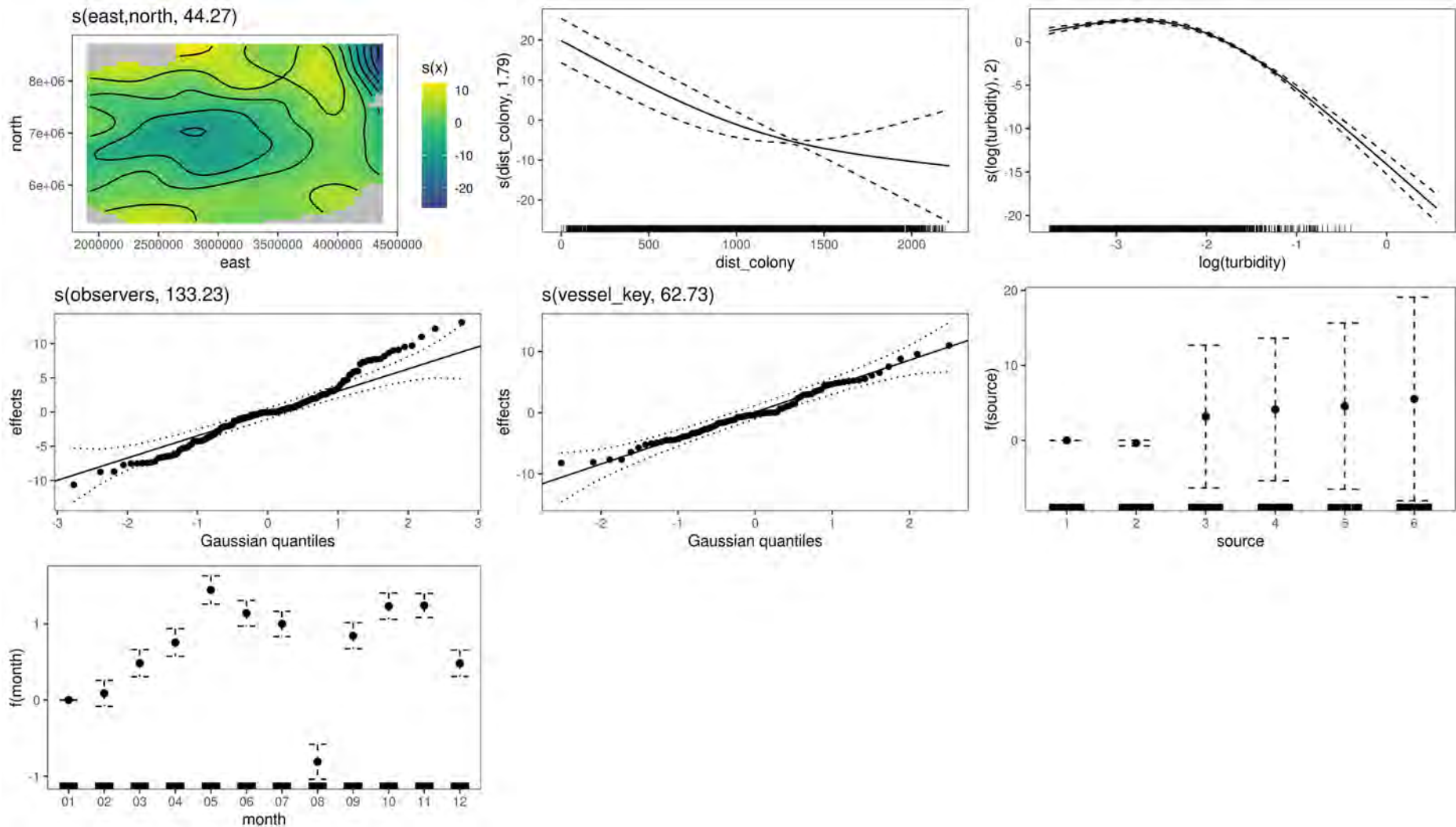


Figure 4: Model terms for the final model for Westland petrel including: the Gaussian process spatial smooth; distance to colony and turbidity splines; observer ID and vessel key random effects; and data source (1 = paper form, 2 = Nomad, 3 = eBird stationary, 4 = eBird travelling, 5 = Te Papa, 6 = tracking) and month fixed effects, where month 01 is January.

3.2.4 White-chinned Petrel

The white-chinned petrel spatial data included paper form, Nomad, eBird, Te Papa, and tracking (GLS) data. The tracking data set was downweighted to 10%, since these were collected by GLS devices only and were deemed to have relatively poor spatial accuracy. Taken together, the spatial information for this species indicates that white-chinned petrels are most abundant to the south of the South Island, although are present as far north as the top of the North Island (Figure D.4).

The initial model for this species included a GP spatial smooth, a random effect for each observer, a random effect for each vessel, and fixed effects for each data source and month. The optimal model added a spline for sea surface turbidity and explained 90.6% of the model deviance, a 0.4% improvement on the initial model (Table 8). As with all of the other species for which turbidity was selected by the optimisation process, the expected count of white-chinned petrel was lower in turbid waters (Figure 5). Based on this model, the expected count was high in October–April and low in the winter period and adjacent months.

There was no obvious spatial pattern in the residuals of the final model for white-chinned petrels (Figure E.13, Figure E.14, and Figure E.15). The residuals by date, month, and data source were all centered about zero (Figure E.16).

The spatial model predictions indicate that white-chinned petrels are most abundant in offshore waters to the south and east of New Zealand (Figure F.10). The predicted monthly distributions are not as centred on the breeding colonies as the old layers (compare Figure F.10 and Figure A.4) and include an area of high density to the east of the North Island that was not present in the old layers.

This model predicted that they are most abundant within the EEZ from October to April (Figure F.10), consistent with the empirical analysis of tracking data only (see Section 3.3). Spatial model predictions indicated minimal variability in the spatial distribution of white-chinned petrels remaining within the EEZ, discernable when the colour scale was allowed to vary by month (Figure F.11, Figure F.12), although the predictions do indicate seasonality in their use of a region on the edge of the EEZ to the east of the North Island.

Table 8: Degrees of freedom (DF) for each term in the final model for white-chinned petrel and percentage deviance explained/Akaike information criterion (AIC) for the fixed terms (above the second horizontal line) and with the addition of each selected term (below the line). The DF was derived from the number of levels for non-splined terms (i.e., without the ‘s’ prefix), and was the effective degrees of freedom reported using ‘summary.gam’ for splined terms.

Model terms	DF	Deviance explained (%)	AIC
s(easting, northing)	33.8		
+ s(observer)	158.0		
+ s(vessel)	72.3		
+ source	5.0		
+ month	11.0	90.2	97 548.1
+ s(log(turbidity))	1.9	90.6	96 808.9

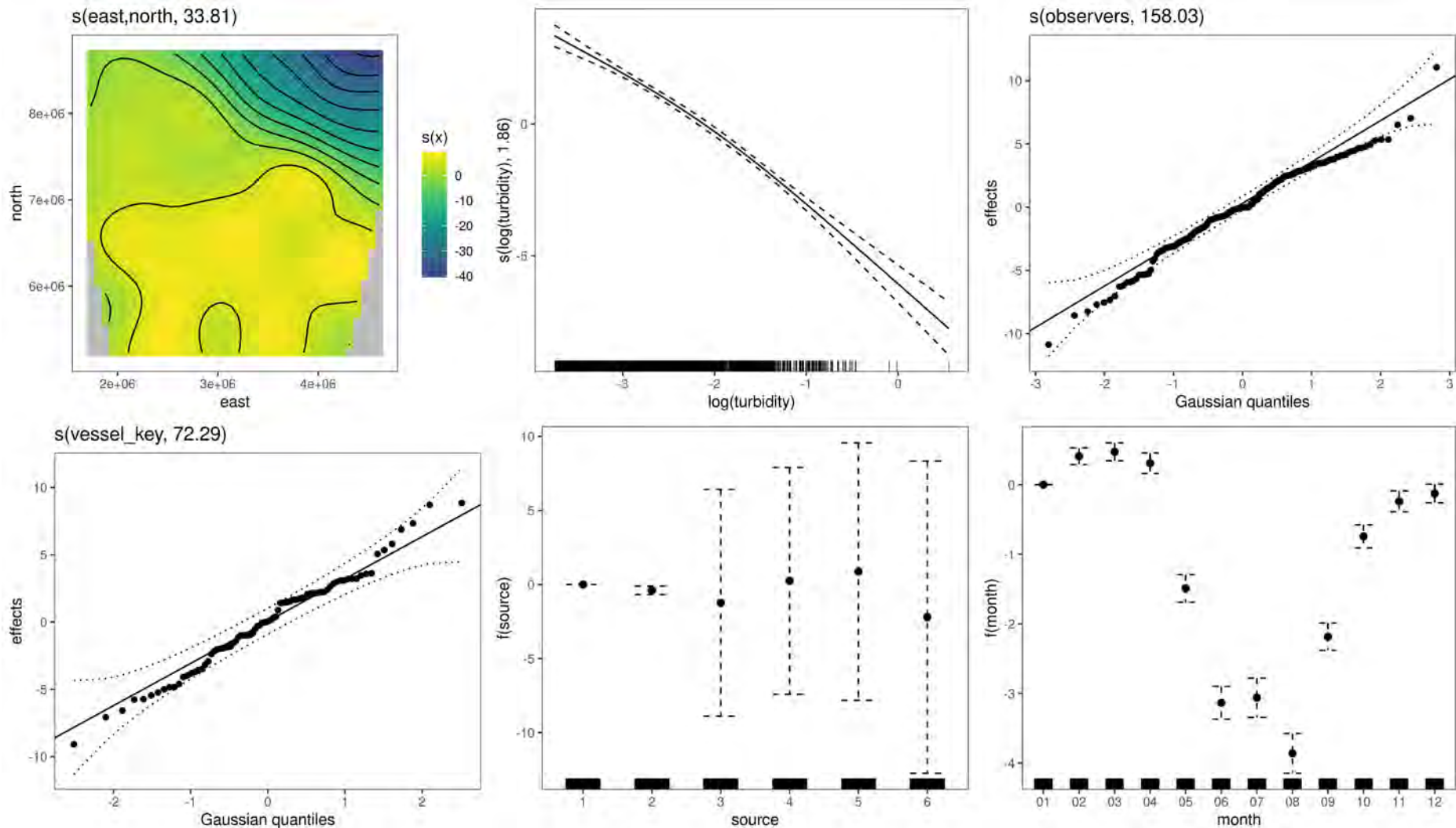


Figure 5: Model terms for the final model for white-chinned petrel including: the Gaussian process spatial smooth; the turbidity spline; observer ID and vessel key random effects; and data source (1 = paper form, 2 = Nomad, 3 = eBird stationary, 4 = eBird travelling, 5 = Te Papa, 6 = tracking) and month fixed effects, where month 01 is January.

3.2.5 Northern and Southern Buller’s albatross

For Northern and Southern Buller’s albatross, the basic approach was to predict their spatial distribution throughout the New Zealand EEZ at the species level, and then to use species identifications from fishery bycaught seabirds (Wold 2017) to spatially disaggregate the species-level prediction by sub-species.

The final data set of spatial information for Northern and Southern Buller’s albatross consisted of paper form, Nomad, eBird, Te Papa, and tracking (GPS, PTT, and GLS) data. Although the sightings-based data were informative of both sub-species combined (fisheries observers are unlikely to be able to differentiate them reliably), the tracking data were almost entirely collected for Southern Buller’s albatross (extremely limited sampling from Northern Buller’s albatross at Chatham Islands, see Table C.5). For this reason, the tracking data set for Southern Buller’s albatross was downweighted to 10% of the sightings data weighting, despite the good quality of these data. For Northern Buller’s albatross, only the zero count grid cells were allocated a relative weighting of 10%, and the positive counts were given the same weighting as the count data. The spatial agreement between the different sources of information was not as good as for other species. For example, the paper form data indicated relatively high abundance off the west coast of the South Island, whereas the other sources of sighting data did not. However, all data sources indicated relatively high abundance to the south of the South Island (Figure D.5).

The initial model for this species included a GP spatial smooth for each of the chick-rearing and non-chick-rearing periods, a random effect for each observer, a random effect for each vessel, and fixed effects for each data source and month. The optimisation process added splines for sea surface turbidity and distance to colony and explained 87.8% of the model deviance—a 0.9% improvement on the initial model (Table 9).

Table 9: Degrees of freedom (DF) for each term in the final model for Northern and Southern Buller’s albatross and percentage deviance explained/Akaike information criterion (AIC) for the fixed terms (above the second horizontal line) and with the addition of each selected term (below the line). The DF was derived from the number of levels for non-splined terms (i.e., without the ‘s’ prefix), and was the effective degrees of freedom reported using ‘summary.gam’ for splined terms.

Model terms	DF	Deviance explained (%)	AIC
s(easting, northing, non-brooding season)	37.8		
+ s(easting, northing, brooding season)	38.9		
+ s(observer)	209.5		
+ s(vessel)	76.6		
+ source	5.0	86.9	139 814.7
+ month	11.0		
+ s(log(turbidity))	1.9	87.6	138 293.0
+ s(distance to colony)	2.0	87.8	137 782.2

The model term plots indicated that expected counts were higher in low turbidity regions. Expected counts also decreased with distance from colony up to ~ 750 km and increased with distance to colony further away than this, although this latter relationship was strongly confounded with the spatial smooths, which have the greatest expected counts around the main colonies (Figure 6).

There was no obvious spatial pattern in the model residuals across all data sources (Figure E.17) or for each source individually (Figure E.18 and Figure E.19). The residuals by date, month, and data source were all centered about zero (Figure E.20).

The model-predicted monthly distributions for the species (i.e., across both sub-species) are shown in Figure F.13, Figure F.14, and Figure F.15.

The spatial prediction for the model fitted to bycatch incidents that were identified to species level is shown in Figure 7. This model (see Section 2.2.5 for a description of this) explained 65.7% of the null model deviance and predicted that Southern Buller's albatross are the dominant subspecies around all of the South Island and off the west coast of the North Island. Whereas Northern Buller's albatross were predicted to be dominant around the Chatham Islands, where their largest breeding colony is located (top-left plot of Figure B.10), and in offshore regions to the north and east of the North Island.

The prediction from this model was then used to partition the species-level monthly predictions into subspecies-level predictions for the Northern Buller's albatross (Figure F.16, Figure F.17, Figure F.18) and Southern Buller's albatross (Figure F.19, Figure F.20, Figure F.21). These predictions were consistent with Northern Buller's albatross being most abundant around their main breeding colony at the Chatham Islands (all months) and over the western Chatham Rise (February to June). These distributions were similar to those used previously, although with a greater affinity to the Chatham Rise than the previous distributions (comparing Figure A.5 with Figure F.20, Figure F.21). By comparison, the predicted Southern Buller's albatross distributions were more centred on the breeding colonies and were very similar to the previous distributions used for the breeding period (comparing Figure A.6 with Figure F.20 and Figure F.21).

For Northern Buller's albatross, the main seasonal variability in model predictions was off the east of the North Island towards the edge of the EEZ, where they were predicted to be present outside the assumed chick-rearing period (July to January) (Figure F.17 and Figure F.18). For Southern Buller's albatross, the region of greatest variability was to the west of the South Island, where they were predicted to have greatest density in December and January, although the predicted density here was low relative to some other regions (Figure F.20 and Figure F.21).

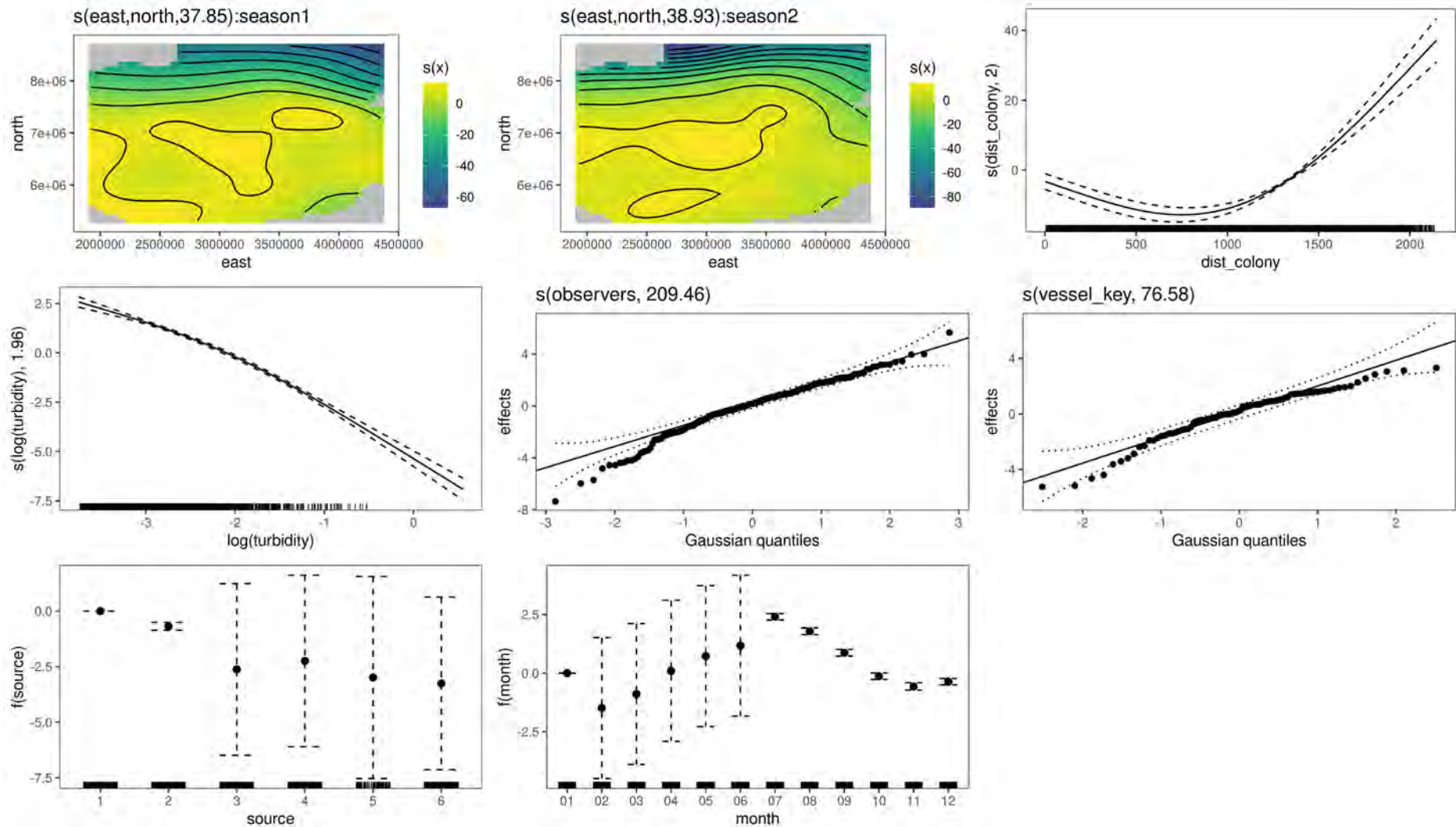


Figure 6: Model terms for the final model for Northern and Southern Buller's albatross (combined) including: the spatial smooths by season (season1 = non-chick-rearing, season2 = chick-rearing); distance to colony (dist_colony) and turbidity splines; the observer ID and vessel key random effects; and data source (1 = paper form, 2 = Nomad, 3 = eBird stationary, 4 = eBird travelling, 5 = Te Papa, 6 = tracking) and month fixed effects, where month 01 is January.

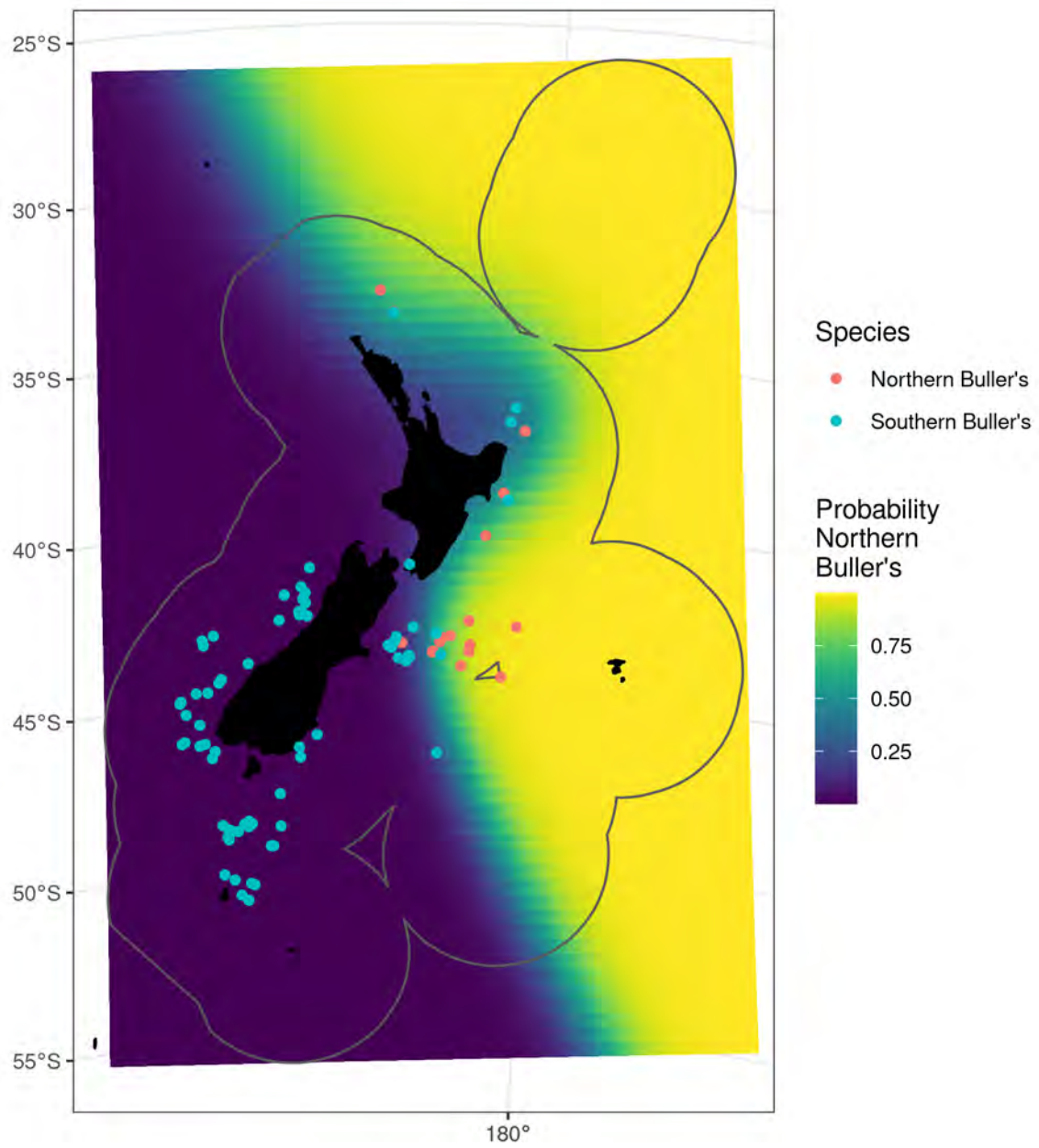


Figure 7: The spatial probability of Northern Buller's albatross and the spatially explicit necropsy data for confirmed Southern and Northern Buller's albatross (points) used to inform the model.

3.2.6 Chatham Island albatross

The final spatial data set for Chatham Island albatross consisted of paper form, Nomad, eBird, Te Papa, and tracking (GLS, GPS, and PTT) data. Generally, all data sources agreed with each other in that most individuals were observed off the east coast of the South Island, particularly around the Chatham Islands, where this species breeds (compare Figure D.6 with the bottom-left plot of Figure B.9). The month of May was not included in the GAM as no Chatham Island albatross were observed during this month in any data set; the distribution during this month was assumed to be the average of the April and June distributions. The tracking data were deemed of relatively good quality and were only downweighted by 50% relative to the sightings data.

The initial model for this species included a GP spatial smooth, a random effect for each observer, a random effect for each vessel, and fixed effects for each data source and month. No additional model terms were added by the model optimisation process. The final model explained 95.5% of the model deviance (Table 10). As with most of the other species, the best spatial information came from the fisheries observer sighting data (paper form and Nomad), evidenced by greater uncertainty in the expected counts for the eBird, Te Papa, and tracking data sets relative to the fisheries observer sightings data sources (Figure 8).

There were no obvious spatial patterns in the model residuals across all data sources (Figure E.21) or when viewed separately for each data source (Figure E.22, Figure E.23). The residuals by date, month, and data source were all centered about zero (Figure E.24).

The spatial model predictions indicated that Chatham Island albatross were most abundant around the Chatham Islands, particularly to the south of these islands (Figure F.22). This is broadly consistent with the previous distributions used for the breeding period (compare Figure F.22 with Figure A.7). The final model predicted that they were most abundant within the EEZ from August to February, with a temporary decrease in December (Figure F.22), which is broadly (although not perfectly) consistent with the empirical analysis of tracking data only (see Section 3.3). The model predictions indicated minimal monthly variability in the spatial distribution of Chatham Island albatross within the EEZ (plotted using different scales for each month in Figure F.23 and Figure F.24).

Table 10: Degrees of freedom (DF) for each term in the final model for Chatham Island albatross and percentage deviance explained/Akaike information criterion (AIC) for the fixed terms (above the second horizontal line) and with the addition of each selected term (below the line). The DF was derived from the number of levels for non-splined terms (i.e., without the ‘s’ prefix), and was the effective degrees of freedom reported using ‘summary.gam’ for splined terms. No additional environmental terms were added to this model.

Model terms	DF	Deviance explained (%)	AIC
s(easting, northing)	31.0		
+ s(observer)	87.7		
+ s(vessel)	42.6		
+ source	5.0		
+ month	11.0	95.5	20 046.0

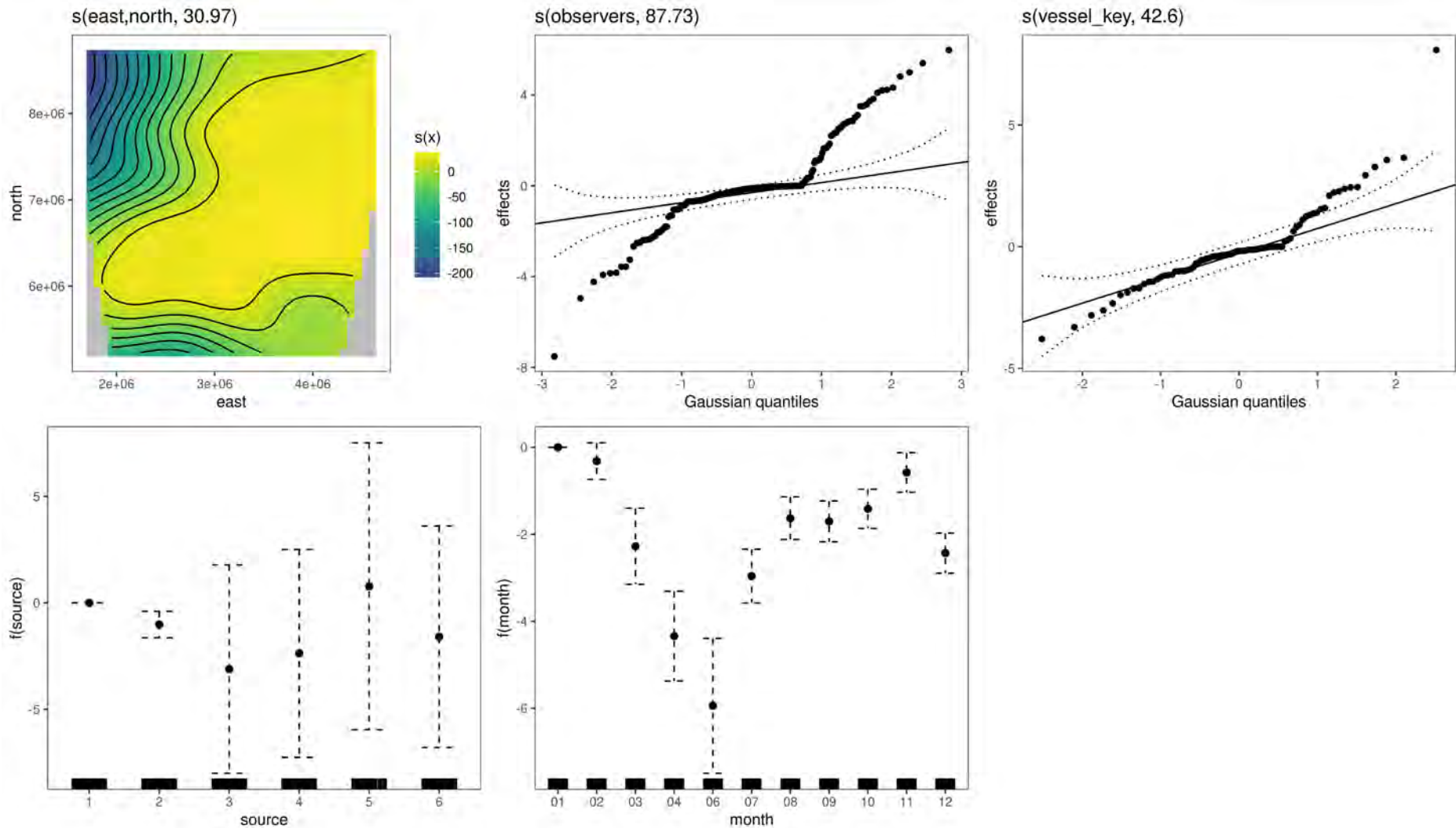


Figure 8: Model terms for the final model for Chatham Island albatross including: the Gaussian process spatial smooth; observer ID and vessel key random effects, and data source (1 = paper form, 2 = Nomad, 3 = eBird stationary, 4 = eBird travelling, 5 = Te Papa, 6 = tracking) and month fixed effects, where month 01 is January.

3.2.7 Salvin's albatross

For Salvin's albatross, the final data set used for spatial modelling consisted of paper form, Nomad, eBird, Te Papa, and tracking (GPS and PTT) data. Based on a visual inspection of the filtered data, the GLS data for this species were deemed to be too low precision for informing distribution within the New Zealand EEZ and were dropped from this analysis. The remaining tracking data were only downweighted by 50% relative to the sightings-based data sources. There was very good agreement in the spatial information between the different data sources, which were consistent with greatest abundance off the east coast of the South Island, including the western Chatham Rise (Figure D.7).

The initial model for this species included a GP spatial smooth for each of the chick-rearing and non-chick-rearing seasons, a random effect for each observer, a random effect for each vessel, and fixed effects for each data source and month (Table 11). The optimal model added splines for sea surface turbidity and distance to colony, and the final model explained 88.7% of the model deviance, a 0.6% improvement on the initial model (Table 11). The model expected counts were greatest in areas of low turbidity and close proximity to the breeding colonies (Figure 9). The term plots indicated low expected counts during the November–February chick rearing period for this species, although this was strongly confounded with the separate surface smooths by season, and the model predictions should instead be used to judge seasonality.

There was no obvious spatial pattern in the model residuals across all data sources (Figure E.25) or when viewed separately for each data source (Figure E.26 and Figure E.27). The residuals by date, month, and data source were all centered about zero (Figure E.28).

The spatial model predictions indicated that Salvin's albatross were most abundant around their largest breeding colony at the Bounty Islands (compare Figure F.25 with bottom-right plot of Figure B.10), although they were also abundant to the east of the South Island in certain months, particularly over the western Chatham Rise. The updated distributions appear to include the main high-density areas from the previous distributions used for the breeding and non-breeding seasons (compare Figure A.8 with Figure E.26 and Figure E.27).

The model predicted that Salvin's albatross were most abundant within the EEZ from September to March (Figure F.25). This finding differs slightly from the empirical analysis of proportion in zone from the tracking data only, which indicated that they were most abundant around New Zealand from July to February (see Section 3.4). The model predictions indicate some monthly variability in the spatial distribution of Salvin's albatross remaining within the EEZ, with a greater density of birds predicted over the western Chatham Rise during the austral summer (Figure F.26 and Figure F.27).

Table 11: Degrees of freedom (DF) for each term in the final model for Salvin's albatross and percentage deviance explained/Akaike information criterion (AIC) for the fixed terms (above the second horizontal line) and with the addition of each selected term (below the line). The DF was derived from the number of levels for non-splined terms (i.e., without the 's' prefix), and was the effective degrees of freedom reported using 'summary.gam' for splined terms.

Model terms	DF	Deviance explained (%)	AIC
s(easting, northing; non-brooding season)	33.0		
+ s(easting, northing; brooding season)	34.4		
+ s(observer)	181.5		
+ s(vessel)	73.5		
+ source	5.0		
+ month	11.0	88.1	144 640.2
+ s(log(turbidity))	2.0	88.5	143 658.7
+ s(distance_to_colony)		88.7	143 010.1

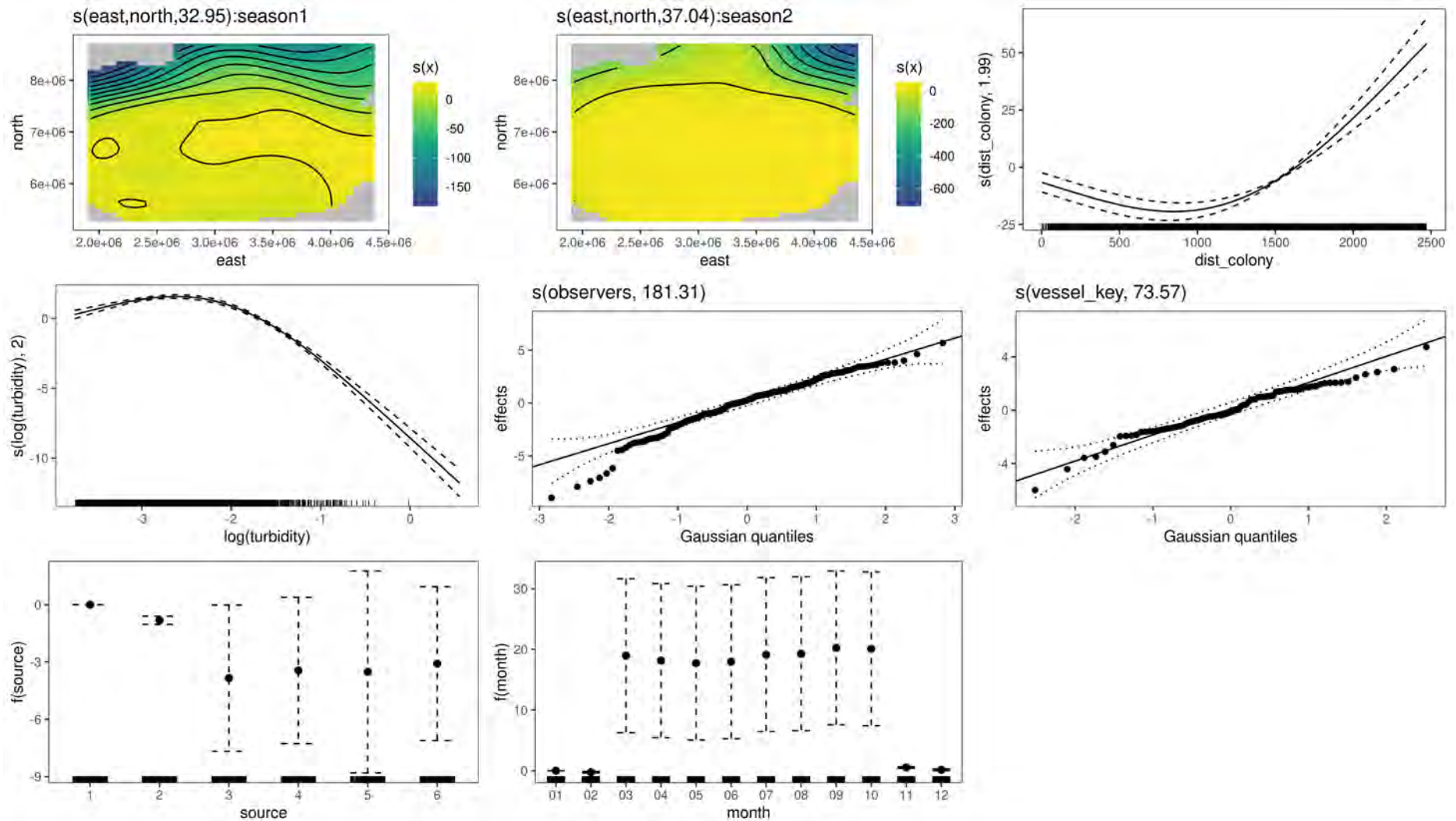


Figure 9: Model terms for the final model for Salvin's albatross including: the spatial smooths by season (season1 = non-chick-rearing, season2 = chick-rearing); the distance to colony and turbidity splines; the observer ID and vessel key random effects, and data source (1 = paper form, 2 = Nomad, 3 = eBird stationary, 4 = eBird travelling, 5 = Te Papa, 6 = tracking) and month fixed effects, where month 01 is January.

3.2.8 White-capped albatross

The final white-capped albatross data set used for spatial modelling consisted of paper form, Nomad, eBird, Te Papa, and tracking (GPS and PTT) data. The available GLS data for this species were deemed of insufficient precision and were dropped from this analysis. The remaining tracking data were deemed to be of good quality and were only downweighted by 50% relative to the sightings-based data. There was a good degree of spatial agreement in the information between the paper form and tracking data, which were the best sources of information for this species. Both data sources indicated the greatest abundance of white-capped albatross was around their main breeding colonies at the Auckland Islands (compare Figure D.8 with the top-left plot of Figure B.11). The degree of spatial agreement with other sources of information was also good based on spatial plots of model residuals (Figure E.30).

The initial model for this species included a GP spatial smooth for each of the chick-rearing and non-chick-rearing seasons, a random effect for each observer, a random effect for each vessel, and fixed effects for each data source and month. The model optimisation process added splines for sea surface turbidity, sea surface temperature, and tidal current speed (Table 12). The final model explained 85.3% of the model deviance, a 2.0% improvement on the initial model. The model expected counts were greatest in areas of low turbidity, intermediate sea surface temperature, and high tidal current speeds (Figure 10).

There was no obvious spatial pattern in the model residuals across all data sources (Figure E.29) or when viewed separately for each data source (Figure E.30 and Figure E.31). The residuals by date, month, and data source were all centered about zero (Figure E.32).

The model predictions indicated that white-capped albatross were most abundant around the southern half of the South Island and Stewart Island and around their main breeding colonies at the Auckland Islands (Figure F.28). This is quite unlike the previously assumed distribution, which had a much greater density around the Auckland Islands breeding colony in the breeding period than anywhere else, and greatest density off the northern west coast South Island in the non-breeding period (compare Figure A.9 with Figure F.29 and Figure F.30).

The final model predicted that white-capped albatross are, to some degree, present around New Zealand throughout the year, which is consistent with the empirical analysis of tracking data only (see Section 3.3). The model predictions indicated they are most abundant around New Zealand from March–October (Figure F.28), which includes most of the assumed chick-rearing period (February–May). The predictions also indicate minimal monthly variability in the spatial distribution of this species around New Zealand, evident when different scales are used for each month (Figure F.29 and Figure F.30).

Table 12: Degrees of freedom (DF) for each term in the final model for white-capped albatross and percentage deviance explained/Akaike information criterion (AIC) for the fixed terms (above the second horizontal line) and with the addition of each selected term (below the line). The DF was derived from the number of levels for non-splined terms (i.e., without the ‘s’ prefix), and was the effective degrees of freedom reported using ‘summary.gam’ for splined terms.

Model terms	DF	Deviance explained (%)	AIC
s(easting, northing; non-brooding season)	45.5		
+ s(easting, northing; brooding season)	40.6		
+ s(observer)	184.3		
+ s(vessel)	79.8		
+ source	5.0		
+ month	11.0	83.3	266 869.6
+ s(log(turbidity))	2.0	84.8	262 564.0
+ s(sst)	2.0	85.1	261 715.0
+ s(currents)	1.0	85.3	260 966.1

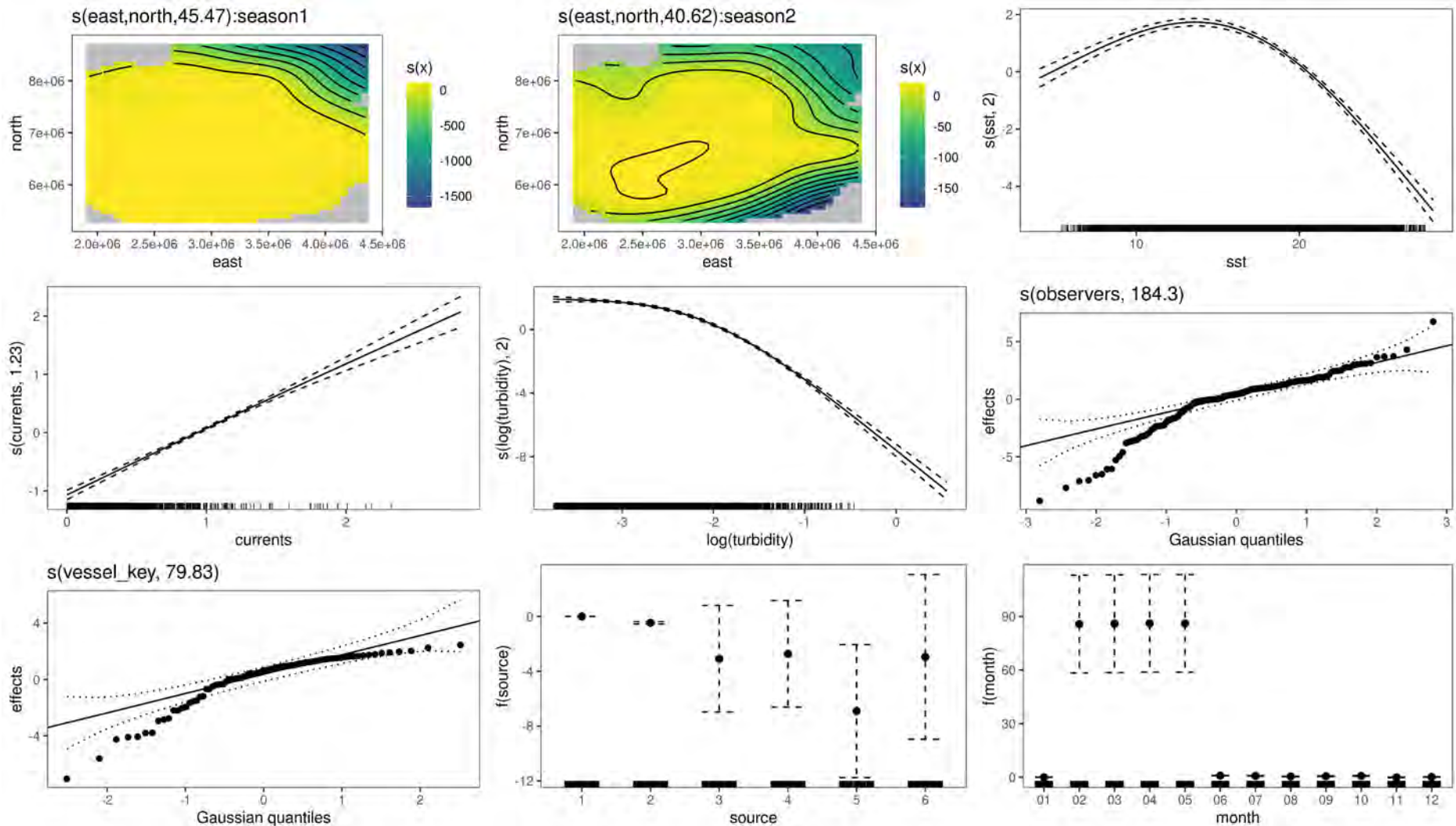


Figure 10: Model terms for the final model for white-capped albatross including the spatial smooths by season (season1 = non-chick-rearing, season2 = chick-rearing), the sea surface temperature (sst), currents, and turbidity splines; the observer ID and vessel key random effects, and data source (1 = paper form, 2 = Nomad, 3 = eBird stationary, 4 = eBird travelling, 5 = Te Papa, 6 = tracking) and month fixed effects.

3.2.9 Antipodean albatross

The final data set used for Antipodean albatross comprised tracking data only, including relatively high-quality GPS and PTT data. The available sightings data attributed to this sub-species were not used because of difficulties differentiating them from Gibson’s albatross and other great albatrosses occurring around New Zealand. The spatial pattern of Antipodean albatross density from the tracking data was obscured by some very high gridded counts around the main breeding colony at the Antipodes Islands (see Figure 1, Figure B.11, and Figure D.9). However, most grid cells around the New Zealand EEZ had positive counts, indicating a wide-ranging distribution for this species (left-hand plot of Figure D.9).

The initial model for this species included a GP spatial smooth for each of the chick-rearing and non-chick-rearing periods, and a random effect for each tag. The optimisation process added non-linear predictors for distance to colony and sea surface temperature (Table 13). The optimal model explained 58.5% of the model deviance, a 0.9% improvement on the initial model. The model expected count was greatest at intermediate sea surface temperatures and close to the main breeding colonies (Figure 11).

There was no obvious spatial pattern in the model residuals, although the model did not fully represent a band of foraging along the slopes around the Chatham Rise (Figure E.33). The residuals by date, month, and data source were all centered about zero (Figure E.34).

The model predictions indicate that Antipodean albatross are most abundant around their main breeding colony at the Antipodes Islands from January to March, although they occur around much of the New Zealand EEZ (obscured by the high prediction near the main breeding colony) (Figure F.31). The model predictions are broadly consistent with the distribution assumed by the most recent seabird SEFRA, with comparatively low density predicted off the west coast of the South Island and around the Auckland Islands (comparing Figure F.32 and Figure F.32 with the left-hand plot of Figure A.10).

The model predictions indicated minimal monthly variability in the spatial distribution of Antipodean albatross around New Zealand, evident when the colour scales were allowed to vary by month (Figure F.32 and Figure F.33).

Table 13: Degrees of freedom (DF) for each term in the final model for Antipodean albatross and percentage deviance explained/Akaike information criterion (AIC) for the fixed terms (above the second horizontal line) and with the addition of each selected term (below the line). The DF was derived from the number of levels for non-splined terms (i.e., without the ‘s’ prefix), and was the effective degrees of freedom reported using ‘summary.gam’ for splined terms.

Model terms	DF	Deviance explained (%)	AIC
s(easting, northing; non-brooding season)	40.5		
+ s(easting, northing; brooding season)	44.9		
+ s(tag)	40.7	57.4	160 080.8
+ distance_to_colony	1.0	58.2	158 812.7
+ s(sst)	2.0	58.5	158 437.3

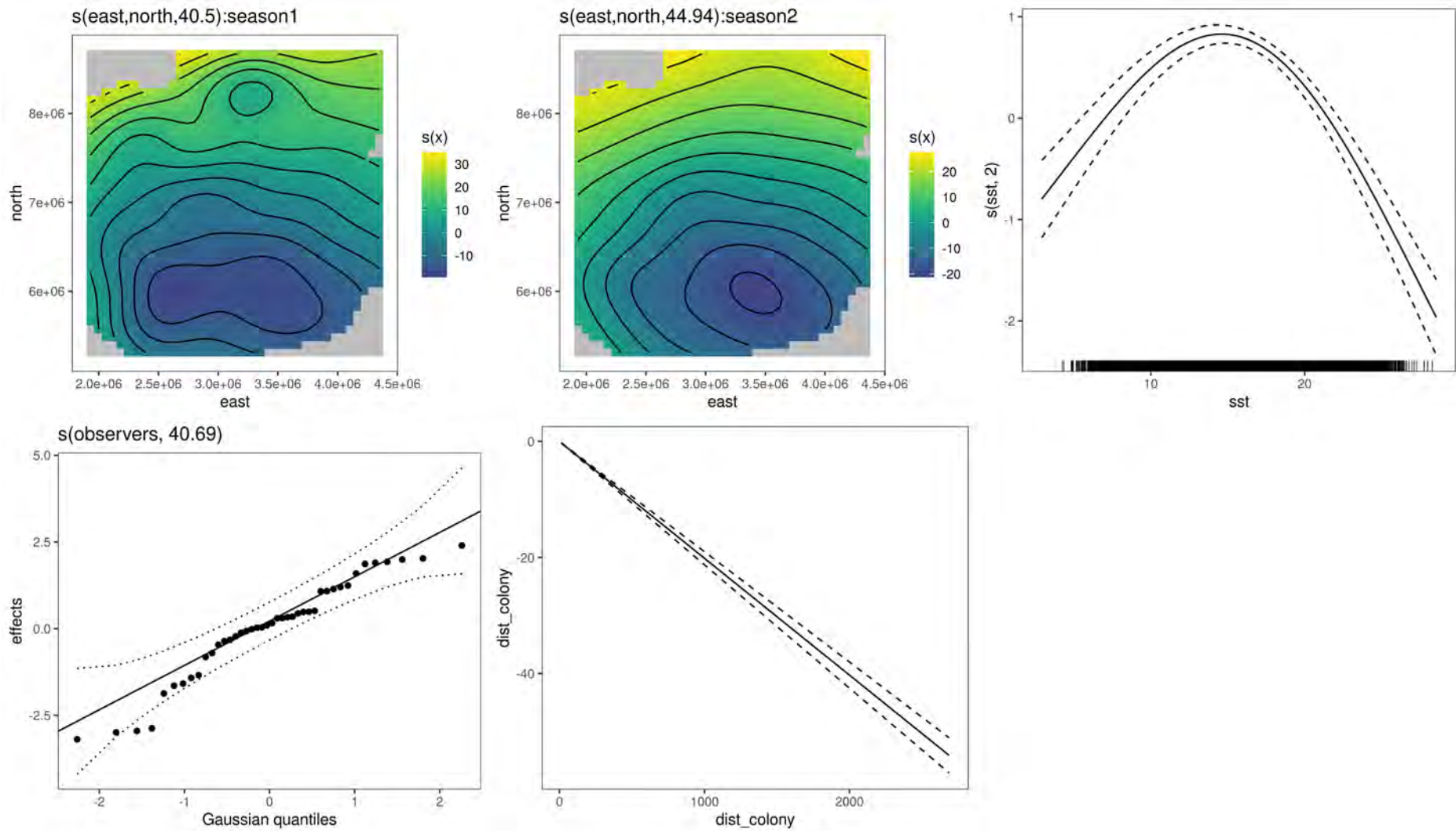


Figure 11: Model terms for the final model for Antipodean albatross including: the spatial smooths by season (season1 = non-chick-rearing, season2 = chick-rearing); the sea surface temperature (sst) and distance to colony (dist_colony) splines; and the observer ID random effects.

3.2.10 Gibson's albatross

As with Antipodean albatross, the final data set used for Gibson's albatross comprised tracking data only, which included high-quality GPS and PTT data (i.e., the available sightings data were not used). The spatial pattern of gridded counts from the tracking data was obscured by very high gridded counts around the main breeding colonies at the Auckland Islands (see Figure 1, Figure B.11, and Figure D.9). The spatial pattern of positive counts by grid cells was different to that for Antipodean albatross (compare the right and left-hand plots of Figure D.9).

The initial model for this species included a GP spatial smooth for each of the chick-rearing and non-chick-rearing periods, and a random effect for each tag. The optimisation process added non-linear predictors for slope, sea surface temperature, distance to colony, and wind speed (Table 14). The optimal model explained 52.9% of the model deviance, a 2.1% improvement over the initial model. The model expected count was greatest in areas of steep bathymetric slope, low and high sea surface temperature (the inverse of the pattern for Antipodean albatross), close proximity to the main breeding colony, and intermediate wind speeds (Figure 12). There was no obvious spatial pattern in the model residuals (Figure E.35). The residuals by date, month, and data source were all centered about zero (Figure E.36).

The model predictions indicated that Gibson's albatross were most abundant around their main breeding colonies at the Auckland Islands, although were present around much of the New Zealand EEZ (obscured by the high prediction near to the main breeding colony) (Figure F.34). The model predictions were quite different from those assumed by the most recent seabird SEFRA, which indicated a much more even distribution around the New Zealand EEZ that is not nearly so centred on the main breeding colony for this species at the Auckland Islands (e.g., comparing Figure F.35 and Figure F.36 with the right-hand plot of Figure A.10). There was minimal monthly variation in this spatial prediction, which is evident when the scale is allowed to vary by month (Figure F.35 and Figure F.36).

Table 14: Degrees of freedom (DF) for each term in the final model for Gibson's albatross and percentage deviance explained/Akaike information criterion (AIC) for the fixed terms (above the second horizontal line) and with the addition of each selected term (below the line). The DF was derived from the number of levels for non-splined terms (i.e., without the 's' prefix), and was the effective degrees of freedom reported using 'summary.gam' for splined terms.

Model terms	DF	Deviance explained (%)	AIC
s(easting, northing; non-brooding season)	35.9		
+ s(easting, northing; brooding season)	39.8		
+ s(tag)	6.9	50.8	20 850.0
+ s(sqrt(slope))	1.9	51.5	20 745.1
+ s(sst)	1.9	52.1	20 668.2
+ distance_to_colony	2.0	52.6	20 584.7
+ s(wind)	2.0	52.9	20 542.3

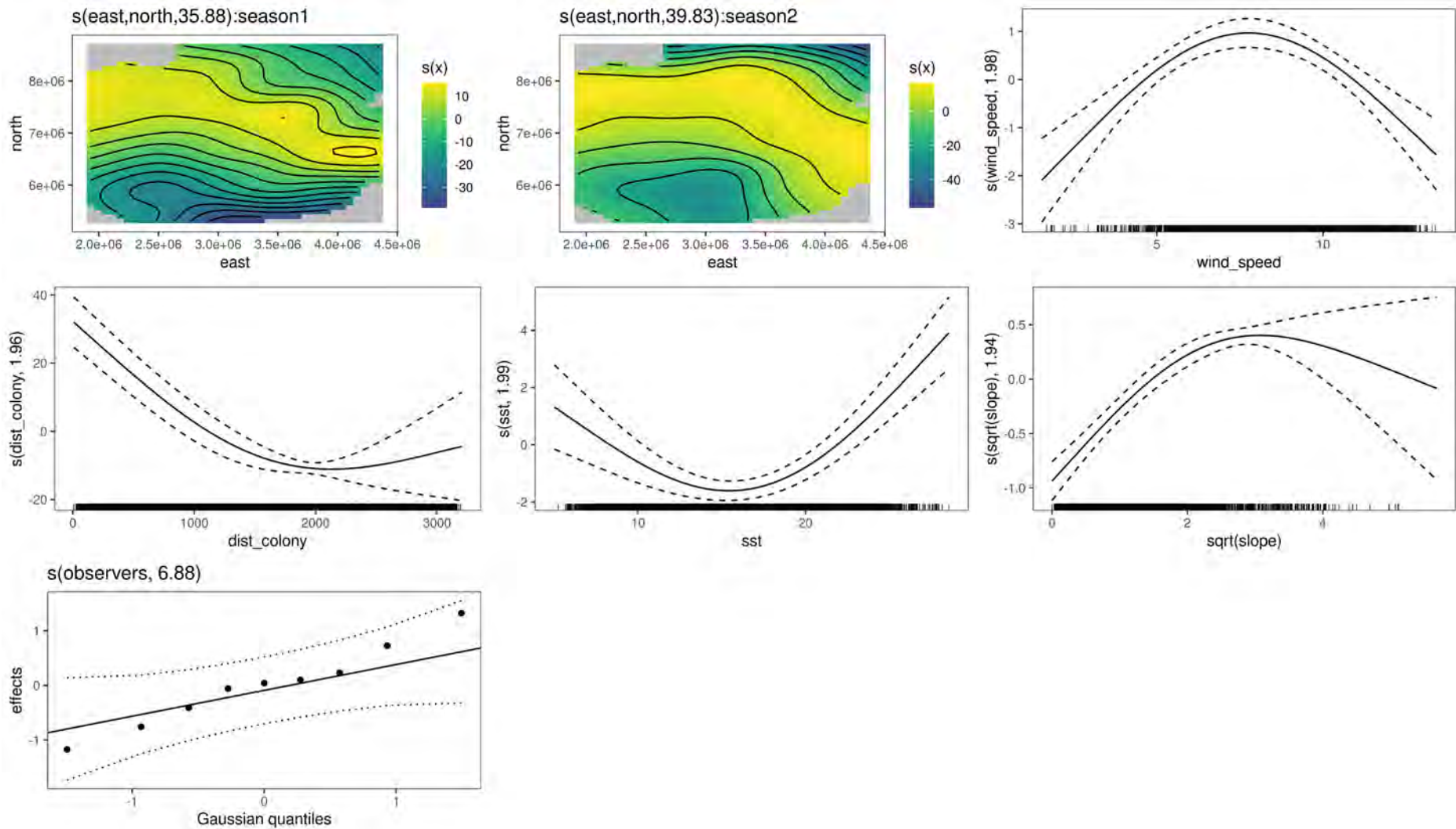


Figure 12: Model terms for the final model for Gibson's albatross including: the Gaussian process spatial smooths by season (season1 = non-chick-rearing, season2 = chick-rearing); the wind speed (wind_speed), distance to colony (dist_colony), sea surface temperature (sst), and slope splines; and the observer ID random effects.

3.2.11 Yellow-eyed penguin

Separate distribution models were fitted to fledglings and adults. For both age stages, the at-sea sightings data were too sparse to be useful for spatial modelling (and are not shown). Note that the previous SEFRA model did not include juvenile yellow-eyed penguin (Richard et al. 2020a).

3.2.11.1 Fledgling yellow-eyed penguin

The fledgling tracking data included PTT data only and were deemed to be of high quality for spatial modelling based on visual inspection.

The initial model for this species included a non-linear predictor for distance to colony, a random slope with respect to distance to colony for each tag ID, and a random intercept for each tag ID. The model optimisation process added non-linear predictors for distance to shore, sea level anomaly, tidal current speed, and surface chlorophyll-a concentration (Table 15). This model explained 61.0% of the model deviance, a 23.4% improvement in deviance explained over the initial model (Table 15).

The term plots for the final model show that expected counts were greatest within 300 km of the location of tagging, within 100 km from the shore, as well as areas of high sea level anomaly, low tidal current speed, and high surface chlorophyll-a concentration (Figure 13). When viewed in natural space, it is possible to see that the expected counts of fledglings peaked at slightly above 200 km from the location of tagging (see grey shaded area of Figure E.37), although this relationship varied by colony of tagging, as illustrated by the random effect plots (coloured lines in Figure E.37). There was no obvious spatial pattern in the model residuals (Figure E.38). The residuals by date, month, and location of tagging were all centered about zero (Figure E.39 and Figure E.40).

The model predictions indicated that fledgling yellow-eyed penguins were most abundant around the sub-Antarctic Islands to the south of New Zealand (where most of the breeding occurs), particularly around Snares Islands and Auckland Islands (Figure F.37), with relatively high predicted densities off the south coast of the South Island and around Campbell Island (Figure F.38, Figure F.39). When the prediction was viewed in log-space, it was possible to see that fledglings were predicted to occur off the east coast of the South Island up to Kaikōura and also around the southern west coast South Island, and that there may be suitable habitat for them as far north as Hawke Bay on the east coast North Island and Taranaki on the west coast (Figure F.40).

Table 15: Degrees of freedom (DF) for each term in the final model for fledgling yellow-eyed penguin and percentage deviance explained/Akaike information criterion (AIC) for the fixed terms (above the second horizontal line) and with the addition of each selected term (below the line). The DF was derived from the number of levels for non-splined terms (i.e., without the ‘s’ prefix), and was the effective degrees of freedom reported using ‘summary.gam’ for splined terms.

Model terms	DF	Deviance explained (%)	AIC
s(distance_to_colony, k = 3)	2.0		
+ s(tag) (random intercept)	20.7		
+ s(tag, distance_to_colony) (random slope)	20.5	37.6	6 171.3
+ s(shore, k = 3)	1.9	53.5	5 584.6
+ s(sea level anomaly, k = 3)	1.8	54.2	5 555.3
+ s(sqrt(currents), k = 3)	1.0	57.7	5 399.3
+ s(log(chlorophyll), k = 3)	2.0	61.0	5 190.9

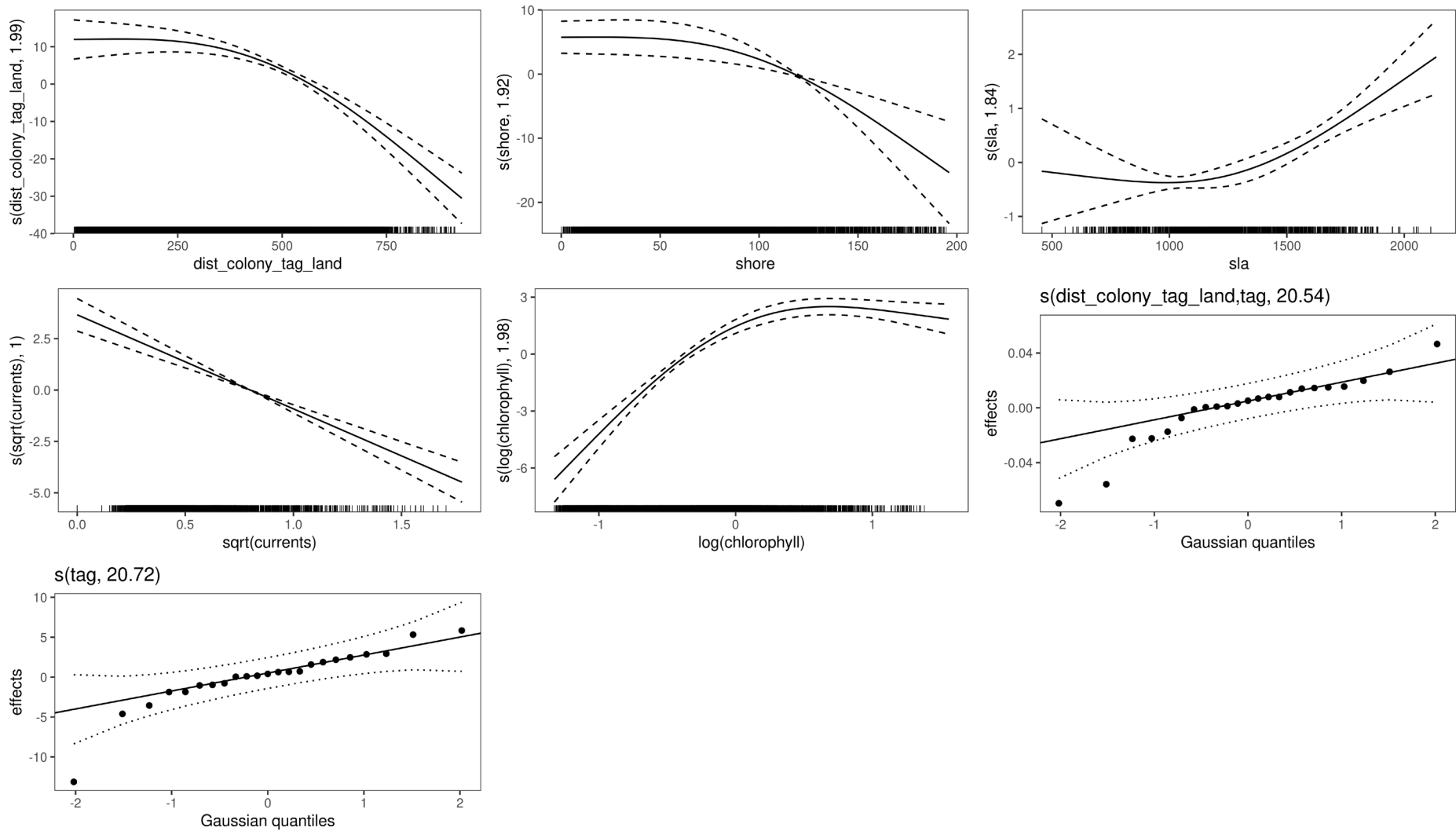


Figure 13: Model terms for the final model for fledgling yellow-eyed penguin including: the splines for distance to colony ($\text{dist_colony_tag_land}$), distance to shore (shore), sea level anomaly (sla), currents, and chlorophyll-a concentration; and the random effects for tag and distance to colony for each tag.

3.2.11.2 Adult yellow-eyed penguin

The adult yellow-eyed penguin data comprised tracking data only (GPS and VHF). The relative data set weighting was set to 100% for grid cells with positive counts or 10% for those cells with counts of zero (i.e., pseudo-zero grid cells).

The initial model for this species did not include a GP spatial smooth. Instead, it included a spline for distance to colony, a random intercept for each tag, and a random slope for each tag × distance to colony interaction (Table 16). The model optimisation process added splines for distance to shore and depth and explained 91.0% of the model deviance, a 1.7% improvement on the initial model (Table 16). Expected counts were greatest over shallow seafloor within 20 km of the breeding colony of tagging and near to shore (Figure 14). The model predictions indicated a degree of variability in the distance to colony relationship by colony of tagging (Figure E.44).

Additional model runs were trialled, based on the findings of previous research (Moore et al. 1995), including a seasonal spline for distance to colony (one each for the chick-rearing and non-chick-rearing periods), and specifying a separate depth spline by region (for each of the Stewart Island, the Catlins Coast, and the North Otago Coast). However, neither of these inputs explained at least an additional 0.2% of the model deviance and so were not retained by the final model. There were no obvious spatial patterns in the final model residuals (Figure E.42). The residuals by date and month were all centered about zero (Figure E.43) and also when plotted by colony of tagging (Figure E.44).

The spatial prediction of adult yellow-eyed penguins was obscured by some very high density cells immediately surrounding the largest breeding colonies at the Auckland Islands and Campbell Island, which together support the majority of the species' breeding population (Figure F.41). When the prediction was plotted in log-space, moderate and lower density regions were more easily visible around the breeding colonies on Stewart Island and the South Island (Figure F.41). This prediction, which was based on count data, estimates a more near-shore distribution relative to the previous layers used for SEFRA (Figure A.11), which were based on presence only data.

Table 16: Degrees of freedom (DF) for each term in the final model for adult yellow-eyed penguin and percentage deviance explained/Akaike information criterion (AIC) for the fixed terms (above the second horizontal line) and with the addition of each selected term (below the line). The DF was derived from the number of levels for non-splined terms (i.e., without the 's' prefix), and was the effective degrees of freedom reported using 'summary.gam' for splined terms.

Model terms	DF	Deviance explained (%)	AIC
s(sqrt(distance_to_colony), k = 5)	3.9		
+ s(tag) (random intercept)	58.4		
+ s(tag, distance_to_colony) (random slope)	54.3	89.3	14 311.1
+ s(sqrt(shore), k = 3)	2.0	90.0	13 724.8
+ s(depth, k = 3)	1.0	91.0	12 966.3

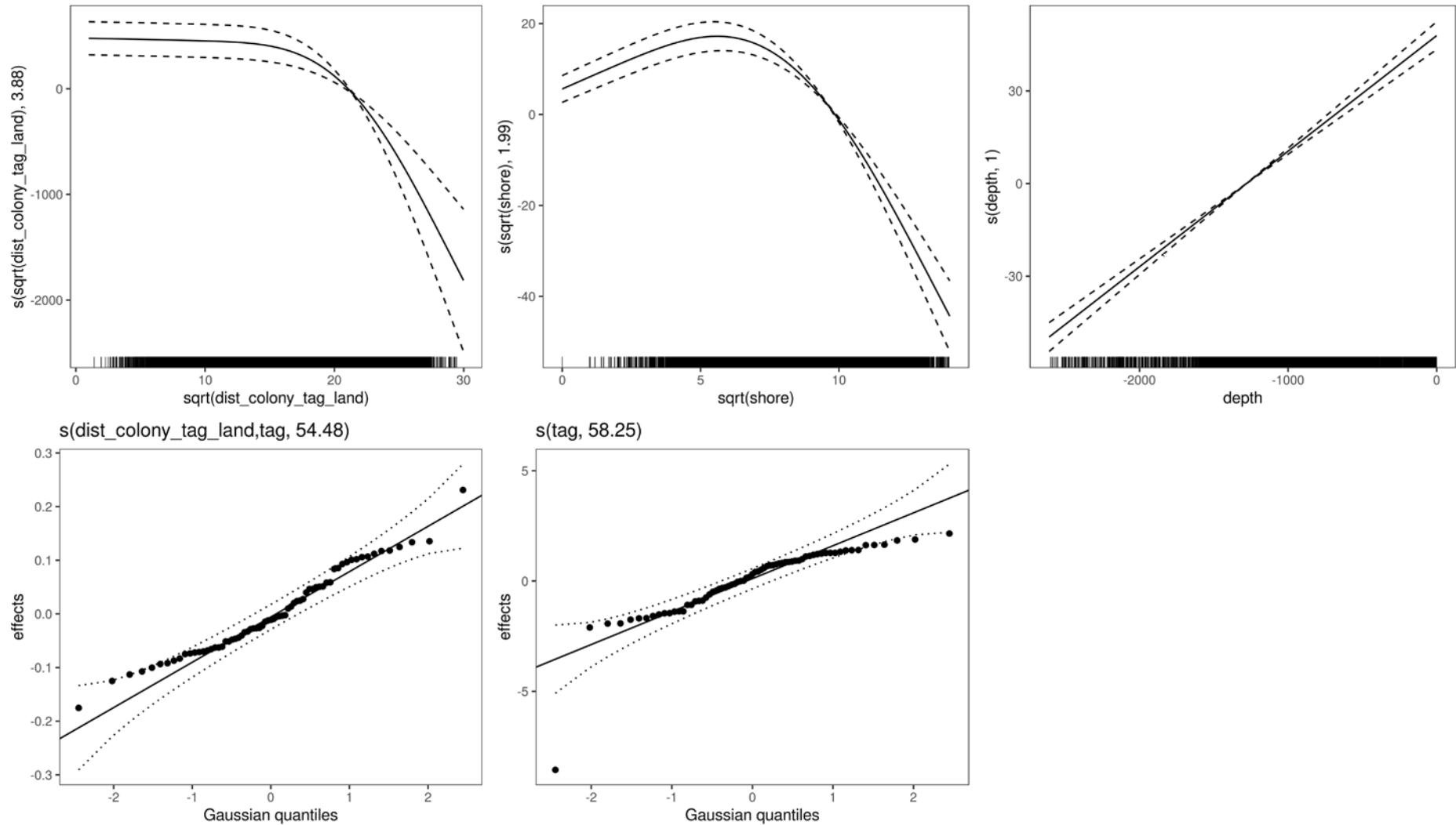


Figure 14: Model terms for the final model for adult yellow-eyed penguin including: the splines for distance to colony (`dist_colony_tag_land`), distance to shore (`shore`), and depth; and the random effects for tag and distance to colony for each tag.

3.3 Proportion of seabirds in zone

Estimating the proportion in zone was not possible for Northern Buller's albatross due to a lack of tracking data. Also, this was not necessary for yellow-eyed penguins, which were assumed to remain within the New Zealand EEZ year-round. It was also not possible to calculate this for Chatham Island albatross during September and October or Gibson's albatross during December due to a lack of tracking data during these months.

The updated proportions in zone by species and month were nearly always lower than the proportions assumed by previous implementations of the seabird SEFRA (Richard et al. 2020a) (Table 17). There were no months where all seabird tracking locations were in zone for the assessed species. However, there were months where all birds were out of zone for some of the assessed species (Figure 15).

Table 17: Average proportion of seabird tracking data locations inside the New Zealand EEZ by month (in black), compared with the previous (Richard et al. 2020a) proportions in zone (in grey). A dash (–) indicates that no tracking data locations were obtained for the respective species in that month, while a zero indicates that all tracking data locations were out of zone.

Taxon	Jan	Feb	Mar	Apr	May	Jun	Jul	Aug	Sep	Oct	Nov	Dec
Flesh-footed shearwater	0.754	0.798	0.545	0.264	0.006	0.001	0.001	0.000	0.000	0.216	0.808	0.892
	1.000	1.000	1.000	1.000	1.000	0.005	0.005	0.005	1.000	1.000	1.000	1.000
Black petrel	0.375	0.584	0.453	0.467	0.253	0.000	0.001	0.000	0.000	0.024	0.186	0.273
	1.000	1.000	1.000	1.000	1.000	0.005	0.005	0.005	0.005	1.000	1.000	1.000
Westland petrel	0.000	0.000	0.006	0.346	0.686	0.846	0.775	0.629	0.415	0.543	0.411	0.030
	0.025	0.025	1.000	1.000	1.000	1.000	1.000	1.000	1.000	1.000	1.000	1.000
White-chinned petrel	0.679	0.400	0.141	0.071	0.091	0.000	0.000	0.000	0.000	0.372	0.647	0.850
	1.000	1.000	1.000	1.000	1.000	0.025	0.025	0.025	0.025	1.000	1.000	1.000
Southern Buller's albatross	0.359	0.510	0.647	0.862	0.851	0.746	0.708	0.508	0.178	0.004	0.000	0.079
	1.000	1.000	1.000	1.000	1.000	1.000	1.000	1.000	0.025	0.025	0.025	1.000
Northern Buller's albatross	–	–	–	–	–	–	–	–	–	–	–	–
	1.000	1.000	1.000	1.000	1.000	1.000	0.025	0.025	0.025	1.000	1.000	1.000
Chatham Island albatross	0.717	0.288	0.066	0.000	0.005	0.002	0.024	0.022	–	–	0.938	0.939
	1.000	1.000	1.000	1.000	1.000	0.025	0.025	1.000	1.000	1.000	1.000	1.000
Salvin's albatross	0.628	0.365	0.177	0.011	0.026	0.178	0.609	0.867	0.841	0.913	0.912	0.881
	1.000	1.000	1.000	1.000	0.100	0.100	0.100	0.100	1.000	1.000	1.000	1.000
White-capped albatross	0.538	0.772	0.500	0.509	0.527	0.526	0.424	0.444	0.374	0.527	0.625	0.558
	1.000	1.000	1.000	1.000	1.000	1.000	1.000	1.000	0.500	0.500	1.000	1.000
Antipodean albatross	0.612	0.596	0.517	0.440	0.314	0.322	0.424	0.432	0.257	0.196	0.199	0.280
	1.000	1.000	1.000	1.000	1.000	1.000	1.000	1.000	1.000	1.000	1.000	1.000
Gibson's albatross	0.668	0.550	0.593	0.455	0.335	0.499	0.387	0.204	0.187	0.231	0.318	–
	1.000	1.000	1.000	1.000	1.000	1.000	1.000	1.000	1.000	1.000	1.000	1.000

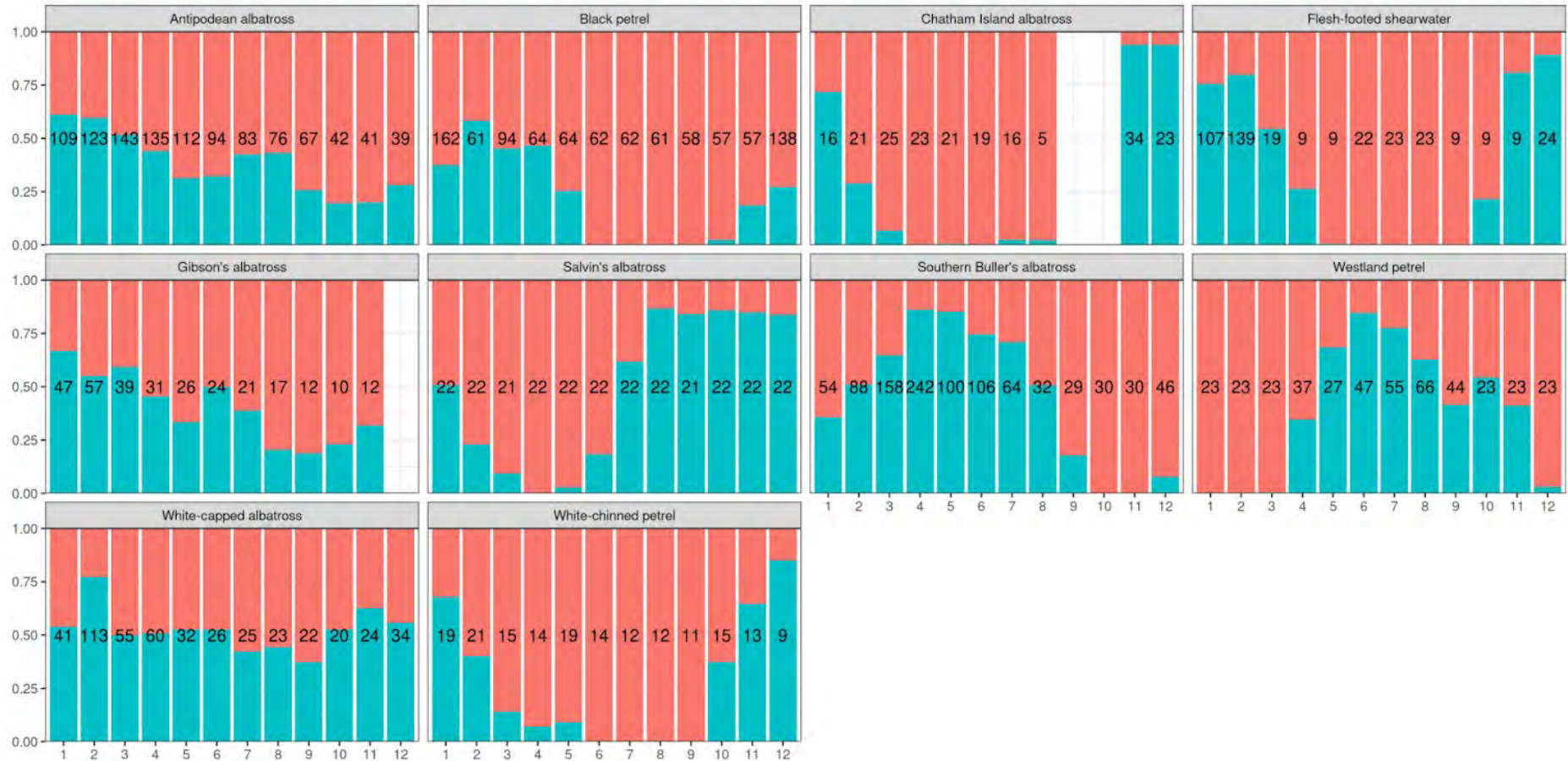


Figure 15: Average proportion of tracking data locations inside the New Zealand EEZ by month for each species. Blue indicates the proportion in zone, red the proportion out of zone, a missing bar indicates no tracking data for that month, and the number at the centre of each bar is the number of tracking device deployments on which the proportion in zone estimate was based.

4 DISCUSSION

4.1 Spatial and seasonal coverage

The various data sources provided differing extents of spatial coverage within the New Zealand EEZ. Fisheries observer sightings data provide good spatial information in regions of relatively high overlap with commercial fishing, particularly in well-observed fisheries. The paper form fisheries observer data had best coverage in offshore waters, including the Chatham Rise and the sub-Antarctic region, whereas the Nomad data had better coverage inshore. Other sources of spatial data (e.g., eBird and Te Papa) provided spatial coverage in regions where fishing effort was minimal. The eBird data tended to have best coverage inshore, with some coverage on the Chatham Rise, and the Te Papa data had best coverage off the west coast of the North Island (e.g., see Figure D.1). The main benefit of using these other sources of sighting data, as well as the tracking data, was to stabilise model predictions in regions of low fisheries observer sighting effort. This was apparent from the preliminary model runs for some species, which produced spurious predictions towards the periphery of the EEZ when tracking data were not used in model fitting.

While some anomalous sightings were identified for some species (e.g., some sightings of black petrels in the sub-Antarctic region), these were typically made by specific observers. As such, these observations did not need to be removed from the fitted data set, because they were accounted for by the inclusion of an observer ID effect in all spatial models, which corrected the relevant species predictions for these events.

The tracking data were also important for the modelling of species/taxa for which taxonomic identifications from boat-based sightings are highly problematic (e.g., differentiating Buller's albatross sub-species or Antipodean albatross from Gibson's albatross), or at-sea sightings are infrequent (e.g., yellow-eyed penguin).

The tracking data typically had best *seasonal* coverage during the breeding period of each respective seabird, which would have been the easiest time to conduct tagging studies. As such, for seabirds that had seasonal spatial smooths, it is likely that model predictions in the non-chick rearing period were primarily influenced by sightings-based information. The monthly coverage of sightings events was good, including the subset used by this analysis (Table 2 and Table 3), which plugged temporal gaps in tracking data information during the non-breeding period.

4.2 Integrating sources of spatial information

During model fitting, we gave equal statistical weighting to observations from the different sources of spatial information. Generally, there was good agreement in the sighting rates of each seabird when data from the different sources are compared (e.g., Figure D.1), and when these were plotted spatially by data source there were no strong patterns in residuals (e.g., Figure E.2) that might have necessitated the exploration of alternative relative statistical weightings by sightings data source.

The spatial modelling analysis used the tracking data to produce gridded counts of tracking data across the EEZ, which were then combined with sightings-based counts. As noted by the project team and the AEWG, this is problematic because, while absences of a species during a sighting event can be considered a true zero, absences of tracking data locations within a grid cell cannot, because only a small fraction of each species population was instrumented with tracking devices. Hence, zero counts in the gridded tracking data should only be considered as pseudo-zeros. This was dealt with differently for each species depending on the quantity and quality of the data from each data source (see column 'Tracking weights' in Table 4). For all seabirds where sightings data were also used, tracking data were given a relatively low data set weighting. The tracking data weighting was further reduced if the quality of the tracking data was relatively poor (e.g., only GLS data were available for white-chinned petrel). For some seabirds (e.g., yellow-eyed penguin and southern Buller's albatross) the pseudo-zero tracking data counts were given a lower weighting than the positive tracking data counts. The selection of the

relative tracking data weighting value used for each species was somewhat arbitrary, although was sufficiently high to prevent the appearance of spurious values in model predictions for all species.

4.3 Environmental covariates of seabird distribution

For all seabirds, the fixed model terms (i.e., the 2-dimensional GP surface smooth, observer and vessel IDs, data source, and month) explained a large proportion of the model deviance (e.g., Table 5), particularly the spatial smooths, which were allowed to be spatially complex and to vary seasonally (except for yellow-eyed penguin, for which distance to colony was used instead). The satellite-derived turbidity proxy was the first selected model term for a number of species (flesh-footed shearwater, Westland petrel, white-chinned petrel, Northern/Southern Buller's albatross, Salvin's albatross, and white-capped albatross), all of which were predicted to avoid turbid waters. A review of the literature found few examples of overseas seabird populations avoiding turbid waters (e.g., Haney & Stone 1988 obtained conflicting evidence for this). However, New Zealand coastal waters are particularly turbid by international standards, due partly to high sediment levels from rivers (Hicks et al. 2011), such that the threshold turbidity levels for avoidance may be more likely to be reached around New Zealand. This analysis used a quarterly climatology for turbidity, to optimise spatial coverage of satellite measurements in the southern EEZ during the winter period, when cloud coverage can prevent measurement. For species that do not occur in the sub-Antarctic region, future spatial analyses could consider using higher temporal resolution turbidity data for model fitting.

Other commonly selected covariates included distance to colony and sea surface temperature. Note that some covariates (e.g., sea surface temperature and wind speed) are correlated in space around New Zealand (compare Figure B.2 and Figure B.4; also compare with air temperature, see Figure B.1), and may be confounded with distance to colony for some species. For example, it seems unlikely that Gibson's and Antipodean albatross truly have opposing sea surface temperature preferences, as the models for these species would suggest (compare Figure 11 and Figure 12). Except for turbidity and distance to colony, this study did not uncover any environmental covariates that consistently improved species habitat models beyond using a surface smooth. For example, bathymetric depth, slope, sea surface temperature, and current speed were all previously found to be influential for Westland petrel (Poupart et al. 2020), although none of these were retained in the optimal model for this species in the current study and may, to some extent, have been represented by the surface smooth (Table 7). It is also likely that the model selection process used by the current study (based on percent model deviance explained and using a threshold value for adding new terms) may favour more simple models compared with the methods used by other studies (e.g., Poupart et al. 2020 used model AIC).

Previous habitat modelling of adult yellow-eyed penguins by Mattern (2020) mostly used tracking data that were unavailable to this analysis and used only a subset of locations consistent with benthic dives. Mattern (2020) used maximum entropy (Maxent) models fitted to presence data and inferred absences (i.e., not counts) and found that bathymetry and colony distance were the best covariates of their distribution, with sediment type a distant third. The adult model developed here included covariates for distance to colony as well as distance to shore and depth, although did not retain any of the benthic sediment types that were offered. This may be because the benthic habitat preferences of adults vary regionally, as was suggested by Mattern (2020). Furthermore, the current assessment obtained limited statistical support for estimating separate layers for chick-rearing and non-chick-rearing periods, contrary to the findings of Mattern (2020), although this could be revisited should more non-breeding data become available.

Previous research has identified environmental covariates for close relative species of this study, that were offered, although not retained in the optimal models based on observations around New Zealand. For example, sea level anomaly was identified as a significant predictor of wandering albatross (*Diomedea exulans*) foraging from Marion Island, Prince Edward Archipelago (Carpenter-Kling et al. 2020), although was not found to be influential around New Zealand for either Gibson's albatross or Antipodean albatross. However, bathymetric slope was influential for both the Marion Island population (Carpenter-Kling et al. 2020) and Gibson's albatross (this study).

4.4 Changes to assumed spatial distributions

In this sub-section, the updated seabird distribution layers (Appendix F) are compared with the distribution layers used by the most recent published multispecies seabird SEFRA model (Appendix A) (Richard et al. 2020a). The updated layers are shown using the same scale across all months (e.g., Figure F.1) and using different scales for each month, so that the spatial distribution can be discerned in months when few birds are present around New Zealand (e.g., Figure F.2 and Figure F.3). For some seabird species/taxa, the updated at-sea distribution layers resemble the previous layers—e.g., black petrel (compare Figure F.5 and Figure F.6 with Figure A.2), Westland petrel (compare Figure F.8 and Figure F.9 with Figure A.3), Chatham Island albatross (compare Figure F.23 and Figure F.24 with Figure A.7), and Antipodean albatross (compare Figure F.32 and Figure F.33 with the left-hand plot of Figure A.10).

For other species, the updated distribution layers are quite different. For example, the updated flesh-footed shearwater layers (Figure F.2 and Figure F.3) give this species a much broader at-sea distribution during the breeding season and more constrained distribution during the non-breeding season than was previously assumed (Figure A.1). The updated Gibson's albatross layers (Figure F.35 and Figure F.36) have a much more constrained distribution around the main breeding colony than was previously assumed (Figure A.10). This is also the case for Antipodean albatross, except centred around the Auckland Islands instead of the Antipodes Islands (Figure F.32 and Figure F.33).

The at-sea distribution of fledgling yellow-eyed penguins was estimated separately using fledgling data. This produced a very different spatial prediction compared with the adult model (Figure F.38 and Figure F.39 compared with Figure F.41), indicating that they are much less constrained by colony of origin than breeders, as might be expected. The foraging of fledglings appears to favour locations with high chlorophyll-a concentration, positive sea level anomaly (associated with upwelling), and low current speed. For adults, no dynamic environmental covariates influencing at-sea distribution were identified. This is consistent with the foraging patterns of individual adult yellow-eyed penguins largely depending on breeding site location, as may be expected given their requirement to regularly feed chicks and their much slower foraging speeds relative to flying seabirds.

The updated adult yellow-eyed penguin distribution layer (Figure F.41), which was based on count data, is quite different from the layers estimated by Mattern (2020) (Figure A.11) for breeding and non-breeding birds, which were based on presence-absence data. The updated layer shows their at-sea distribution being centred closer to the shore than was assumed by the previous SEFRA. Based on previous research (Moore et al. 1995), it was expected that the model optimisation process would result in a distance to colony function that varies by chick-rearing versus non-chick-rearing periods. However, including a seasonal interaction term did not add much in terms of deviance explained, and a seasonally constant layer was predicted instead.

It is anticipated that updating the spatial layer inputs to the SEFRA model may change the estimated vulnerabilities for some species, which could have implications for estimated captures for several species, given that vulnerabilities may be shared across taxa (Richard et al. 2020a). The switch to monthly seabird layers (compared with breeding versus non-breeding layers) should also cause some minor improvements to model predictions.

4.5 Changes to proportion in zone

For each of the seabird species/taxa, this study estimated the proportion of birds located within the New Zealand EEZ by month, calculated empirically using the better-quality tracking data. For most species, the resulting proportions were quite different from those used by the most recent seabird SEFRA model (Table 17). The derived monthly proportions in-zone were nearly always lower than the previous values, and, apart from yellow-eyed penguin, no seabird species/taxon was found to forage entirely in-zone in any month (as was previously assumed for many species). However, for some species, there

were still months where all birds were out of zone (when all birds vacated the New Zealand EEZ for the non-breeding period).

For many species, the breeding season for the average bird would be quite different to what was previously assumed based on the updated proportions. For example, all flesh-footed shearwaters were previously assumed to be present within the EEZ in April–May as well as September–October (either side of the main summer/autumn breeding season), when the tracking data show most birds being out of zone (Table 17). This general pattern (i.e., the average bird was not present around New Zealand for as long as was previously assumed) was evident in the outputs for most other species also.

It is anticipated that using the updated monthly proportion in zone values in the seabird SEFRA models will have a major effect on model estimates of vulnerability to capture for the study species and also for species that are taxonomically linked in the SEFRA model.

4.6 Future research

This project gained access to most, although not all, of the known tracking data sets for some of the study seabirds. For example, a large number of yellow-eyed penguin tracks were requested although were not obtained. Where tracking data were obtained for other species, it was often not clear if grooming algorithms had already been applied to the data. Also, different data formats made it difficult to collate data for some species. Some of these issues would be addressed by collating the existing data into a single data repository, which would be advantageous for future assessments of New Zealand seabird species distributions. This process could begin with the collation of spatial information and associated metadata (e.g., identifiers that would allow a specific track to correspond to an individual's age stage or breeding status) from government-funded research.

We identified one environmental covariate (sea surface turbidity) that appeared to influence foraging patterns across a range of species, and a handful of others (e.g., SST) that appear to be relevant to some species. The lack of any strong environmental covariates for some species may be due to the use of 2-dimensional GP smooths, which were used by this study without much issue, due to the good spatial and temporal coverage of data for all species around New Zealand. This approach may be problematic when fitting models to data across regions/ocean basins, where a patchy coverage of spatial information may cause problems for estimating spatial smooths. It is likely that other environmental covariates of seabird foraging have not yet been identified, and it would be particularly advantageous to uncover these for predicting outside the New Zealand EEZ.

We did not compare the spatial/monthly distribution of the model predictions with the observed fishery captures. This is best done using SEFRA models, which account for spatial overlap with fishing effort and species-gear variability in capture rate.

This study demonstrated the utility of tracking data for estimating the proportions of birds in zone by month. This was done empirically, but future research should develop model-based approaches for predicting these proportions, which would provide estimates of uncertainty around estimates and can account for potential sources of bias relating to the sample being used.

5 ACKNOWLEDGEMENTS

The authors would like to thank B. Sharp and W. Gibson at Fisheries New Zealand; I. Debski, S. Bose, and G. Taylor at DOC; and L. Pearmain at BirdLife International for help to source seabird tracking data. We also thank Fisheries New Zealand for funding the projects PRO2019-09 and PSB2020-04.

The tracking data used are the product of a lot of field time by many people, often in arduous conditions. In attempt to fully acknowledge all contributors, primary report authors have been added as authors and

any within-report acknowledgements are listed here, with DOC and Fisheries New Zealand credits covering various staff members.

Antipodean albatross: S. Hamilton, A. Wiltshire, I. West and J. Burgess, P. Tyree, M. Renner, D. Houston, L. Davis, A. Schulze, Fisheries New Zealand, DOC, Southern Seabird Solutions, Campbelltown Cargo Services, Akademik Shokalskiy, Tranquil Image, HMZS Wellington, Evohe, and Live Ocean.

Buller's albatross. C. Robertson, A. Bartle, D. Sagar, L. Sanson, A. Cox, J. Carroll, J. Molloy, DOC, CNRS, Evohe, and Awesome.

Black petrel: S. Bettany, M. Brown, DOC, M. Imber, N. Marriott, L. Bull, P. Trevathan, C. Duncan, M. Fraser, P. Garner-Richards, C. Rothschild, H. Floyd, T. Guilford, H. Williams, S. Williams, Great Barrier Local Board, Southern Seabird Solutions, Auckland Council, Hauraki Gulf Forum, The Guardians of the Sea Charitable Trust, J. Atkins, M. Fraser, T. Macdonald, C. Mischler, N. Nieuwenhove, S. O'Reilly, B. Issler, T. Dennis, A. Clow, L. Clow, Z. Olsen, J. Williamson, J. Teman, T. Higham, H. Higham, F. Pressnell, Wildlife Management International. The authors thank DOC, Fisheries New Zealand, and Ngāti Rehua Ngāti Wai ki Aotea for permission to release the black petrel data.

Chatham Island albatross: Ian Potter Foundation, WWF, W.V. Scott Estate, La Trobe University, DOC Wild Press, M. Harger, M. Murray, Southlight Farm, Chisholm Institute, D. Bell, H. Rook, Daymond Estate, and M. Fraser.

Flesh-footed shearwater: K. Willis, D. Butler, P. Harborne, El Pescador Charters, DOC, S. Ray, K. Ritchie, J. Lewis, T. Bliss, D. Burgin, T. Hellesland, H. Ricardo, G. Malowski, T. Jackson, L. Pickford, J. Ward, A. Ward, Ngatiwai, Ngati Hei, D. Boyle, T. Bell, J. Arnould, A. Tennyson, B. Baker, P. Gaze, G. Hedley, Ngati Kuia, Woodward Family, R. Blyth, A. Burnett, L. Crotty, S. Hayward, I. Hutzler, K. Lewis, C. Miskelly, L. Miskelly, K. Miskelly, K. Morrison, L. Shepard, G. Stone, P. Stone, R. Thorley, C. Barbraud, D. Sim, S. Patrick, G. and B. Moore Foundation, D. and L. Packard Foundation, and A. Sloane Foundation.

Gibson's albatross: S. King, Tiama, HMNZS Wellington, R. Buckingham, P. Aplin, Marine Countess, I. West, A. Furgus, Tranquil Image, Awesome, DOC, E. Sommer, K.A. Edge, M. Renner, A. Schultz, G. Clark, R. Sale, K. Lay, D. Anderson, P. Moore, M. Pryde, and Tiama.

Salvin's albatross: Evohe, R. Calder, and Tiama.

White-chinned petrel: K. Clemens-Seely, DOC, H. Haazen, B. Baker, B. Robertson, University of Otago, NIWA, Parker Conservation, Linnaeus Taxonomy Fellowship (Otago Museum), J.S. Watson Trust award, New Zealand Federation of Graduate Women fellowship, Tiama, HMNZS Wellington, and Baltazar.

White-capped albatross: DOC, Fisheries New Zealand, Evohe, K. Parker, C. Miskelly, A. Tennyson, N. Atkinson, Tranquil Image, Awesome, Tiama, Clan McCleod, and F. Proffitt.

Westland petrel: NIWA, S. Bartle, P. Ryan, A.B. Freeman, DOC, University of Auckland, Auckland War Museum, Auckland Council, Brian Mason Scientific & Technical Trust, JS Watson Trust, S. Ismar, C. Millar, Punakaiki Department of Conservation staff, (particularly G. C. Wood), National banding Office, New Zealand Lottery, D. Lincoln University, Microwave Telemetry, Sirtrack Ltd. C. Miskelly, L. Shepherd, Katu Waewae Runanga, DOC, G. Coleman, S. Freeman, P. Doherty, M. Hauber, T. Dennis, and S. van Dijken.

6 REFERENCES

- Abraham, E.; Richard, Y.; Bell, E.; Landers, T. (2016). Overlap of the distribution of black petrel (*Procellaria parkinsoni*) with New Zealand trawl and longline fisheries. *New Zealand Aquatic Environment and Biodiversity Report No. 161*. 30 p.
- Bell, E.; Burgin, D.; Sim, J.; Dunleavy, K.; Fleishman, A.; Schofield, P. (2018). Population trends, breeding distribution and habitat use of black petrels (*Procellaria parkinsoni*) – 2016/2017 operational report. *New Zealand Aquatic Environment and Biodiversity Report No. 198*. 50 p.
- Bell, E.; Mischler, C.; Sim, J.; Schofield, P.; Francis, C.; Abraham, E.; Landers, T. (2014). At-sea distribution and population parameters of the black petrels (*Procellaria parkinsoni*) on Great Barrier Island (Aotea Island), 2013/14. Department of Conservation, Wellington, New Zealand. 98 p.
- Bell, E.; Sim, J.; Schofield, P. (2006). Population parameters and distribution of the black petrel (*Procellaria parkinsoni*), 2005/06. Department of Conservation, Wellington, New Zealand. 47 p.
- Bell, E.; Sim, J.; Schofield, P. (2008). Population parameters and distribution of the black petrel (*Procellaria parkinsoni*) on Great Barrier Island (Aotea Island), 2007/08. Department of Conservation, Wellington, New Zealand. 38 p.
- Bell, E.; Sim, J.; Schofield, P.; Francis, C.; Landers, T. (2013). At-sea distribution and population parameters of the black petrels (*Procellaria parkinsoni*) on Great Barrier Island (Aotea Island), 2012/13. Department of Conservation, Wellington, New Zealand. 95 p.
- Bostock, H.; Jenkins, C.; Mackay, K.; Carter, L.; Nodder, S.; Orpin, A.; Pallentin, A.; Wysoczanski, R. (2019a). Distribution of surficial sediments in the ocean around New Zealand/Aotearoa. Part A: continental slope and deep ocean. *New Zealand Journal of Geology and Geophysics* 62: 1–23.
- Bostock, H.; Jenkins, C.; Mackay, K.; Carter, L.; Nodder, S.; Orpin, A.; Pallentin, A.; Wysoczanski, R. (2019b). Distribution of surficial sediments in the ocean around New Zealand/Aotearoa. Part B: continental shelf. *New Zealand Journal of Geology and Geophysics* 62: 24–45.
- Broekhuizen, N.; Stahl, J.C.; Sagar, P.M. (2003). Simulating the distribution of southern Buller's albatross using an individual-based population model. *Journal of Applied Ecology* 40: 678–691.
- Carpenter-Kling, T.; Reisinger, R.R.; Orgeret, F.; Connan, M.; Stevens, K.L.; Ryan, P.G.; Makhado, A.; Pistorius, P.A. (2020). Foraging in a dynamic environment: response of four sympatric sub-Antarctic albatross species to interannual environmental variability. *Ecology and Evolution* 10: 11277–11295.
- CLS [Collection Localisation Satellites]. (2011). Argos user's manual. Available at www.argos-system.org/wp-content/uploads/2016/08/r363_9_argos_users_manual-v1.6.6.pdf
- Crowe, P. (2018). Foraging distribution and behaviour of flesh-footed shearwaters (*Puffinus carneipes*) breeding on Lady Alice Island – January 2018. Department of Conservation, Wellington, New Zealand. 21 p.
- Crowe, P. (2020). Flesh-footed shearwater population monitoring and at-sea distribution: 2019/20 season. Department of Conservation, Wellington, New Zealand. 39 p.
- Croxall, J.P.; Butchart, S.H.; Lascelles, B.; Stattersfield, A.J.; Sullivan, B.; Symes, A.; Taylor, P. (2012). Seabird conservation status, threats and priority actions: A global assessment. *Bird Conservation International* 22: 1–34.
- Deppe, L.; McGregor, K.; Tomasetto, F.; Briskie, J.; Scofield, R. (2014). Distribution and predictability of foraging areas in breeding Chatham albatrosses *Thalassarche eremita* in relation to environmental characteristics. *Marine Ecology Progress Series* 498: 287–301.
- Elliott, G.; Walker, K. (2014). Gibson's wandering albatross at Adams Island – population study. Department of Conservation, Wellington, New Zealand. 13 p.

- Elliott, G.; Walker, K. (2017). Antipodean wandering albatross census and population study 2017. Department of Conservation, Wellington, New Zealand. 20 p.
- Elliott, G.; Walker, K. (2020). Antipodean wandering albatross: Satellite tracking and population study Antipodes Island 2020. Department of Conservation, Wellington, New Zealand. 35 p.
- Fisheries New Zealand (2020). Aquatic Environment and Biodiversity Annual Review 2019–20. Compiled by the Fisheries Science Team, Ministry for Primary Industries, Wellington New Zealand. 765 p.
- Freeman, A.N.D. (1997). The influence of hoki fishing vessels on Westland Petrel (*Procellaria westlandica*) distribution at sea. *Notornis* 44: 159–164.
- Freeman, A.N.D.; Nicholls, D.G.; Wilson, K.-J.; Bartle, J.A. (1997). Radio and satellite tracking Westland Petrels *Procellaria westlandica*. *Marine Ornithology* 25: 31–36.
- Freeman, A.N.D.; Wilson, K.-J. (1997). Results of the Westland petrel satellite tracking programme 1995 season. Department of Conservation, Wellington, New Zealand. 4 p.
- Freeman, A.N.D.; Wilson, K.-J.; Nicholls, D.G. (2001). Westland Petrels and the Hoki fishery: Determining co-occurrence using satellite telemetry. *Emu - Austral Ornithology* 101: 47–56.
- Freeman, R.; Dennis, T.; Landers, T.; Thompson, D.; Bell, E.; Walker, M.; Guilford, T. (2010). Black Petrels (*Procellaria parkinsoni*) Patrol the Ocean Shelf-Break: GPS Tracking of a Vulnerable Procellariiform Seabird. *PLOS ONE* 5: e9236.
- Hamilton, S.; Wiltshire, A.; Walker, K.; Elliott, G. (2002). Monitoring Antipodean wandering albatross, 1999/2000. *DOC Science Internal Series* 78. Department of Conservation, Wellington, New Zealand. 24 p.
- Haney, J.C.; Stone, A.E. (1988). Seabird foraging tactics and water clarity: are plunge divers really in the clear? *Marine Ecology Progress Series* 49: 1–9.
- Hicks, D.M.; Shankar, U.; McKerchar, A.I.; Basher, L.; Lynn, I.; Page, M.; Jessen, M. (2011). Suspended sediment yields from New Zealand rivers. *Journal of Hydrology (New Zealand)* 50: 81–142.
- Kirk, H.; Crowe, P.; Bell, M. (2017). Foraging distribution and behaviour of flesh-footed shearwaters (*Puffinus carneipes*) breeding on Lady Alice Island – February 2017. Department of Conservation, Wellington, New Zealand. 24 p.
- Landers, T.J.; Rayner, M.J.; Phillips, R.A.; Hauber, M.E. (2011). Dynamics of seasonal movements by a trans-Pacific migrant, the Westland Petrel. *The Condor* 113: 71–79.
- Leathwick, J.; Elith, J.; Francis, M.; Hastie, T.; Taylor, P. (2006). Variation in demersal fish species richness in the oceans surrounding New Zealand: An analysis using boosted regression trees. *Marine Ecology Progress Series* 321: 267–281.
- Mattern, T. (2020). Modelling marine habitat utilisation by yellow-eyed penguins along their mainland distribution: baseline information. *New Zealand Aquatic Environment and Biodiversity Report No. 243*. 29 p.
- Moore, P.J.; Wakelin, M.; Douglas, M.E.; McKinlay, B.; Nelson, D.; Murphy, B. (1995). Yellow-eyed penguin foraging study, South-eastern New Zealand, 1991–1993. *Science and Research Series No. 83*. New Zealand Department of Conservation. 41 p.
- Mormede, S.; Webber, D.; Edwards, E. (2022). Creating standardised grids for New Zealand marine science outputs. *New Zealand Aquatic Environment and Biodiversity Report No. 283*. 7 p.
- Phillips, R.A.; Silk, J.R.D.; Croxall, J.P.; Afanasyev, V.; Briggs, D.R. (2004). Accuracy of geolocation estimates for flying seabirds. *Marine Ecology Progress Series* 266: 265–272.
- Poupart, T.A.; Waugh, S.M.; Kato, A.; Arnould, J.P.Y. (2020). Foraging niche overlap during chick-rearing in the sexually dimorphic Westland petrel. *Royal Society Open Science* 7: 191511.
- Poupart, T.; Waugh, S.; Miskelly, C.; Kato, A.; Angel, L.; Rogers, K.; Arnould, J. (2019). Fine-scale foraging behaviour of southern Buller’s albatross, the only Thalassarche that provisions chicks through winter. *Marine Ecology Progress Series* 625: 163–179.

- Rakhimberdiev, E.; Saveliev, A.; Piersma, T.; Karagicheva, J. (2017). FLightR: an R package for reconstructing animal paths from solar geolocation loggers. *Methods in Ecology and Evolution* 8: 1482–1487.
- Rayner, M.J.; Taylor, G.A.; Thompson, D.R.; Torres, L.G.; Sagar, P.M.; Shaffer, S.A. (2011). Migration and diving activity in three non-breeding flesh-footed shearwaters *Puffinus carneipes*. *Journal of Avian Biology* 42: 266–270.
- Reid, T.A.; Tuck, G.N.; Hindell, M.A.; Thalmann, S.; Phillips, R.A.; Wilcox, C. (2013). Nonbreeding distribution of flesh-footed shearwaters and the potential for overlap with north Pacific fisheries. *Biological Conservation* 166: 3–10.
- Rexer-Huber, K. (2017). White-chinned petrel distribution, abundance and connectivity have circumpolar conservation implications. PhD thesis, University of Otago, Dunedin. 166 p.
- Rexer-Huber, K.; Elliott, G.; Walker, K.; Thompson, D.; Parker, G. (2020). Gibson’s albatross and white-capped albatross in the Auckland Islands 2019–20. Department of Conservation, Wellington, New Zealand. 30 p.
- Richard, Y.; Abraham, E.; Berkenbusch, K. (2020a). Assessment of the risk of commercial fisheries to New Zealand seabirds, 2006–07 to 2016–17. *New Zealand Aquatic Environment and Biodiversity Report* 237. 57 p.
- Richard, Y.; Abraham, E.; Berkenbusch, K. (2020b). Counts of seabirds around commercial fishing vessels within New Zealand waters, 2007–08 to 2018–19. Department of Conservation, Wellington, New Zealand. 43 p.
- Roberts, J.O.; Webber, D.N.; Roe, W.T.; Edwards, C.T.T.; Doonan, I.J. (2019). Spatial risk assessment of threats to Hector’s/Māui dolphins (*Cephalorhynchus hectori*). *New Zealand Aquatic Environment and Biodiversity Report No. 214*. 168 p.
- Sagar, P.M.; Parker, G.; Rexer-Huber, K.; Thompson, D. (2018). Salvin’s albatross: Bounty Islands population project, ground component. Department of Conservation, Wellington, New Zealand. 18 p.
- Sagar, P.M.; Weimerskirch, H. (1996). Satellite tracking of southern Buller’s albatrosses from the Snares, New Zealand. *The Condor* 98: 649–652.
- Stahl, J.C.; Sagar, P.M. (2000). Foraging strategies and migration of southern Buller’s albatrosses *Diomedea b. bulled* breeding on the Solander Is, New Zealand. *Journal of the Royal Society of New Zealand* 30: 319–334.
- Stahl, J.-C.; Sagar, P.M. (2006). Long and short trips in nonbreeding Buller’s albatrosses: relationships with colony attendance and body mass. *The Condor* 108: 348–365.
- Stephenson, F.; Goetz, K.; Sharp, B.R.; Mouton, T.L.; Beets, F.J.; Roberts, J.; MacDiarmid, A.B.; Constantine, R.; Lundquist, C.J. (2020). Modelling the spatial distribution of cetaceans in New Zealand waters. *Diversity and Distributions* 26: 495–516.
- Thalmann, S.J.; Baker, G.B.; Hindell, M.; Tuck, G.N. (2009). Longline fisheries and foraging distribution of flesh-footed shearwaters in Eastern Australia. *The Journal of Wildlife Management* 73: 399–406.
- Thompson, D.; Sagar, P.M. (2006). Conduct a population and distributional study on white-capped albatross at the Auckland Islands. Department of Conservation, Wellington, New Zealand. 11 p.
- Thompson, D.; Sagar, P.M. (2008). A population and distributional study of white-capped albatross (Auckland Islands), 2006-07 Annual report. Contract Number: POP 2005/02. Department of Conservation, Wellington, New Zealand. 22 p.
- Thompson, D.; Sagar, P.M.; Briscoe, D.; Parker, G.; Rexer-Huber, K.; Charteris, M. (2020). Salvin’s albatross: Bounty Islands population project. Ground component. Department of Conservation, Wellington, New Zealand. 18 p.
- Thompson, D.; Sagar, P.M.; Torres, L.G. (2009). A population and distributional study of white-capped albatross (Auckland Islands) Contract Number: POP 2005/02. Department of Conservation, Wellington, New Zealand. 17 p.

- Thompson, D.; Sagar, P.M.; Torres, L.G.; Charteris, M. (2014). Salvin's albatrosses at the Bounty Islands: at-sea distribution. Department of Conservation, Wellington, New Zealand. 15 p.
- Torres, L.; Thompson, D.; Bearhop, S.; Votier, S.; Taylor, G.; Sagar, P.; Robertson, B. (2011). White-capped albatrosses alter fine-scale foraging behavior patterns when associated with fishing vessels. *Marine Ecology Progress Series 428*: 289–301.
- Walker, K.; Elliott, G. (2002a). Monitoring Antipodean wandering albatross, 1997/98. *DOC Science Internal Series 76*. Department of Conservation, Wellington, New Zealand. 20 p.
- Walker, K.; Elliott, G. (2002b). Monitoring Gibson's wandering albatross, 1998/99. *DOC Science Internal Series 70*. Department of Conservation, Wellington, New Zealand. 20 p.
- Walker, K.; Elliott, G. (2002c). Monitoring Gibson's wandering albatross, 2001/02. *DOC Science Internal Series 73*. Department of Conservation, Wellington, New Zealand. 29 p.
- Walker, K.; Elliott, G. (2006). At-sea distribution of Gibson's and Antipodean wandering albatrosses, and relationships with longline fisheries. *Notornis 53*: 265–290.
- Walker, K.; Elliott, G. (2015). Gibson's wandering albatross population study 2014/15. Department of Conservation, Wellington, New Zealand. 16 p.
- Walker, K.; Elliott, G. (2019). Antipodean wandering albatross census and population study on Antipodes Island 2019. Department of Conservation, Wellington, New Zealand. 27 p.
- Walker, K.; Elliott, G.; Hamilton, S.; Wiltshire, A. (2002). Monitoring Antipodean wandering albatross, 1998/99. *DOC Science Internal Series 77*. Department of Conservation, Wellington, New Zealand. 19 p.
- Waugh, S.; Jamieson, S.; Stahl, J.-C.; Fillipi, D.P.; Taylor, G.A.; Booth, A. (2014). Flesh-footed shearwater – population study and foraging areas (POP2011-02). Department of Conservation, Wellington, New Zealand. 68 p.
- Waugh, S.M.; Griffiths, J.W.; Poupart, T.A.; Filippi, D.P.; Rogers, K.; Arnould, J.Y.P. (2018). Environmental factors and fisheries influence the foraging patterns of a subtropical seabird, the Westland Petrel (*Procellaria westlandica*), in the Tasman Sea. *The Condor 120*: 371–387.
- Waugh, S.M.; Patrick, S.C.; Fillipi, D.P.; Taylor, G.A.; Arnould, J.Y.P. (2016). Overlap between Flesh-footed Shearwater *Puffinus carneipes* foraging areas and commercial fisheries in New Zealand waters. *Marine Ecology Progress Series 551*: 249–260.
- Wold, J.R. (2017). Phylogenetic relationships, population connectivity, and the development of genetic assignment testing in Buller's albatross (*Thalassarche bulleri bulleri*). PhD Thesis, Victoria University of Wellington. 101 p.
- Wood, B.; Finucci, B.; Black, J. (2022). A standardised approach for creating spatial grids for New Zealand marine environment and species data. *New Zealand Aquatic Environment and Biodiversity Report No. 288*. 6 p.
- Wood, S.N.; Goude, Y.; Shaw S. (2015) Generalized additive models for large datasets. *Journal of the Royal Statistical Society, Series C 64*: 139–155.

APPENDIX A. PREVIOUS SEABIRD DISTRIBUTION LAYERS

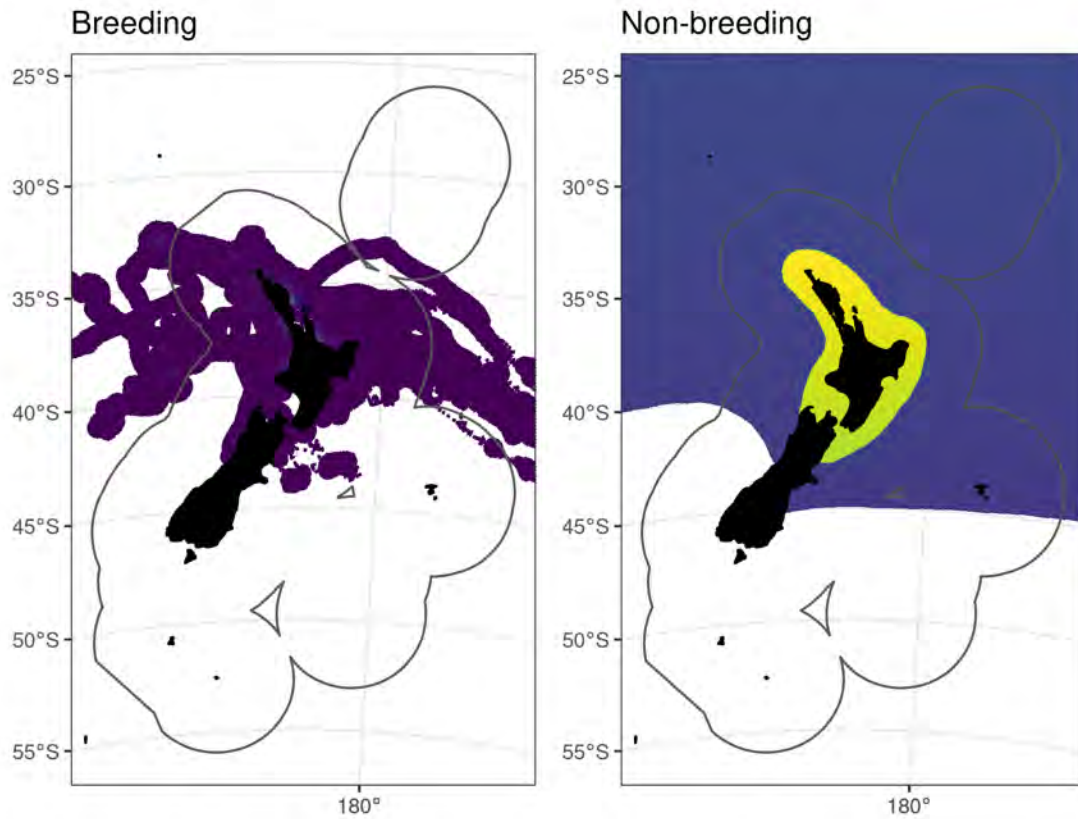


Figure A.1: Previous flesh-footed shearwater distribution layers. The breeding season was assumed to be September–May.

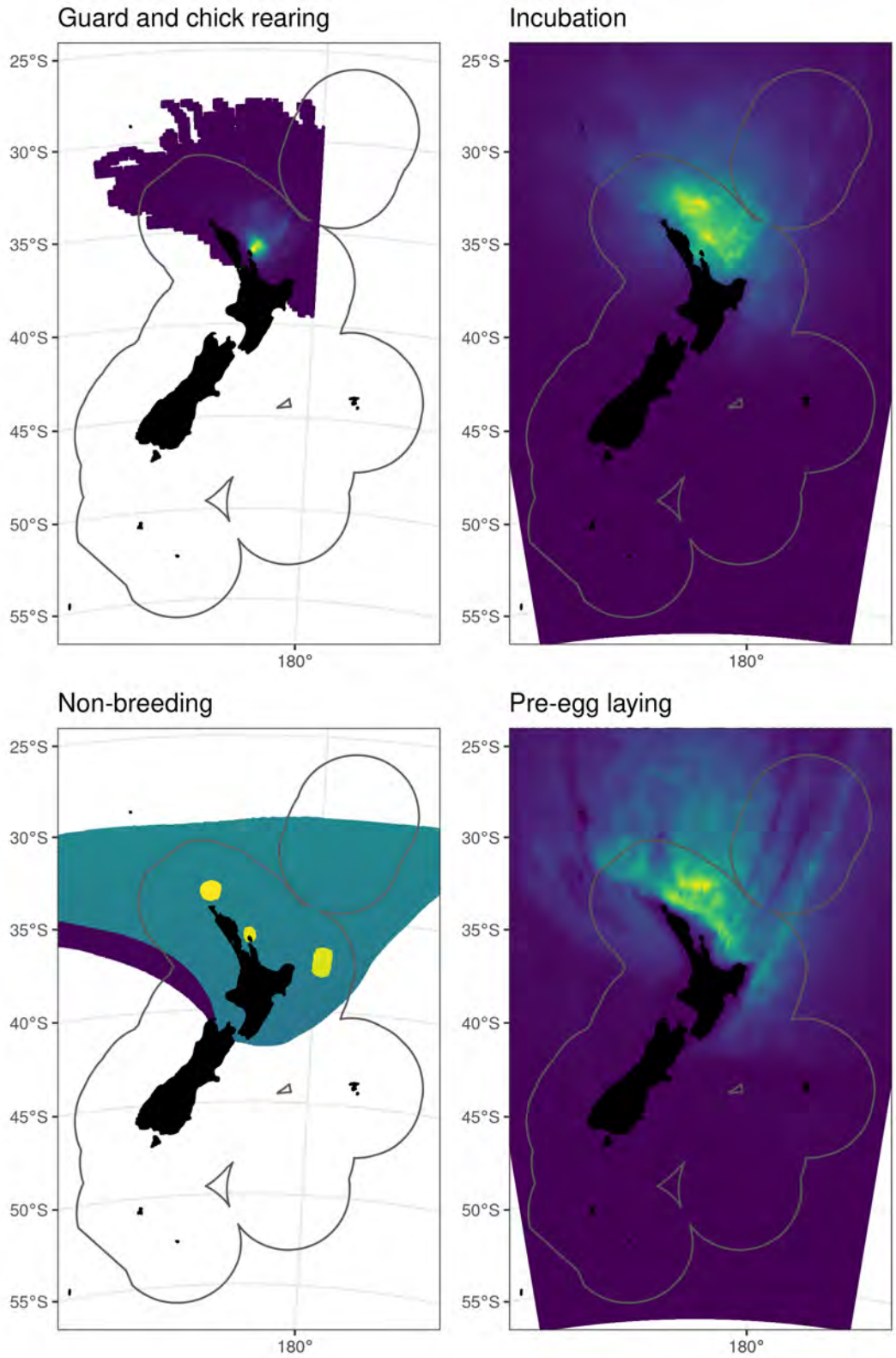


Figure A.2: Previous black petrel distribution layers. The breeding seasons were assumed to be October–November for Pre-egg laying, December–January for Incubation, February–May for Guard and chick-rearing.

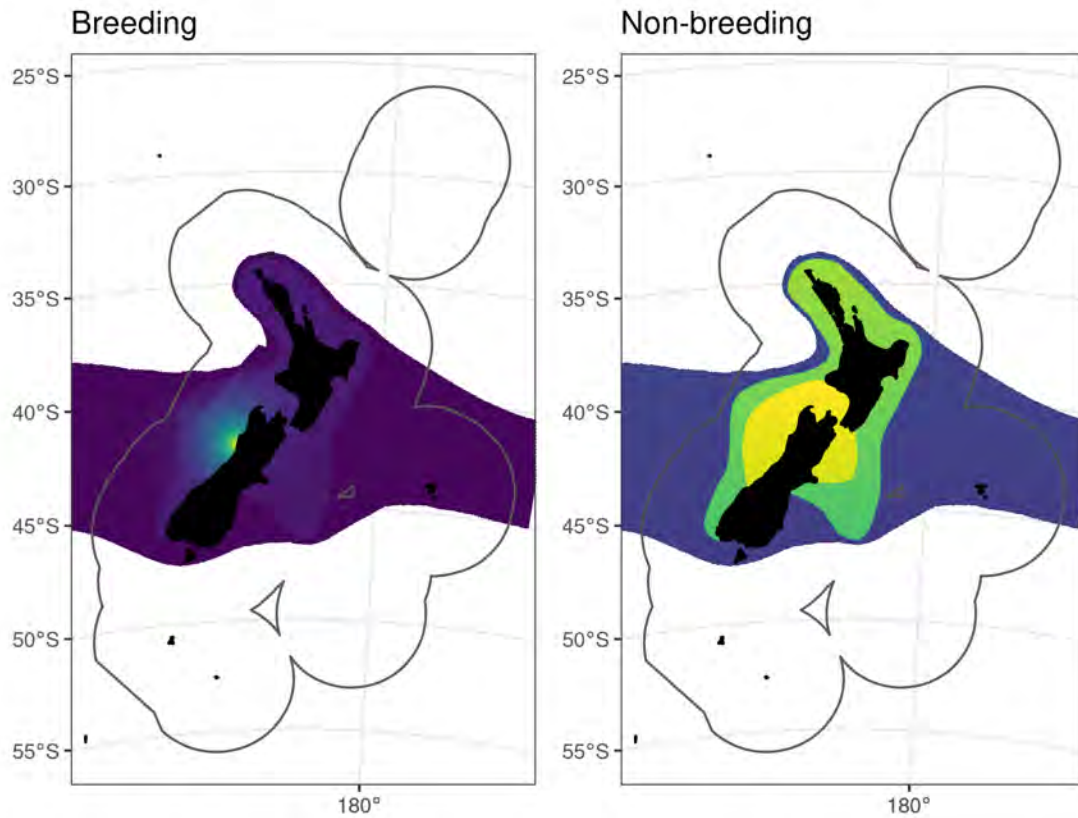


Figure A.3: Previous Westland petrel distribution layers. The breeding season was assumed to be March–December.

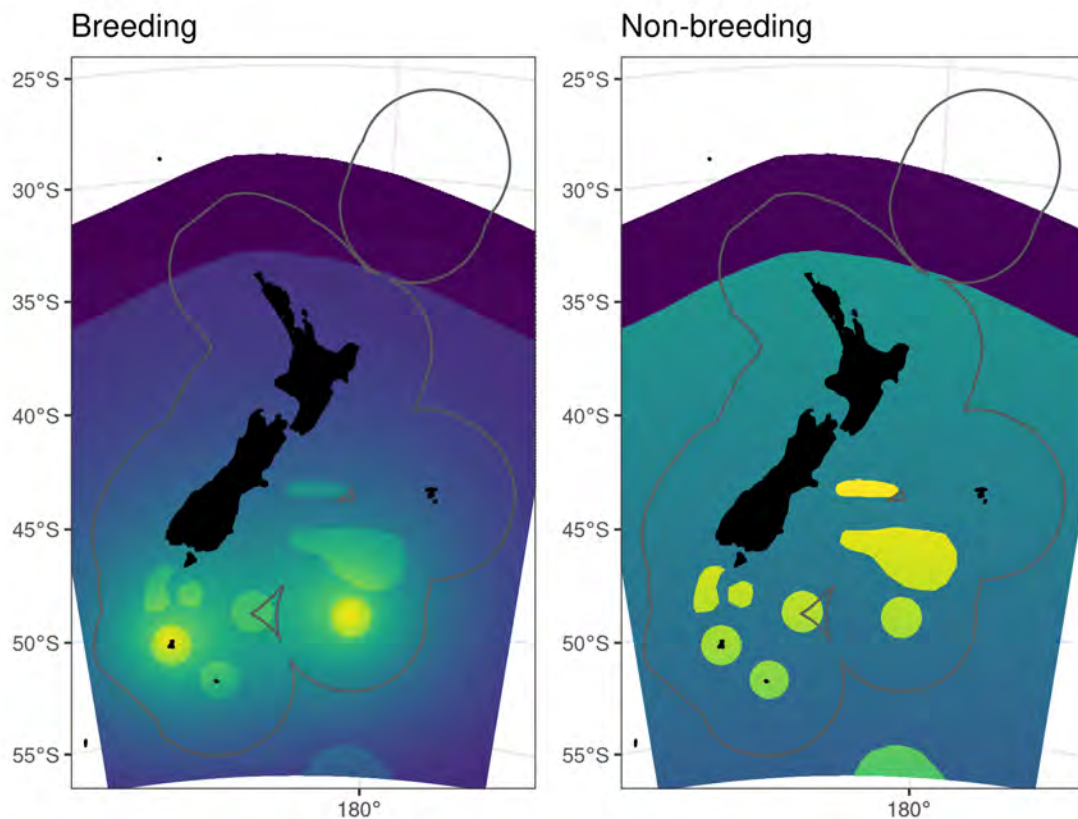


Figure A.4: Previous white-chinned petrel distribution layers. The breeding season was assumed to be November–May.

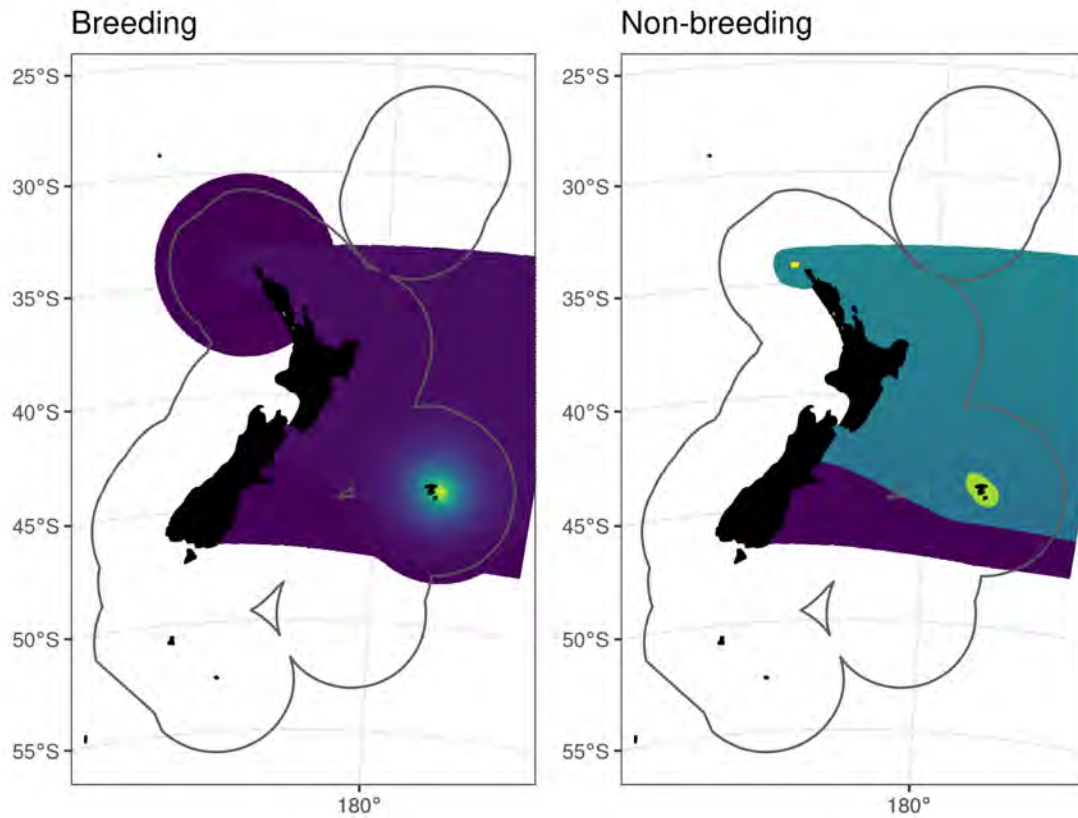


Figure A.5: Previous Northern Buller's albatross distribution layers. The breeding season was assumed to be October–June.

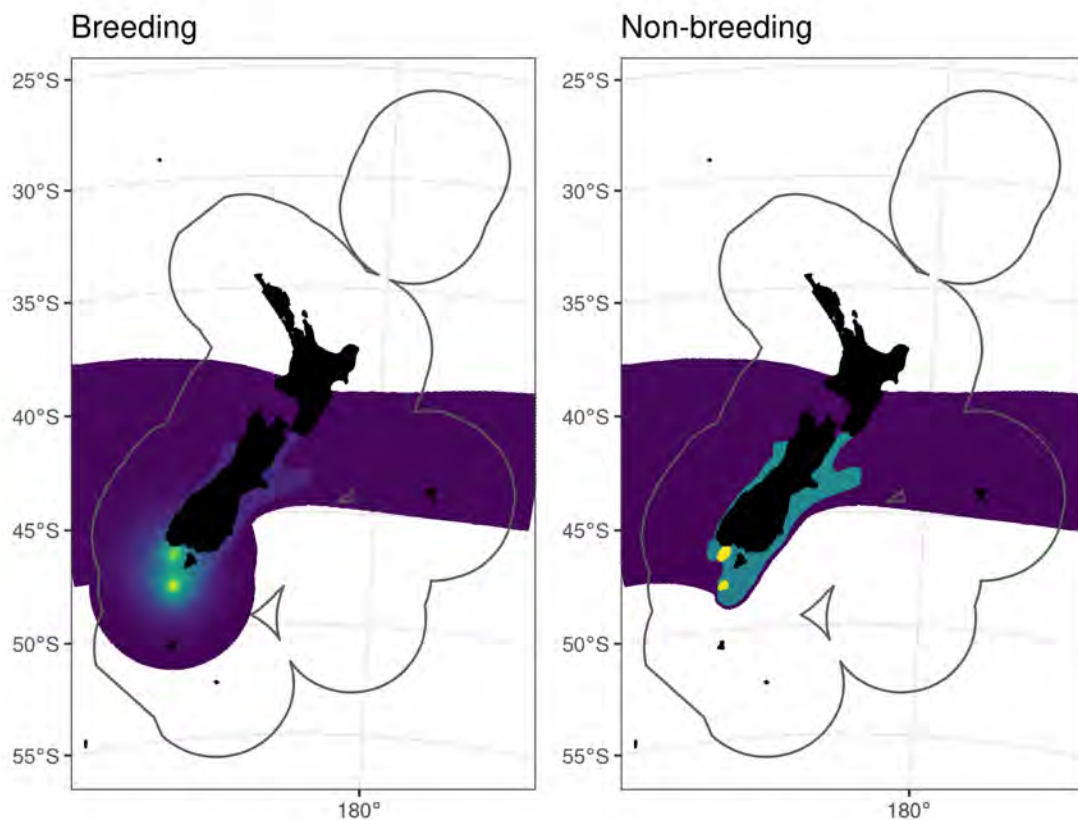


Figure A.6: Previous Southern Buller's albatross distribution layers. The breeding season was assumed to be December–August.

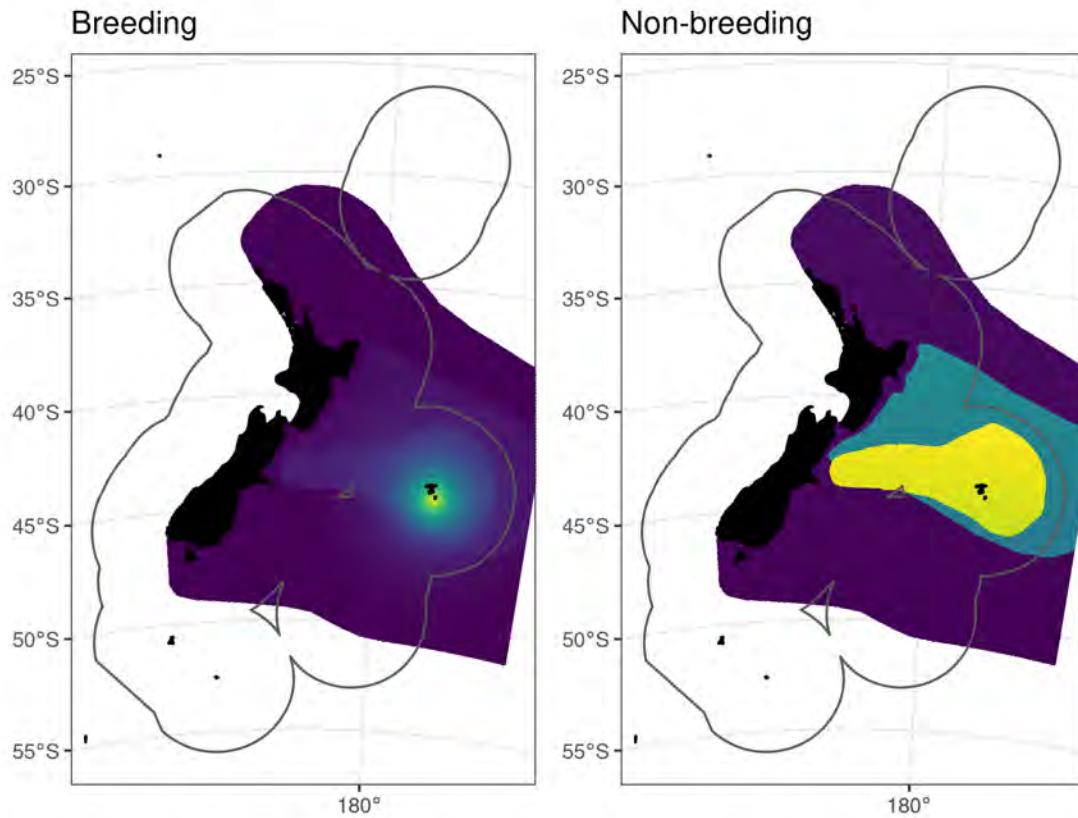


Figure A.7: Previous Chatham Island albatross distribution layers. The breeding season was assumed to be August–May.

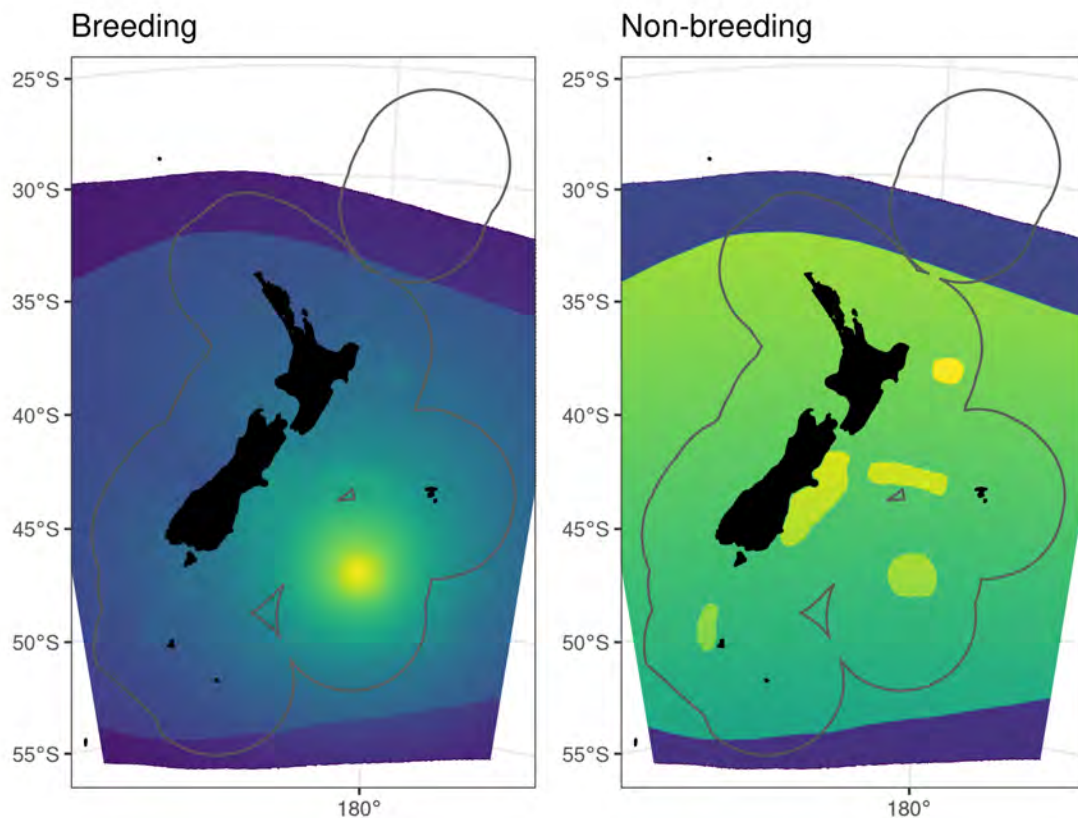


Figure A.8: Previous Salvin's albatross distribution layers. The breeding season was assumed to be September–April.

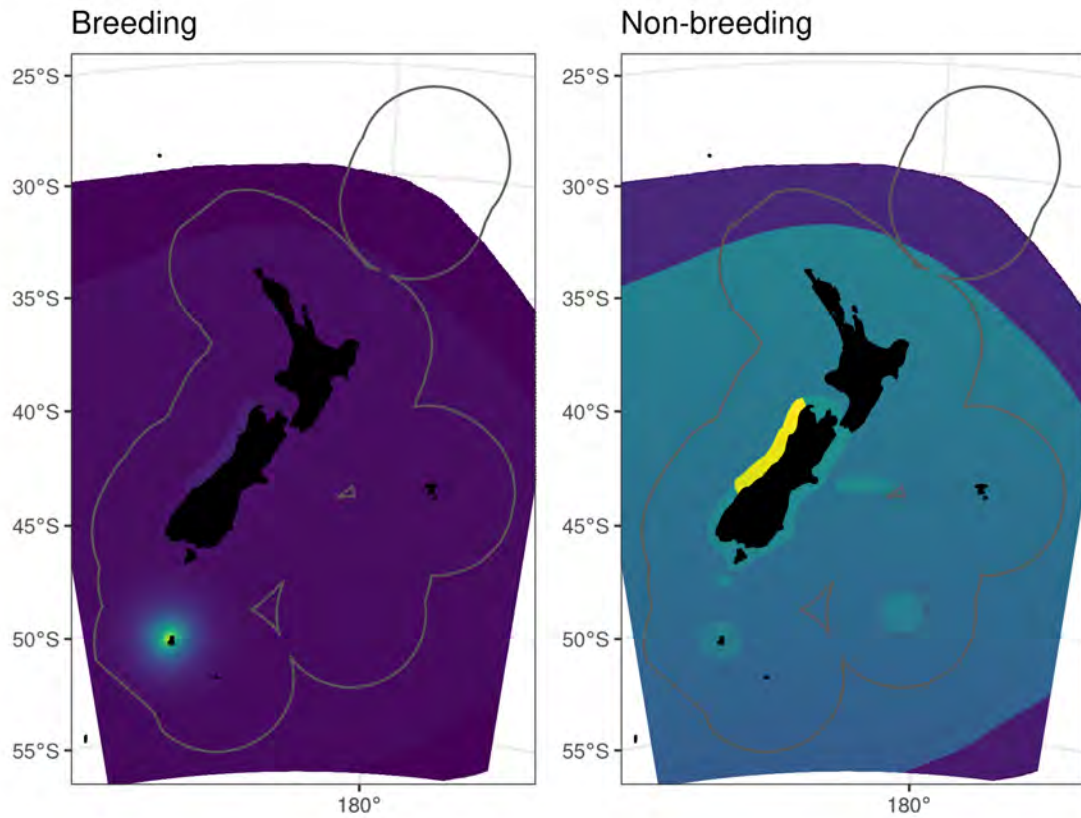


Figure A.9: Previous white-capped albatross distribution layers. The breeding season was assumed to be November–August.

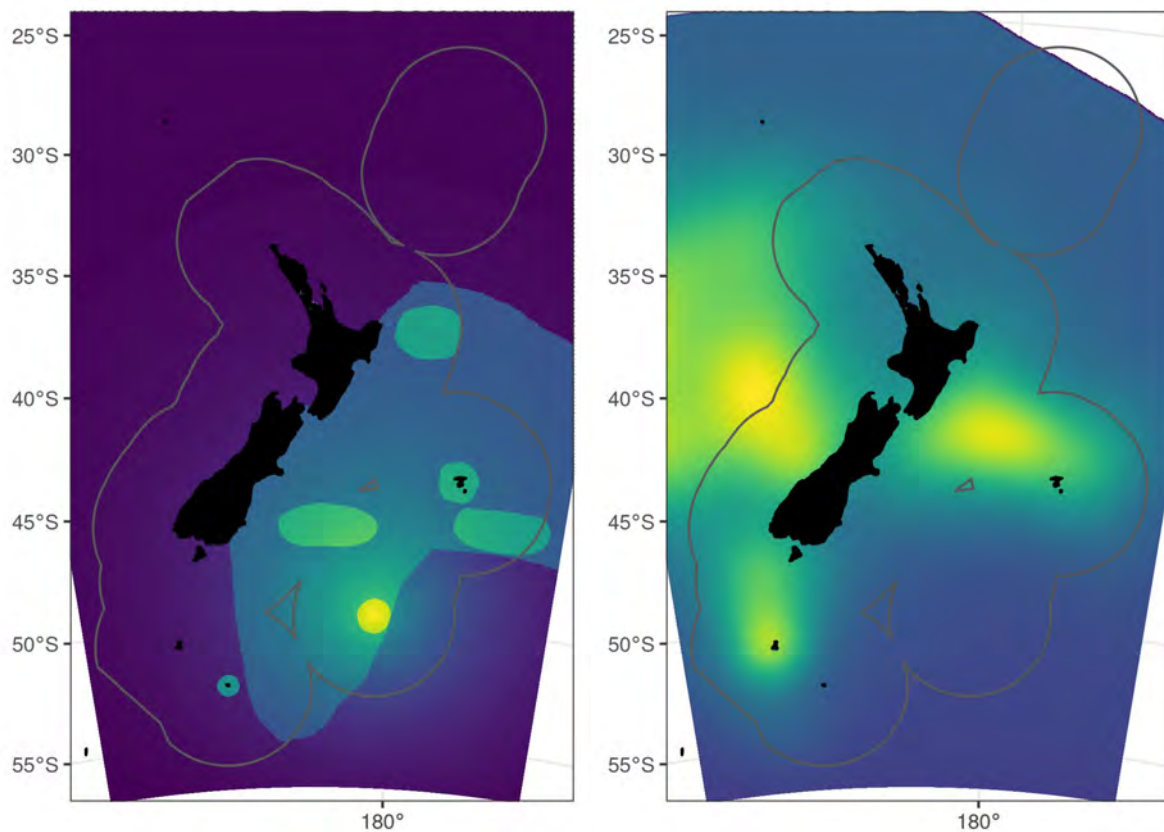


Figure A.10: Previous Antipodean [left] and Gibson's [right] albatross distribution layers.

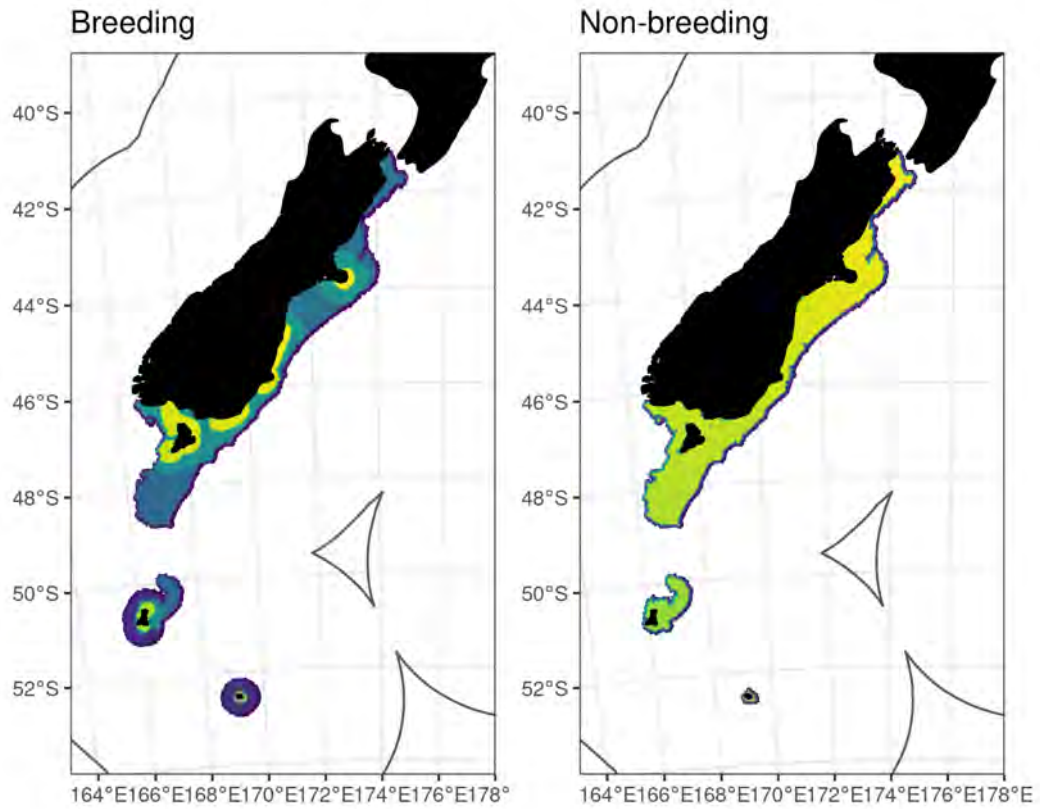


Figure A.11: Previous yellow-eyed penguin distribution layers. The breeding season was assumed to be August–May.

APPENDIX B. CANDIDATE SPATIAL COVARIATES OF SEABIRD DISTRIBUTION

The spatial environmental covariates offered to seabird distribution models were monthly (Figure B.1 to Figure B.5), quarterly (Figure B.6 and Figure B.7), or temporally static (Figure B.8 to Figure B.13).

Table B.1: Summary of all spatial environmental covariates offered to spatial predictive models of Hector's dolphin sighting rate.

Covariate	Spatial resolution	Temporal resolution	Source
Bathymetric depth (depth)	250 m	Static	NIWA (https://niwa.co.nz/our-science/oceans/bathymetry/download-the-data)
Bathymetric slope (slope)	1 km	Static	Derived from bathymetry
Distance to colony (distance_to_colony)	1 km	Static	Derived from known breeding colony locations, including only colonies that comprised at least 1% of the total seabird breeding population
Sea surface temperature (sst)	~0.25 degree	Monthly, 1979-2020	ERA5 climate data re-analysis (https://cds.climate.copernicus.eu/cdsapp#!/dataset/reanalysis-era5-single-levels-monthly-means?tab=overview)
Wind speed (wind)	~0.25 degree	Monthly, 1979-2020	ERA5 climate data re-analysis (https://cds.climate.copernicus.eu/cdsapp#!/dataset/reanalysis-era5-single-levels-monthly-means?tab=overview)
SST gradient (sst_gradient)	~0.25 degree	Monthly, 1979-2020	Calculated from SST data
Sea level anomaly (sea_level_anomaly)	0.25 degree	Monthly, 1993-2020	Satellite altimetry data processed and provided by Copernicus Climate Change Service (C3S) (https://cds.climate.copernicus.eu/cdsapp#!/dataset/satellite-sea-level-global?tab=overview)
Tidal current speed (currents)	1 km	Static	Leathwick et al. (2012), processed by Stephenson et al. (2020).
Surface chlorophyll-a concentration (chlorophyll)	4 km	Quarterly climatology, 2003-2020	Satellite ocean colour data processed and provided by NASA GIOVANNI (https://giovanni.gsfc.nasa.gov/giovanni/)
Surface turbidity proxy (turbidity)	4 km	Quarterly climatology, 2003-2020	Satellite ocean colour data product (Kd490) processed and provided by NASA GIOVANNI (https://giovanni.gsfc.nasa.gov/giovanni/)
% sand of benthic sediments (sand)	1 km	Static	Bostock et al. (2019a, 2019b)
% mud of benthic sediments (mud)	1 km	Static	Bostock et al. (2019a, 2019b)
% gravel of benthic sediments (gravel)	1 km	Static	Bostock et al. (2019a, 2019b)
% carbonate of benthic sediments (carbonate)	1 km	Static	Bostock et al. (2019a, 2019b)
Probability of presence of the top seven prey species (prey)	1 km	Static	Derived from spatial model fitted to research trawl survey catch data. Layers originally produced for MPI project PRO2017-12 (Roberts et al. 2019). Seven prey taxa selected that comprised at least 10% of the estimated total dietary mass from any published dietary study: arrow squid species (<i>Nototodarus</i> spp.; species codes 'NOS', 'NOG', 'SQU', and 'SQX'), red cod (<i>Pseudophycis bachus</i> ; 'RCO'), blue cod (<i>Parapercis colias</i> , 'BCO'), sprat species (<i>Sprattus</i> sp.; 'SPR', 'SPM', 'SPA'), silverside (<i>Argentina elongata</i> , 'SSI'), opalfish (<i>Hemerocoetes</i> sp., 'OPA'), ahuru (<i>Auchenoceros punctatus</i> , 'PCO').

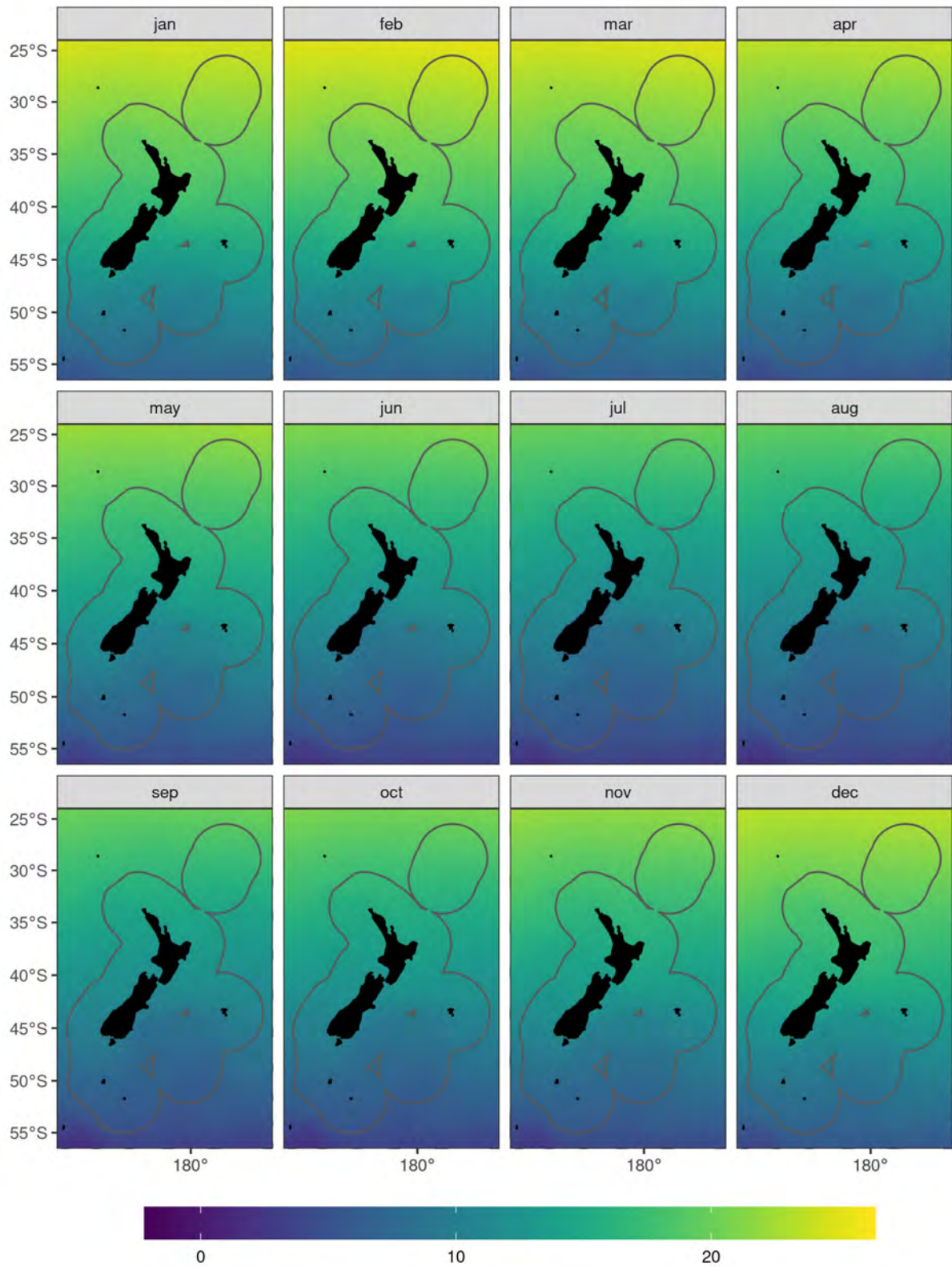


Figure B.1: Mean air temperature (°C) by month. Note that monthly climatologies are shown here, which were used for model predictions, although models were fitted to monthly data in the respective year of observation.

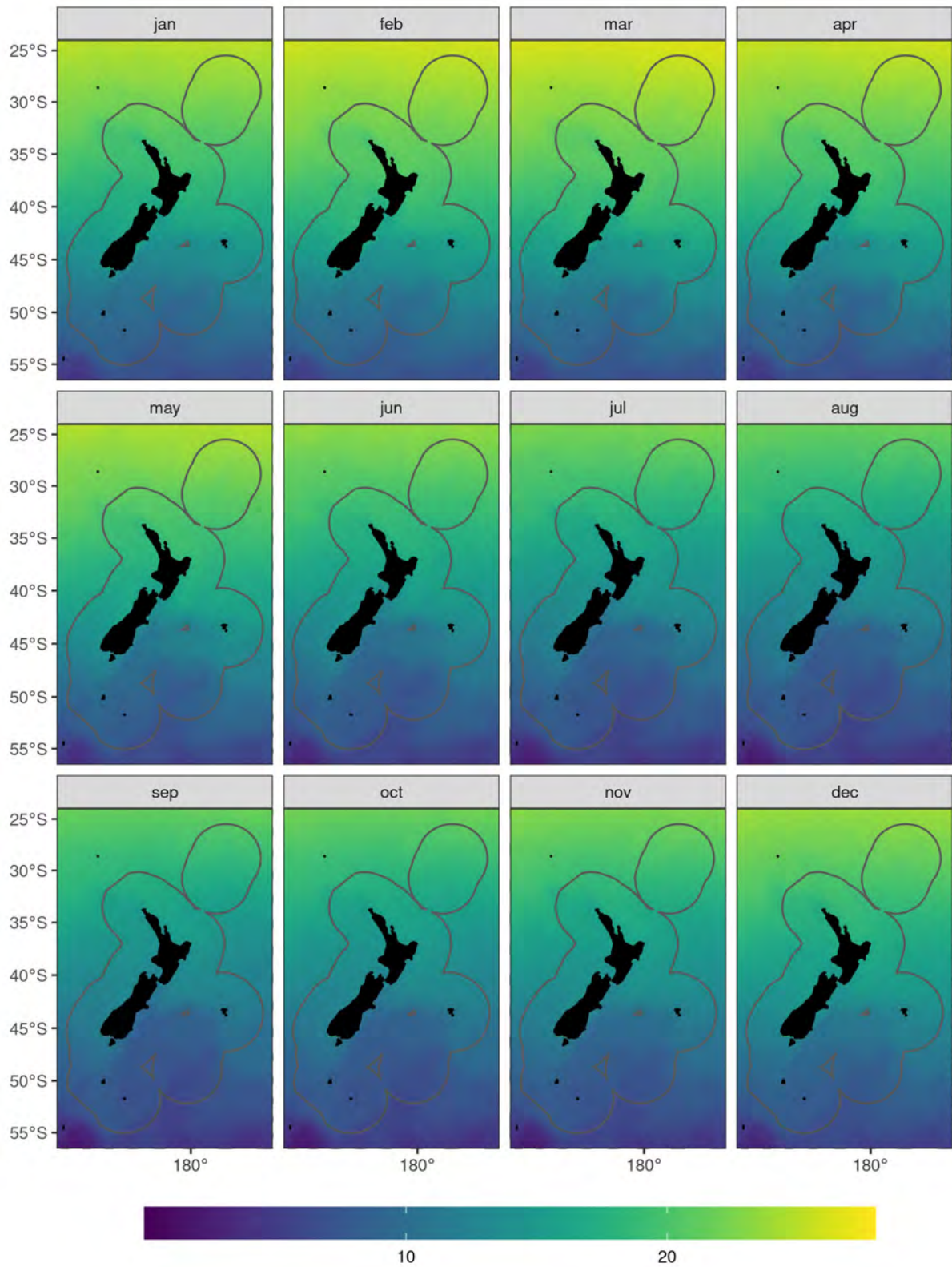


Figure B.2: Mean sea surface temperature (SST, °C) by month. Note that monthly climatologies are shown here, which were used for model predictions, although models were fitted to monthly data in the respective year of observation.

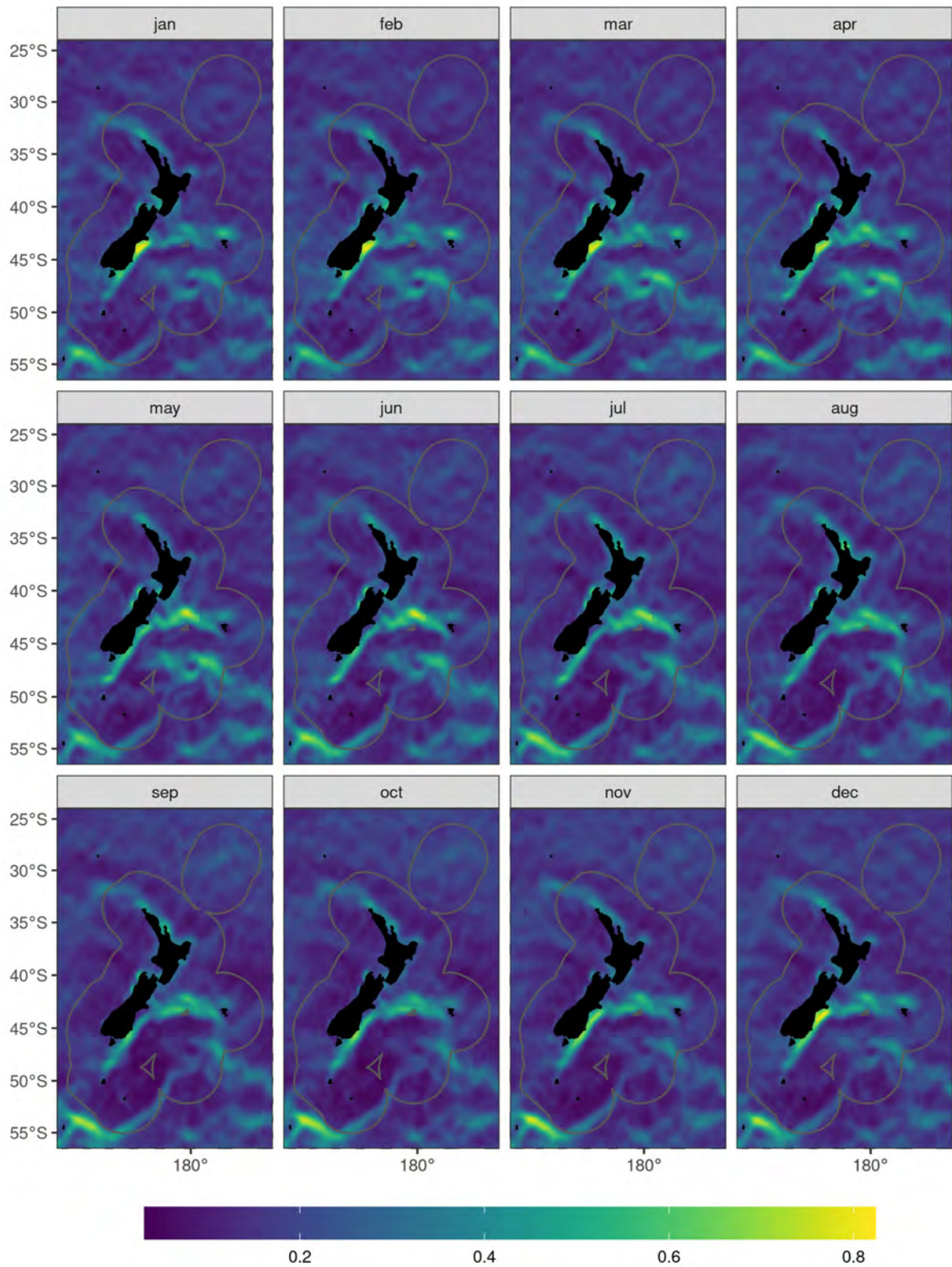


Figure B.3: Mean sea surface temperature (SST) gradient by month. Note that monthly climatologies are shown here, which were used for model predictions, although models were fitted to monthly data in the respective year of observation.

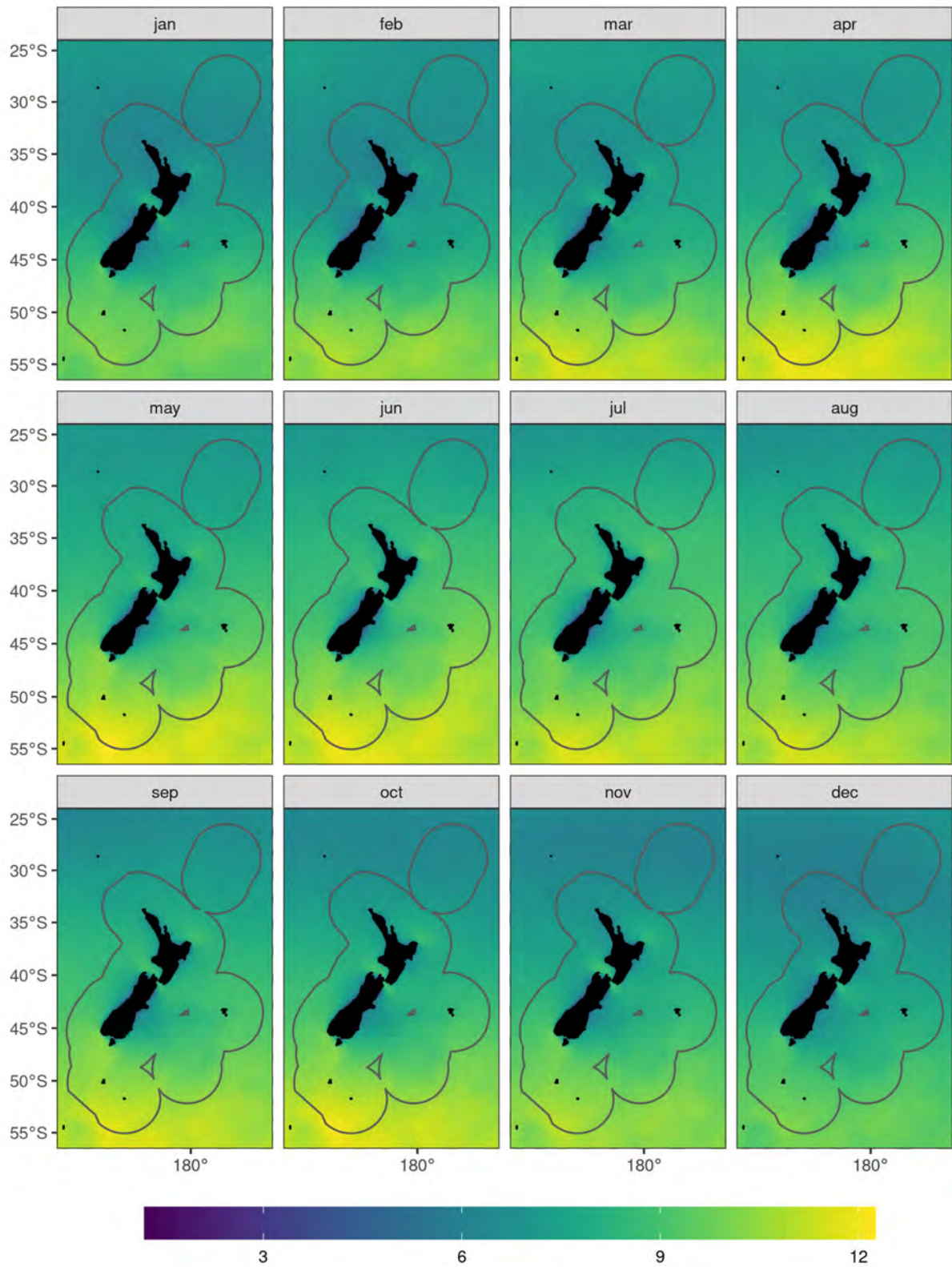


Figure B.4: Mean wind speed (m s^{-1}) by month. Note that monthly climatologies are shown here, which were used for model predictions, although models were fitted to monthly data in the respective year of observation.

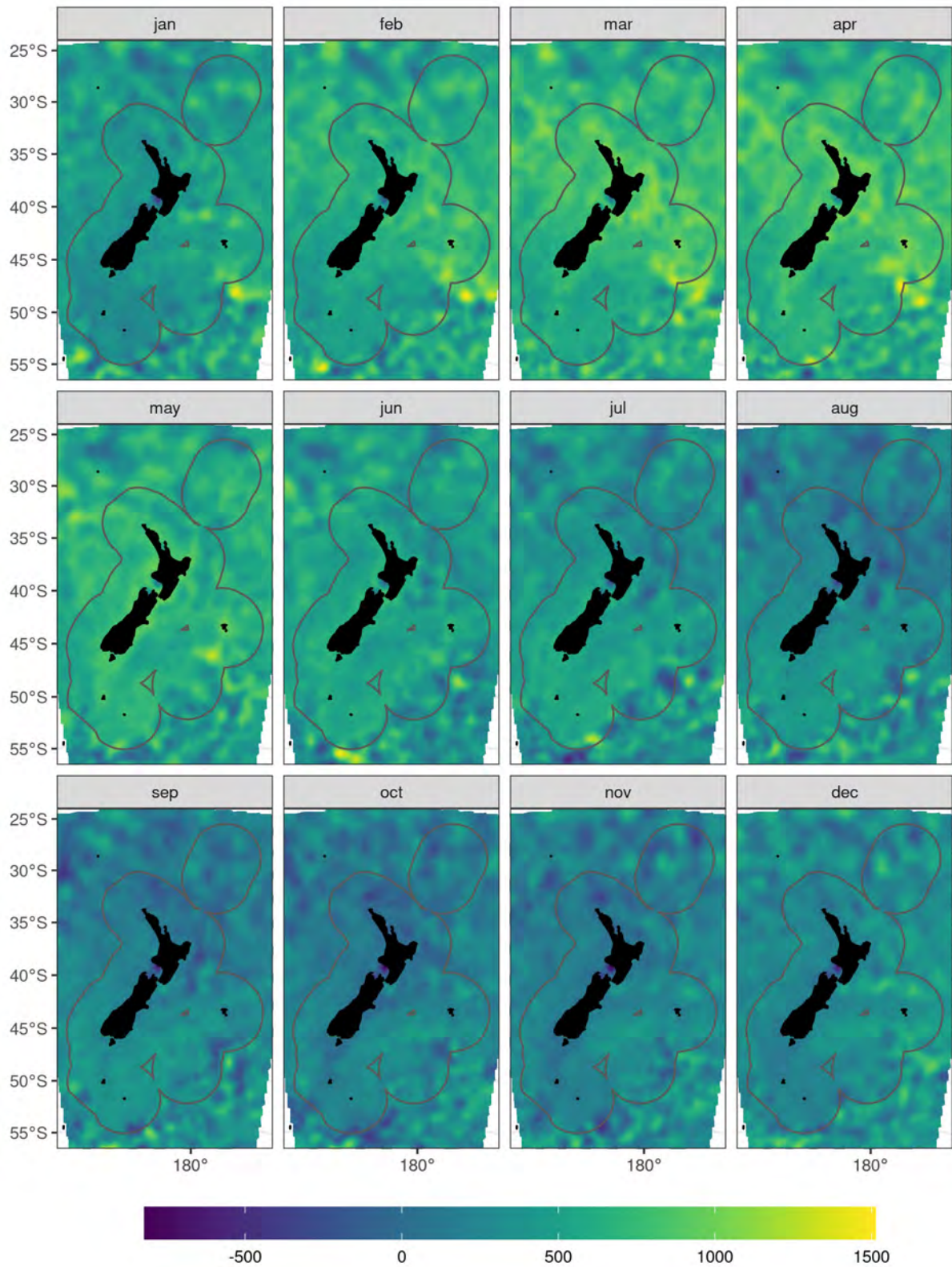


Figure B.5: Mean sea level anomaly (sea surface height above the geoid, in metres) by month. Note that monthly climatologies are shown here, which were used for model predictions, although models were fitted to monthly data in the respective year of observation.

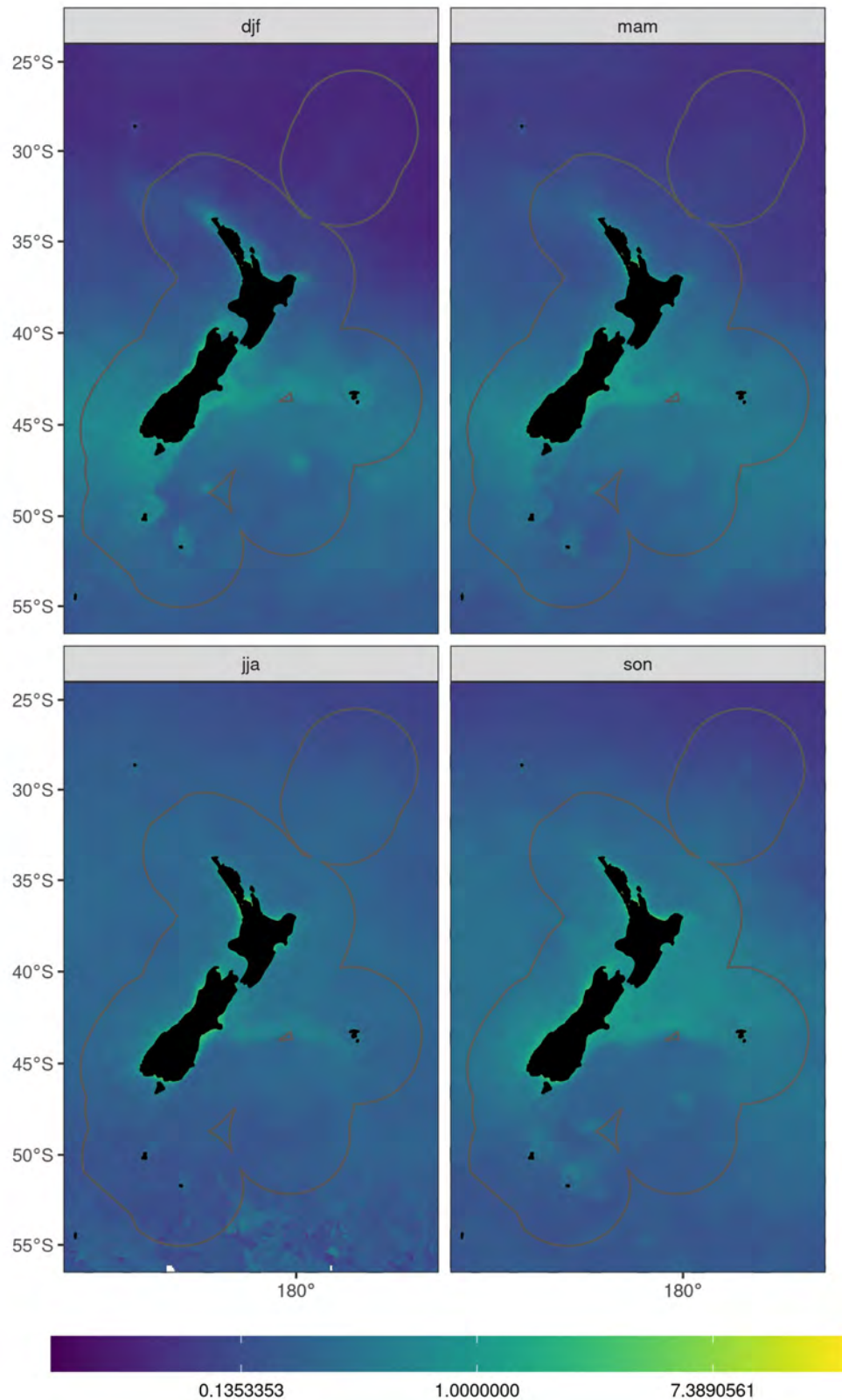


Figure B.6: Mean sea surface chlorophyll-a concentration (mg m^{-3}) by quarter ('djf' = December-February, 'mam' = March-May, 'jja' = June-August, 'son' = September-November). These quarterly climatologies were used for both model fitting and prediction.

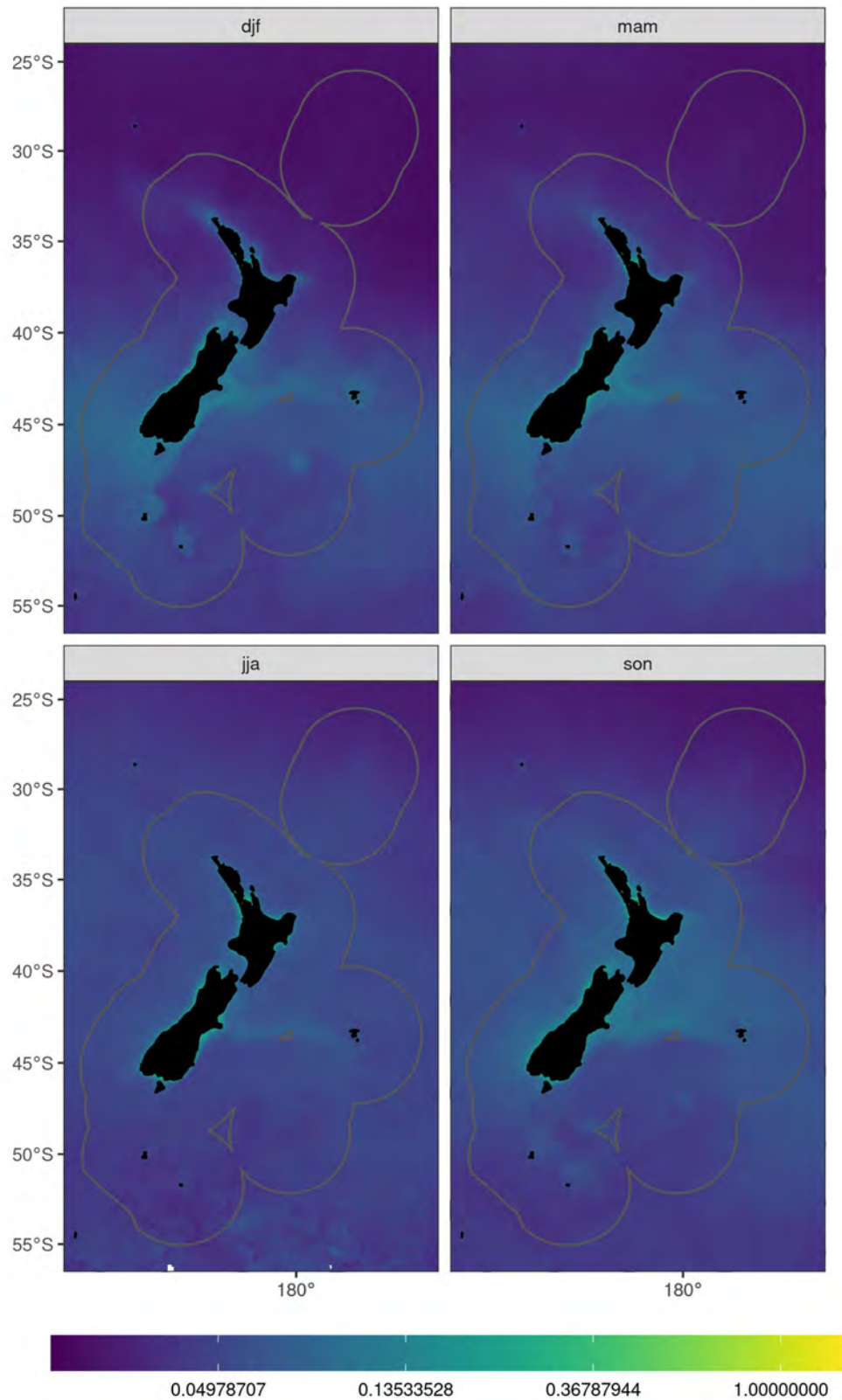


Figure B.7: Mean sea surface turbidity (diffuse attenuation coefficient for downwelling irradiance at 490 nm, 1 m^{-1}) by quarter ('djf' = December-February, 'mam' = March-May, 'jja' = June-August, 'son' = September-November). These quarterly climatologies were used for both model fitting and prediction.

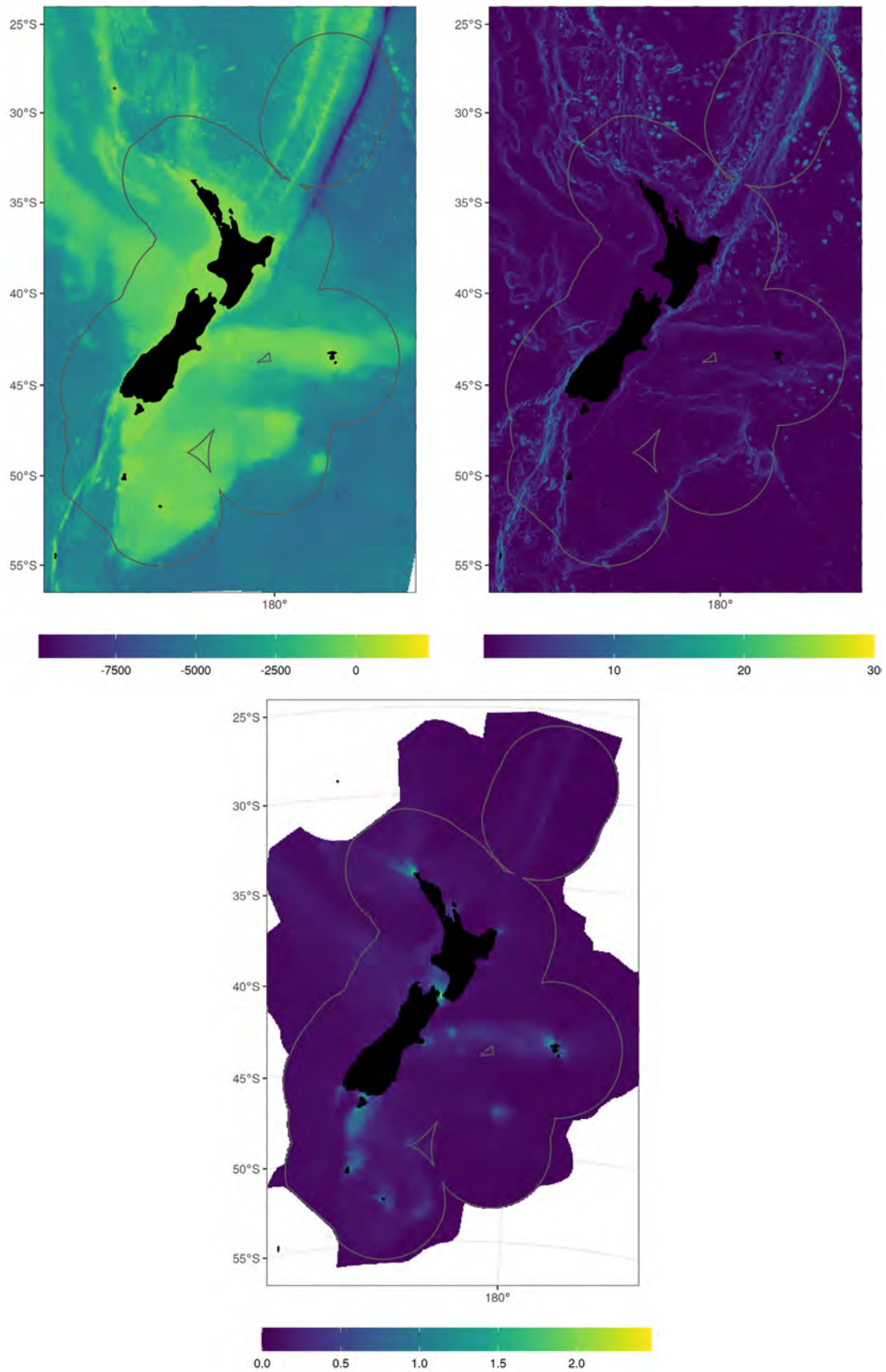


Figure B.8: Bathymetric depth (m) [top-left], bathymetric slope (%) [top-right], and tidal current speed (m s^{-1}) [bottom].

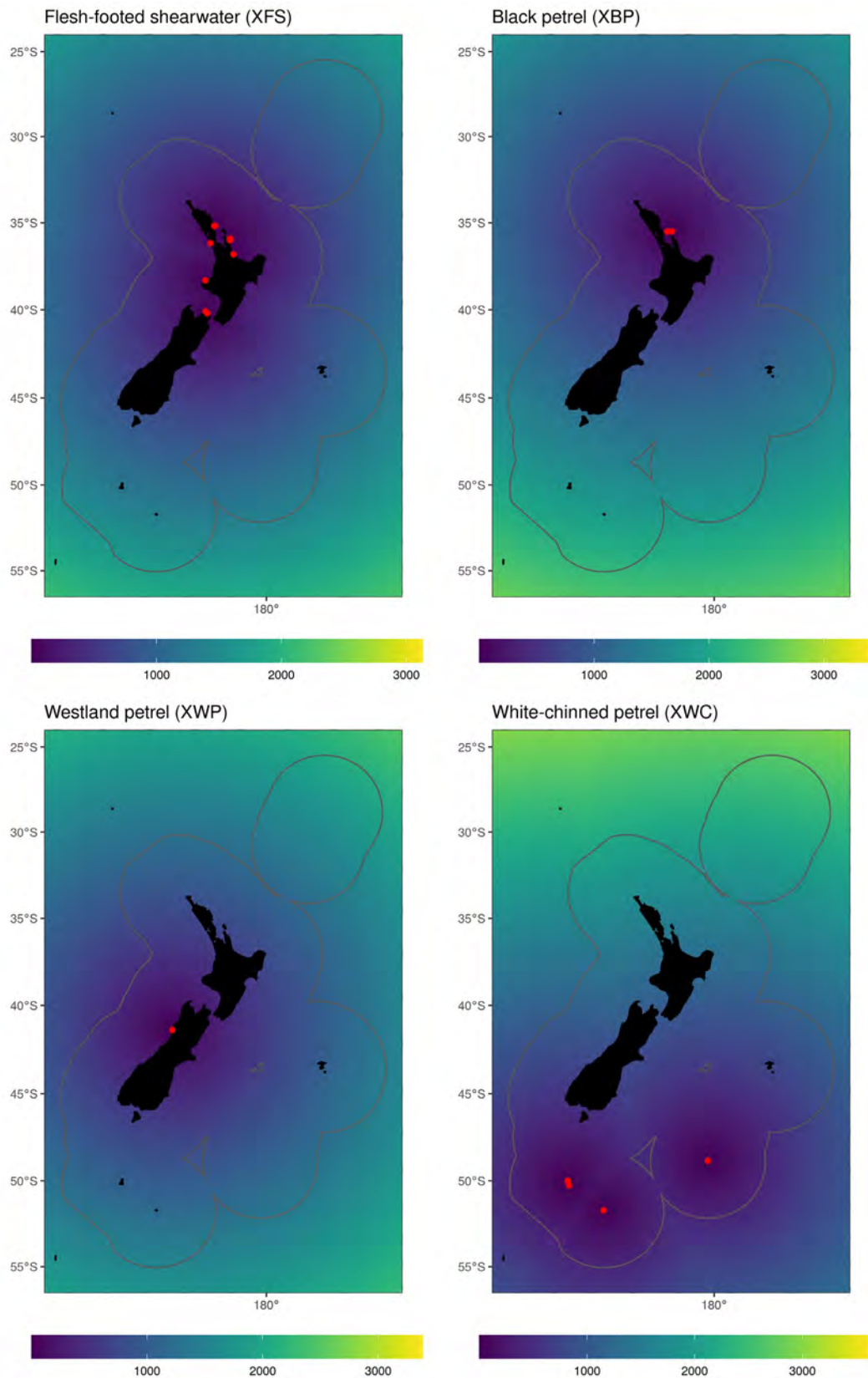


Figure B.9: Distance from colony (km) for flesh-footed shearwater [top-left], black petrel [top-right], Westland petrel [bottom-left], and white-chinned petrel [bottom-right]. The red points indicate the locations of each of the colonies.

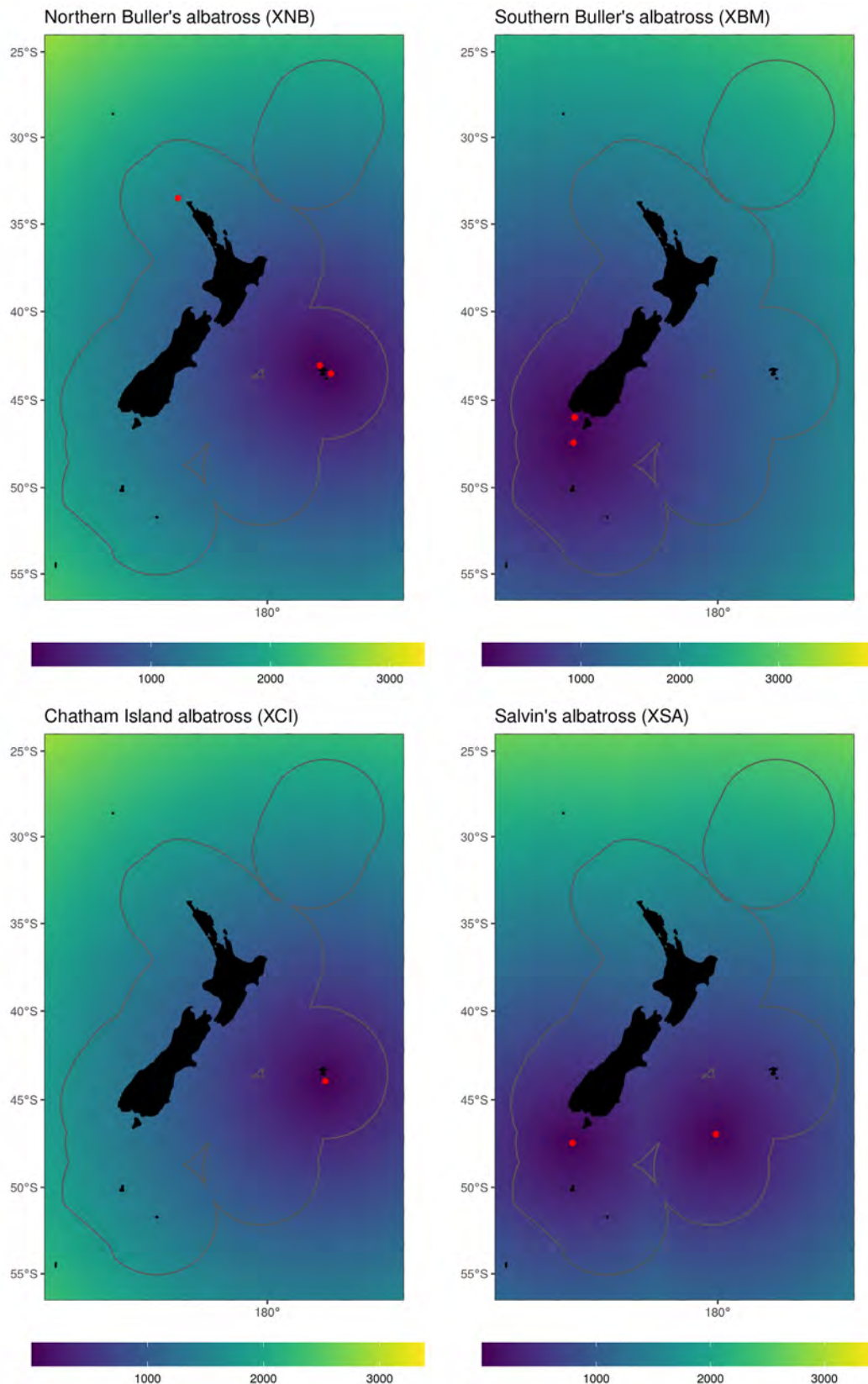


Figure B.10: Distance from colony (km) for Northern and Southern Buller's albatross [top-left and top-right], Chatham Island albatross [bottom-left], and Salvin's albatross [bottom-right]. The red points indicate the locations of each of the colonies, only including colonies that comprise at least 1% of the total breeding population.

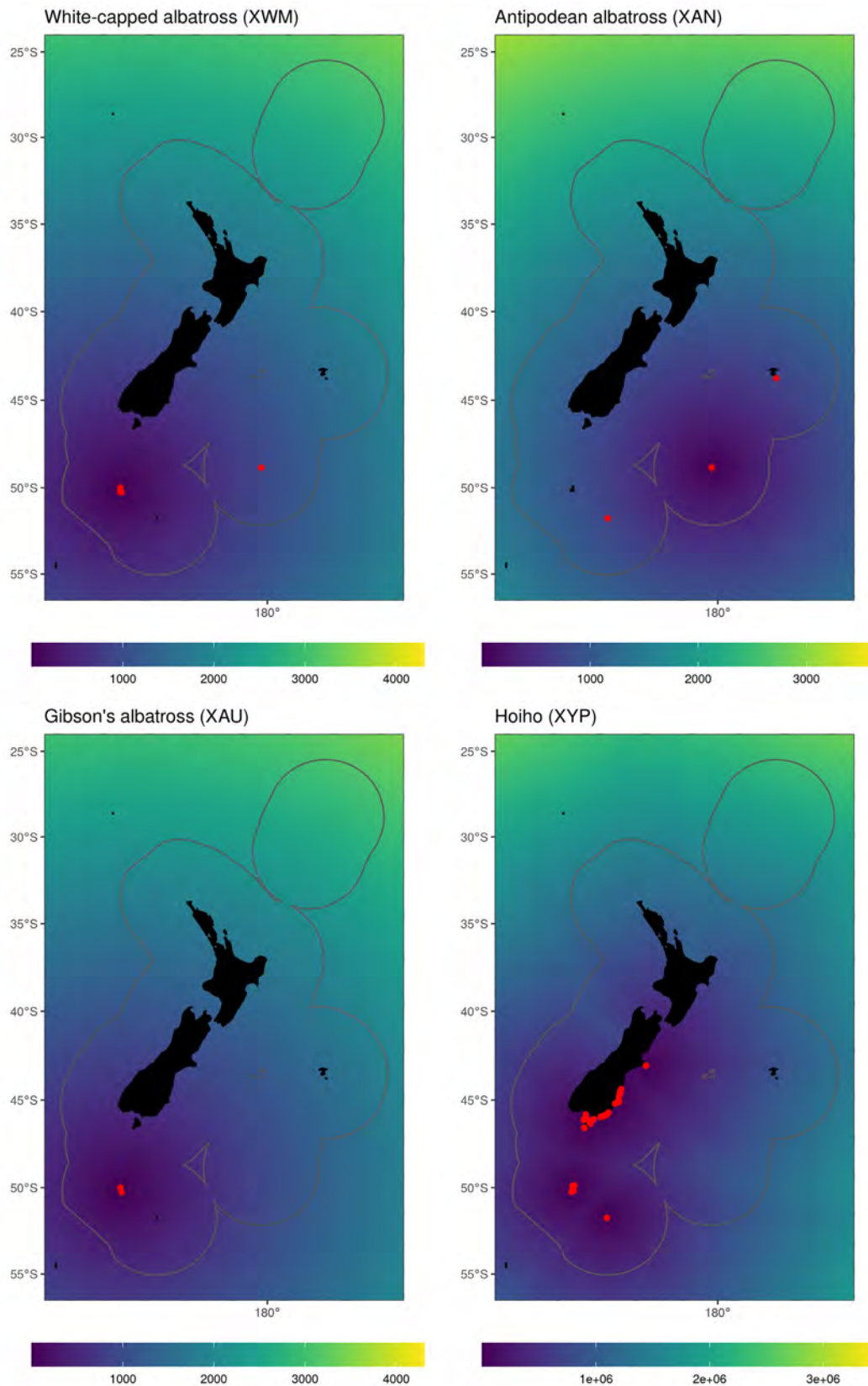


Figure B.11: Distance from colony (km) for white-capped albatross [top-left], Antipodean albatross [top-right], Gibson's albatross [bottom-left], and yellow-eyed penguin [bottom-right]. The red points indicate the locations of each of the colonies, only including colonies that comprise at least 1% of the total breeding population (except for yellow-eyed penguin, for which all known breeding sites are shown).

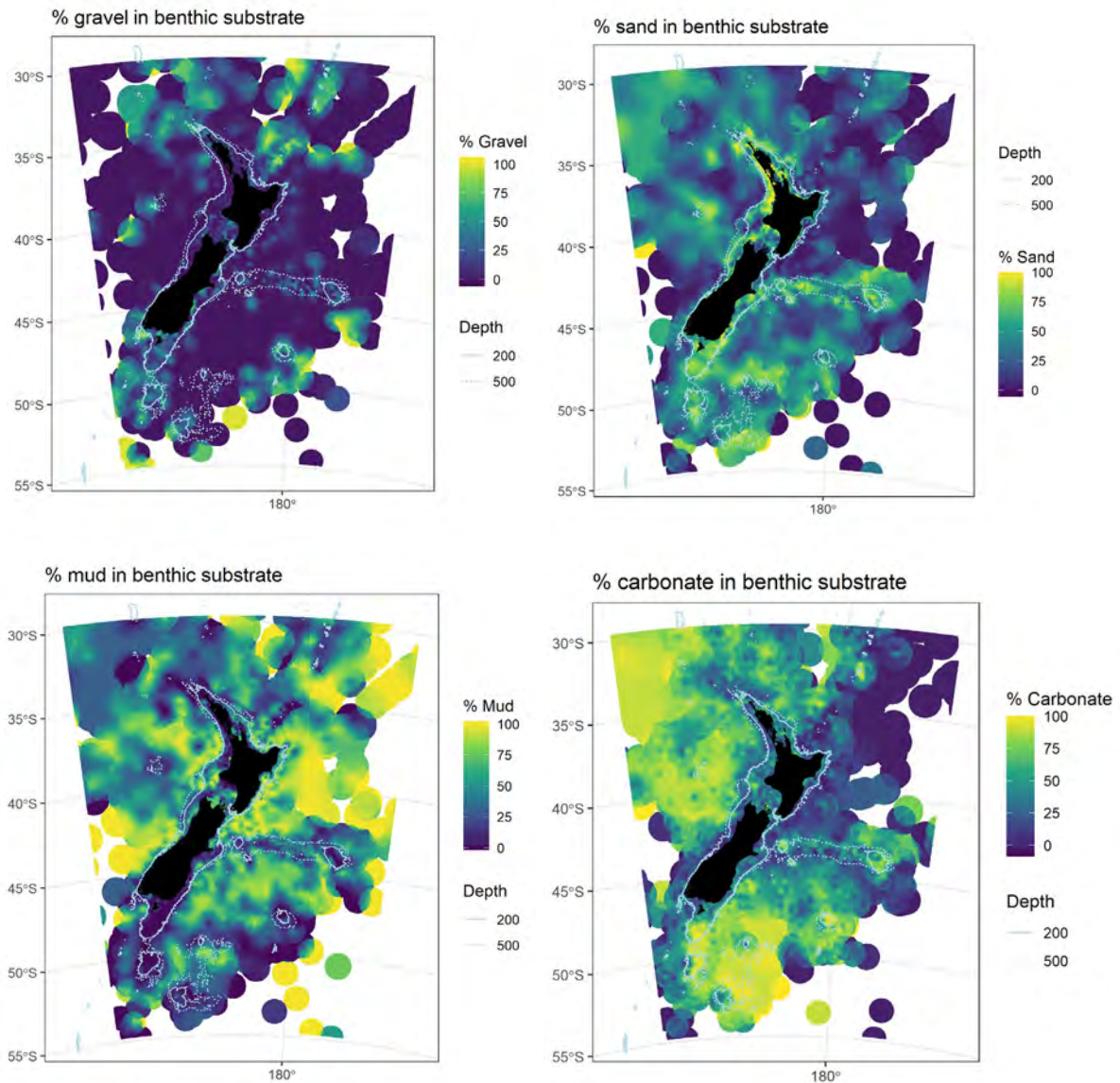


Figure B.12: Percentage sand, gravel, mud, and carbonate in benthic surface sediments. Offered to yellow-eyed penguin models only.

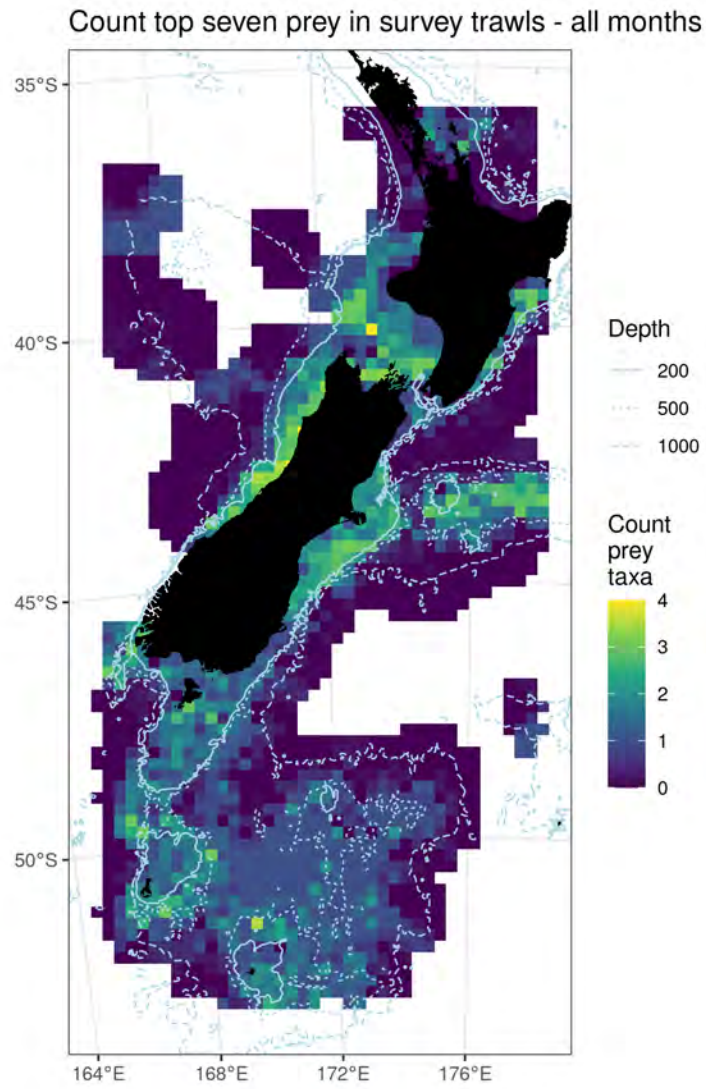


Figure B.13: Count of top seven prey taxa of yellow-eyed penguin in survey bottom trawls.

APPENDIX C. SEABIRD TRACKING DATA SUMMARIES

Flesh-footed shearwater

The tracking data for this species were sourced from several researchers (Table C.1). Susan Waugh provided the earlier GPS data from colonies on Lady Alice Island, Titi Island, and Ohinau Island, including breeding stage. Graeme Taylor at DOC provided GLS data from Bethells Beach, and Patrick Crowe at Wildlife Management International Limited (WMIL) provided recent GPS data from Lady Alice and Ohinau Islands.

Fieldwork and data analysis has been described in a series of reports to DOC and published in journals (Crowe 2018, 2020; Kirk et al. 2017; Rayner et al. 2011; Waugh et al. 2014, 2016). Similar work has been carried out on populations in Australia (Reid et al. 2013; Thalmann et al. 2009).

Table C.1: Flesh-footed shearwater tracking data expressed as the count of bird-days by month and year for which locations were collected. Colony: BB = Bethells Beach, LA = Lady Alice Island, T = Titi Island, O = Ohinau Island. Breeding stage: I = incubation, C = chick-rearing, NB = non-breeding, nd = no data. Source: DOC = Department of Conservation, SW = Susan Waugh, WMIL = Wildlife Management International Limited.

Colony	Year	Tag type	Raw GLS	Sex	Stage	Month												Source
						Jan	Feb	Mar	Apr	May	Jun	Jul	Aug	Sep	Oct	Nov	Dec	
BB	2010	GLS	-	nd	nd	31	53	62	60	62	60	62	62	60	58	58	76	DOC
BB	2011	GLS	Yes	nd	nd	103	153	193	175	185	172	182	194	185	164	180	124	DOC
BB	2012	GLS	Yes	nd	nd	66	101	123	91	93	89	89	91	86	88	85	23	DOC
LA	2012	GPS	Yes	nd	nd	5	0	0	0	0	0	0	0	0	0	0	0	SW
T	2013	GPS	-	nd	I	10	0	0	0	0	0	0	0	0	0	0	0	SW
O	2014	GPS	-	nd	I	238	88	0	0	0	0	0	0	0	0	0	0	SW
LA	2017	GPS	-	nd	I, C, NB	2	184	0	0	0	0	0	0	0	0	0	0	WMIL
LA	2018	GPS	-	Yes	nd	168	1	0	0	0	0	0	0	0	0	0	0	WMIL
LA	2020	GPS	-	Yes	nd	240	249	33	0	0	0	0	0	0	0	0	0	WMIL
O	2020	GPS	-	Yes	nd	257	182	0	0	0	0	0	0	0	0	0	0	WMIL

Black petrel

All tracking data for this species were provided by Biz Bell at WMIL (Table C.2). For some GPS data, additional calculated fields were available. GLS data were provided as calculated positions, and some later files had additional light level information included. Tag files included band number and sex (where determined) and metadata included breeding stage.

Fieldwork and data analysis to date has been described in a series of reports for DOC and lately Fisheries New Zealand as well as published in a journal (Abraham et al. 2016; Bell et al. 2006, 2008, 2013, 2014, 2018; Freeman et al. 2010).

Table C.2: **Black petrel tracking data expressed as the count of bird-days by month and year for which locations were collected. Colony: GB = Great Barrier Island. Breeding stage: I = incubation, C = chick-rearing, M = migration, S = successful breeder, F = failed breeder. Source: WMIL = Wildlife Management International Limited.**

Colony	Year	Tag type	Raw GLS	Sex	Stage	Month												Source		
						Jan	Feb	Mar	Apr	May	Jun	Jul	Aug	Sep	Oct	Nov	Dec			
GB	2005	GLS	No	Yes	I	0	0	0	0	0	0	0	0	0	0	0	0	179	WMIL	
GB	2006	GLS	No	Yes	I	73	0	0	0	0	0	0	0	0	0	0	0	0	0	WMIL
GB	2007	GLS	No	Yes	I, C, M	27	0	0	0	0	0	0	0	0	0	0	0	134	WMIL	
GB	2008	GLS	No	Yes	I, C, M	266	339	394	379	375	344	336	221	227	125	210	146	WMIL		
GB	2009	GLS	No	Yes	I, C, M	141	116	131	149	155	150	155	155	112	154	144	546	WMIL		
GB	2010	GLS	No	Yes	I, C	612	36	0	0	0	0	0	0	0	0	0	0	0	WMIL	
GB	2012	GPS	—	Yes	I, C	1	0	0	0	0	0	0	0	0	0	0	0	4	WMIL	
GB	2013	GPS	—	Yes	I, C	3	53	0	0	0	0	0	0	0	0	0	0	0	WMIL	
GB	2014	GPS	—	Yes	I, C	26	37	0	0	0	0	0	0	0	0	0	0	0	WMIL	
GB	2018	GPS	—	Yes	C	0	0	284	7	0	0	0	0	0	0	0	0	0	WMIL	
GB	2018	GLS	Yes	Yes	S, F	0	0	649	1280	1239	1304	1334	1312	1239	1112	1038	900	WMIL		
GB	2019	GLS	Yes	Yes	S, F	340	0	0	0	0	0	0	0	0	0	0	0	0	WMIL	

Westland petrel

Earlier PTT data were sourced through BirdLife International's seabird tracking database and released by David Nicholls and Amanda Freeman. GLS data were provided by Todd Landers, with original tag files. GPS data, including breeding stage, were provided by Susan Waugh and Timothy Poupart (Table C.3).

Fieldwork and data analysis are described in several publications (Freeman 1997, Freeman & Wilson 1997; Freeman et al. 1997, 2001; Landers et al. 2011; Poupart et al. 2020; Waugh et al. 2018).

Table C.3: Westland petrel tracking data expressed as the count of bird-days by month and year for which locations were collected. Colony: P = Punakaiki. Breeding stages: PG = post-guard, PE = pre-egg, I = incubation, C = chick-rearing, B = breeding, NB = non-breeding. Source: BL = BirdLife International, SW = Susan Waugh, TL = Todd Landers, TP = Timothy Poupart.

Colony	Year	Tag type	Raw GLS	Sex	Stage	Month												Source
						Jan	Feb	Mar	Apr	May	Jun	Jul	Aug	Sep	Oct	Nov	Dec	
P	1995	PTT	—	Yes	PG	0	0	0	0	0	0	0	33	18	0	0	0	BL
P	1996	PTT	—	Yes	PG	0	0	0	0	0	0	0	74	4	0	0	0	BL
P	2007	GLS	Yes	Yes	B, NB	0	0	0	0	0	0	81	139	87	247	240	248	TL
P	2008	GLS	Yes	Yes	B, NB	248	231	248	182	181	138	329	430	448	464	448	462	TL
P	2009	GLS	Yes	Yes	B, NB	463	419	455	372	390	256	337	86	20	21	0	0	TL
P	2011	GPS	—	Yes	PE, I,	0	0	0	68	8	27	44	0	0	0	0	0	SW
P	2012	GPS	—	Yes	I, C	0	0	0	0	0	40	2	10	114	0	0	0	SW
P	2015	GPS	—	Yes	I, C	0	0	0	0	0	107	56	0	35	0	0	0	SW
P	2016	GPS	—	Yes	I, C	0	0	0	0	0	0	122	53	0	0	0	0	SW
P	2017	GPS	—	Yes	PG	0	0	0	0	0	0	0	60	0	0	0	0	TP

White-chinned Petrel

The GLS data used by this assessment were collected from birds instrumented during 2008–2009 at the Antipodes Islands, which were sourced from the BirdLife International database, via DOC (Table C.4). Note that GLS data were collected from birds at the Auckland Islands (Table 1, Rexer-Huber 2017), although these were provided as raw light data files and were not used by this analysis.

Table C.4: White-chinned petrel tracking data expressed as the count of bird-days by month and year for which locations were collected. Colony: AN = Antipodes Islands. Breeding stage: B = breeding, NB = non-breeding. Source: BL = BirdLife International.

Colony	Year	Tag type	Raw GLS	Sex	Stage	Month												Source
						Jan	Feb	Mar	Apr	May	Jun	Jul	Aug	Sep	Oct	Nov	Dec	
AN	2008	GLS	No	No	B, NB	46	242	177	255	340	341	324	304	95	145	204	147	BL
AN	2009	GLS	No	No	B	122	3	0	0	0	0	0	0	0	0	0	0	BL

Northern and Southern Buller's albatross

The tracking data for Northern and Southern Buller's albatross were sourced through BirdLife International and released by Henri Weimerskirch, Lorna Deppe, Paul Sagar, Leigh Torres, Jean-Claude Stahl, and via DOC (Table C.5). Fieldwork and data analysis are described in several publications (Broekhuizen et al. 2003; Poupart et al. 2019; Sagar & Weimerskirch 1996; Stahl & Sagar 2000, 2006).

Table C.5: Northern and Southern Buller's albatross (combined) tracking data expressed as the count of bird-days by month and year for which locations were collected. Colony: SN = Snares Islands, SO = Solander Islands (both Southern Buller's albatross), CH = Chatham Islands (Northern Buller's albatross). Breeding stage: BG = brood-guard, PG = post-guard, PE = pre-egg, I = incubation, M = migration, B = breeding, NB = non-breeding. Source: BL = BirdLife International.

Colony	Year	Tag type	Raw GLS	Sex	Stage	Month												Source	
						Jan	Feb	Mar	Apr	May	Jun	Jul	Aug	Sep	Oct	Nov	Dec		
SN	1995	PTT	-	Yes	I	0	20	44	0	0	0	0	0	0	0	0	0	0	BL
SN	1995	PTT	-	Yes	I	0	20	43	0	0	0	0	0	0	0	0	0	0	BL
SN	1996	PTT	-	Yes	I, BG, PG	0	0	173	146	94	129	72	0	0	0	0	0	0	BL
SN	1997	PTT	-	Yes	I	0	0	52	0	0	0	0	0	0	0	0	0	0	BL
SO	1997	PTT	-	Yes	I, BG, PG, M	0	5	125	119	73	130	30	0	0	0	0	0	0	BL
SN	1999	PTT	-	Yes	I, BG, PG	0	2	130	151	84	35	2	0	0	0	0	0	0	BL
SN	2000	PTT	-	Yes	NB	0	20	145	79	0	0	0	0	0	0	0	0	0	BL
SN	2001	PTT	-	Yes	PE	0	0	0	0	7	115	81	4	0	0	0	0	59	BL
SN	2002	PTT	-	Yes	PE, I, M	137	86	0	0	0	0	0	0	0	0	0	0	0	BL
SO	2002	PTT	-	Yes	NB	0	34	169	129	76	89	41	0	0	0	0	0	0	BL
CH	2008	GPS	-	Nd	I	0	0	0	0	0	0	0	0	0	0	0	11	0	BL
SN	2008	GPS	-	Yes	BG	0	0	0	28	0	0	0	0	0	0	0	0	0	BL
SN	2008	GLS	No	Yes	B, NB	0	0	0	260	622	633	654	654	162	588	641	663	BL	
SN	2009	GPS	-	Yes	BG	0	0	0	63	0	0	0	0	0	0	0	0	0	BL
SN	2009	GLS	No	Yes	B, NB	591	380	143	191	373	356	389	394	103	323	387	387	BL	
SN	2010	GPS	-	Yes	BG	0	0	0	77	0	0	0	0	0	0	0	0	0	BL
SN	2010	GLS	No	Yes	I	0	20	44	0	0	0	0	0	0	0	0	0	0	BL
SN	2011	GPS	-	Yes	BG	0	0	0	71	8	0	0	0	0	0	0	0	0	BL

Chatham Island albatross

The tracking data for Chatham Island albatross were sourced through BirdLife International and released by Chris Robertson, David Nicholls, Lorna Deppe, David Thompson, Paul Schofield and Susan Waugh, and have been published (Deppe et al. 2014) (Table C.6).

Table C.6: Chatham Island albatross tracking data expressed as the count of bird-days by month and year for which locations were collected. Colony: CH = Chatham Islands. Breeding stage: B = breeding, NB = non-breeding, C = chick rearing. Source: BL = BirdLife International.

Colony	Year	Tag type	Raw GLS	Sex	Stage	Month												Source
						Jan	Feb	Mar	Apr	May	Jun	Jul	Aug	Sep	Oct	Nov	Dec	
CH	1997	PTT	–	Yes	B, NB	0	12	31	29	30	7	0	0	0	12	26	27	BL
CH	1998	PTT	–	Yes	B, NB	29	29	42	45	49	52	50	25	0	0	213	249	BL
CH	1999	PTT	–	Yes	B, NB	218	186	76	28	11	11	43	9	0	0	0	0	BL
CH	2006	GLS	No	Yes	C	8	11	0	0	0	0	0	0	0	0	0	0	BL
CH	2008	GLS	No	Yes	NB	3	95	202	421	456	398	202	12	0	0	0	0	BL
CH	2008	GLS	No	Yes	B	0	0	0	0	0	0	0	0	0	0	133	2	BL

Salvin's albatross

The PTT Salvin's albatross tracking data were sourced from the DOC albatross tracker web page (Table C.7). Raw GLS data were received from David Thompson, and processed positions were supplied from the BirdLife International database, via DOC. These data are described in reports to DOC (Sagar et al. 2018; Thompson et al. 2014, 2020).

Table C.7: Salvin's albatross tracking data expressed as the count of bird-days by month and year for which locations were collected. Colony: SN = Snares Islands, BO = Bounty Islands. Breeding stage: B = breeding, NB = non-breeding, nd = no data. Source: BL = BirdLife International, DOC = Department of Conservation.

Colony	Year	Tag type	Raw GLS	Sex	Stage	Month												Source
						Jan	Feb	Mar	Apr	May	Jun	Jul	Aug	Sep	Oct	Nov	Dec	
SN	2008	GLS	Yes	nd	B, NB	0	0	0	0	0	0	0	0	0	305	545	656	BL
SN	2009	GLS	Yes	nd	B, NB	637	554	314	451	587	607	613	464	155	77	30	30	BL
SN	2010	GLS	Yes	nd	B, NB	28	23	15	14	30	30	29	31	9	0	0	0	BL
BO	2018	PTT	–	nd	nd	0	0	0	0	0	0	0	0	0	138	358	366	DOC
BO	2019	PTT	–	nd	nd	330	227	156	97	25	21	10	0	0	29	120	118	DOC
BO	2020	PTT	–	nd	nd	92	58	33	9	0	0	0	0	0	0	0	0	DOC
BO	2019	GPS	–	nd	nd	0	0	0	0	0	0	0	0	0	91	352	346	DOC
BO	2020	GPS	–	nd	nd	313	189	104	63	0	0	0	0	0	0	0	0	DOC

White-capped albatross

For white-capped albatross, David Thompson supplied some raw GLS data, and some of the published GPS data (Torres et al. 2011). Other tracking data, from the BirdLife International database, were supplied by DOC (Table C.8). The relevant fieldwork and data processing methods are described across several reports (Rexer-Huber et al. 2020; Thompson et al. 2009; Thompson & Sagar 2006, 2008).

Table C.8: White-capped albatross tracking data expressed as the count of bird-days by month and year for which locations were collected. Colony: SWC = Southwest Cape, DI = Disappointment Island, AI = Auckland Islands. Breeding stage: B = breeding, NB = non-breeding, BG = brood guard, PG = post-guard. Source: BL = BirdLife International, DT = David Thompson.

Colony	Year	Tag type	Raw GLS	Sex	Stage	Month												Source
						Jan	Feb	Mar	Apr	May	Jun	Jul	Aug	Sep	Oct	Nov	Dec	
SWC	2006	GPS	–	nd	nd	0	124	0	0	0	0	0	0	0	0	0	0	DT
DI	2006	GLS	Yes	nd	B, NB	0	166	210	163	269	274	296	260	82	187	214	213	BL
DI	2007	GLS	Yes	nd	B, NB	240	236	187	262	408	415	434	401	141	291	255	322	BL
DI	2008	GLS	Yes	nd	B, NB	311	308	184	232	337	322	316	265	79	174	160	37	BL
DI	2009	GLS	Yes	nd	B, NB	31	28	20	26	31	30	31	26	3	5	19	28	BL
DI	2010	GLS	Yes	nd	B, NB	27	21	0	0	0	0	0	0	0	0	0	0	BL
AI	2006	PTT	–	Yes	BG, PG	0	82	0	0	0	0	0	0	0	0	0	0	BL
AI	2007	PTT	–	Yes	BG, PG, NB	0	0	31	152	45	22	4	0	0	0	0	0	BL
AI	2008	PTT	–	nd	I	0	0	0	0	0	0	0	0	0	0	0	179	BL
AI	2009	PTT	–	nd	I, BG, PG, NB	134	166	168	42	0	0	0	0	0	0	0	0	BL

Antipodean albatross

For Antipodean albatross, the GLS data were collected by Graeme Elliott and Kath Walker and processed by and sourced from DOC. PTT data were sourced from Graeme Elliott, including some data owned by Fisheries New Zealand and DOC. David Nicholls collected the early PTT data and this was sourced through BirdLife International, but duplicated in the data set from Graeme Elliott (Table C.9). The fieldwork and data processing methods are described across several reports (Elliott & Walker 2017, 2020; Hamilton et al. 2002; Walker et al. 2002; Walker & Elliott 2002a, 2006, 2019).

Table C.9: Antipodean albatross tracking data expressed as the count of bird-days by month and year for which locations were collected. Breeding stage was not available for all data points and in some cases was inferred from timing and flight paths. Colony: AN = Antipodes Islands. Breeding stage: B = breeding, NB = non-breeding, N = nester, FB = failed breeder, BOG = bird on ground, D = deserted, I = incubation, PB = post breeding, H/G = hatch/guard, C = chick rearing, nd = no data. Source: BL = BirdLife International, DOC = Department of Conservation.

Colony	Year	Tag type	Raw GLS	Sex	Stage	Month												Source
						Jan	Feb	Mar	Apr	May	Jun	Jul	Aug	Sep	Oct	Nov	Dec	
AN	1996	PTT	-	Yes	D, I, PB	82	264	93	41	14	14	13	13	13	13	12	11	DN
AN	1997	PTT	-	Yes	D, H/G, I, PB	46	70	64	42	28	22	7	0	0	0	0	0	DN
AN	1998	PTT	-	Yes	I, H/G, C, D	0	23	175	133	39	15	0	0	0	0	0	0	GE
AN	1999	PTT	-	Yes	I, H/G, C	13	176	265	193	175	33	0	0	0	0	0	0	GE
AN	2000	PTT	-	Yes	I, H/G, C, D	32	179	210	179	165	134	88	112	123	102	86	92	GE
AN	2001	PTT	-	Yes	C	16	9	0	0	0	0	0	0	0	0	0	0	GE
AN	2002	PTT	-	Yes	nd	0	0	0	0	0	0	0	0	0	0	18	0	GE
AN	2003	PTT	-	Yes	C, NB	0	17	87	55	49	37	33	27	18	0	0	29	GE
AN	2004	PTT	-	Yes	FF, NB	72	85	92	86	88	82	69	79	47	45	27	21	GE
AN	2005	PTT	-	Yes	FF, NB	11	8	0	0	0	0	0	0	0	0	0	0	GE
AN	2018	PTT	-	Yes	NB	0	0	0	0	0	0	0	0	0	1	0	0	GE
AN	2019	PTT	-	Yes	I, FF, H/G, NB	918	1588	1556	1306	1019	770	684	706	551	376	312	293	GE
AN	2020	PTT	-	Yes	nd	225	16	534	1175	1112	1039	960	716	100	0	0	0	GE
AN	2011	GLS	Yes	Yes	N, FB, BOG	5	308	429	367	412	416	457	426	441	370	375	358	DOC
AN	2012	GLS	Yes	Yes	N, FB, BOG	240	214	278	216	228	248	271	262	276	226	235	243	DOC
AN	2013	GLS	Yes	Yes	N, FB, BOG	68	103	194	174	193	188	198	197	165	138	132	158	DOC
AN	2014	GLS	Yes	Yes	N, FB, BOG	154	31	24	20	29	28	30	28	29	31	30	29	DOC
AN	2015	GLS	Yes	Yes	N, FB, BOG	15	150	213	189	213	206	216	213	206	214	207	216	DOC
AN	2016	GLS	Yes	Yes	N, FB, BOG	182	245	296	278	303	296	302	306	296	291	295	298	DOC
AN	2017	GLS	Yes	Yes	N, FB, BOG	174	209	268	251	271	268	277	268	264	266	256	263	DOC
AN	2018	GLS	Yes	Yes	N, FB, BOG	118	0	0	0	0	0	0	0	0	0	0	0	DOC
AN	2019	PTT	-	Yes	B, NB, FB	693	1307	1230	965	718	488	459	420	330	242	163	173	DOC
AN	2020	PTT	-	Yes	B, NB, FB	106	24	619	1003	807	0	0	0	0	0	0	0	DOC
AN	1996	PTT	-	Yes	NB	9	21	39	38	13	9	11	10	11	11	11	10	BL
AN	1997	PTT	-	Yes	NB	8	1	0	0	0	0	0	0	0	0	0	0	BL

Gibson's albatross

For Gibson's albatross, the tracking data were sourced from Graeme Elliott and included data collected by David Nicholls, which was also sourced through BirdLife International (Table C.10). The relevant fieldwork and data analysis methods have been described across several reports (Elliott & Walker 2014; Rexer-Huber et al. 2020; Walker & Elliott 2002b, 2002c, 2006, 2015).

Table C.10: Gibson's albatross tracking data expressed as the count of bird-days by month and year for which locations were collected. Breeding stage was not available for all data points and in some cases was inferred from timing and flight paths. Colony: AI = Auckland Islands. Breeding stage: B = breeding, NB = non-breeding, nd = no data, D = deserted, I = incubation, PB = post breeding, H/G = hatch/guard, C = chick-rearing. Source: BL = BirdLife International, DOC = Department of Conservation, GE = Graeme Elliott.

Colony	Year	Tag type	Raw GLS	Sex	Stage	Month												Source
						Jan	Feb	Mar	Apr	May	Jun	Jul	Aug	Sep	Oct	Nov	Dec	
AI	1994	PTT	-	Yes	I, C, H/G, PB	4	25	12	11	7	0	0	0	0	0	0	1	GE
AI	1995	PTT	-	Yes	I, PB, D	197	149	0	0	0	0	0	0	0	0	0	0	GE
AI	1999	PTT	-	Yes	I, H/G, D	38	230	197	169	34	19	0	0	0	0	0	0	GE
AI	2000	PTT	-	Yes	I, H/G, C, D	0	87	206	190	153	111	84	40	20	20	15	9	GE
AI	2001	PTT	-	Yes	C, D	8	0	0	0	0	66	127	103	79	45	18	0	GE
AI	2002	PTT	-	Yes	C	25	54	58	59	58	54	55	21	24	32	45	0	GE
AI	2003	PTT	-	Yes	NB	0	27	30	28	29	29	15	0	0	33	7	0	GE
AI	2019	PTT	-	Yes	nd	53	256	197	135	126	118	87	87	41	0	0	0	DOC
AI	2019	PTT	-	Yes	B, NB	63	297	209	142	125	112	76	78	39	0	0	0	DOC
AI	1994	PTT	-	nd	nd	0	0	0	0	0	0	0	22	31	18	0	BL	
AI	1994	PTT	-	Yes	nd	8	37	14	11	7	0	0	0	0	0	0	0	BL
AI	1995	PTT	-	Yes	nd	62	36	0	0	0	0	0	0	0	0	0	0	BL

Yellow-eyed penguin

Yellow-eyed penguin fledgling data were supplied, pre-publication, by Melanie Young, and were collected as part of DOC's Conservation Services Programme (POP2016-05, 2017-2018) (Table C.11).

Table C.11: Fledgling yellow-eyed penguin tracking data expressed as the count of bird-days by month and year for which locations were collected. Sex: nd = no data, Breeding stage: F = fledgling, Source: MY = Melanie Young.

Colony Area	Year	Tag type	Raw GLS	Sex	Stage	Month												Source
						Jan	Feb	Mar	Apr	May	Jun	Jul	Aug	Sep	Oct	Nov	Dec	
Various	2017	PTT	-	nd	F		2	69	30									MY
Various	2028	PTT	-	nd	F		166	436	170									MY

Adult VHF data were sourced from Bruce McKinlay at DOC and methods have been published by Moore et al. (1995). Adult GPS data were sourced from Thomas Mattern and were collected under a project for DOC's Conservation Services Programme (POP2018-02) and is described by Mattern (2020) (Table C.12).

Table C.12: Adult yellow-eyed penguin tracking data expressed as the count of bird-days by month and year for which locations were collected. Sex: nd = no data, Breeding stage: W = winter, I = incubation, CG = chick-guard, PG = post guard, PM = pre moult, Source: BM = Bruce McKinlay, TM = Thomas Mattern.

Colony Area	Year	Tag type	Raw GLS	Sex	Stage	Month												Source	
						Jan	Feb	Mar	Apr	May	Jun	Jul	Aug	Sep	Oct	Nov	Dec		
Otago	1990	VHF	-	nd	nd													8	BM
Otago	1990	VHF	-	nd	nd	344												8	BM
Otago	1990	VHF	-	nd	nd	380			12	1	12	1	1						BM
Otago	1990	VHF	-	nd	nd	195			8	344	8	380	195						BM
Catlins	1990	VHF	-	nd	nd		86												BM
Catlins	1990	VHF	-	nd	nd		84												BM
Various	2018	GPS	-	Yes	W I CG PG PM													15	TM
Various	2019	GPS	-	Yes	W I CG PG PM	4	61	18		19		22	22		5	3	33		TM
Various	2020	GPS	-	Yes	W I CG PG PM	94	57	21		51	19	6	9						TM

APPENDIX D. FINAL SEABIRD DATA SUMMARIES

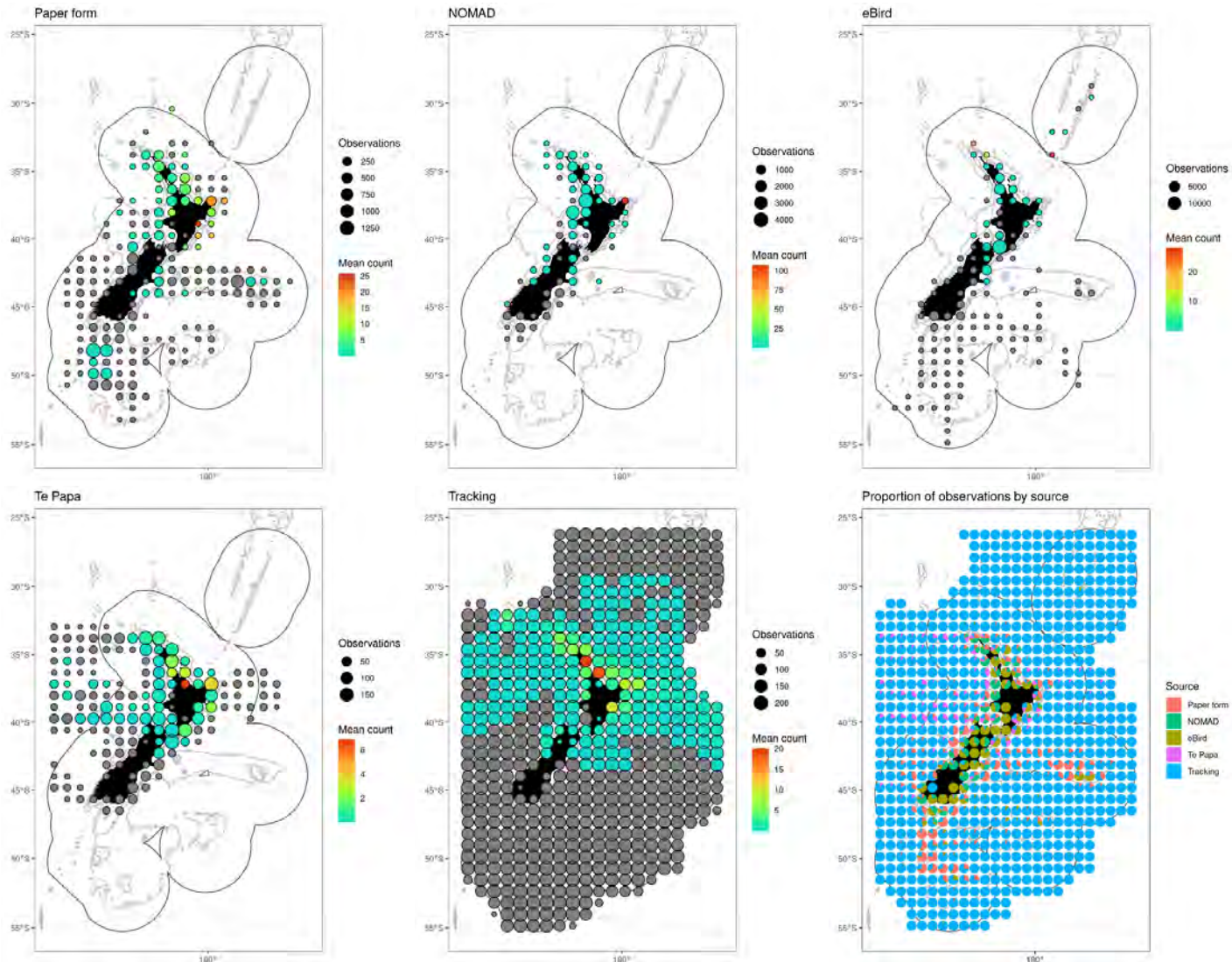


Figure D.1: Spatially explicit mean count of flesh-footed shearwater by data source for the paper form, Nomad, eBird, Te Papa, and tracking data sources. Grey circles represent a mean count of zero, and each circle's size is scaled by the number of observations represented by that circle. The bottom right panel shows the spatial proportion of data for each data source.

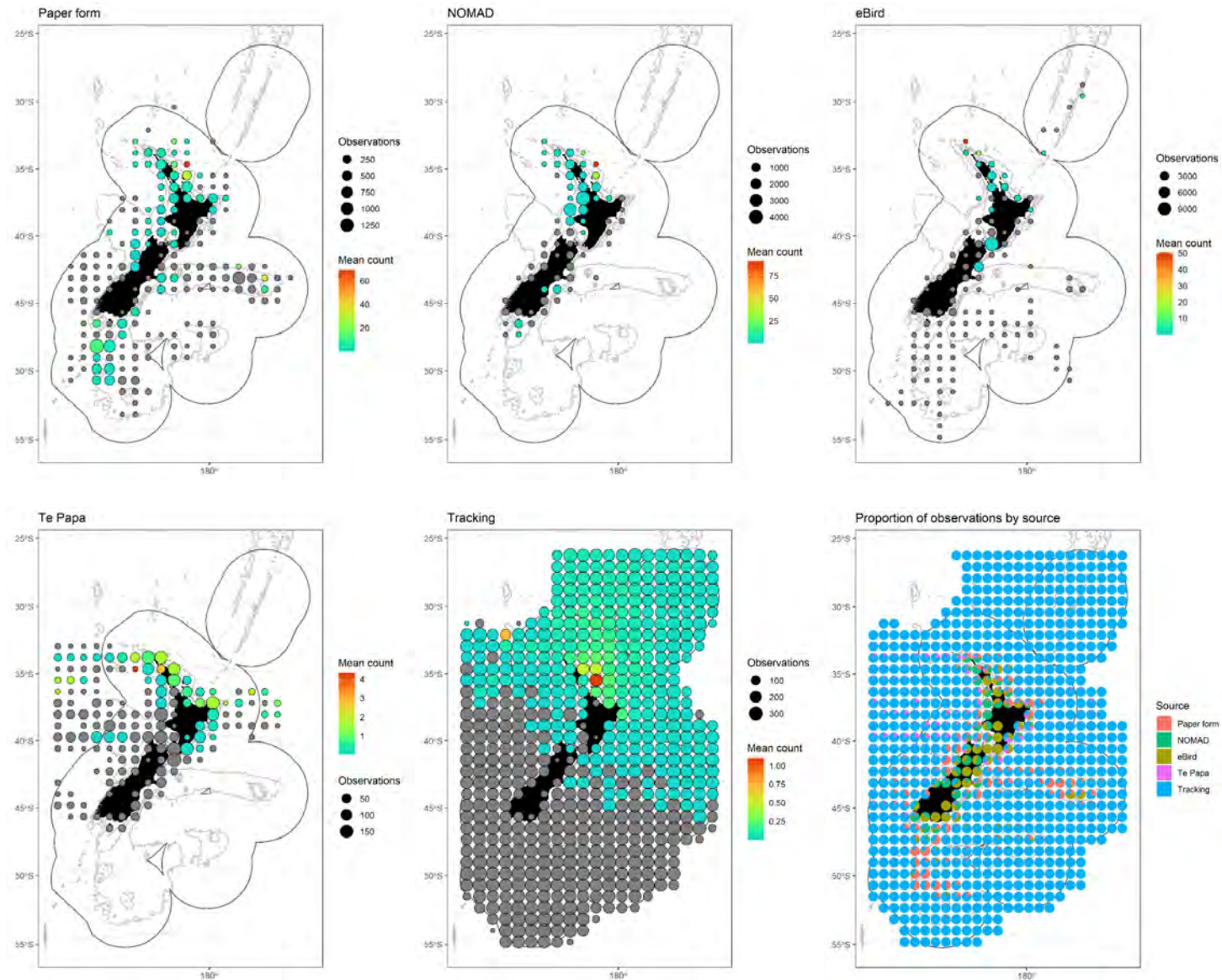


Figure D.2: Spatially explicit mean count of black petrel by data source for the paper form, Nomad, eBird, Te Papa, and tracking data sources. Grey circles represent a mean count of zero, and each circle's size is scaled by the number of observations represented by that circle. The bottom right panel shows the spatial proportion of data for each data source.

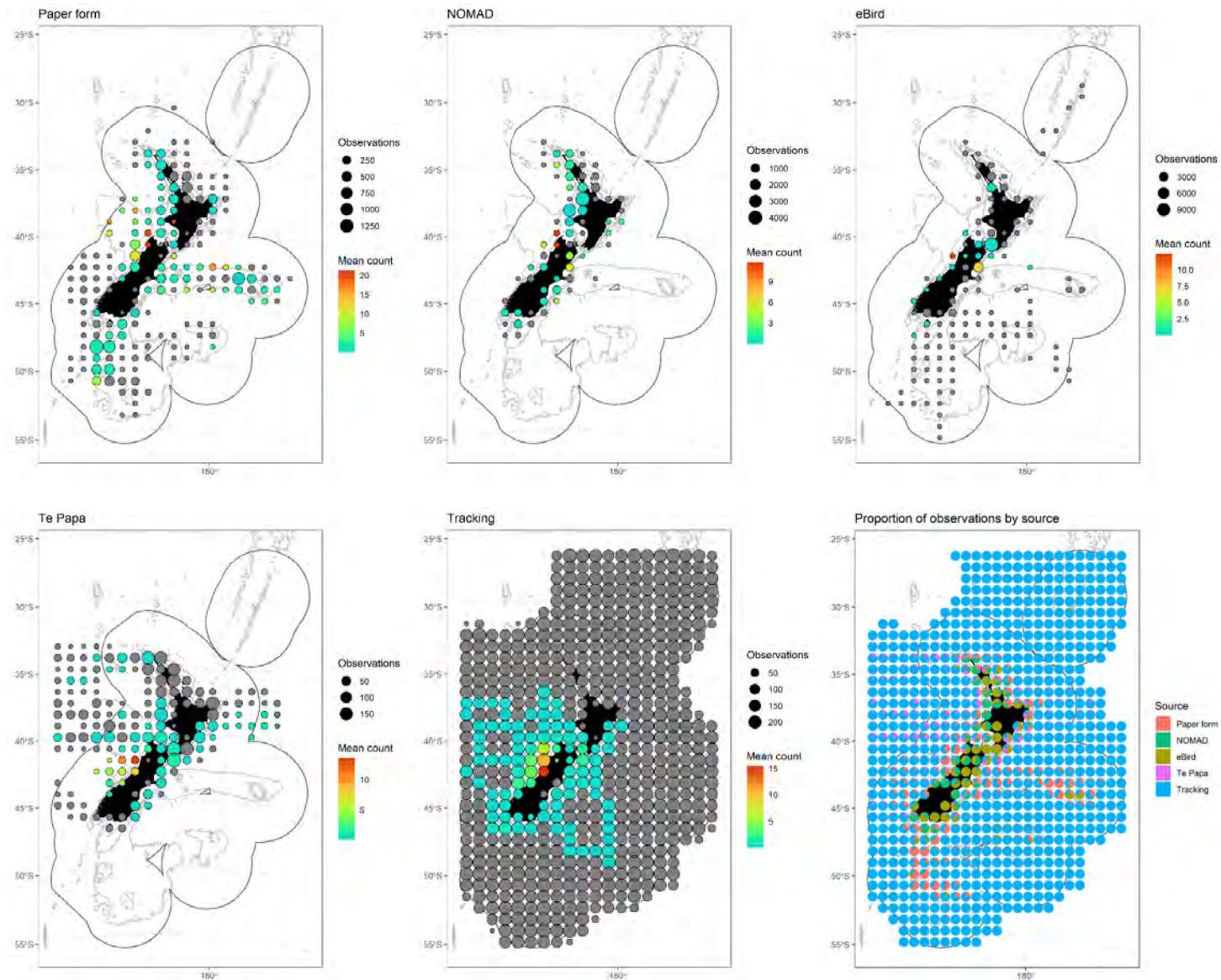


Figure D.3: Spatially explicit mean count of Westland petrel by data source for the paper form, Nomad, eBird, Te Papa, and tracking data sources. Grey circles represent a mean count of zero, and each circle's size is scaled by the number of observations represented by that circle. The bottom right panel shows the spatial proportion of data for each data source.

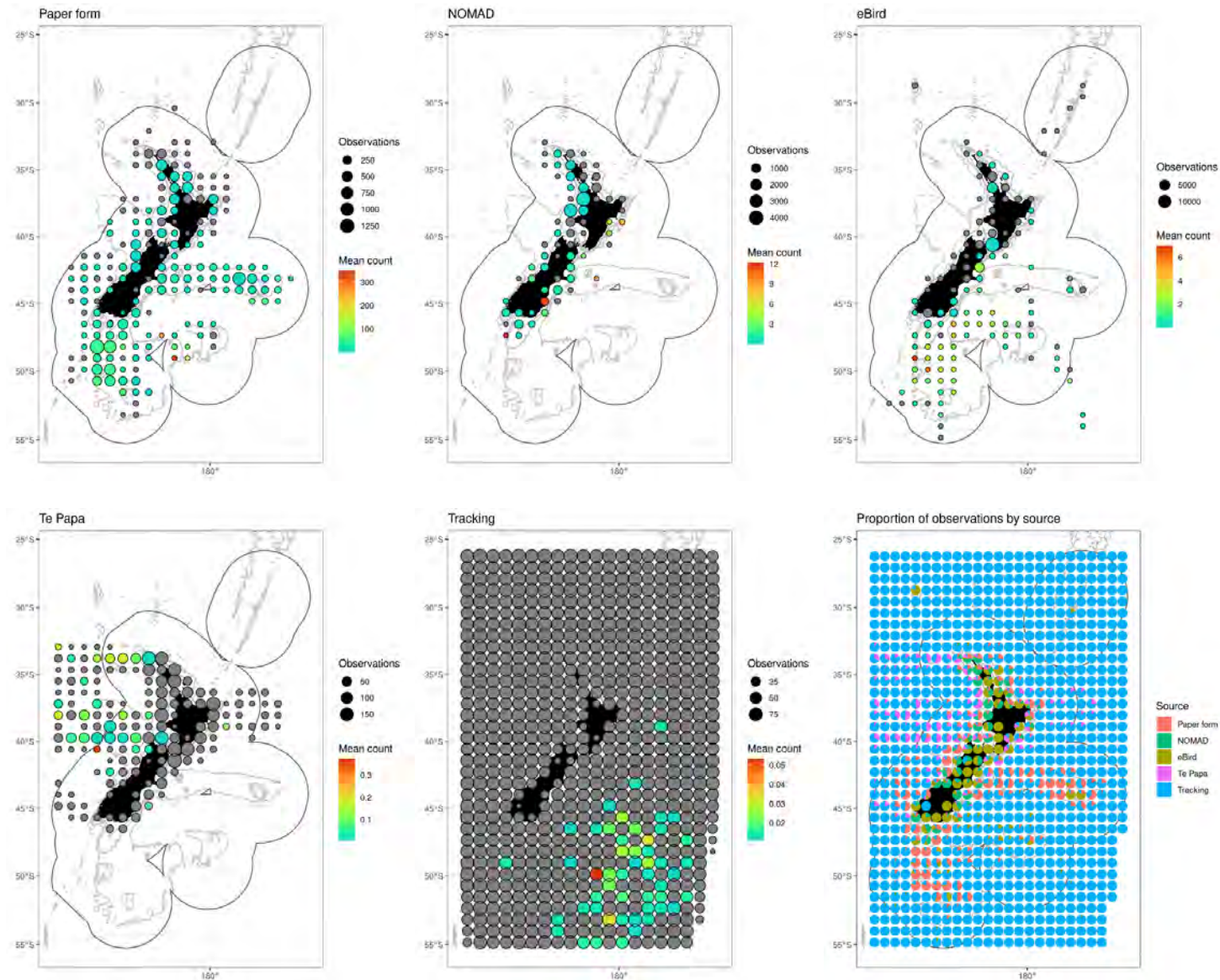


Figure D.4: Spatially explicit mean count of White-chinned petrel by data source for the paper form, Nomad, eBird, Te Papa, and tracking data sources. Grey circles represent a mean count of zero, and each circle's size is scaled by the number of observations represented by that circle. The bottom right panel shows the spatial proportion of data for each data source.

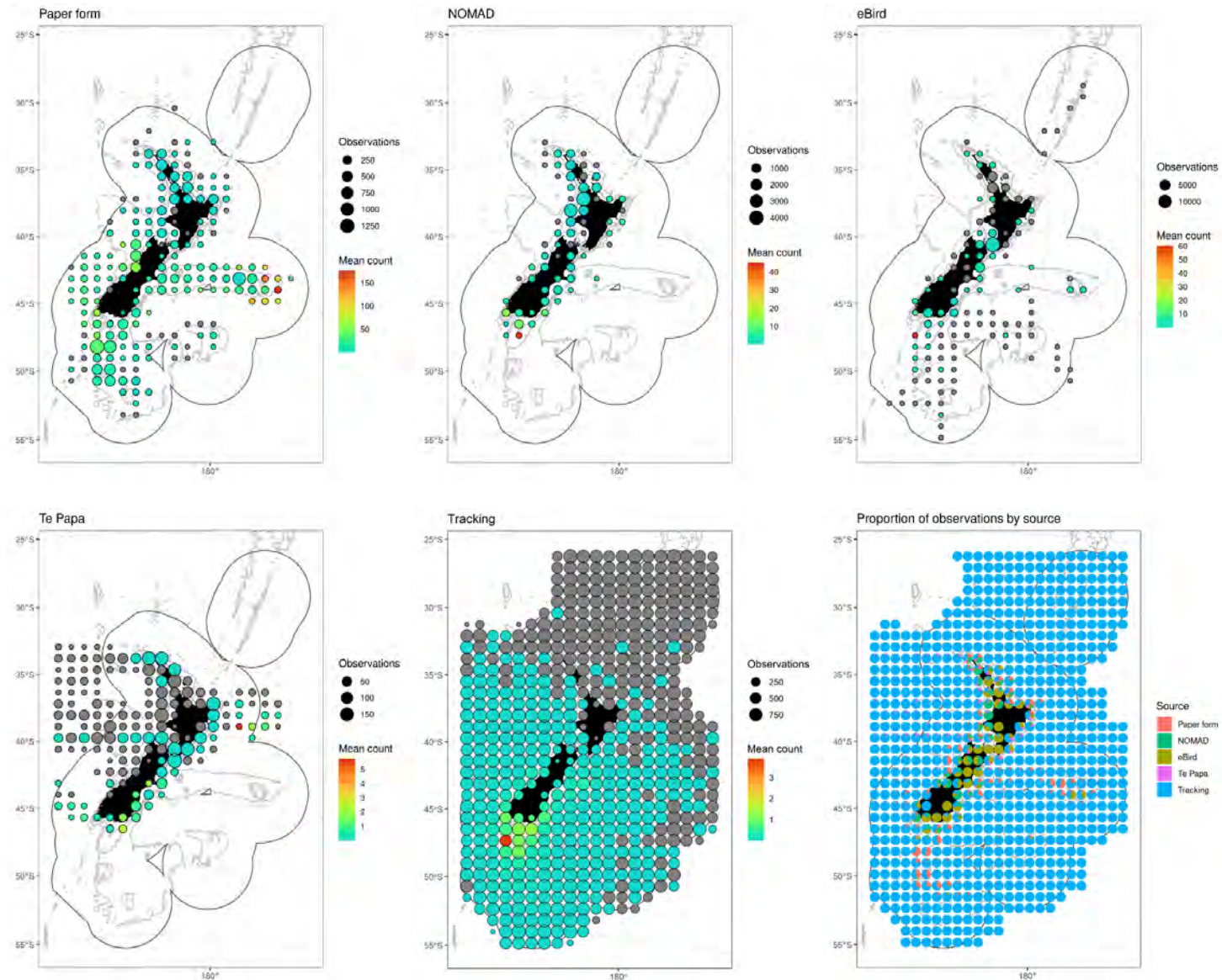


Figure D.5: Spatially explicit mean count of Northern and Southern Buller's albatross (combined) by data source for the paper form, Nomad, eBird, Te Papa, and tracking data sources. Grey circles represent a mean count of zero, and each circle's size is scaled by the number of observations represented by that circle. The bottom right panel shows the spatial proportion of data for each data source.

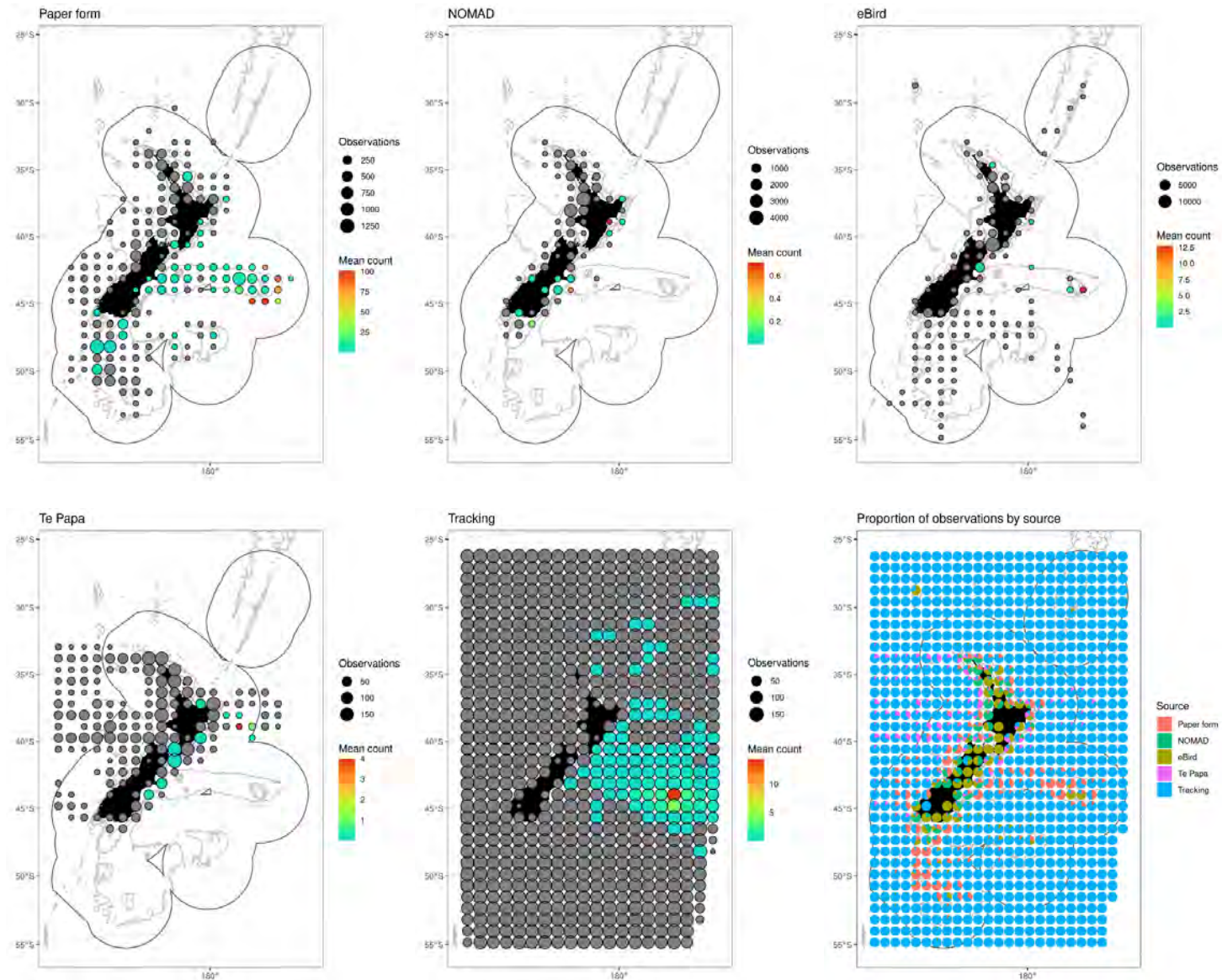


Figure D.6: Spatially explicit mean count of Chatham Island albatross by data source for the paper form, Nomad, eBird, Te Papa, and tracking data sources. Grey circles represent a mean count of zero, and each circle's size is scaled by the number of observations represented by that circle. The bottom right panel shows the spatial proportion of data for each data source.

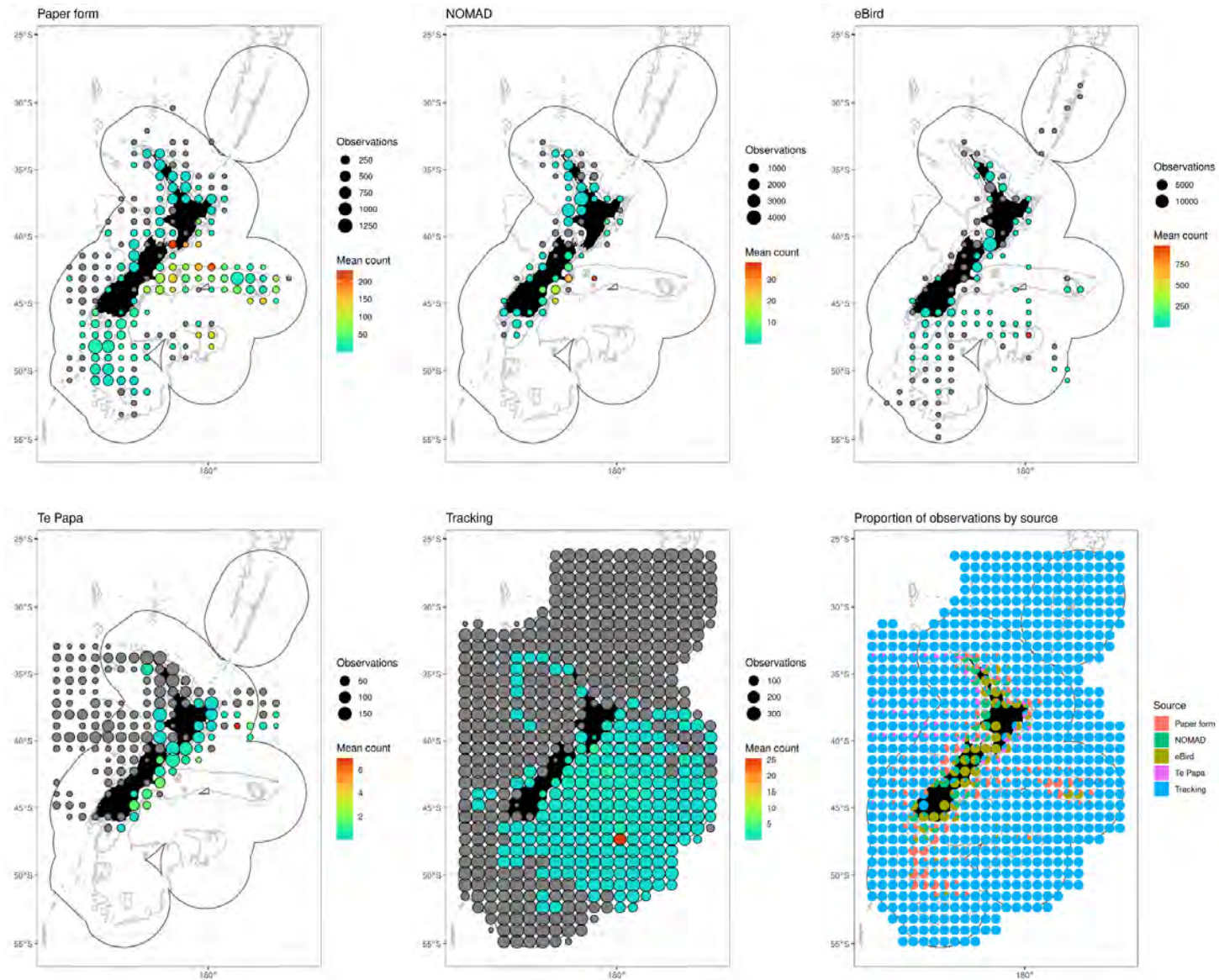


Figure D.7: Spatially explicit mean count of *Salvin's albatross* by data source for the paper form, Nomad, eBird, Te Papa, and tracking data sources. Grey circles represent a mean count of zero, and each circle's size is scaled by the number of observations represented by that circle. The bottom right panel shows the spatial proportion of data for each data source.

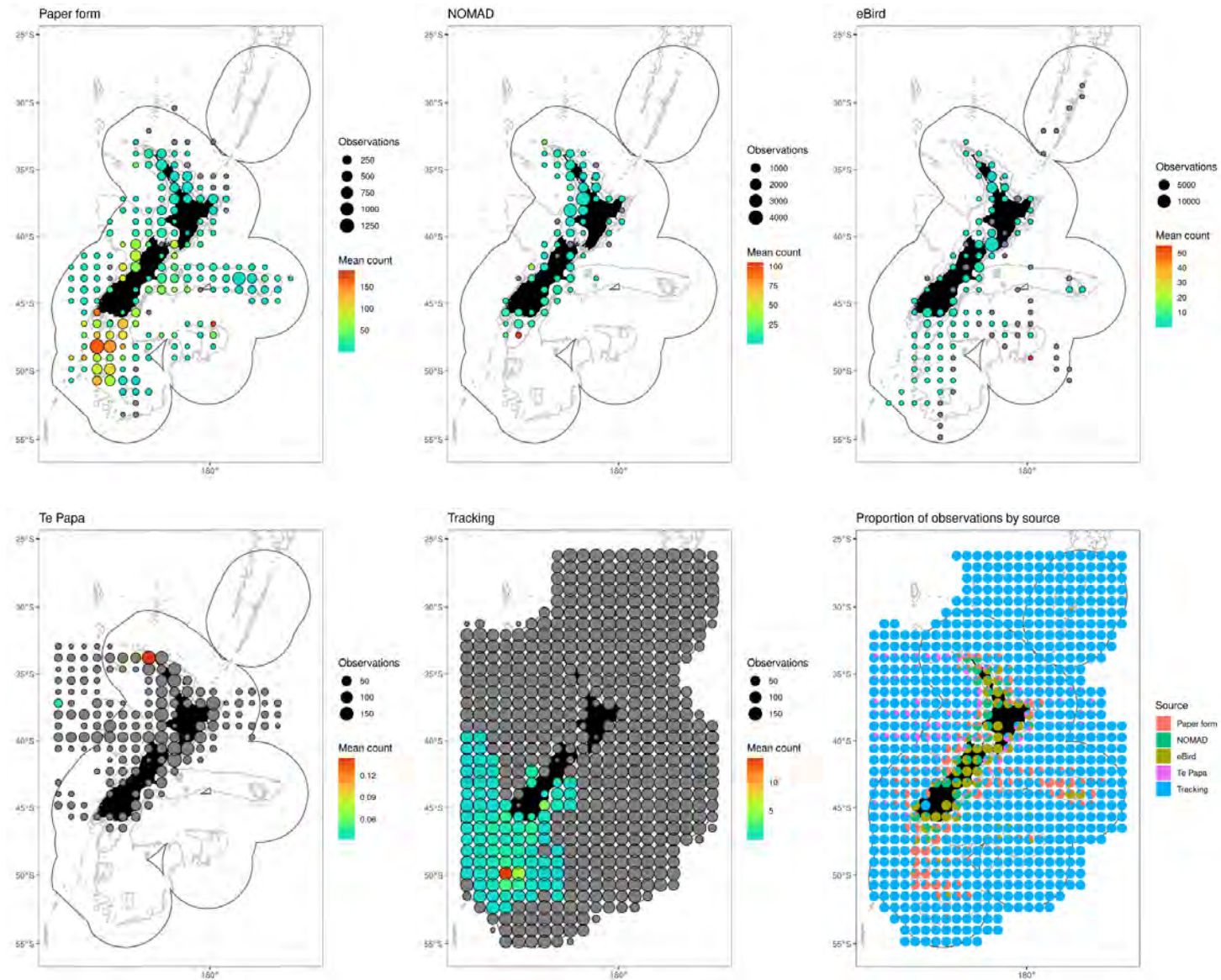


Figure D.8: Spatially explicit mean count of White-capped albatross by data source for the paper form, Nomad, eBird, Te Papa, and tracking data sources. Grey circles represent a mean count of zero, and each circle's size is scaled by the number of observations represented by that circle. The bottom right panel shows the spatial proportion of data for each data source.

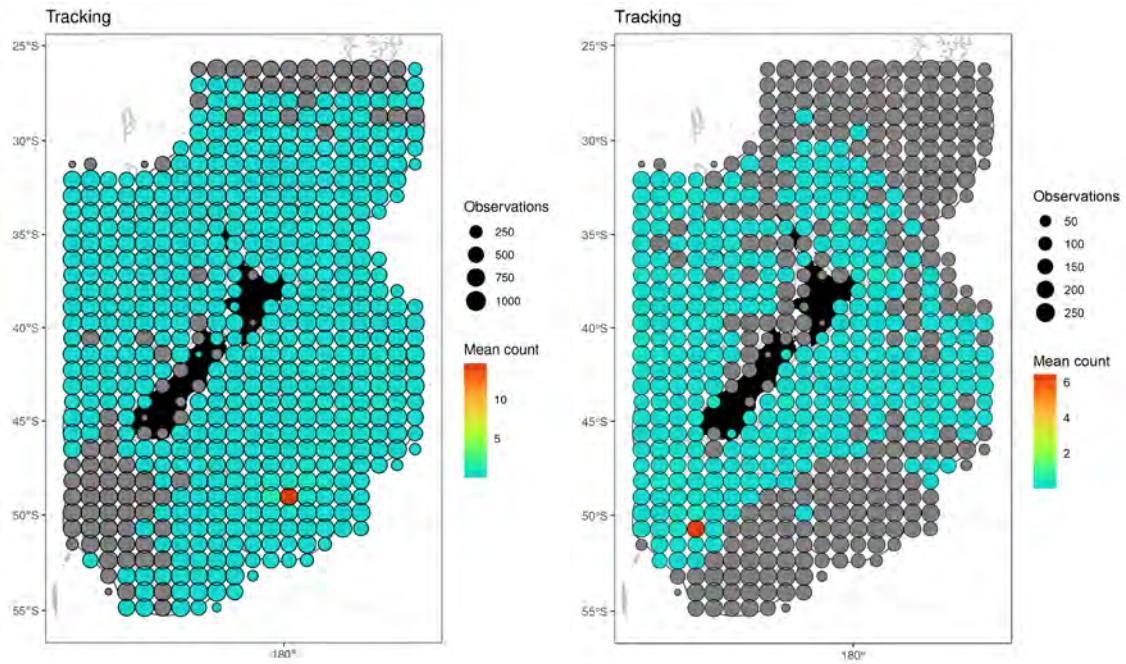


Figure D.9: Spatially explicit mean count of Antipodean albatross (left) and Gibson's albatross (right) from gridded tracking data. Grey circles represent a mean count of zero, and each circle's size is scaled by the number of observations represented by that circle.

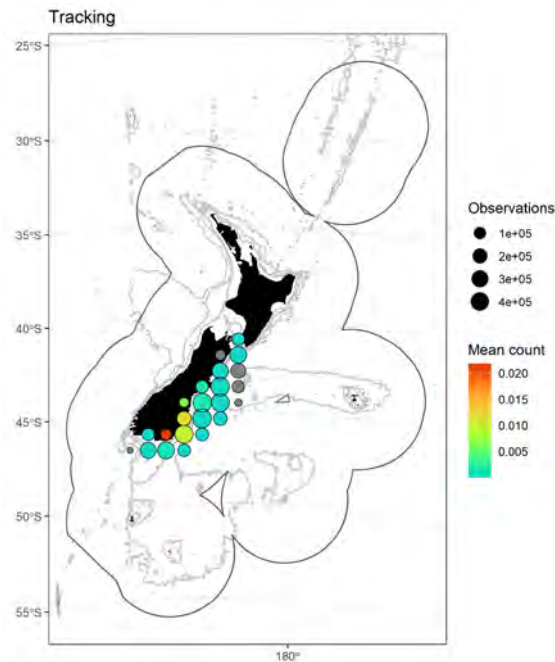


Figure D.10: Spatially explicit mean count of hoiho (all life stages) from gridded tracking data. Grey circles represent a mean count of zero, and each circle's size is scaled by the number of observations represented by that circle.

APPENDIX E. SEABIRD DISTRIBUTION MODEL DIAGNOSTIC PLOTS

Flesh-footed shearwater

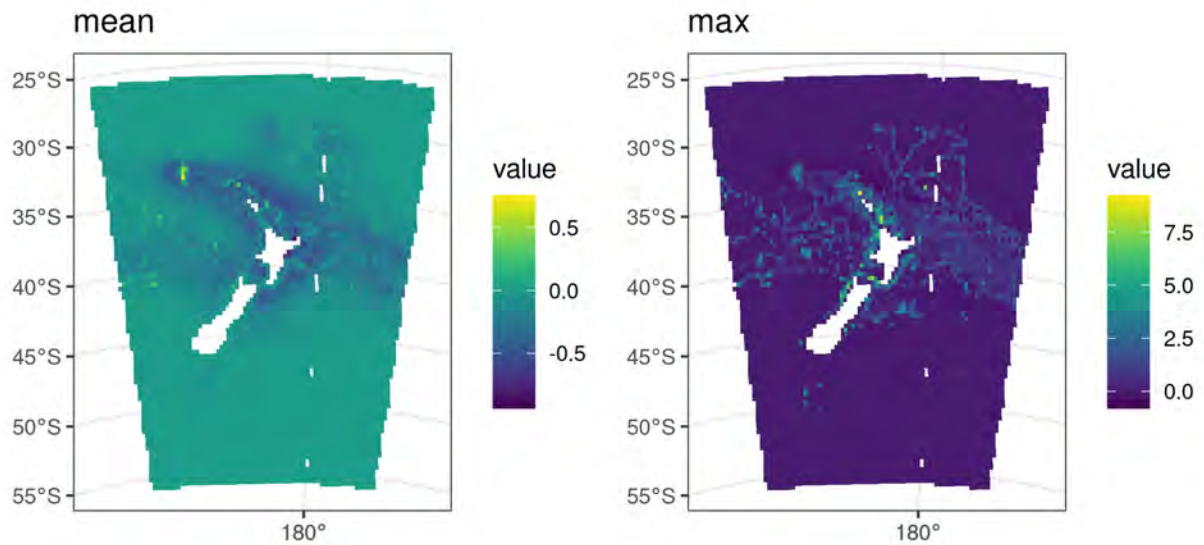


Figure E.1: Spatially-explicit residuals showing the mean residual [left] and the maximum residual [right] for the final flesh-footed shearwater model.

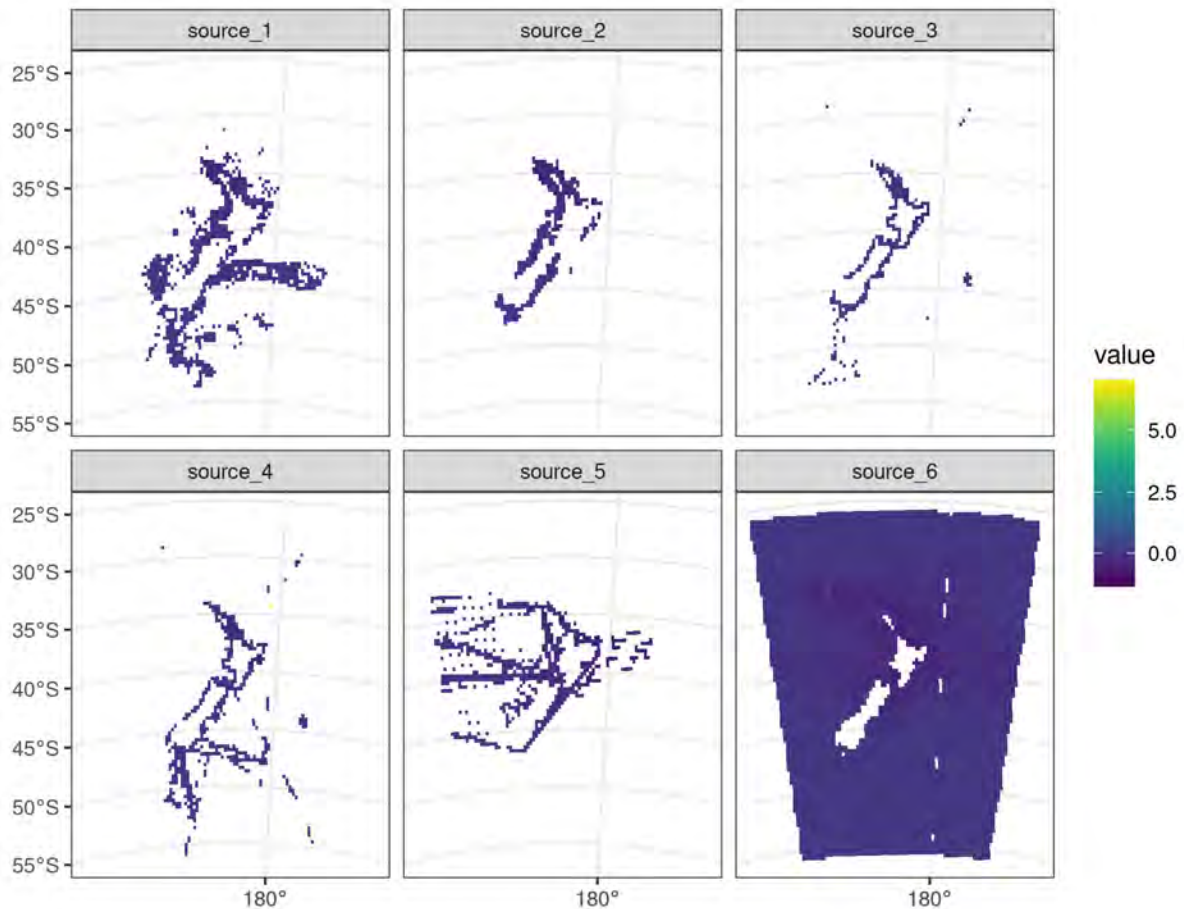


Figure E.2: Mean spatially-explicit residuals by data source (1 = paper form, 2 = Nomad, 3 = eBird stationary, 4 = eBird travelling, 5 = Te Papa, 6 = tracking) for the final flesh-footed shearwater model.

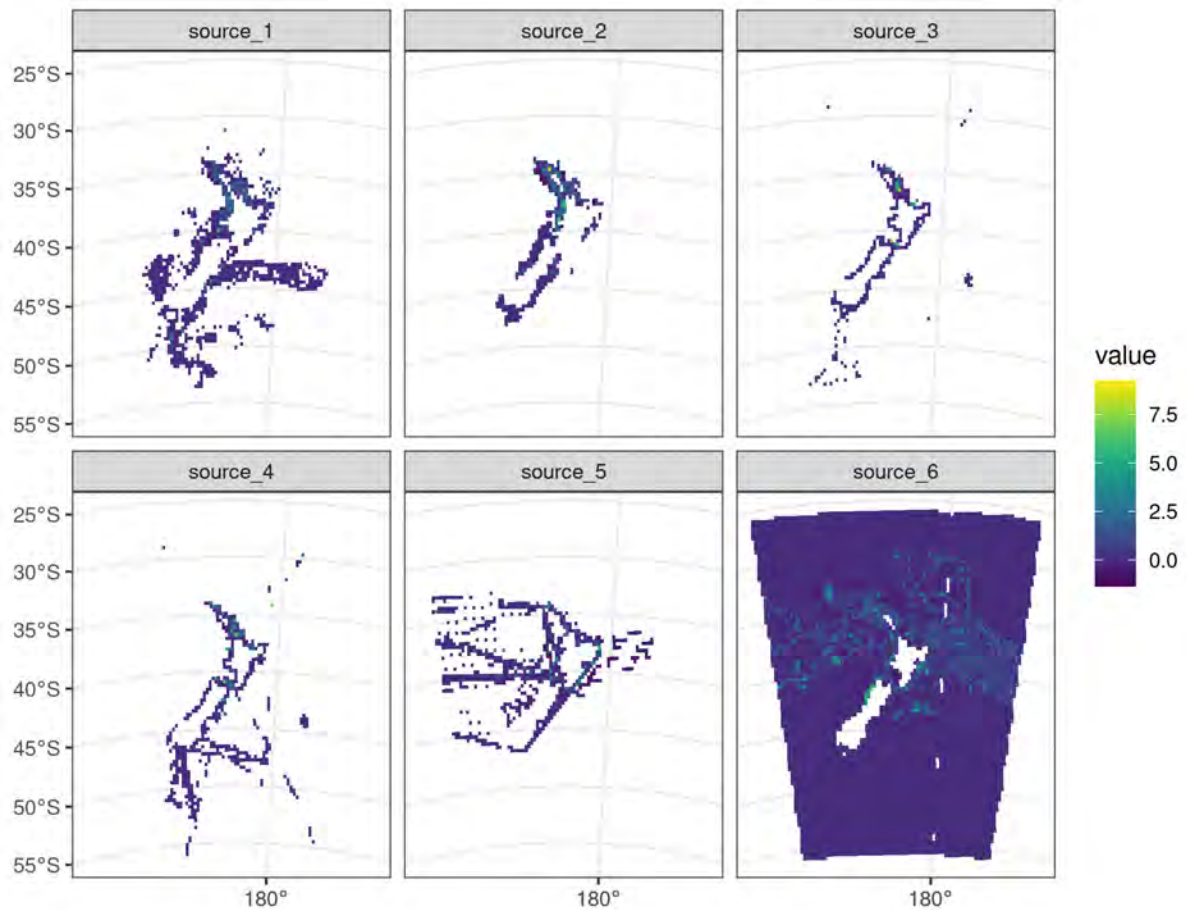


Figure E.3: Maximum spatially-explicit residuals by data source (1 = paper form, 2 = Nomad, 3 = eBird stationary, 4 = eBird travelling, 5 = Te Papa, 6 = tracking) for the final flesh-footed shearwater model.

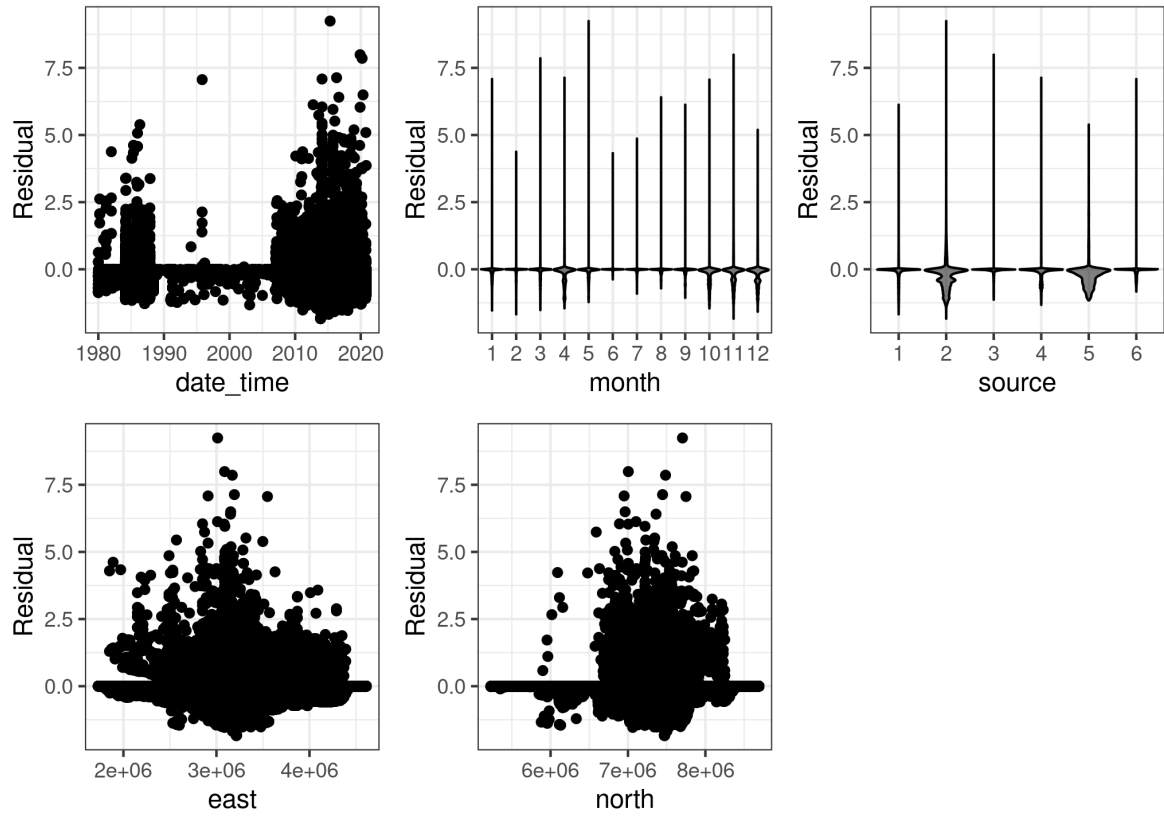


Figure E.4: Residual plots for the final flesh-footed shearwater model by date, month, source, easting, and northing.

Black petrel

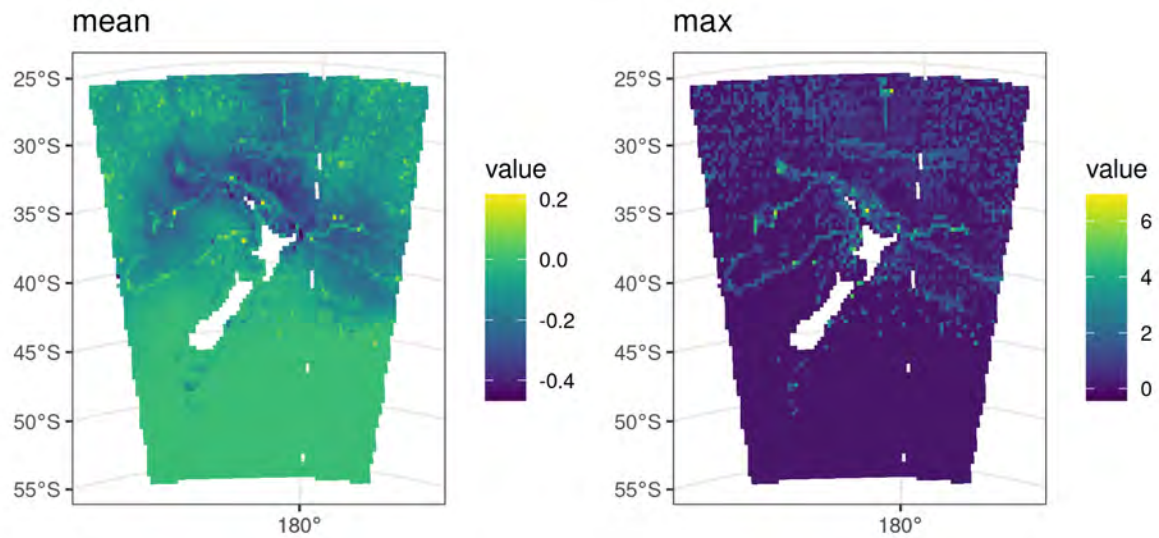


Figure E.5: Spatially-explicit residuals showing the mean and the maximum residual for the final **black petrel** model.

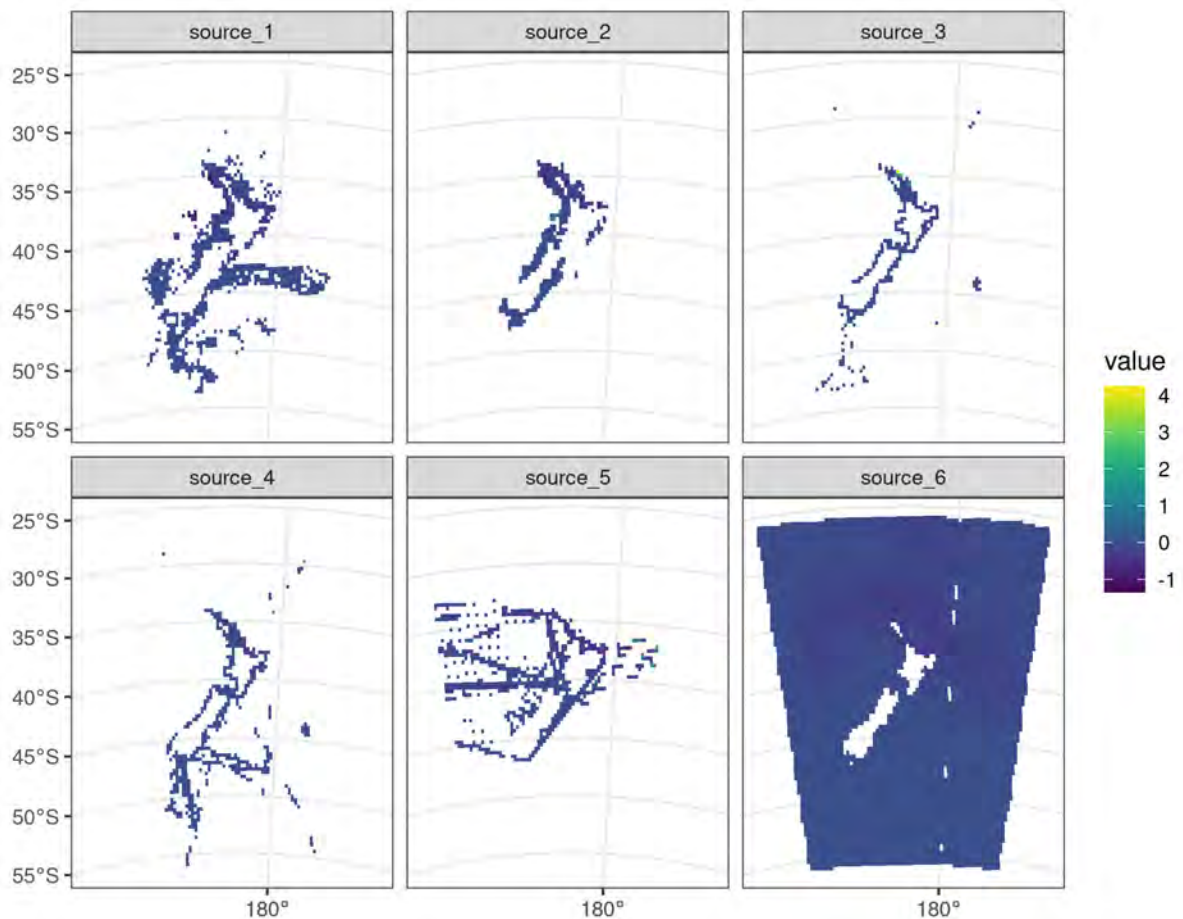


Figure E.6: Mean spatially-explicit residuals by data source (1 = paper form, 2 = Nomad, 3 = eBird stationary, 4 = eBird travelling, 5 = Te Papa, 6 = tracking) for the final **black petrel** model.

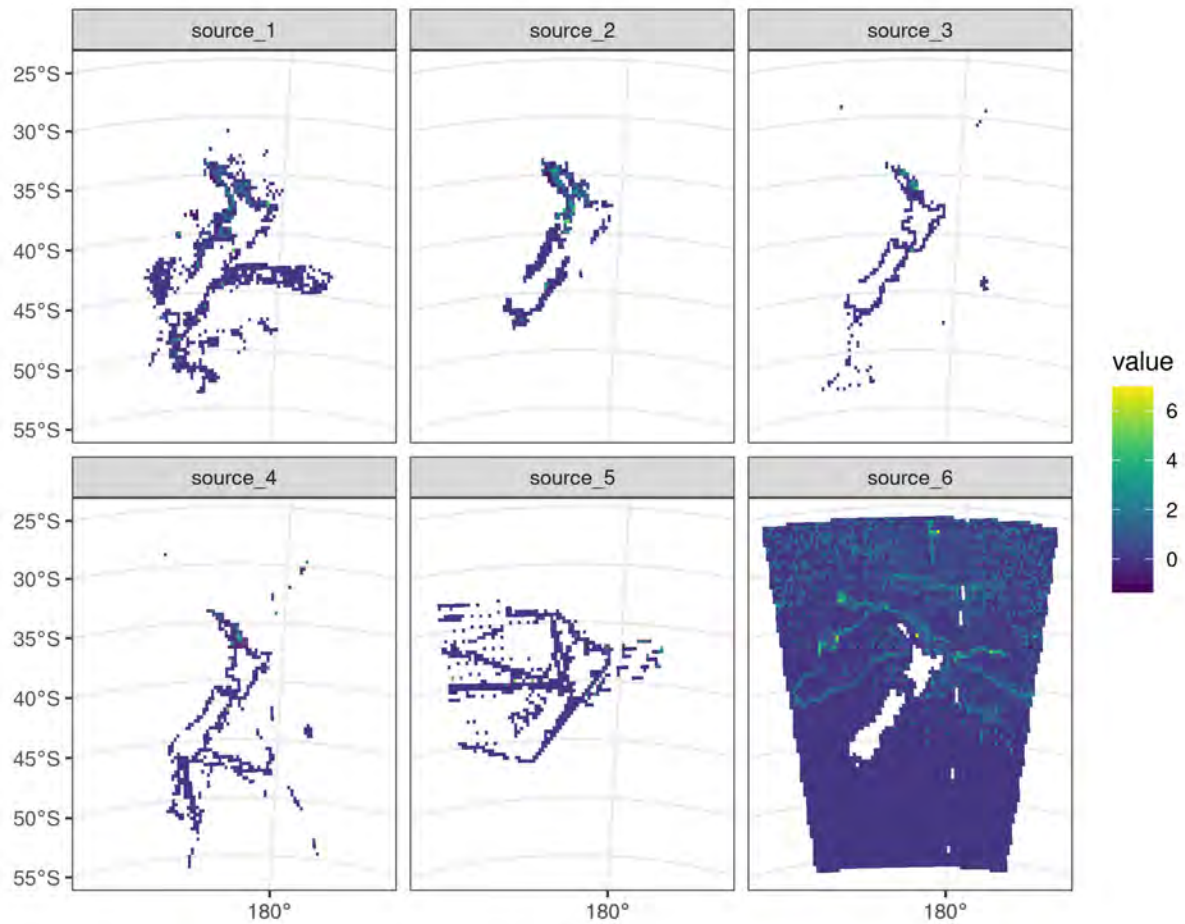


Figure E.7: Maximum spatially-explicit residuals by data source (1 = paper form, 2 = Nomad, 3 = eBird stationary, 4 = eBird travelling, 5 = Te Papa, 6 = tracking) for the final black petrel model.

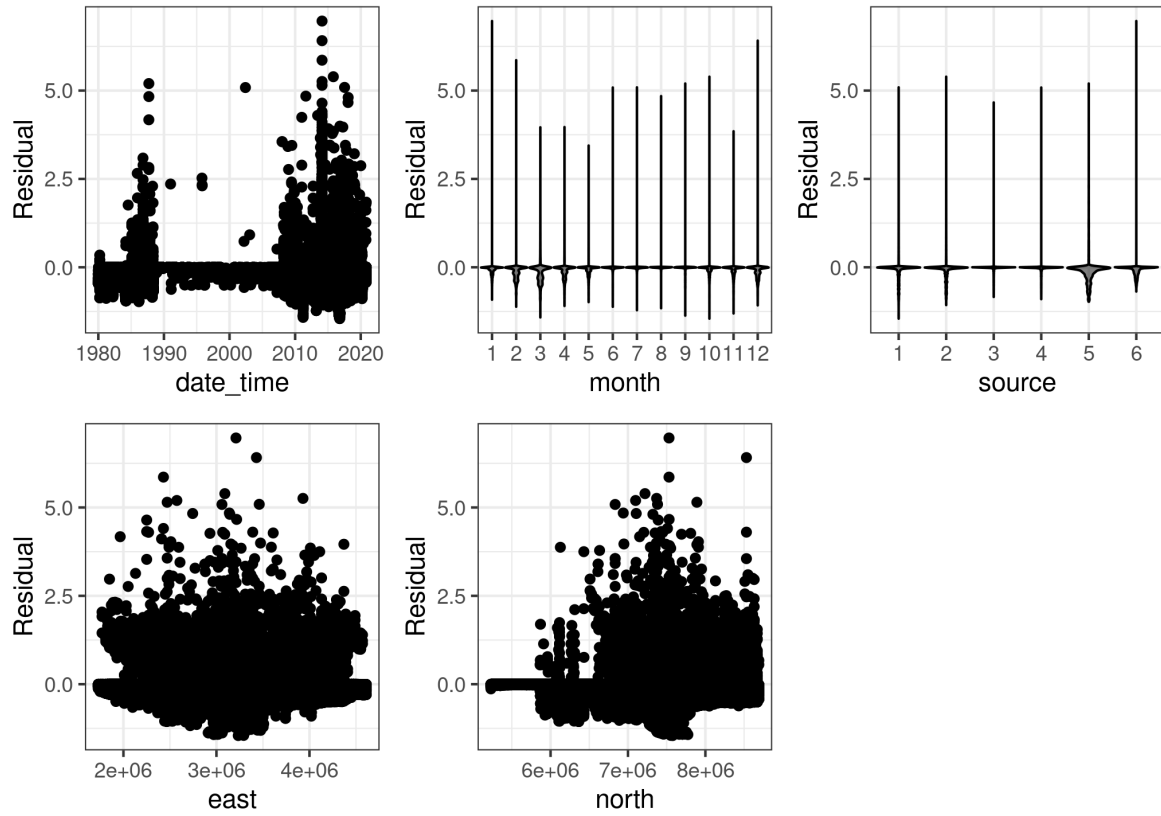


Figure E.8: Residual plots for the final black petrel model by date, month, source, easting, and northing.

Westland petrel

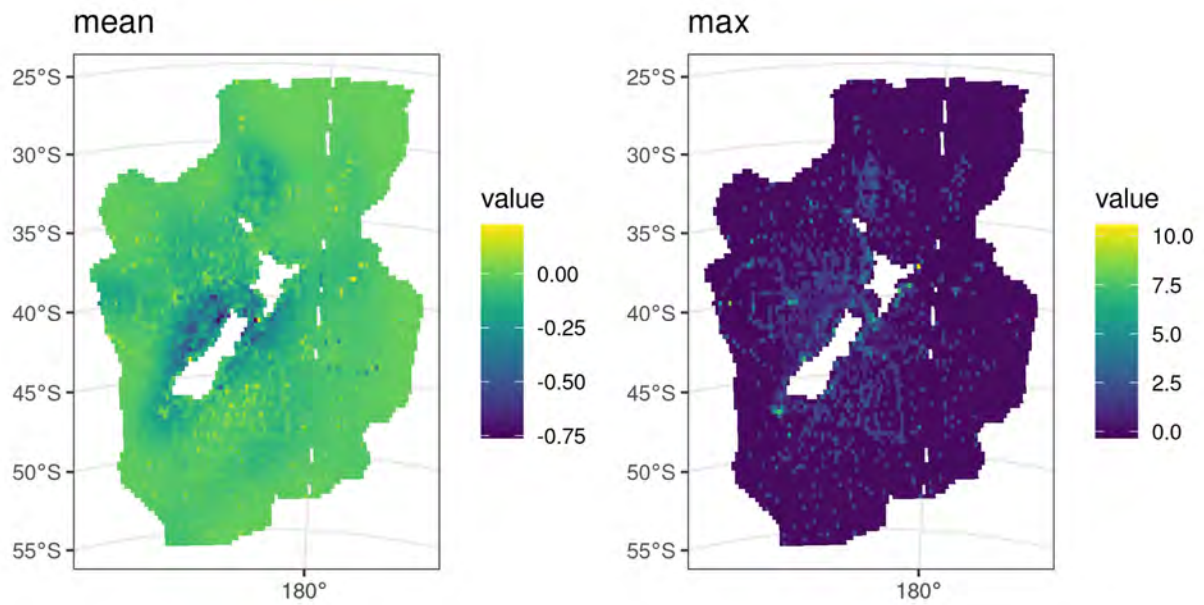


Figure E.9: Spatially-explicit residuals showing the mean residual [left] and the maximum residual [right] for the final Westland petrel model.

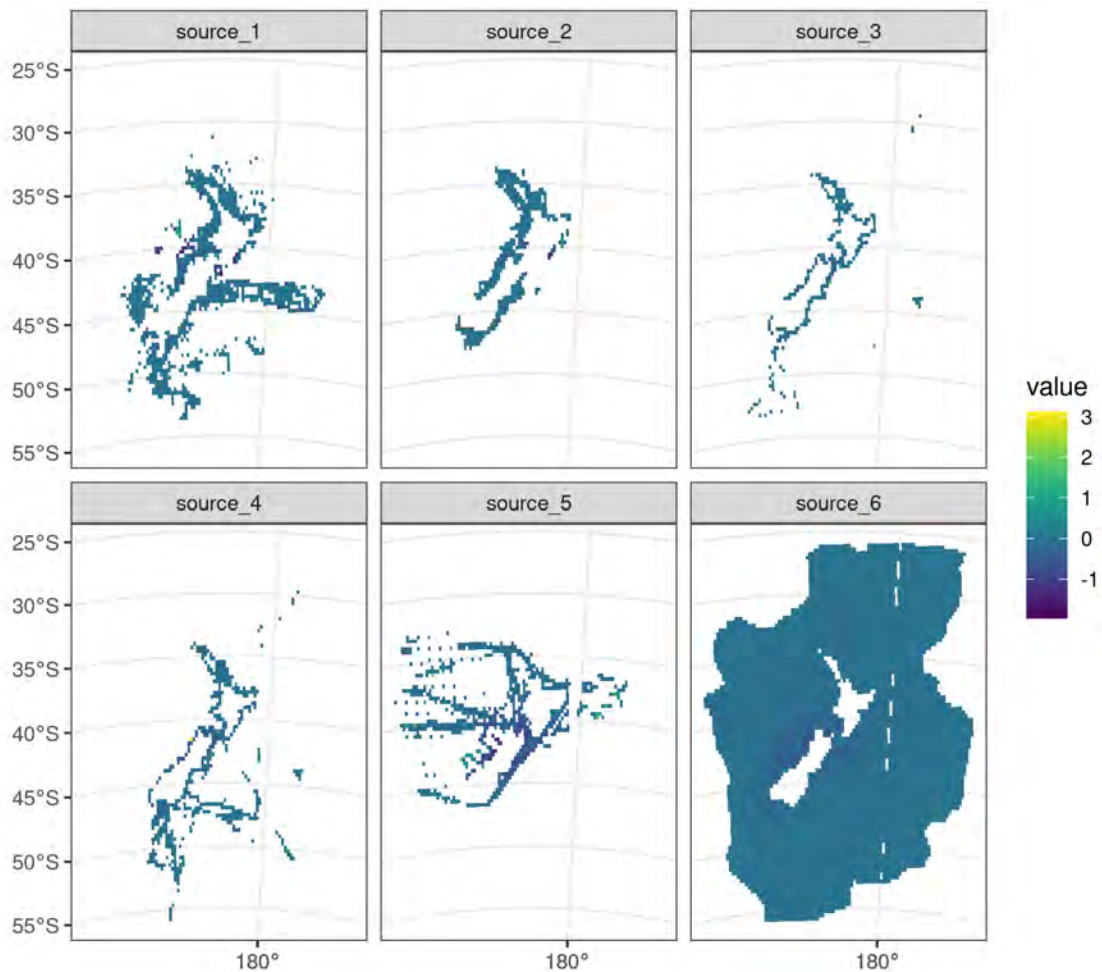


Figure E.10: Mean spatially-explicit residuals by data source (1 = paper form, 2 = Nomad, 3 = eBird stationary, 4 = eBird travelling, 5 = Te Papa, 6 = tracking) for the final Westland petrel model.

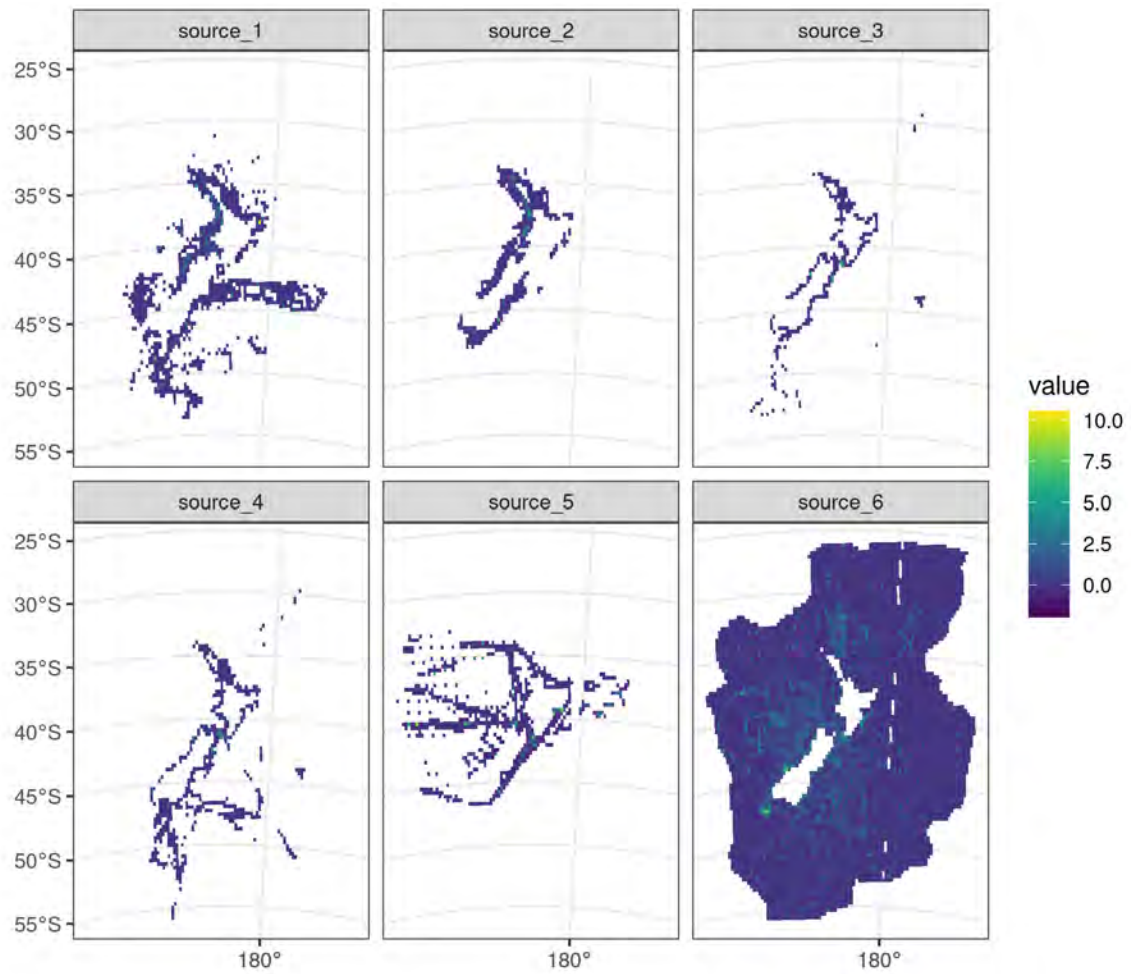


Figure E.11: Maximum spatially-explicit residuals by data source (1 = paper form, 2 = Nomad, 3 = eBird stationary, 4 = eBird travelling, 5 = Te Papa, 6 = tracking) for the final Westland petrel model.

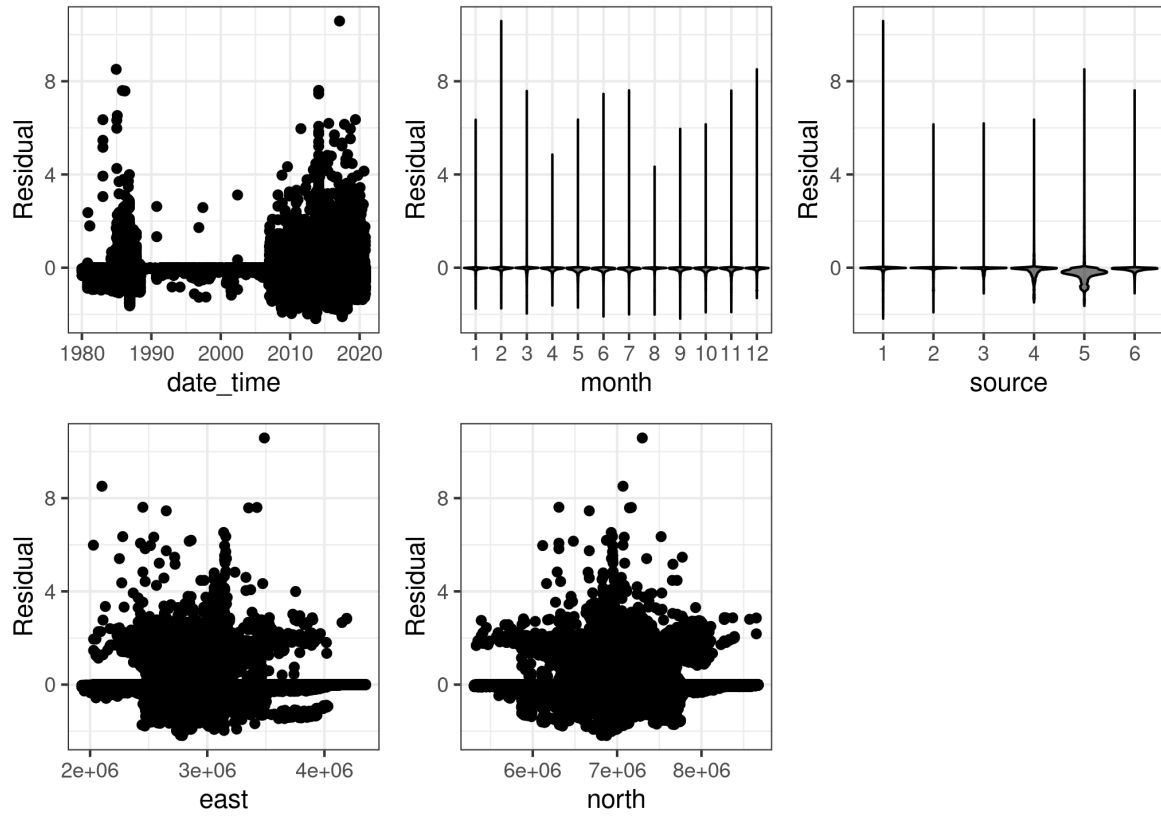


Figure E.12: Residual plots for final Westland petrel model by date, month, source, easting, and northing.

White-chinned petrel

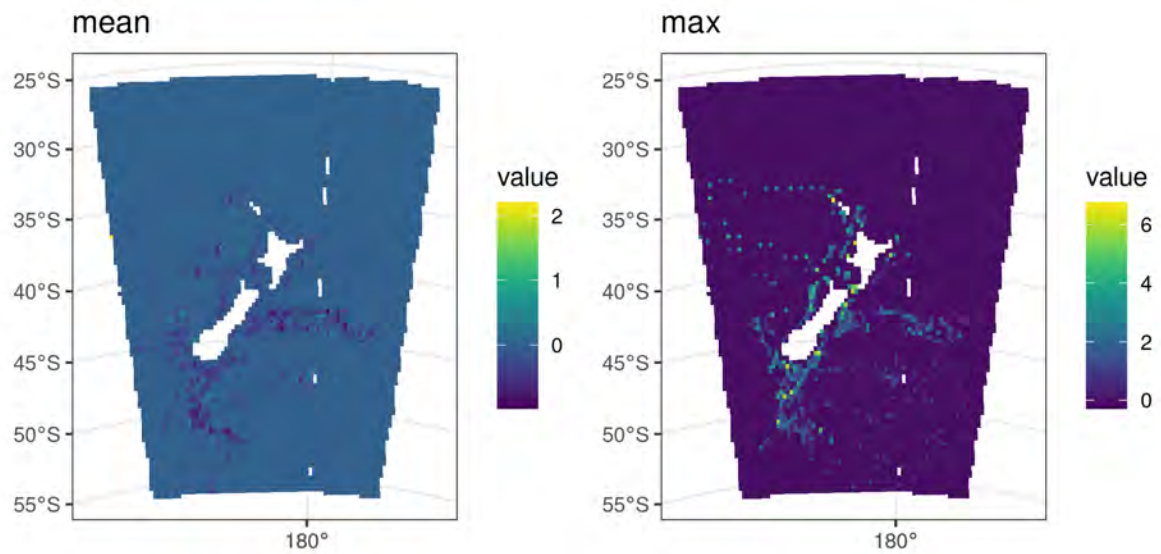


Figure E.13: Spatially-explicit residuals showing the mean residual [left] and the maximum residual [right] for the final white-chinned petrel model.

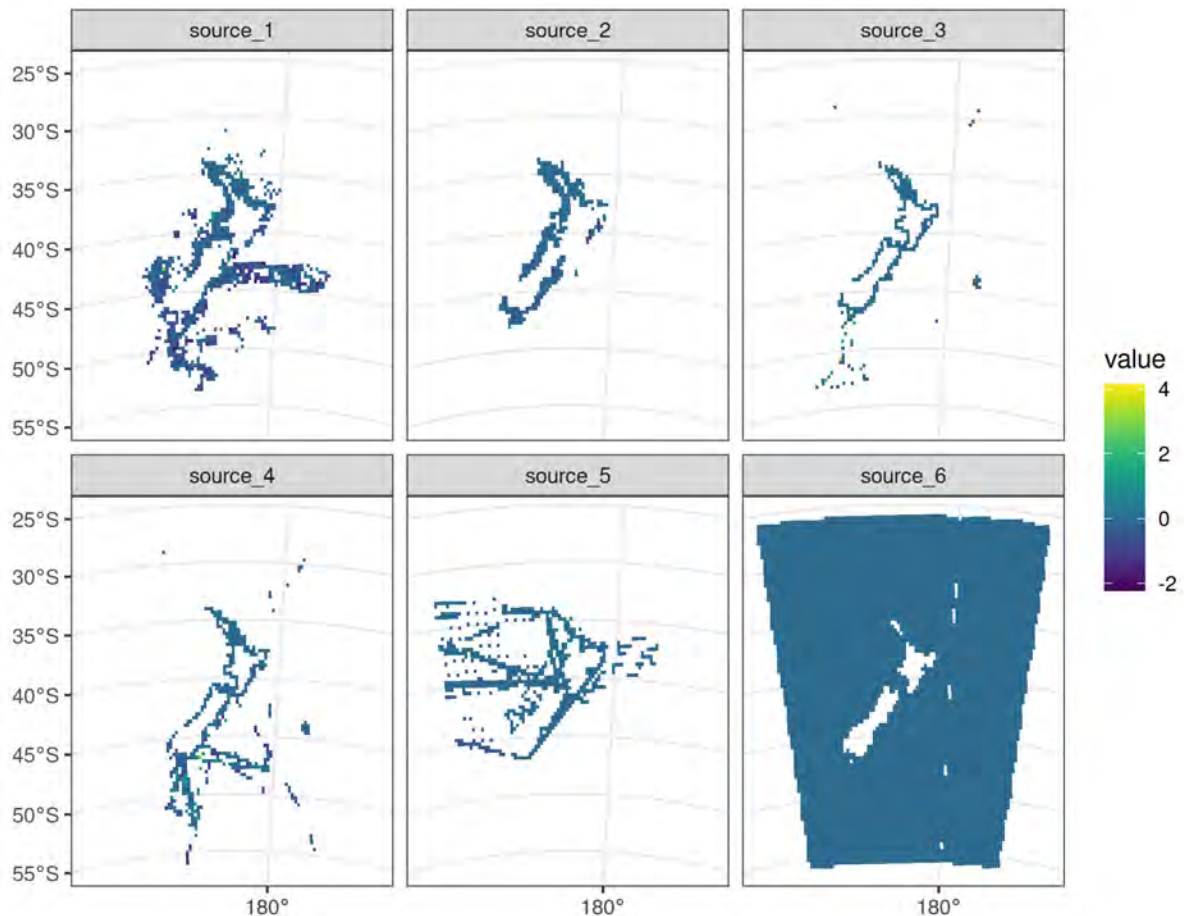


Figure E.14: Mean spatially-explicit residuals by data source (1 = paper form, 2 = Nomad, 3 = eBird stationary, 4 = eBird travelling, 5 = Te Papa, 6 = tracking) for the final white-chinned petrel model.

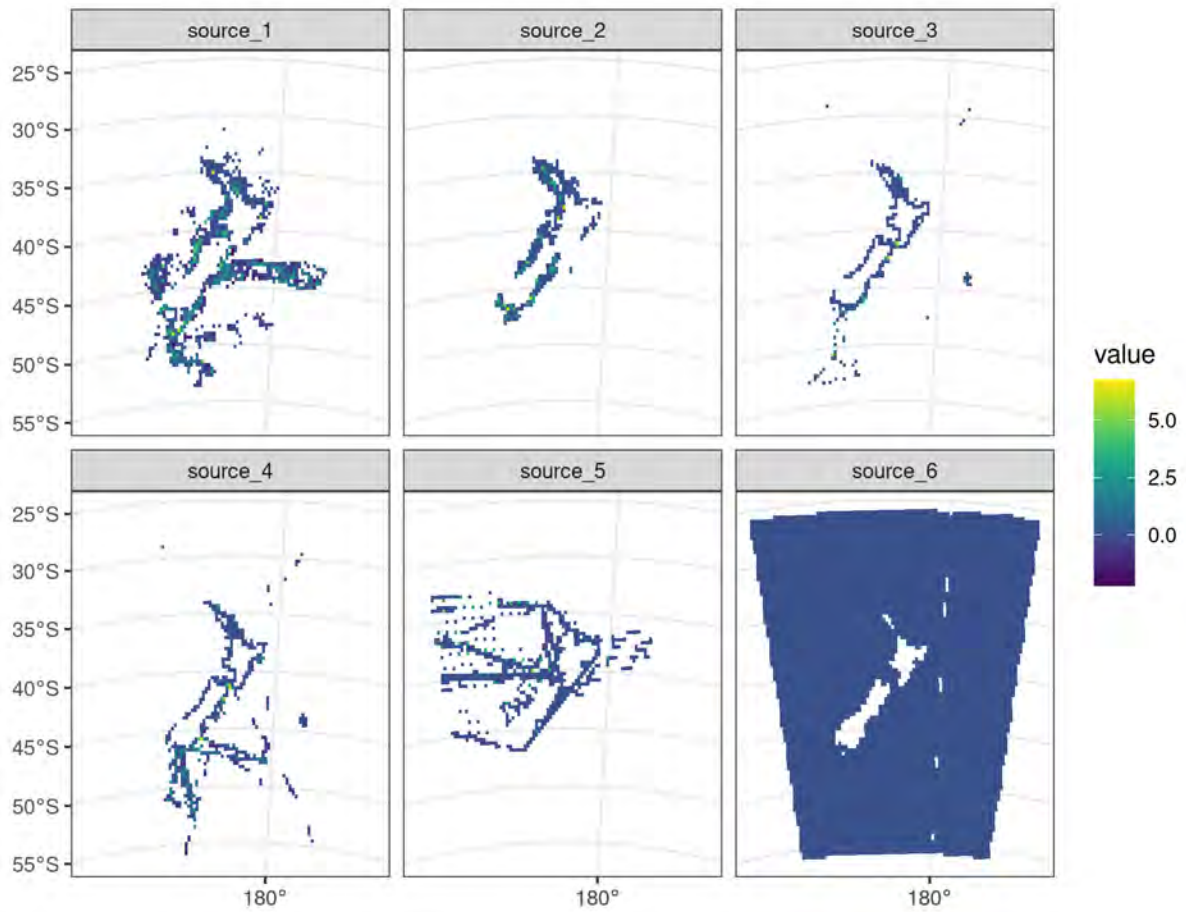


Figure E.15: Maximum spatially-explicit residuals by data source (1 = paper form, 2 = Nomad, 3 = eBird stationary, 4 = eBird travelling, 5 = Te Papa, 6 = tracking) for the final white-chinned petrel model.

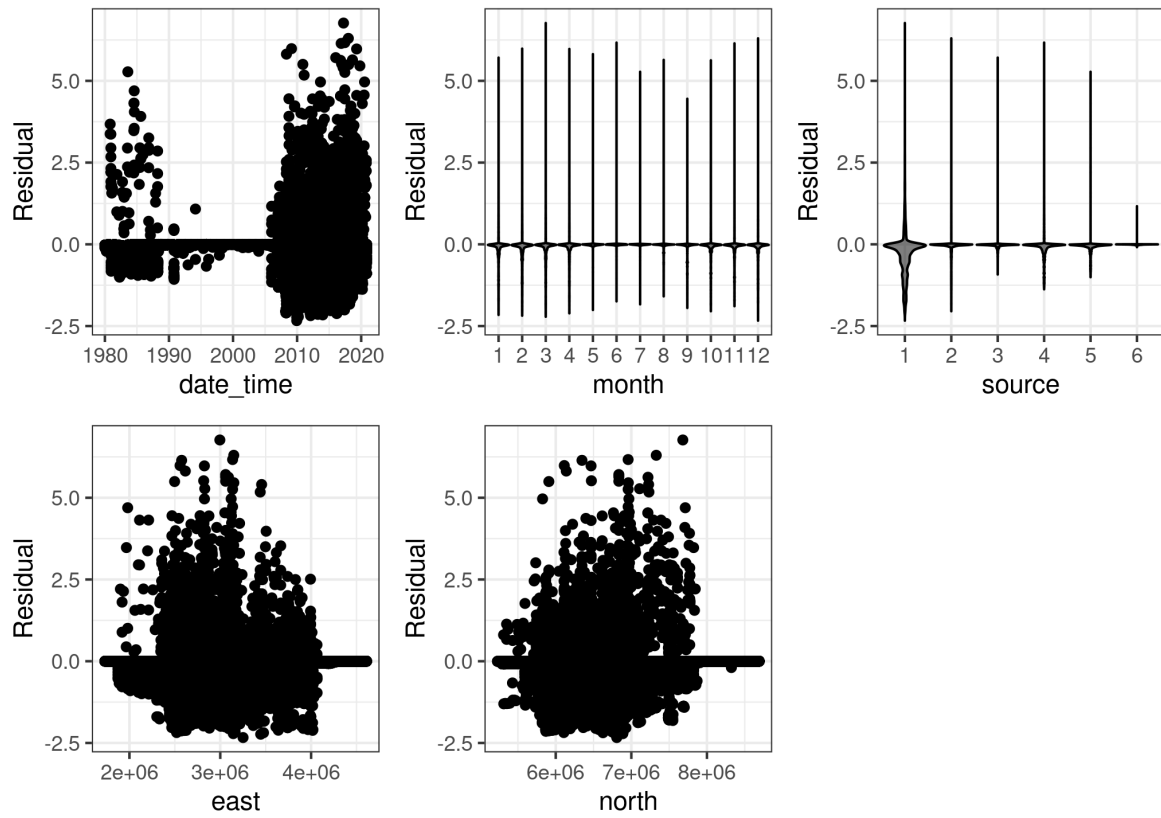


Figure E.16: Residual plots for final white-chinned petrel model by date, month, source, easting, and northing.

Northern and Southern Buller's albatross

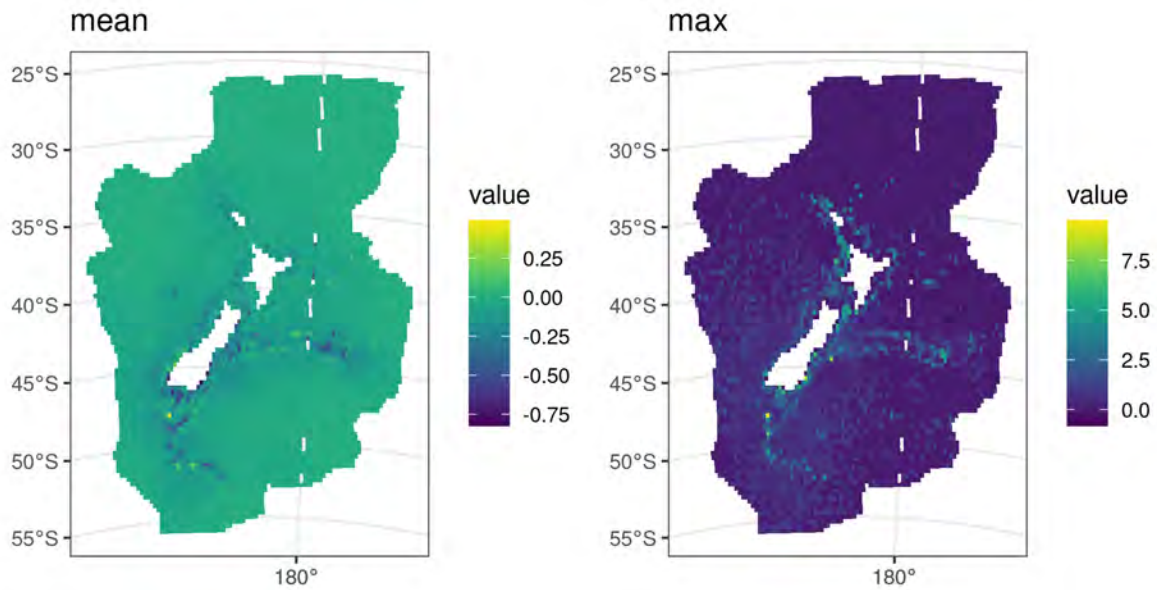


Figure E.17: Spatially-explicit residuals showing the mean residual [left] and the maximum residual [right] for the final Northern and Southern Buller's albatross (combined) model.

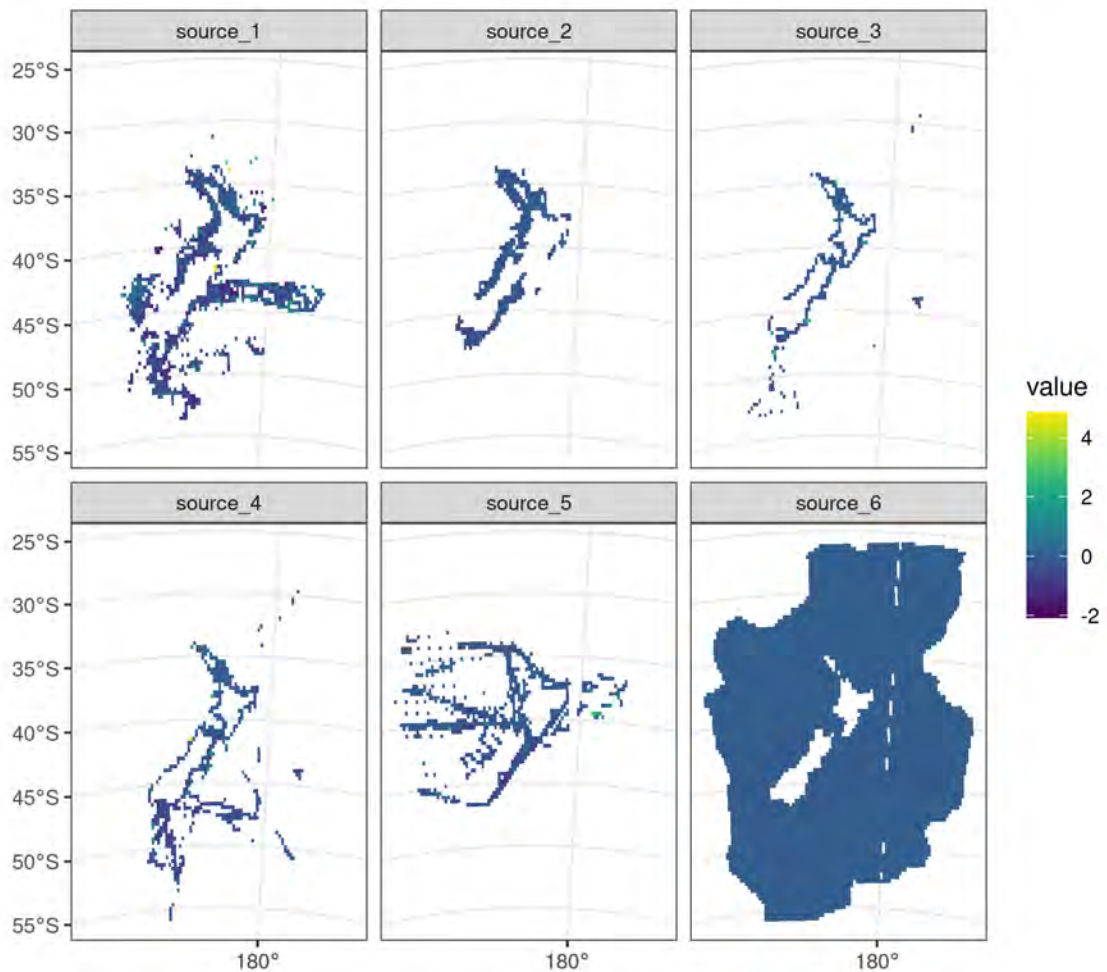


Figure E.18: Mean spatially-explicit residuals by data source (1 = paper form, 2 = Nomad, 3 = eBird stationary, 4 = eBird travelling, 5 = Te Papa, 6 = tracking) for the final Northern and Southern Buller's albatross (combined) model.

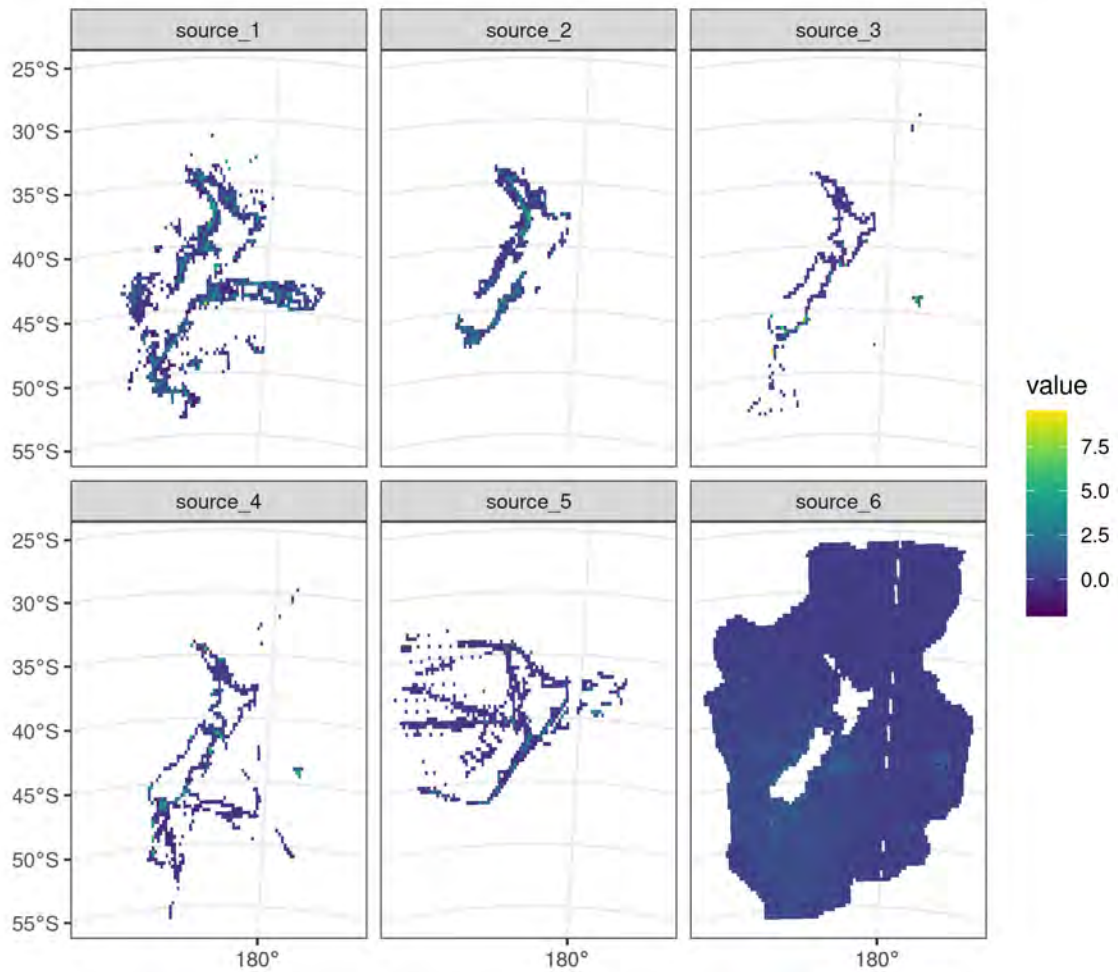


Figure E.19: Maximum spatially-explicit residuals by data source (1 = paper form, 2 = Nomad, 3 = eBird stationary, 4 = eBird travelling, 5 = Te Papa, 6 = tracking) for the final Northern and Southern Buller's albatross (combined) model.

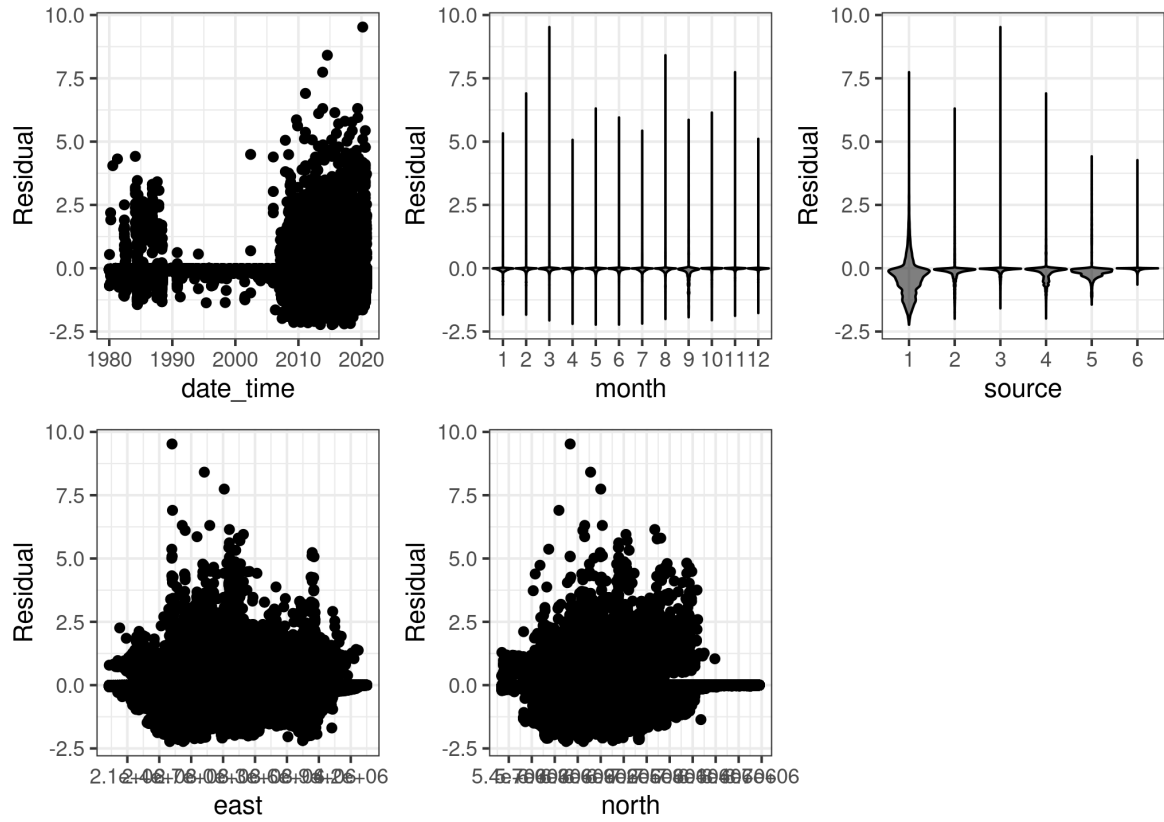


Figure E.20: Residual plots for final Northern and Southern Buller's albatross (combined) model by date, month, source, easting, and northing.

Chatham Island albatross

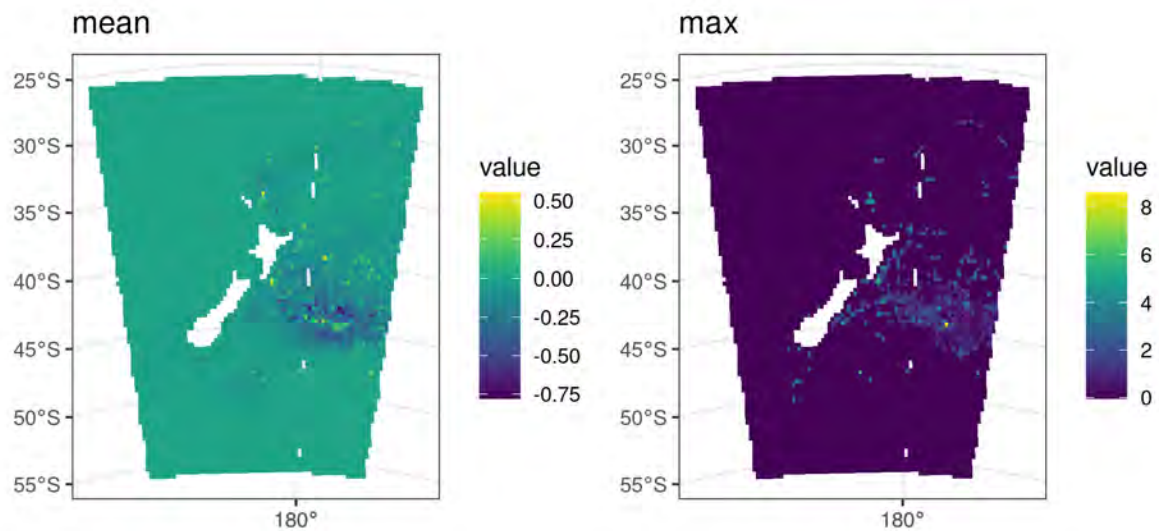


Figure E.21: Spatially-explicit residuals showing the mean residual [left] and the maximum residual [right] for the final Chatham Island albatross model.

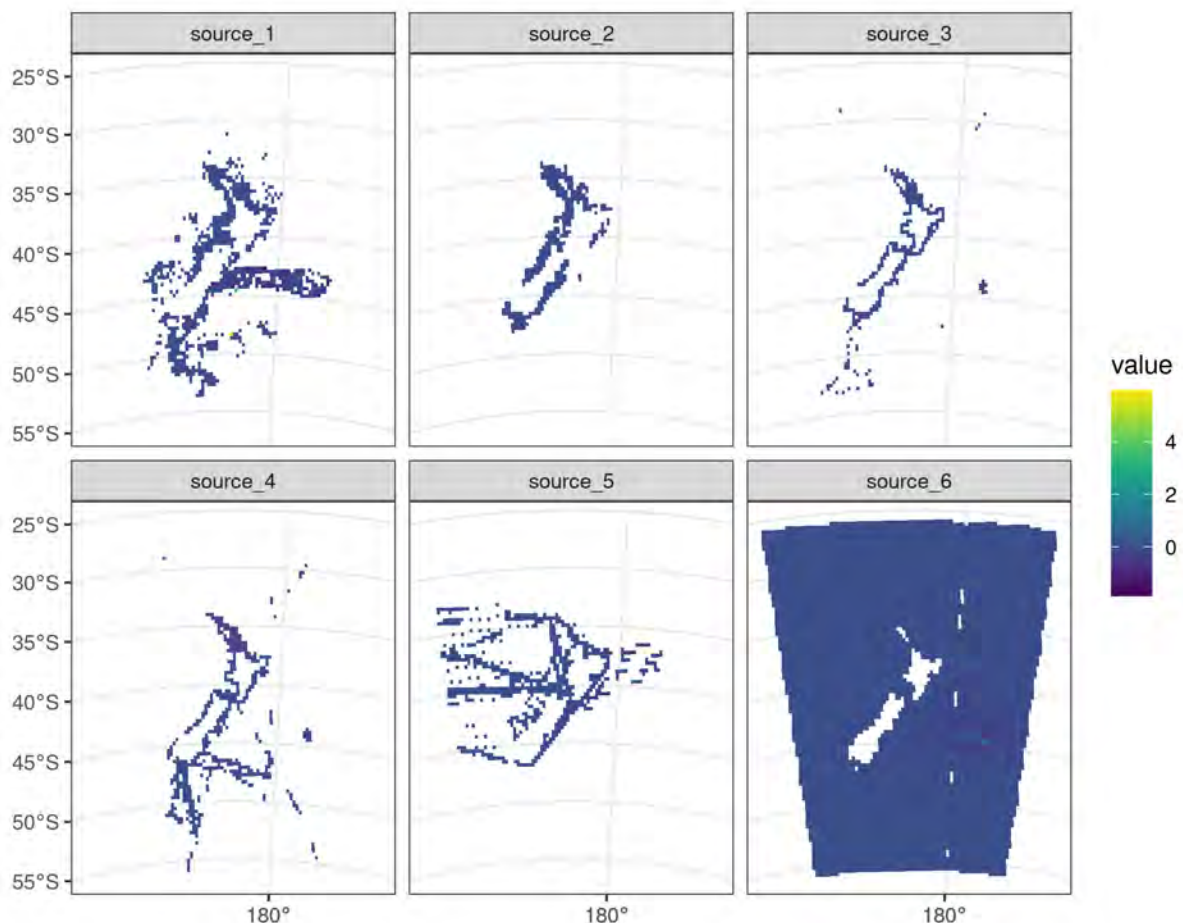


Figure E.22: Mean spatially-explicit residuals by data source (1 = paper form, 2 = Nomad, 3 = eBird stationary, 4 = eBird travelling, 5 = Te Papa, 6 = tracking) for the final Chatham Island albatross model.

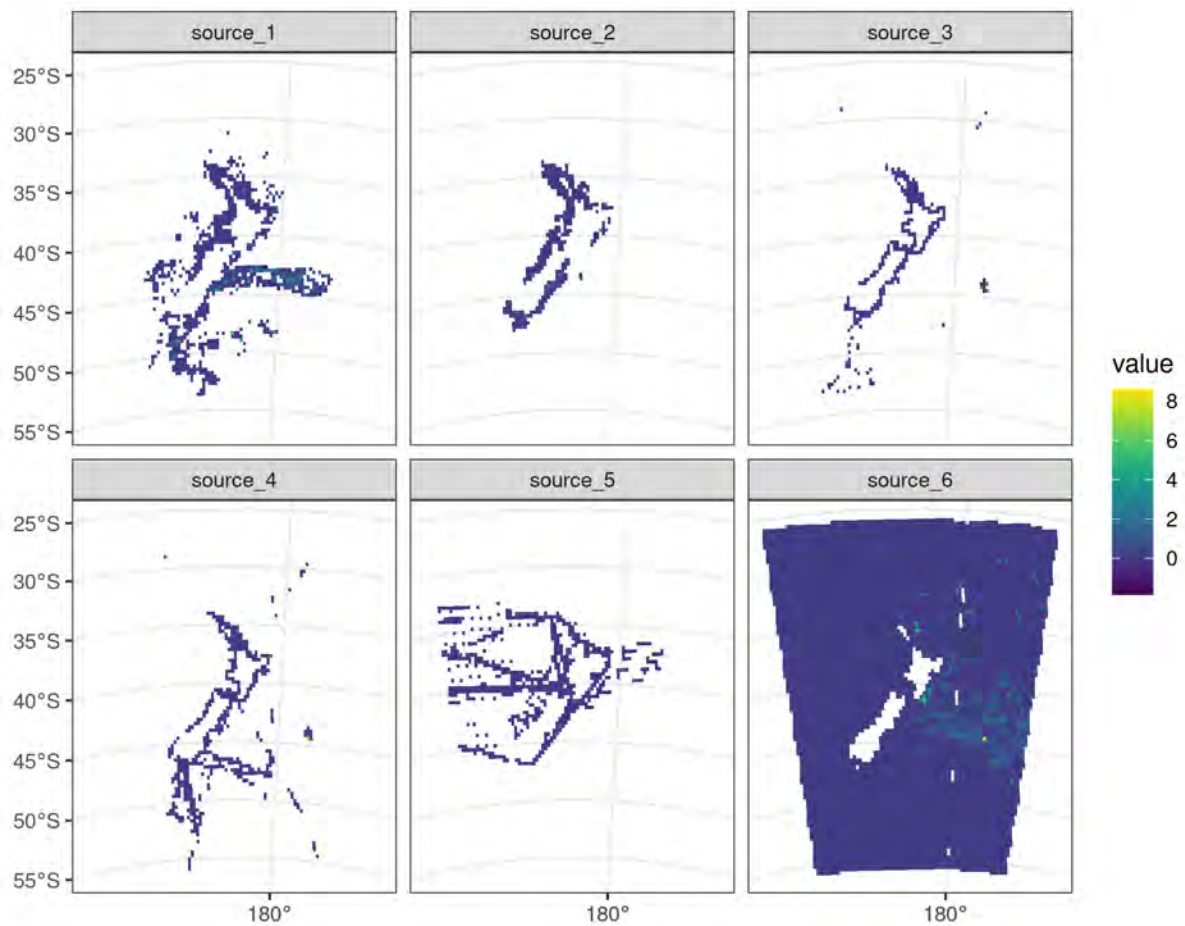


Figure E.23: Maximum spatially-explicit residuals by data source (1 = paper form, 2 = Nomad, 3 = eBird stationary, 4 = eBird travelling, 5 = Te Papa, 6 = tracking) for the final Chatham Island albatross model.

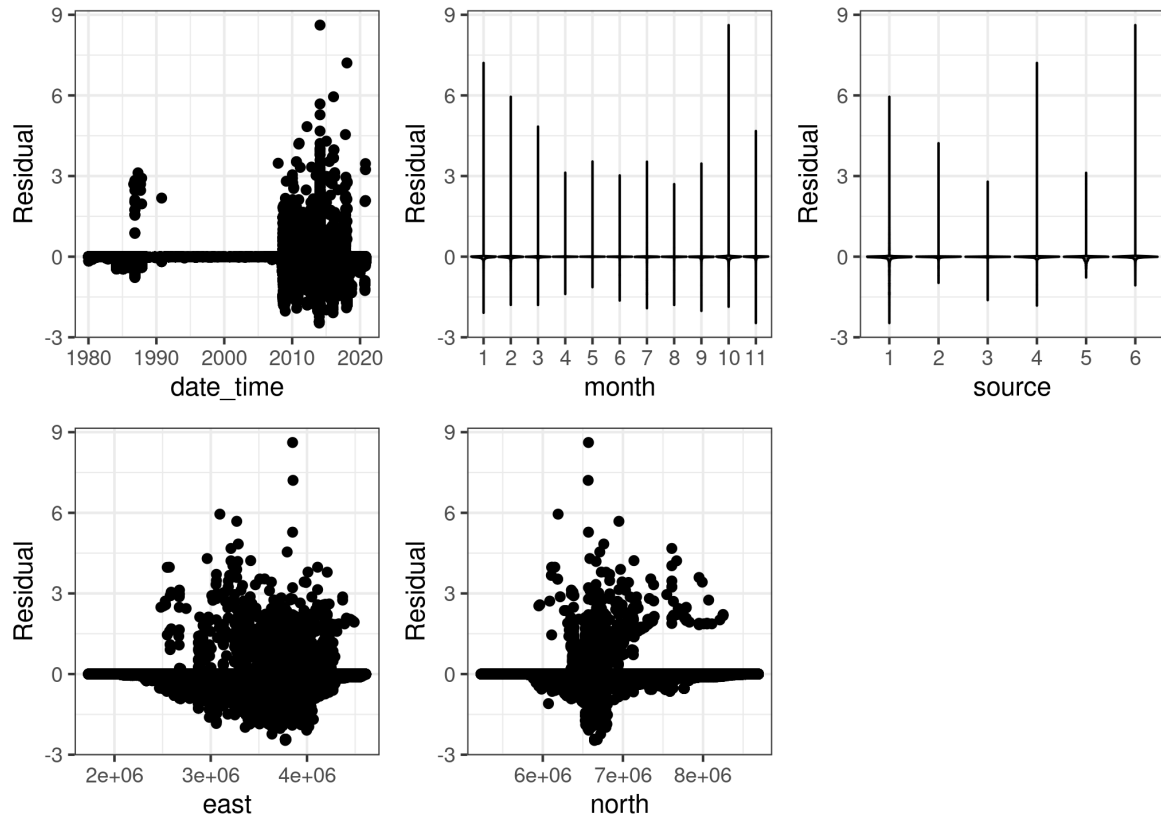


Figure E.24: Residual plots for the final Chatham Island albatross model by date, month, source, easting, and northing.

Salvin's albatross

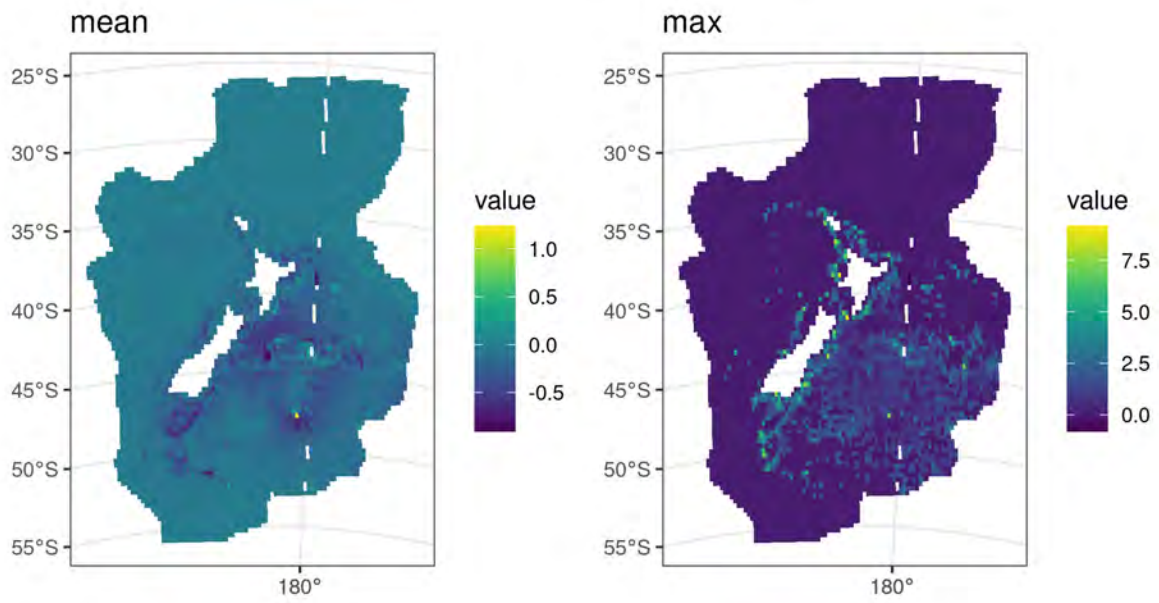


Figure E.25: Spatially-explicit residuals showing the mean residual [left] and the maximum residual [right] for the final Salvin's albatross model.

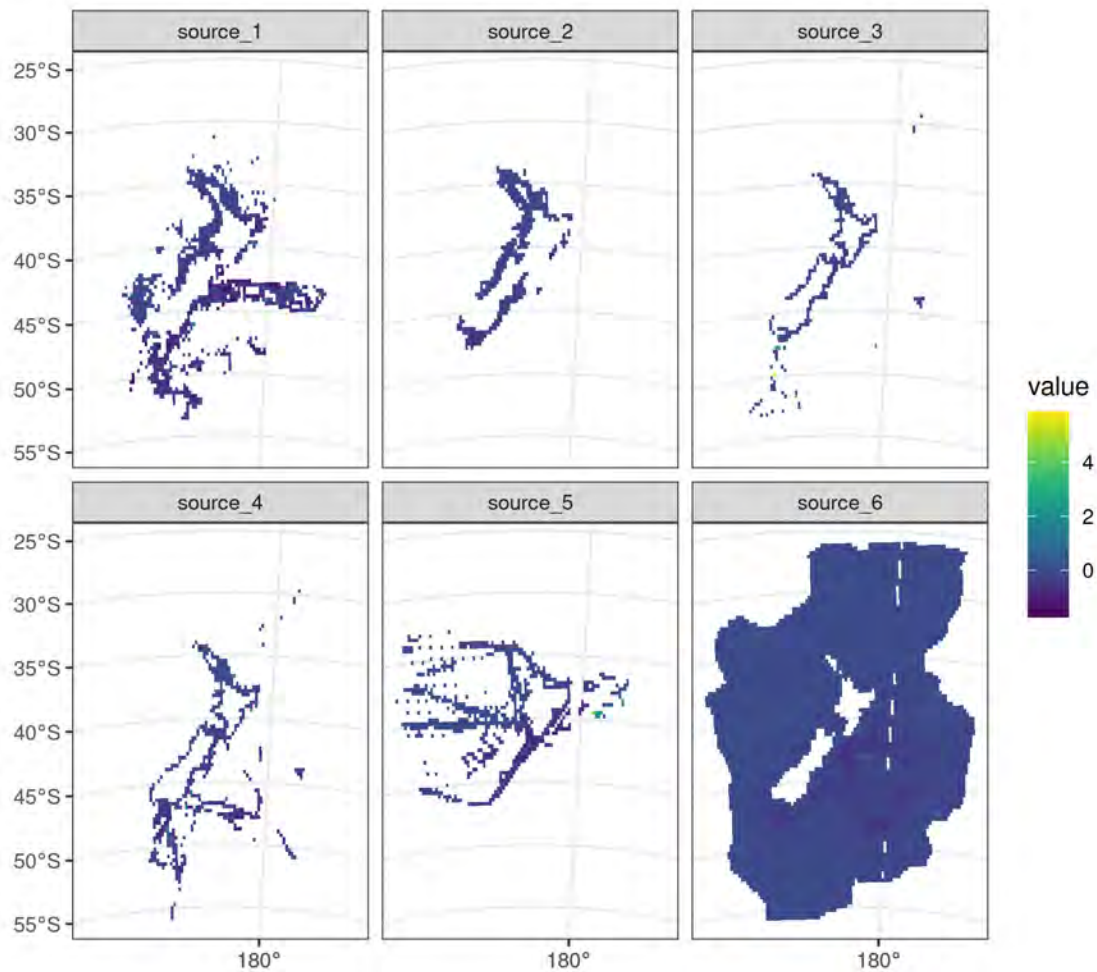


Figure E.26: Mean spatially-explicit residuals by data source (1 = paper form, 2 = Nomad, 3 = eBird stationary, 4 = eBird travelling, 5 = Te Papa, 6 = tracking) for the final Salvin's albatross model.

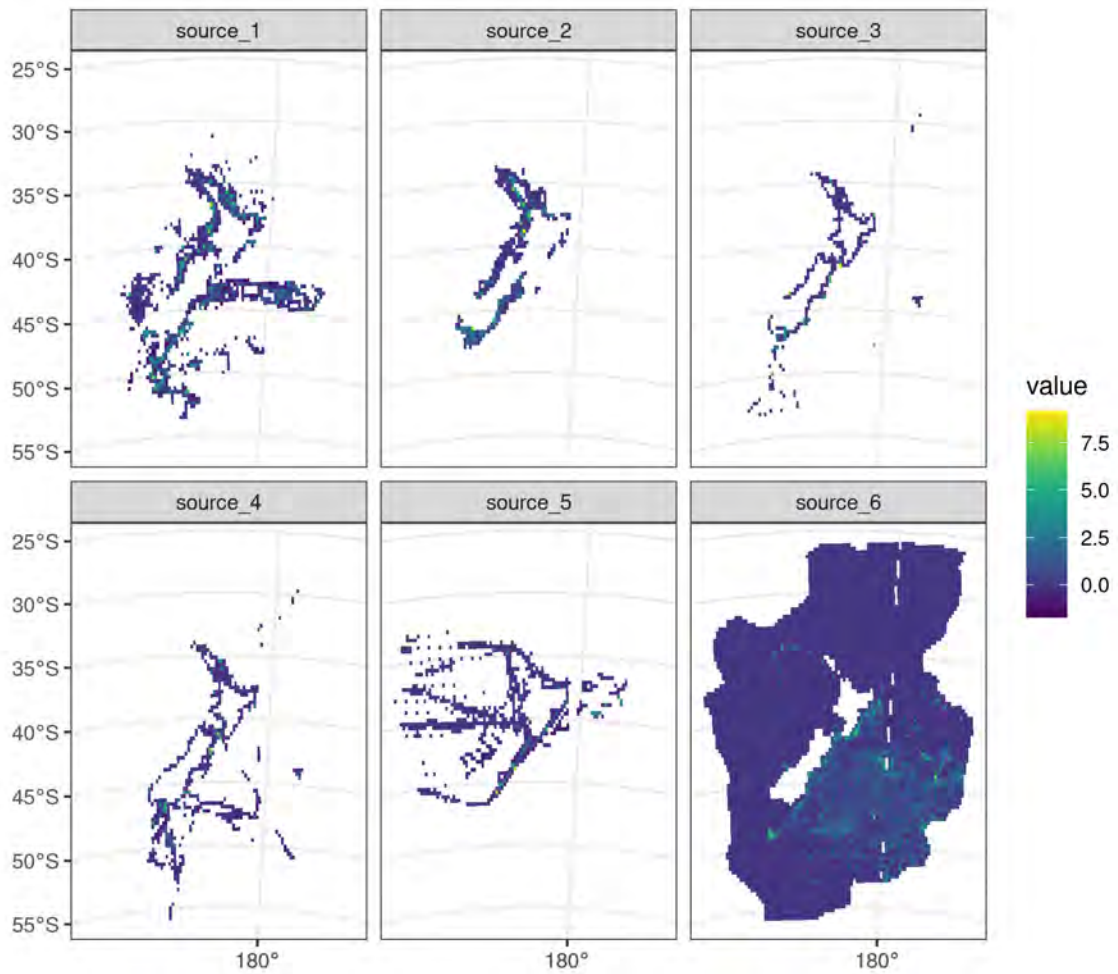


Figure E.27: Maximum spatially-explicit residuals by data source (1 = paper form, 2 = Nomad, 3 = eBird stationary, 4 = eBird travelling, 5 = Te Papa, 6 = tracking) for the final Salvin's albatross model.

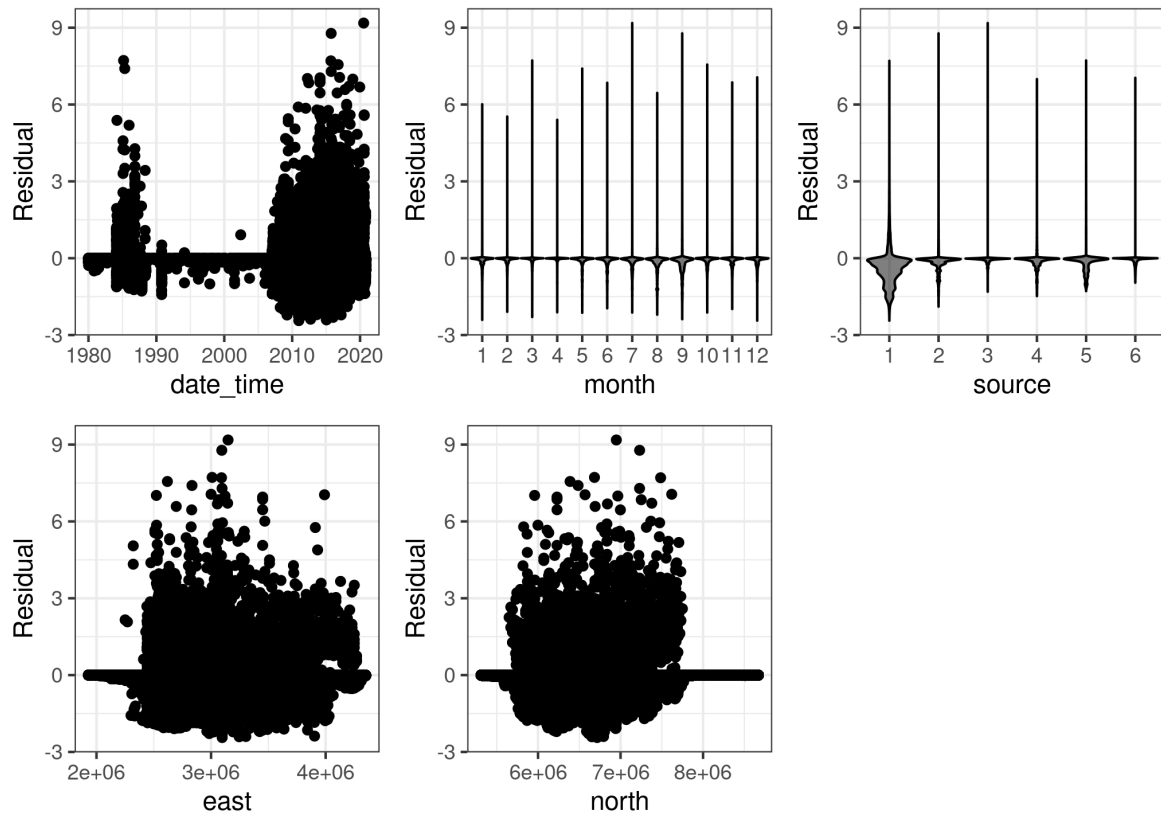


Figure E.28: Residual plots for the final Salvin's albatross model by date, month, source, easting and northing.

White-capped albatross

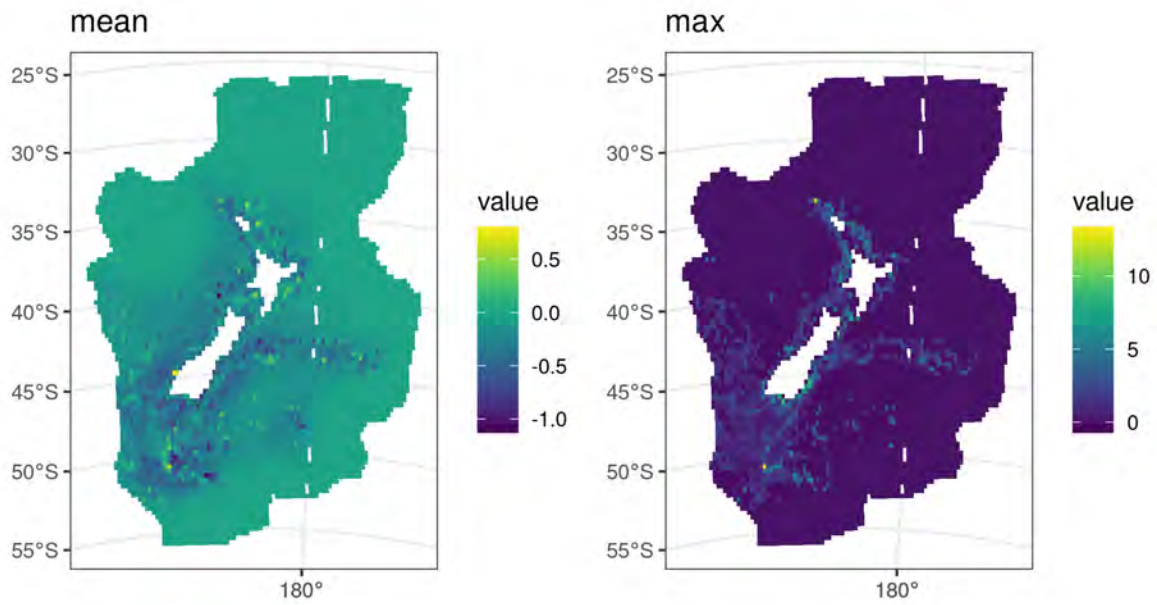


Figure E.29: Spatially-explicit residuals showing the mean residual [left] and the maximum residual [right] for the final white-capped albatross model.

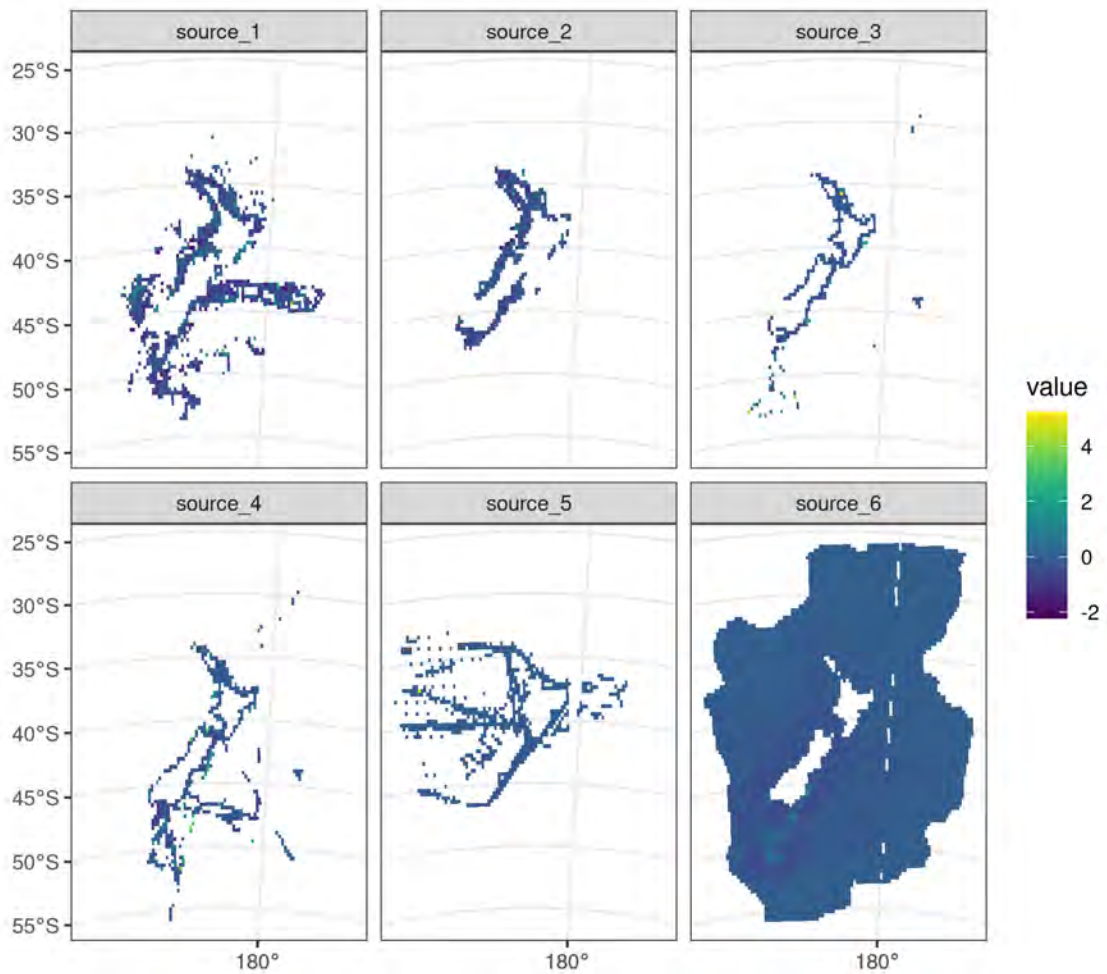


Figure E.30: Mean spatially-explicit residuals by data source (1 = paper form, 2 = Nomad, 3 = eBird stationary, 4 = eBird travelling, 5 = Te Papa, 6 = tracking) for the final white-capped albatross model.

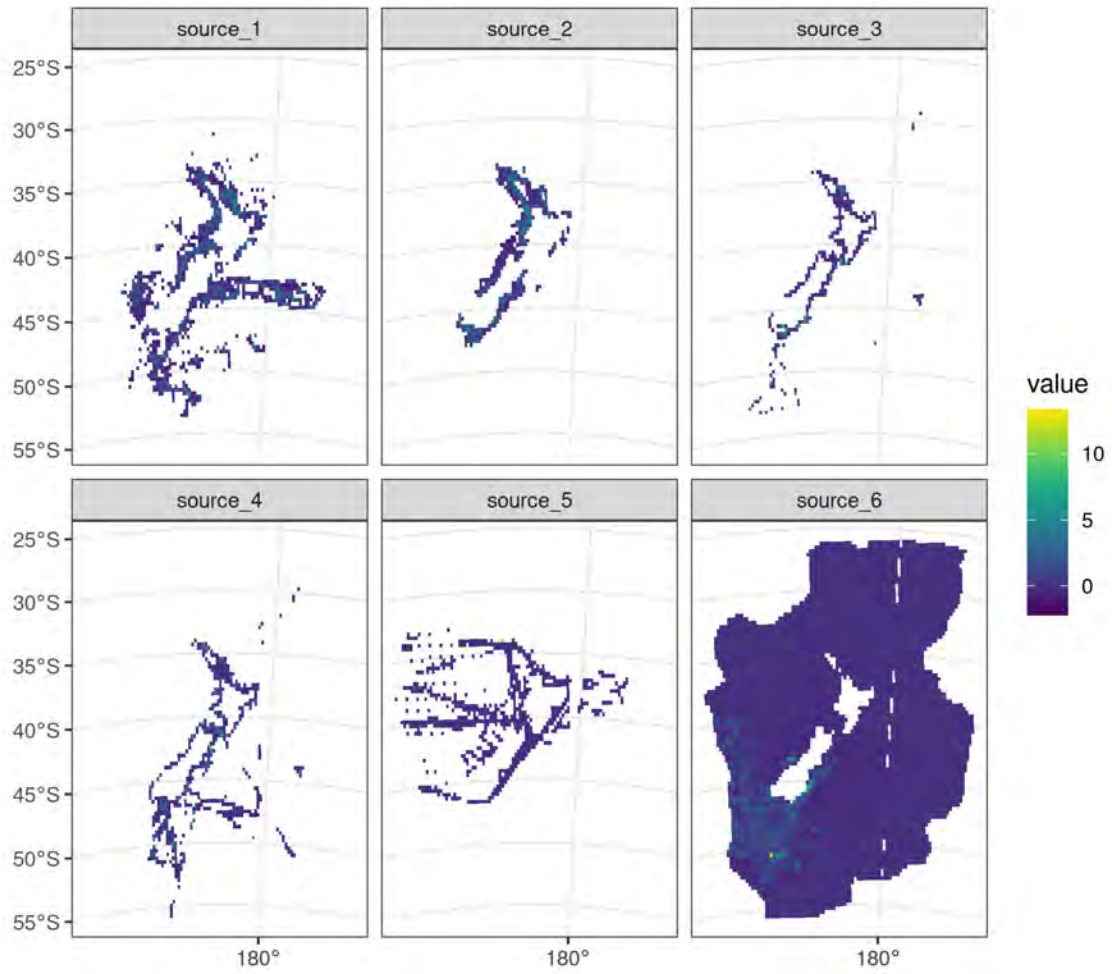


Figure E.31: Maximum spatially-explicit residuals by data source (1 = paper form, 2 = Nomad, 3 = eBird stationary, 4 = eBird travelling, 5 = Te Papa, 6 = tracking) for the final white-capped albatross model.

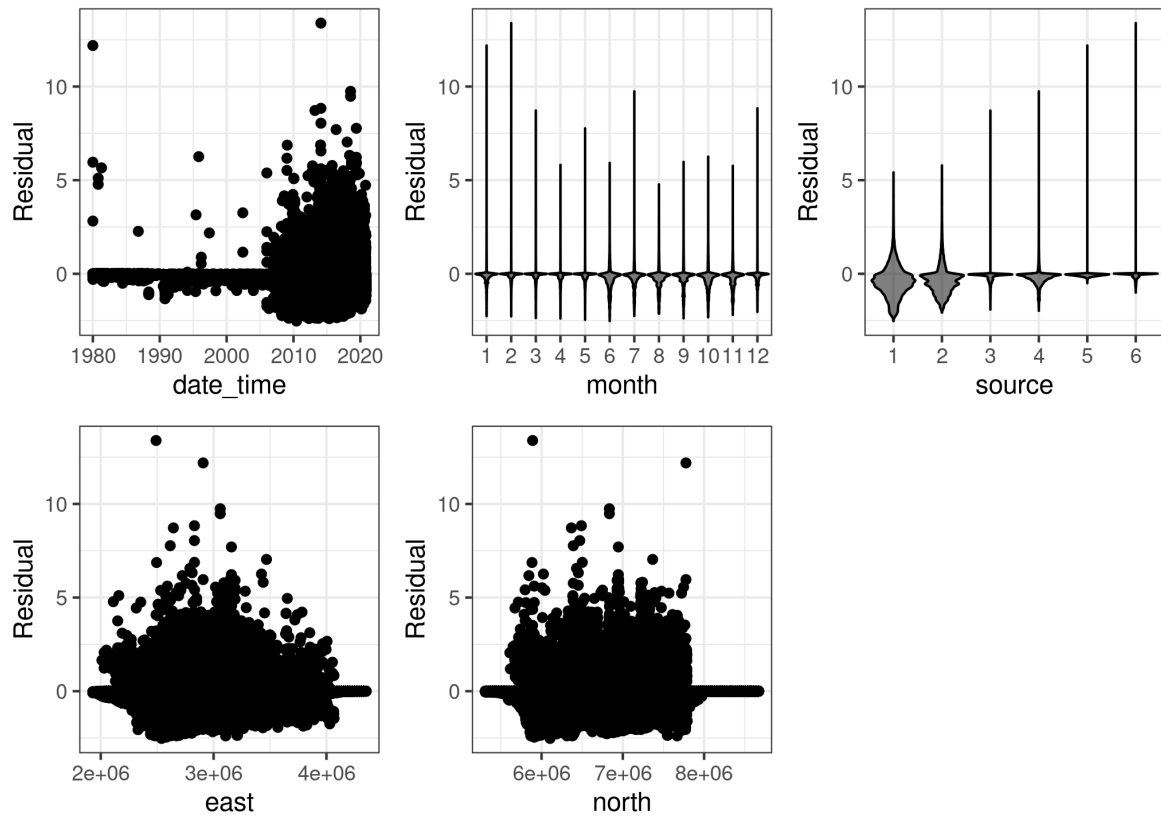


Figure E.32: Residual plots for final white-capped albatross model by date, month, source, easting, and northing.

Antipodean albatross

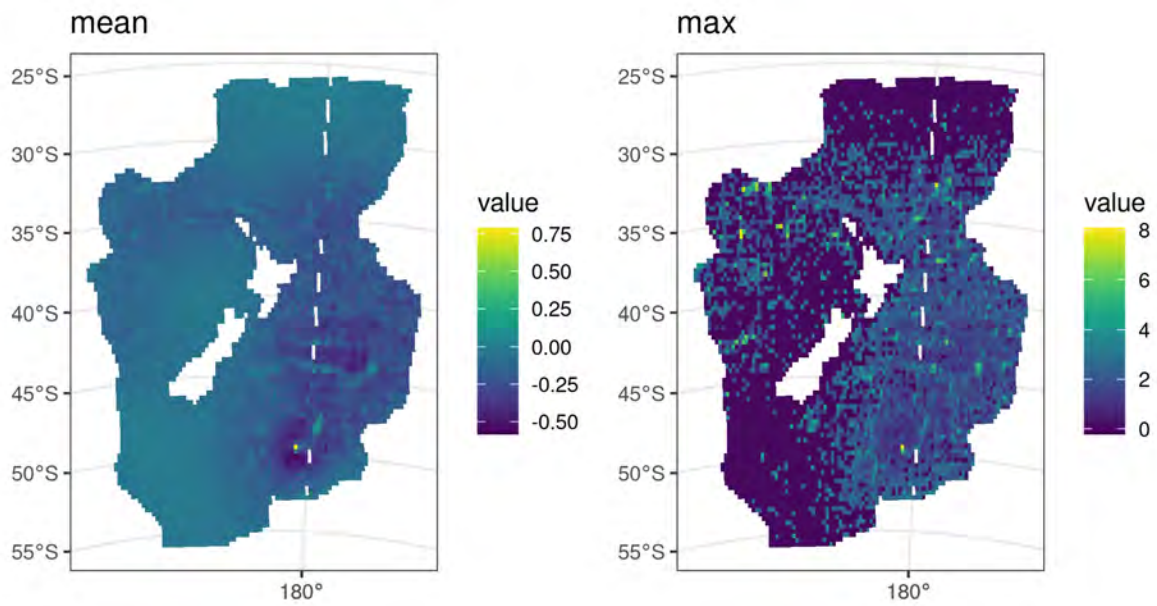


Figure E.33: Spatially-explicit residuals showing the mean residual [left] and the maximum residual [right] for the final Antipodean albatross model.

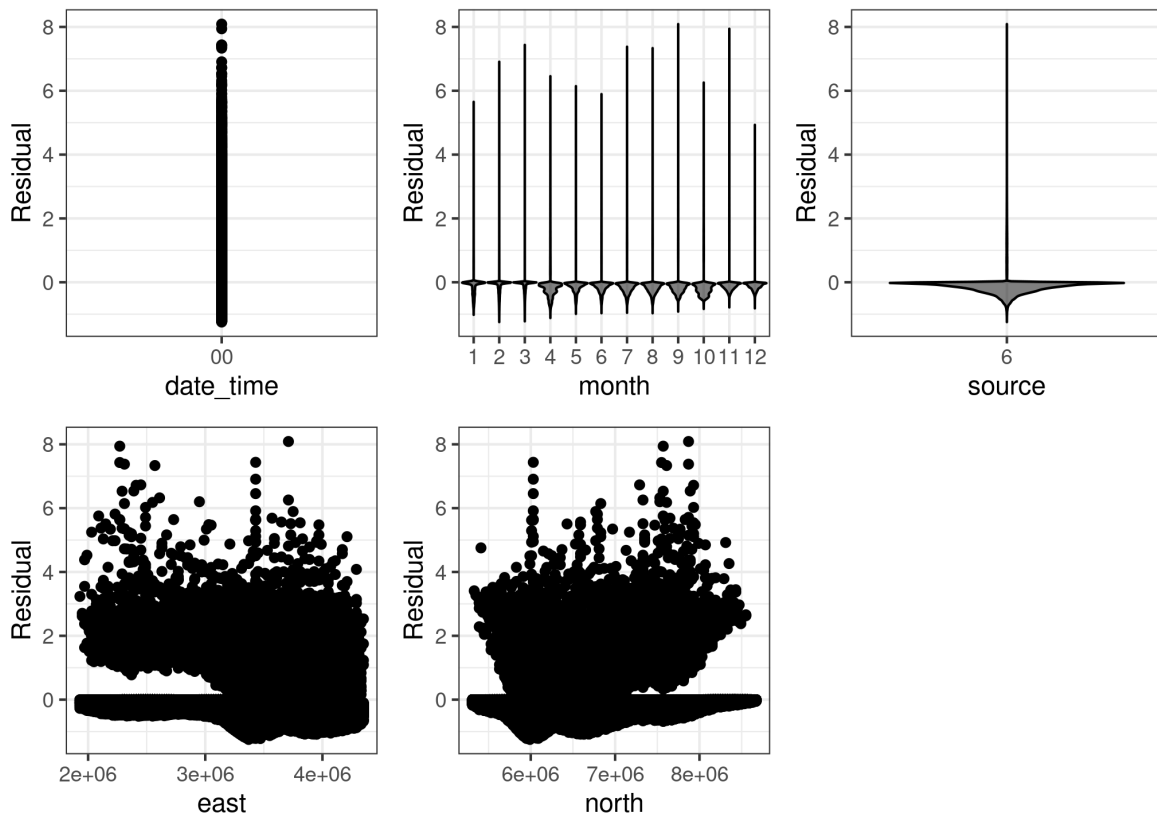


Figure E.34: Residual plots for final Antipodean albatross model by date, month, source, easting, and northing.

Gibson's albatross

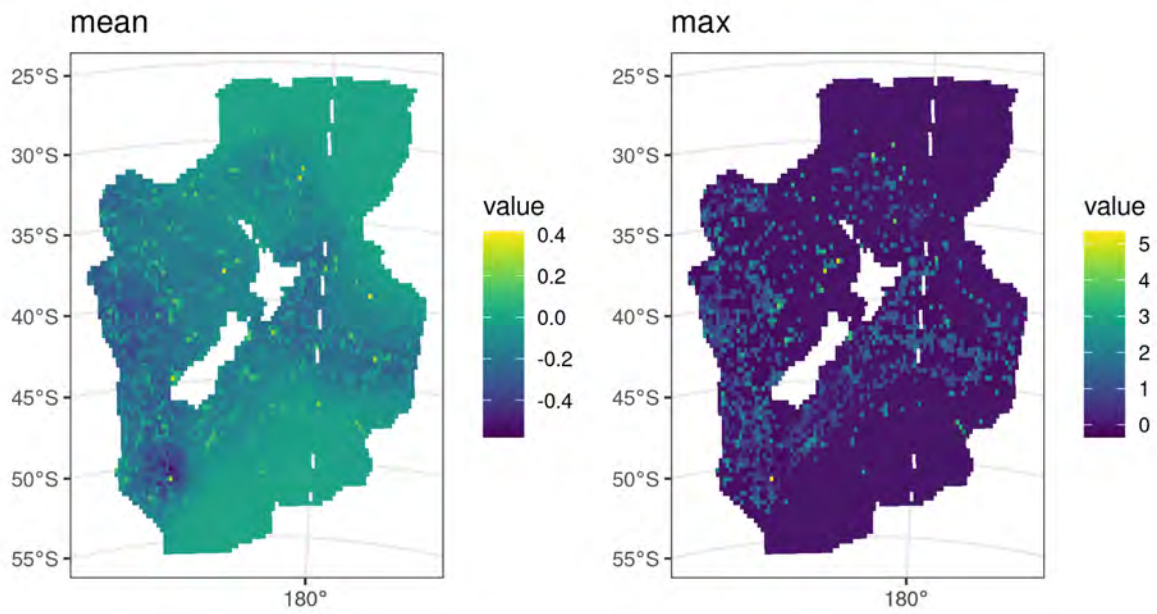


Figure E.35: Spatially-explicit residuals showing the mean residual [left] and the maximum residual [right] for the final Gibson's albatross model.

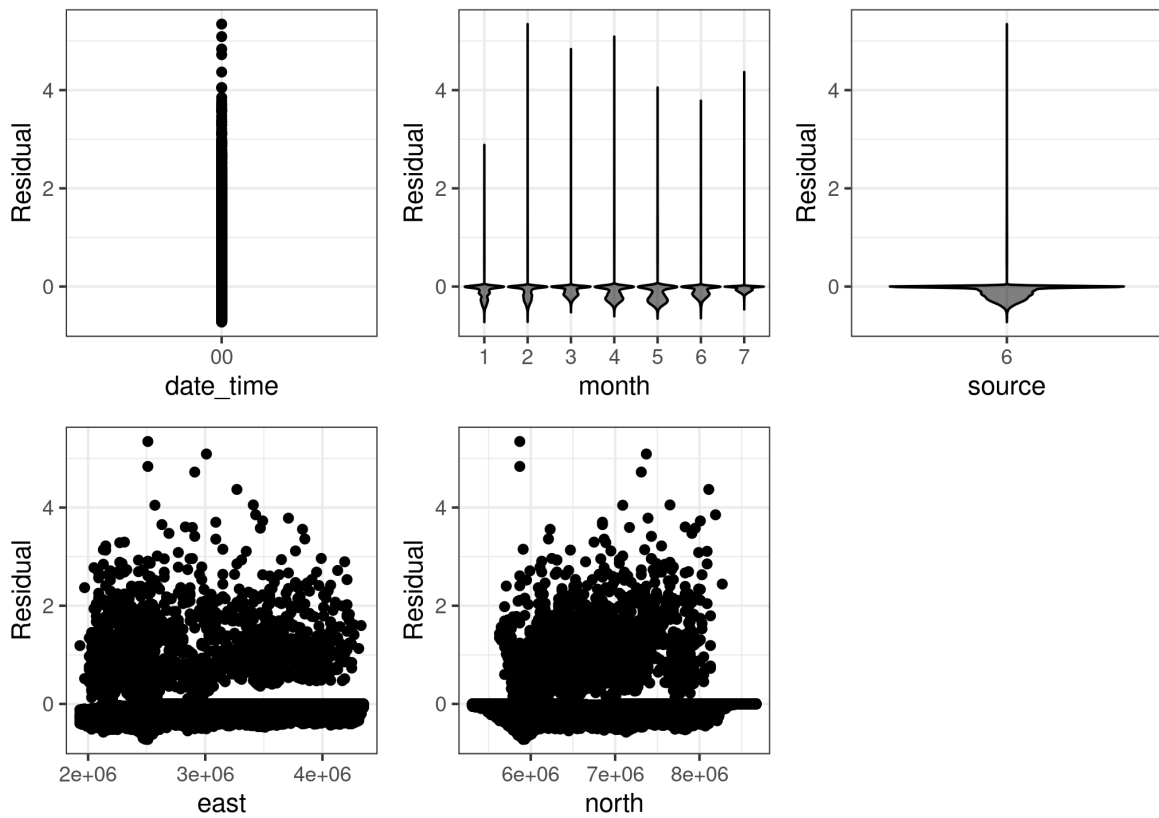


Figure E.36: Residual plots for final Gibson's albatross model by date, month, source, easting, and northing.

Yellow-eyed penguin

Fledglings

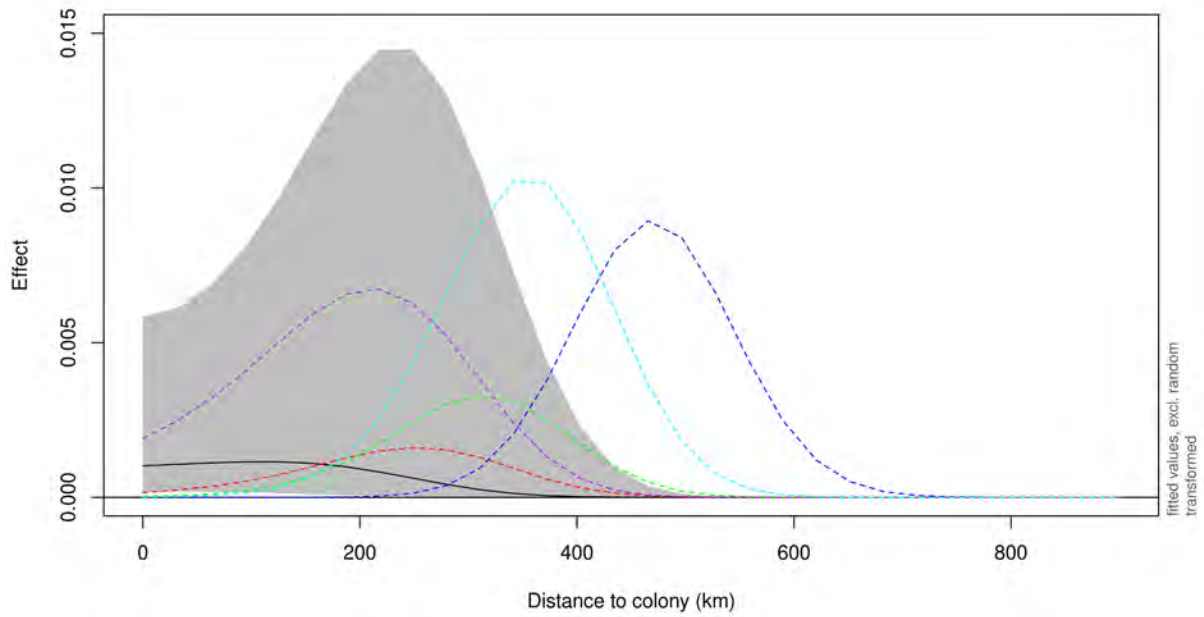


Figure E.37: The distance to colony random effect in the final fledgling yellow-eyed penguin model. Shaded area represents the main effect, coloured lines represent selected random effects.

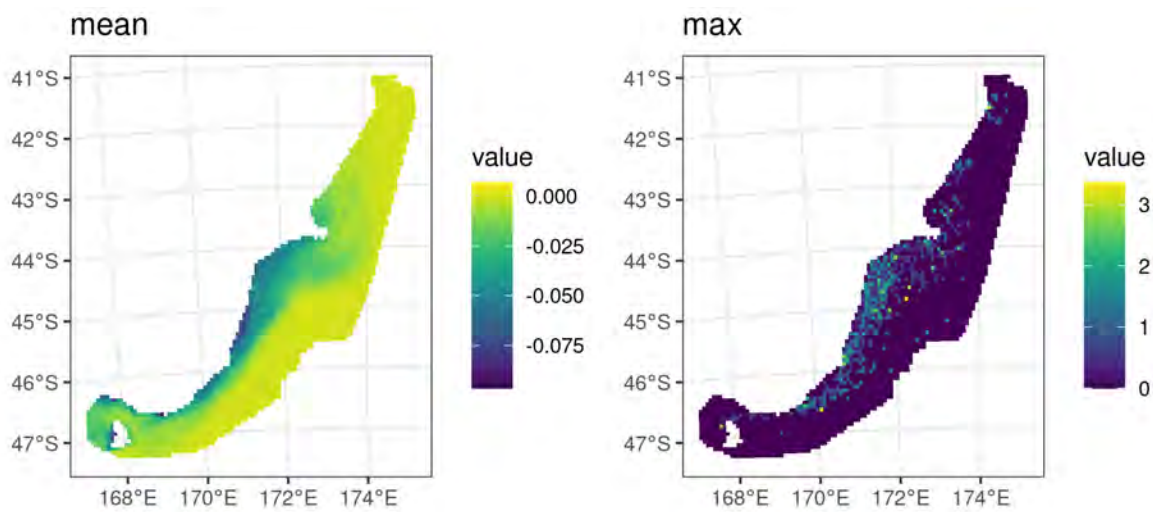


Figure E.38: Spatially-explicit residuals showing the mean residual [left] and the maximum residual [right] for the final fledgling yellow-eyed penguin model.

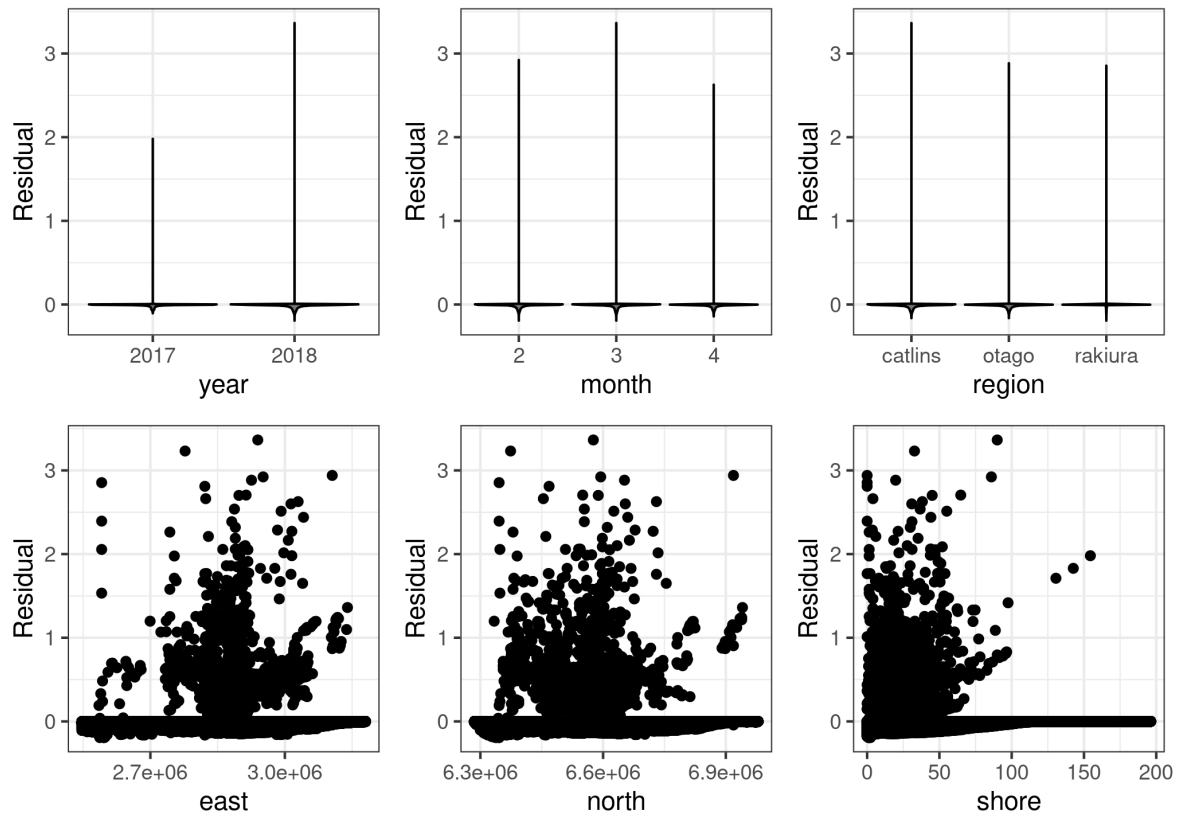


Figure E.39: Residuals for the final fledgling yellow-eyed penguin model by year, month, region, easting and northing, and distance to shore (km).

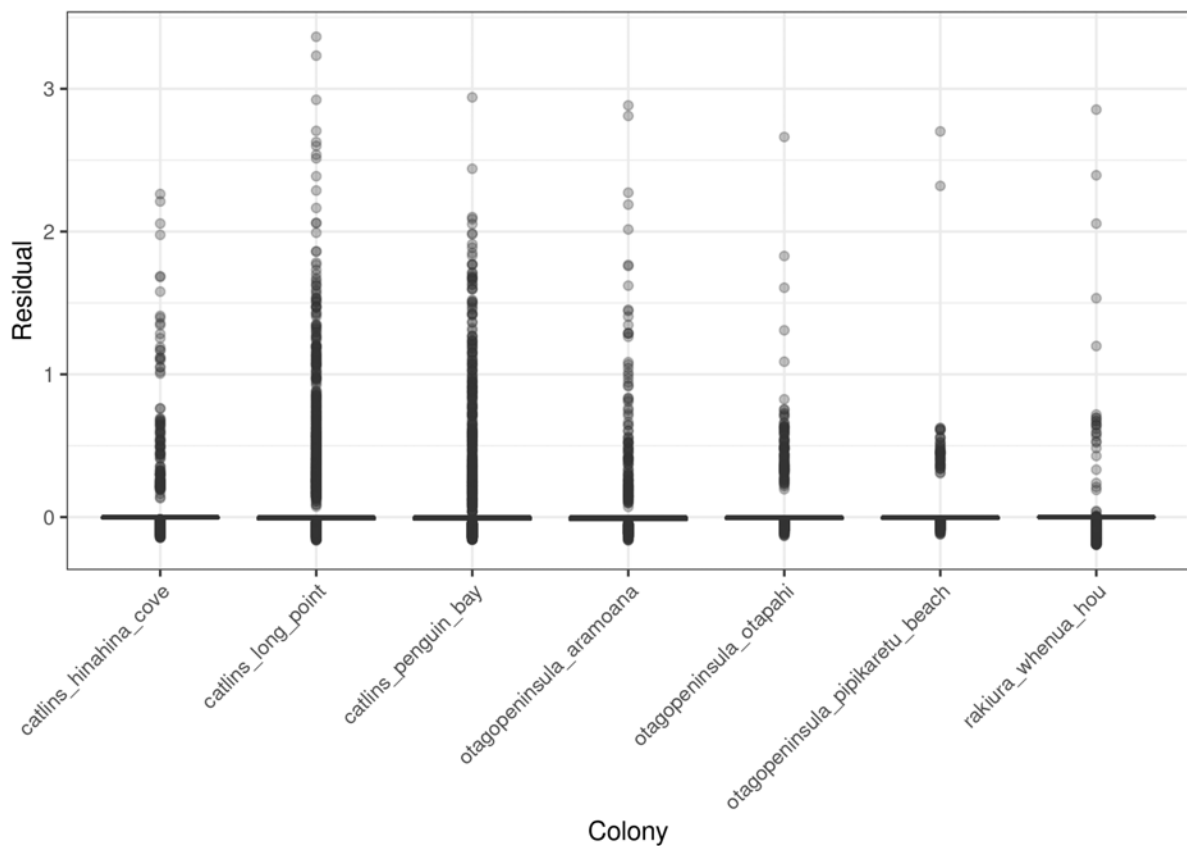


Figure E.40: Residuals for the final fledgling yellow-eyed penguin model by location of tagging.

Adults

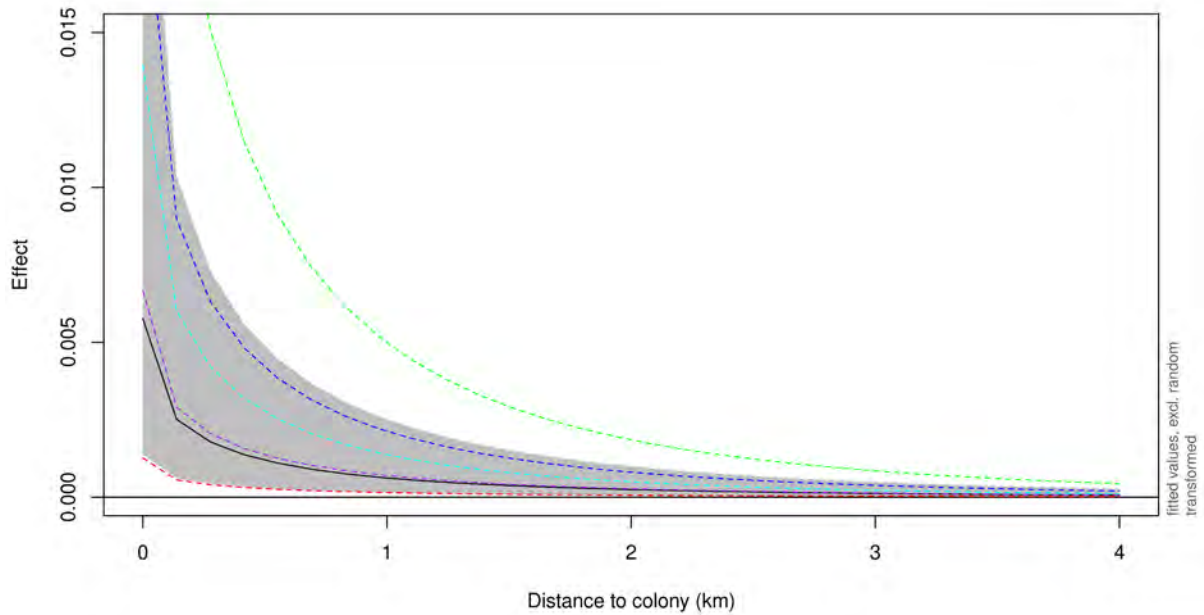


Figure E.41: The distance to colony random-effect in the final adult yellow-eyed penguin model. Shaded area represents the main effect, coloured lines represent selected random effects.

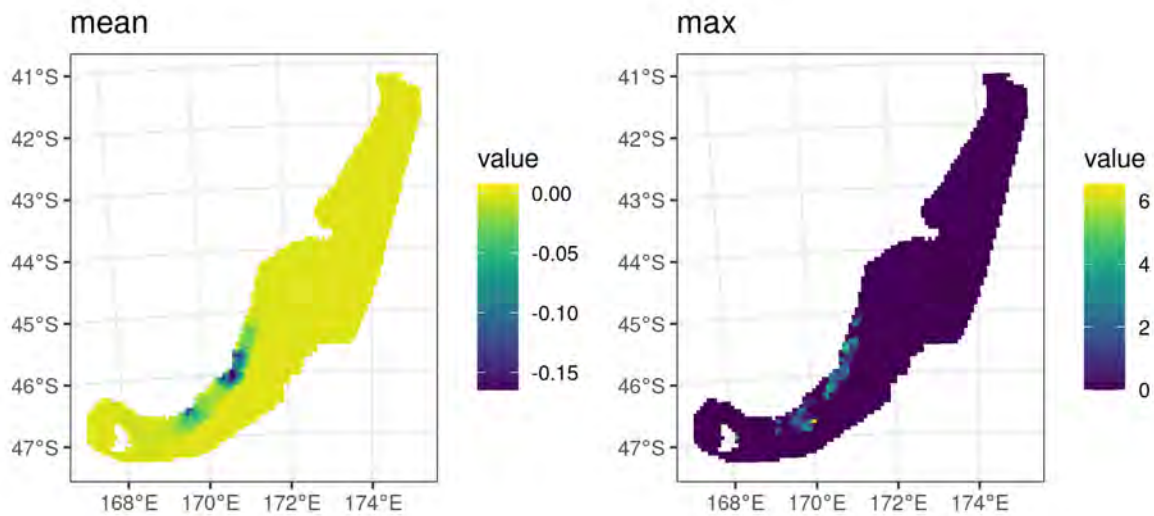


Figure E.42: Spatially-explicit residuals showing the mean residual [left] and the maximum residual [right] for the final adult yellow-eyed penguin model.

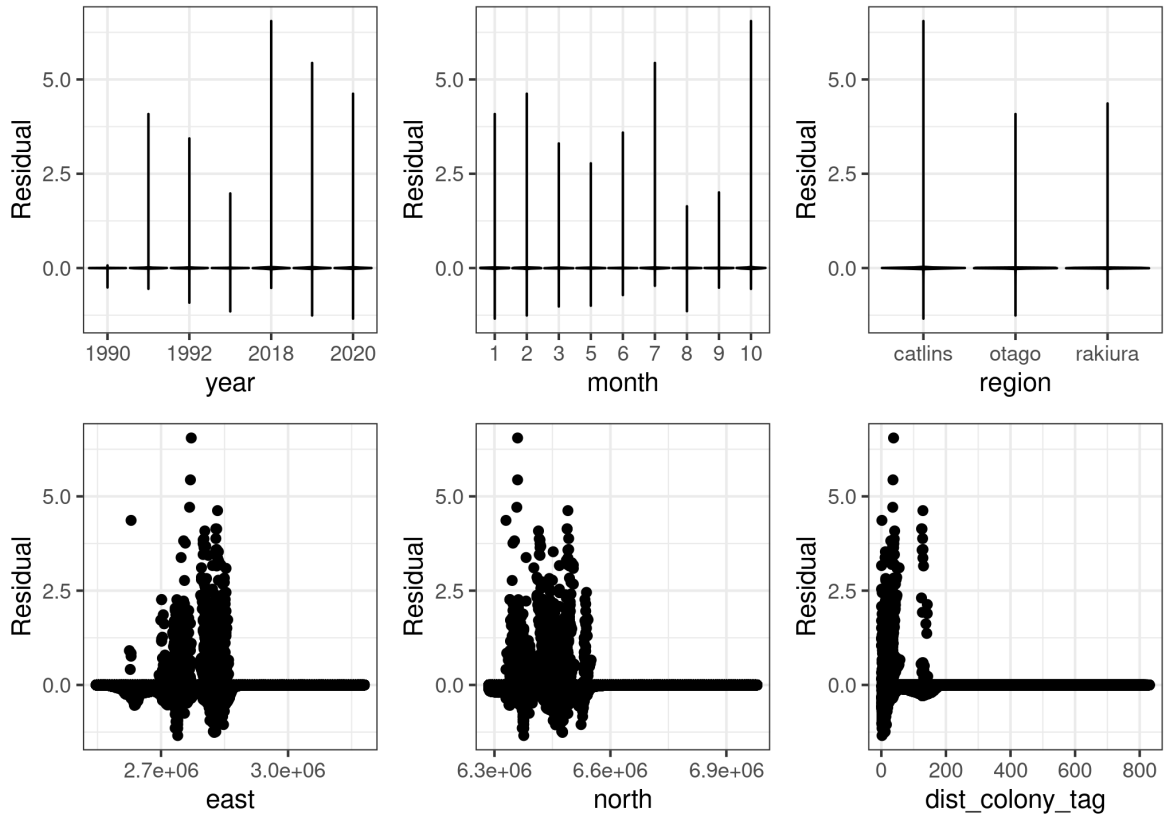


Figure E.43: Residuals for the final adult yellow-eyed penguin model by year, month, region, easting and northing, and distance to colony (km).

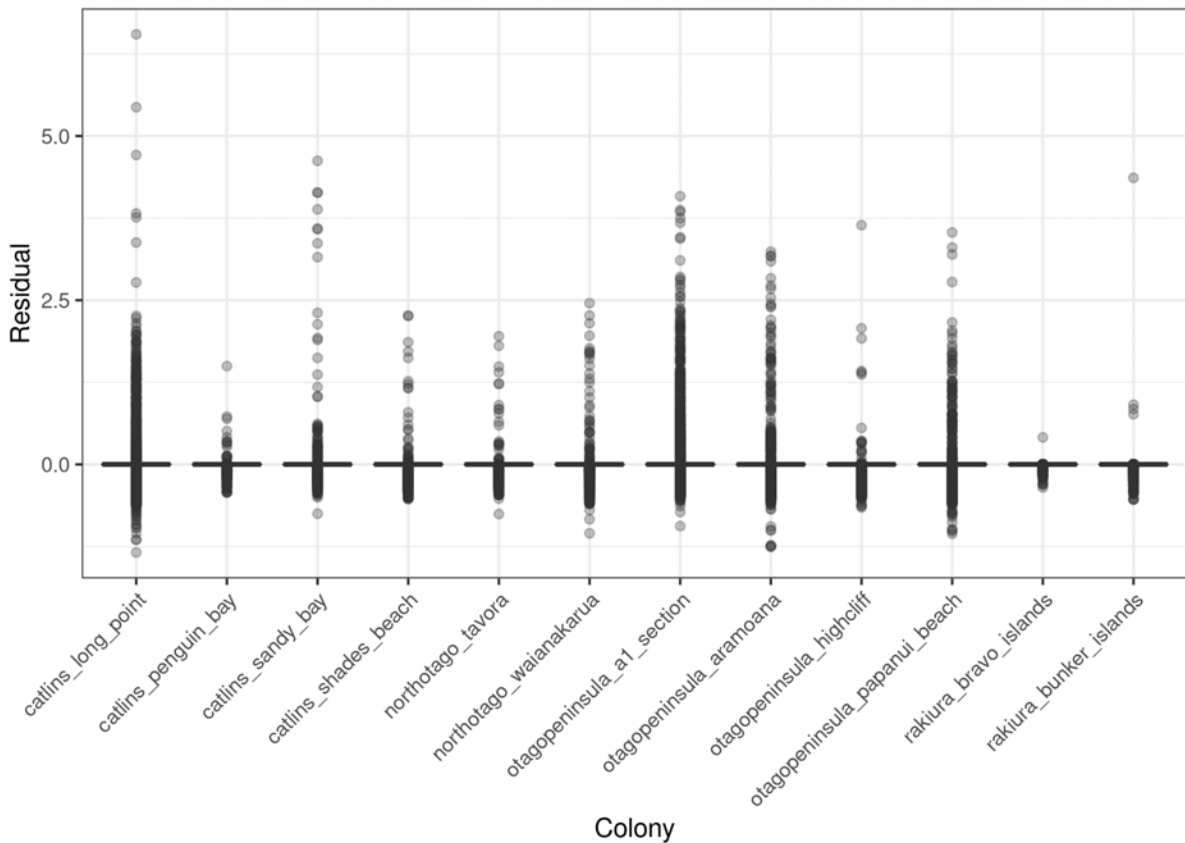


Figure E.44: Residuals for the final adult yellow-eyed penguin model by location of tagging.

APPENDIX F. NEW SEABIRD DISTRIBUTION LAYERS

In this Appendix the monthly predictions from the optimal model for each seabird taxon are shown in two ways:

1. using the same scale across all months; and
2. using a different scale in each month, so that the spatial distribution can be discerned in months when most individuals have migrated away from New Zealand.

Note that these model predictions were not rescaled for population size. The colours in each plot represent *relative density* (yellow is high, blue is low) and the *absolute* values are meaningless.

Flesh-footed shearwater

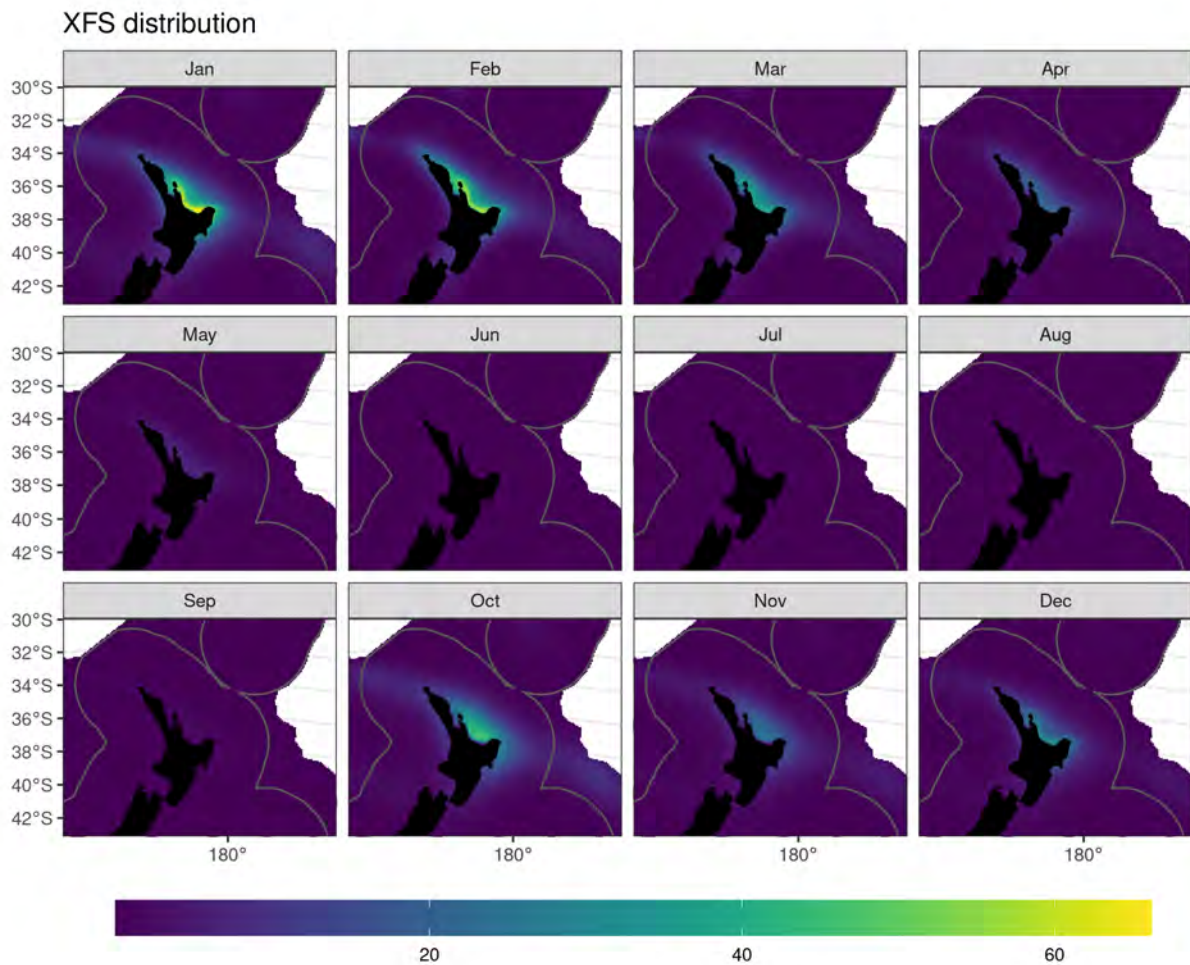


Figure F.1: Predicted relative spatial density of flesh-footed shearwater by month. The colour scale for this figure is shared across all months.

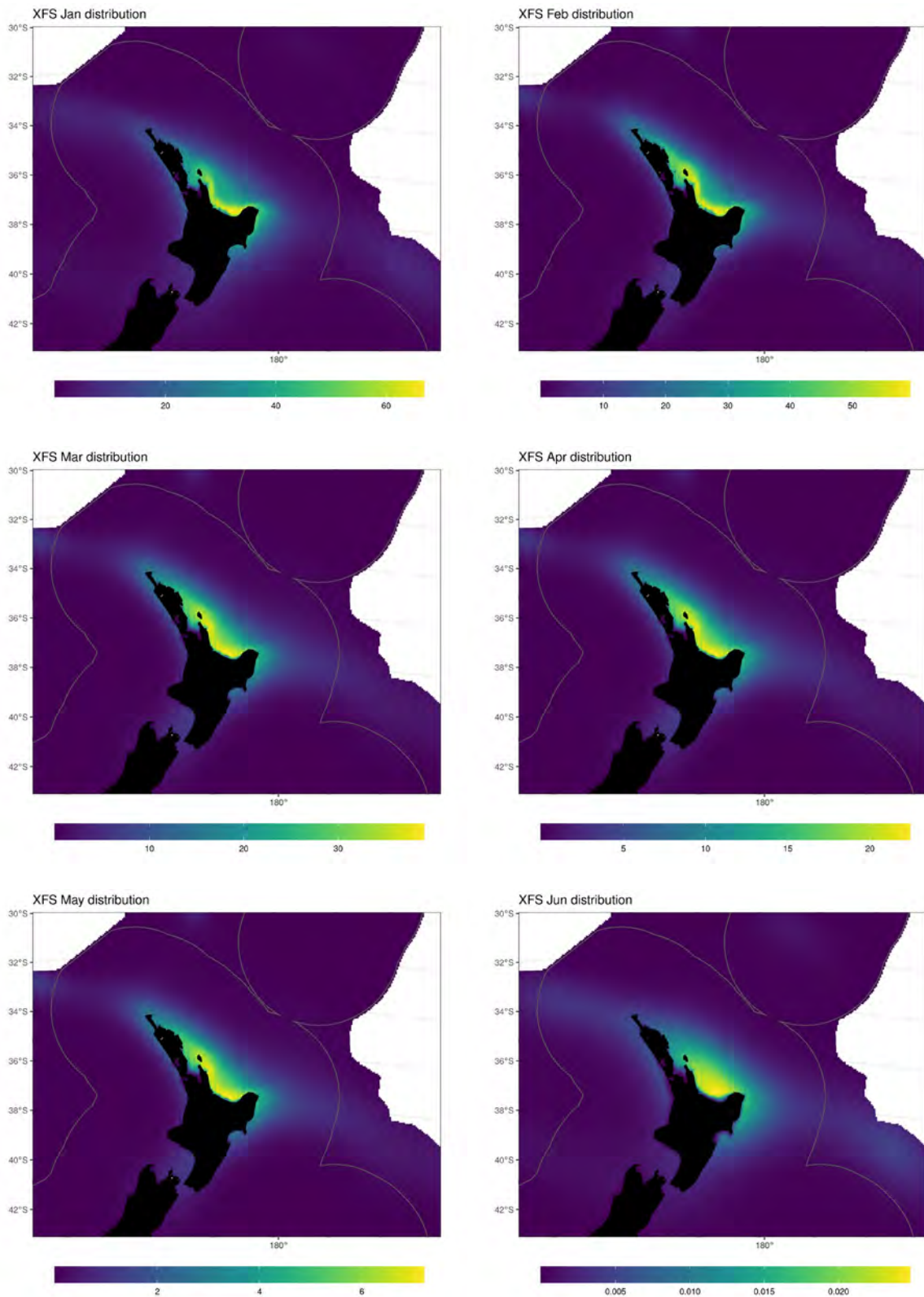


Figure F.2: Predicted relative spatial density of flesh-footed shearwater by month, for January-June. The colour scale for this figure is different for each month.

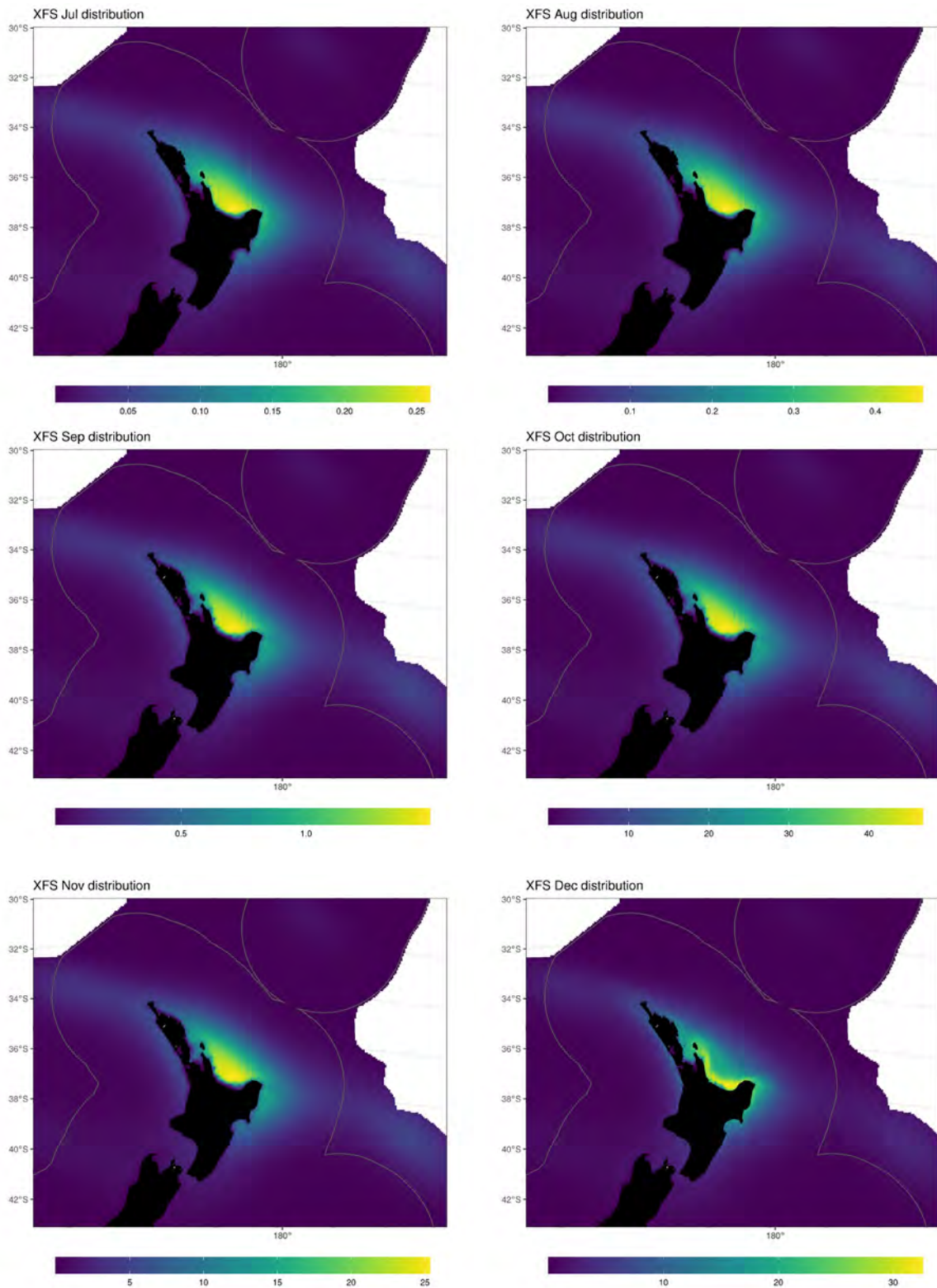


Figure F.3: Predicted relative spatial density of flesh-footed shearwater by month, for July-December. The colour scale for this figure is different for each month.

Black petrel

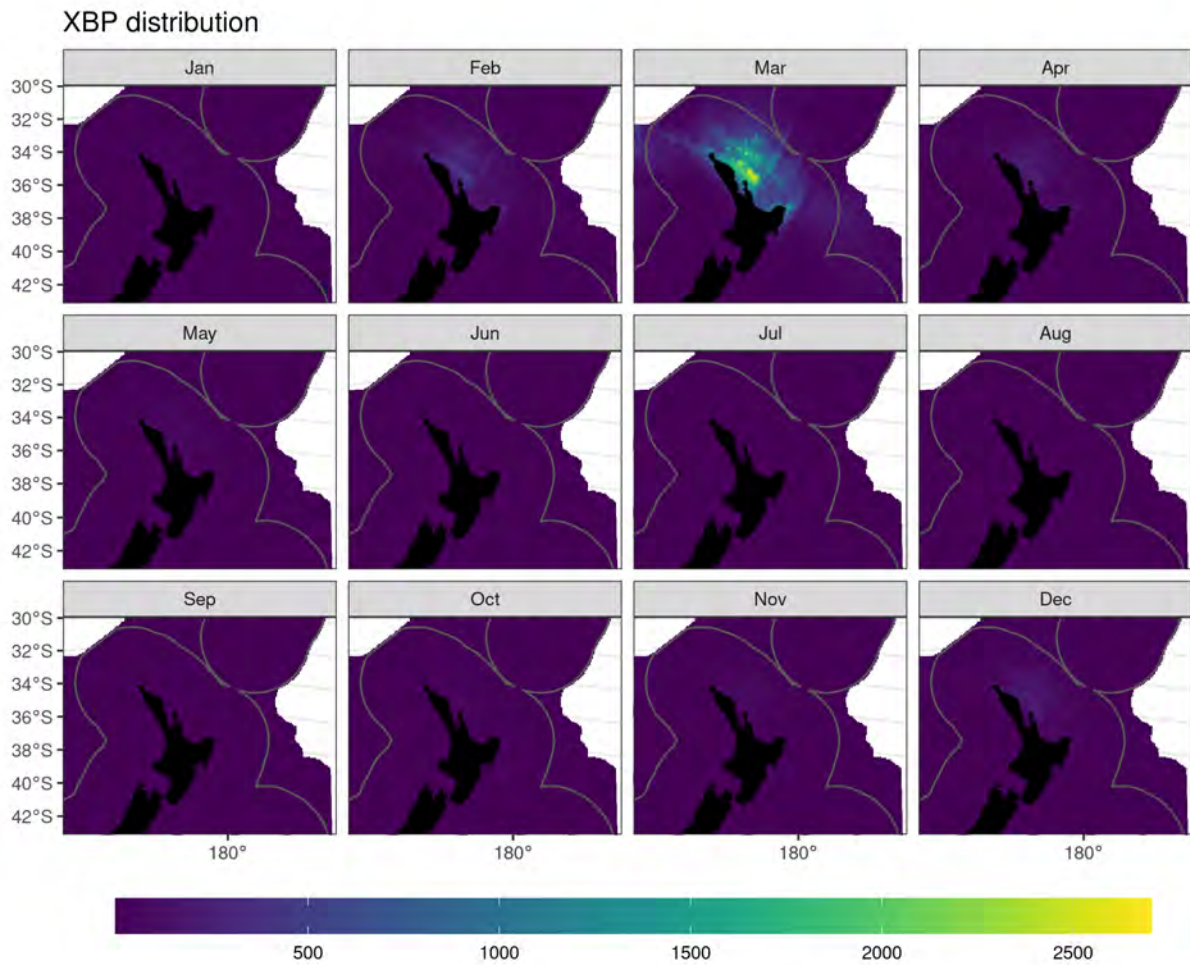


Figure F.4: Predicted relative spatial density of black petrel by month. The colour scale for this figure is shared across all months.

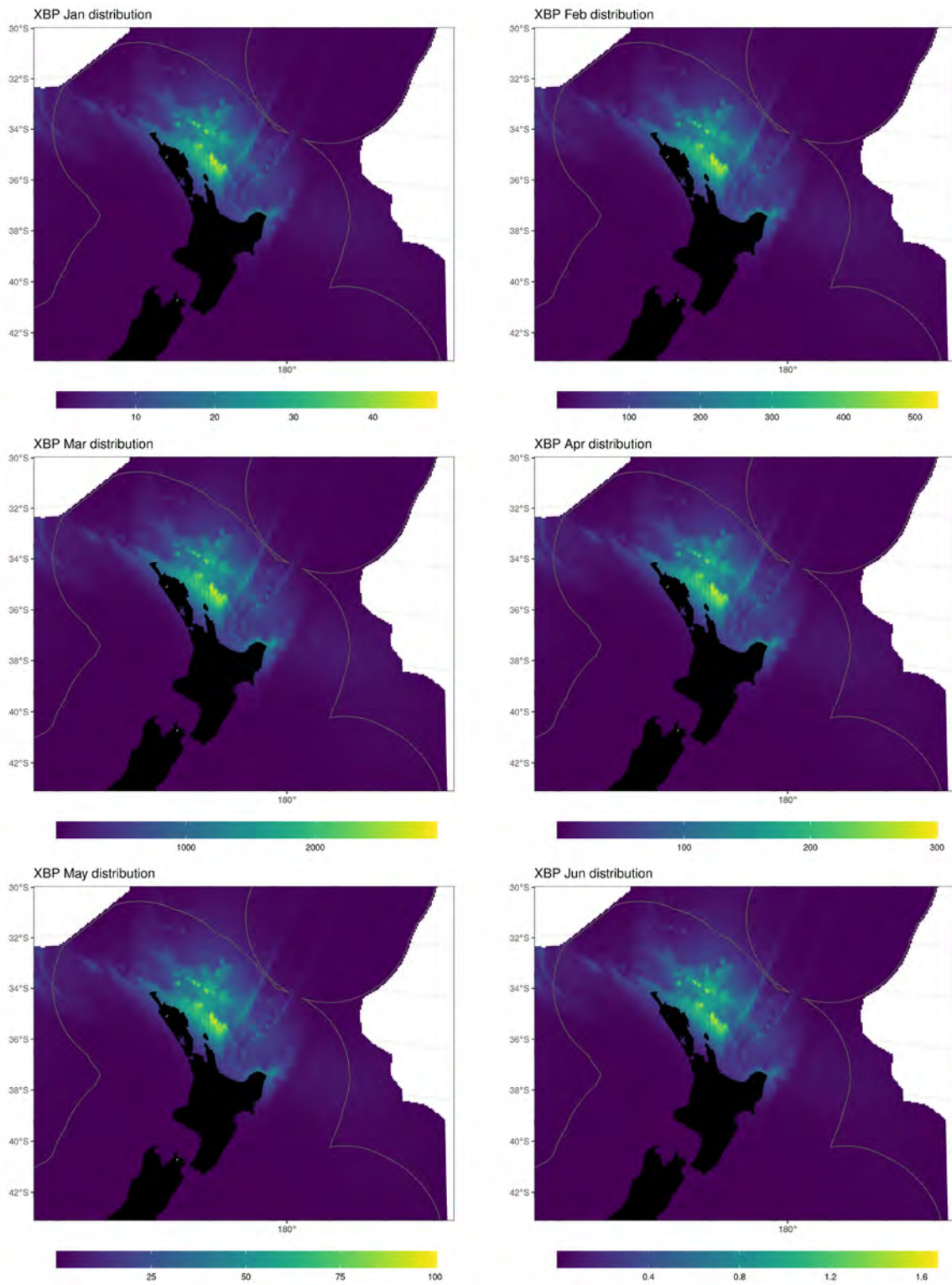


Figure F.5: Predicted relative spatial density of black petrel by month, for January-June. The colour scale for this figure is different for each month.

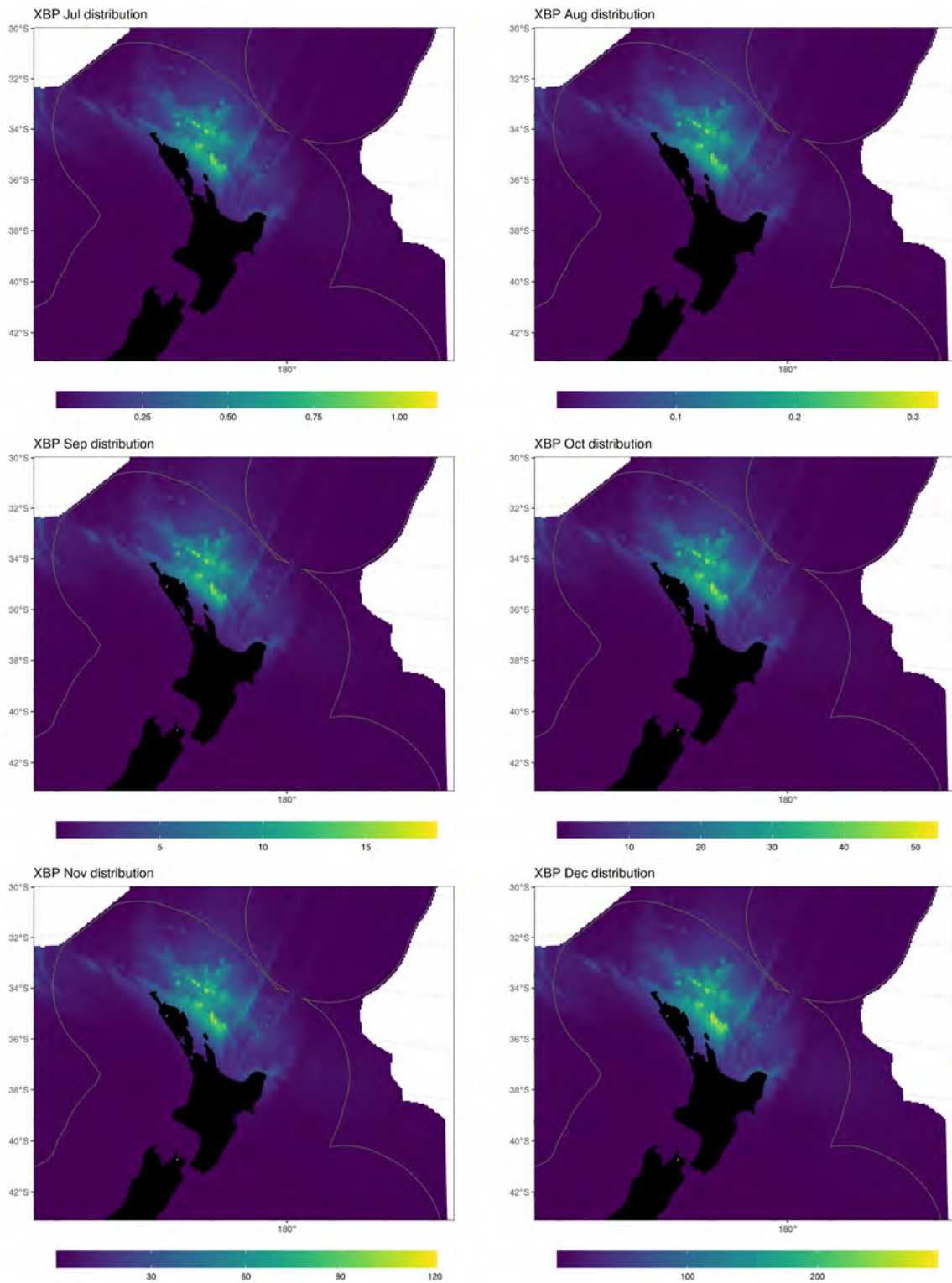


Figure F.6: Predicted relative spatial density of black petrel by month, for July-December. The colour scale for this figure is different for each month.

Westland petrel

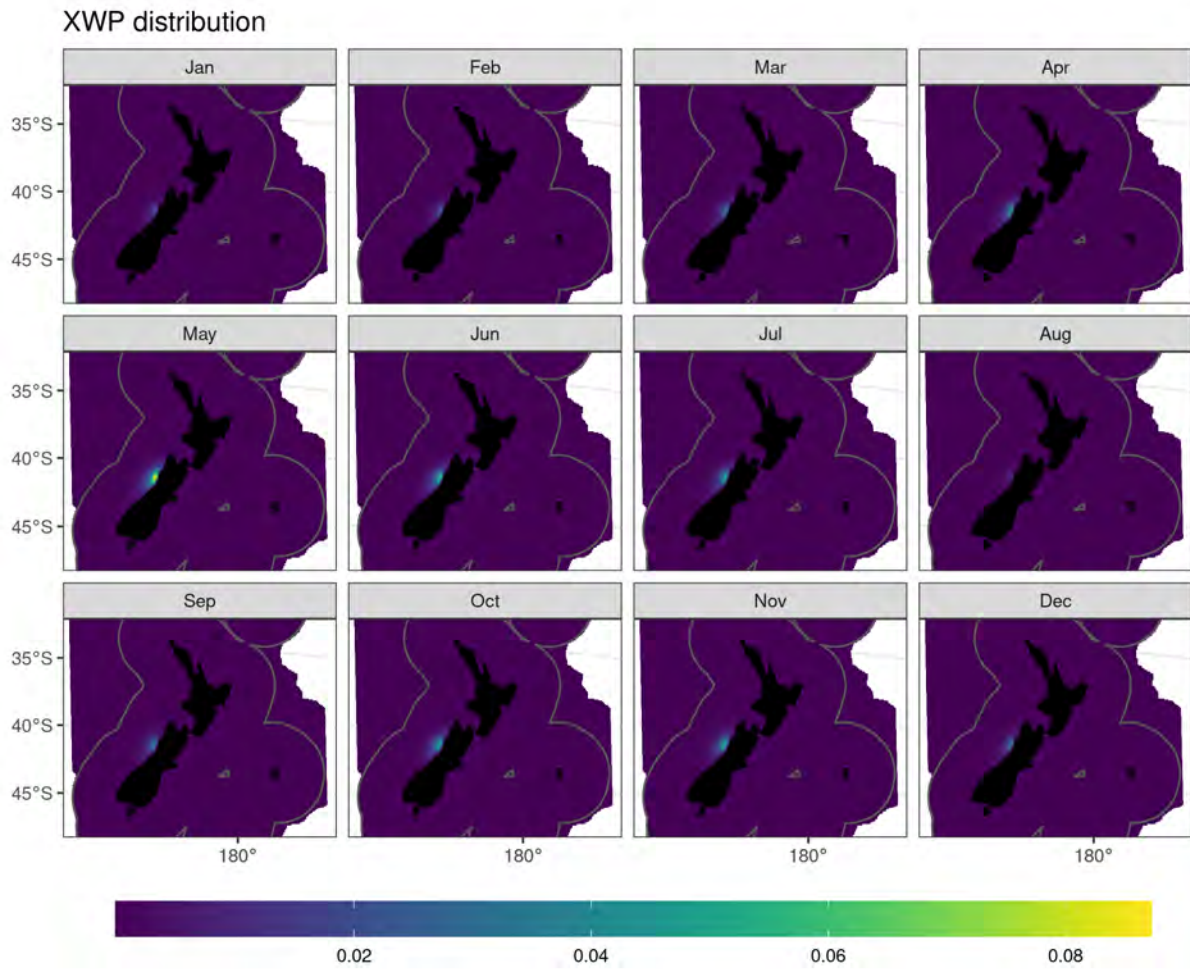


Figure F.7: Predicted relative spatial density of Westland petrel by month. The colour scale for this figure is shared across all months.

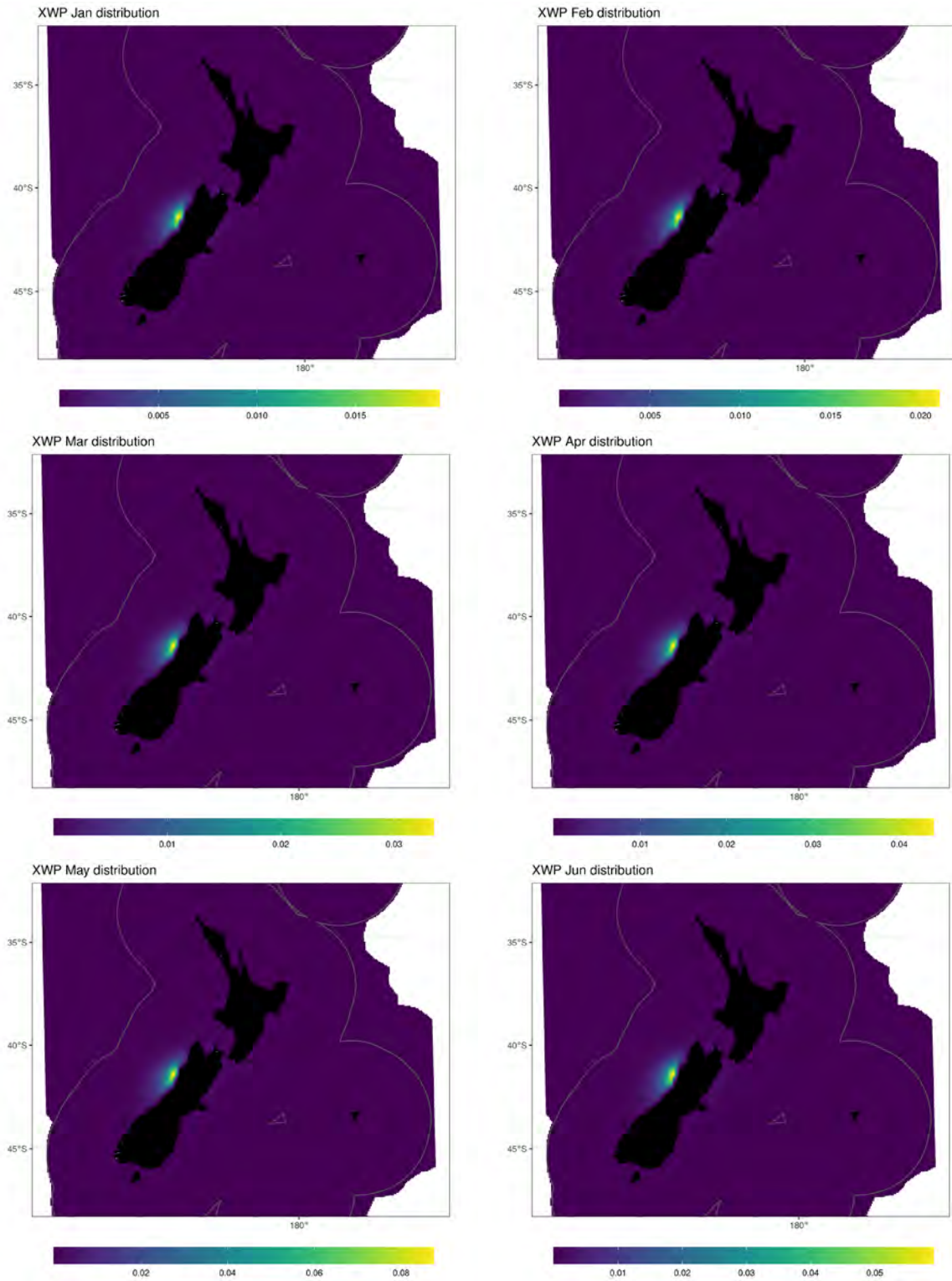


Figure F.8: Predicted relative spatial density of Westland petrel by month, for January-June. The colour scale for this figure is different for each month.

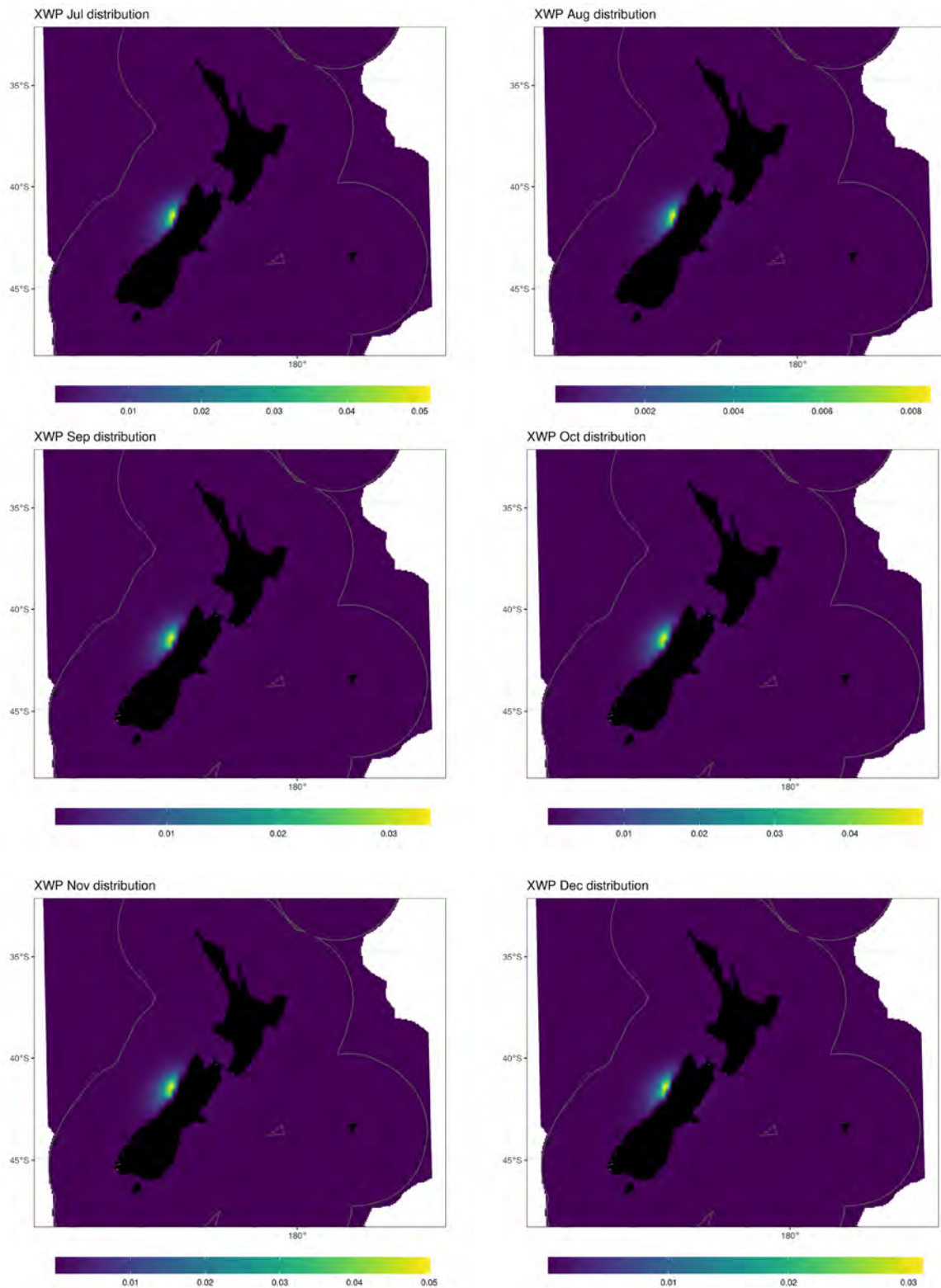


Figure F.9: Predicted relative spatial density of Westland petrel by month, for July-December. The colour scale for this figure is different for each month.

White-chinned petrel

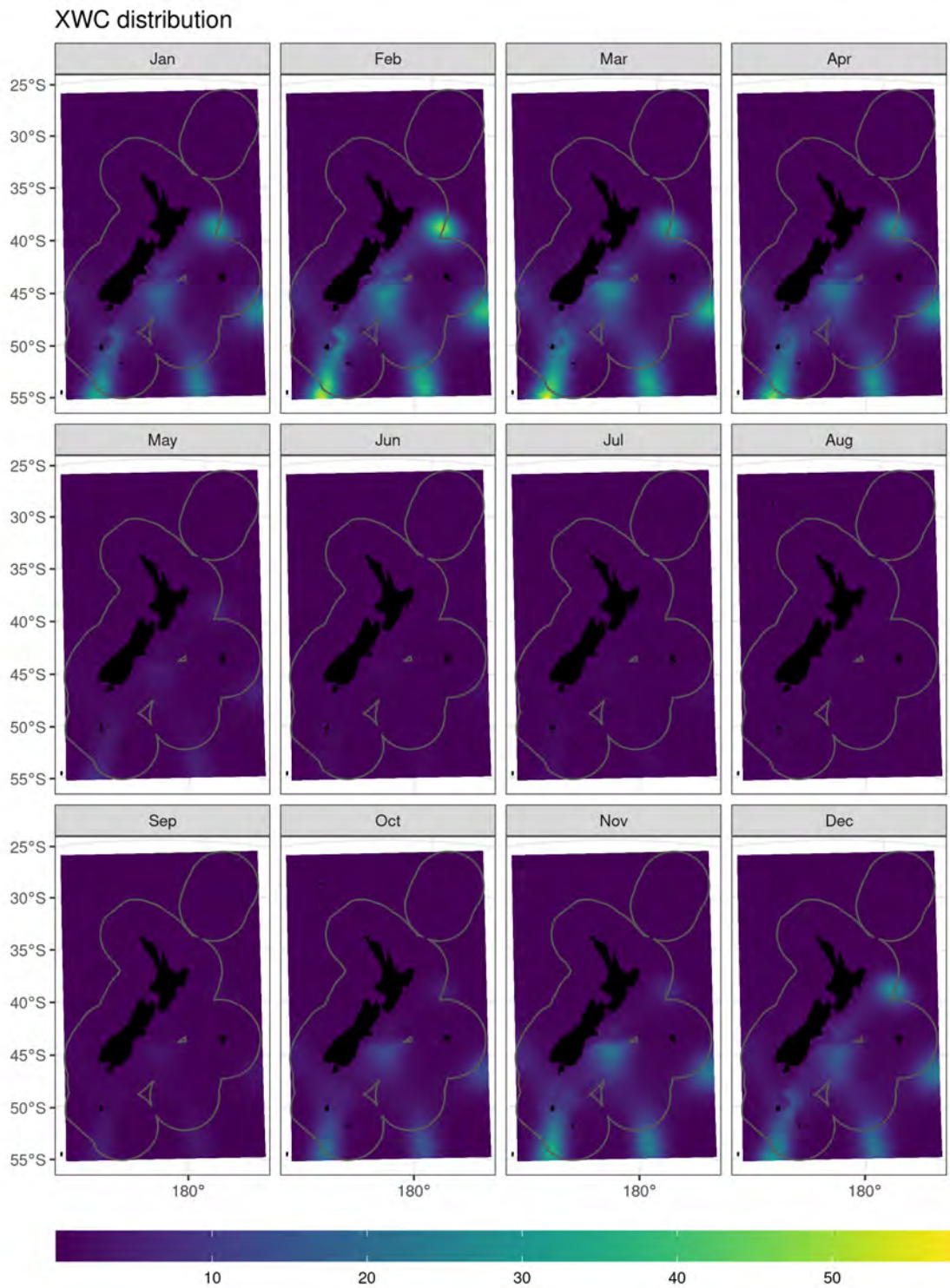


Figure F.10: Predicted relative spatial density of white-chinned petrel by month. The colour scale for this figure is shared across all months.

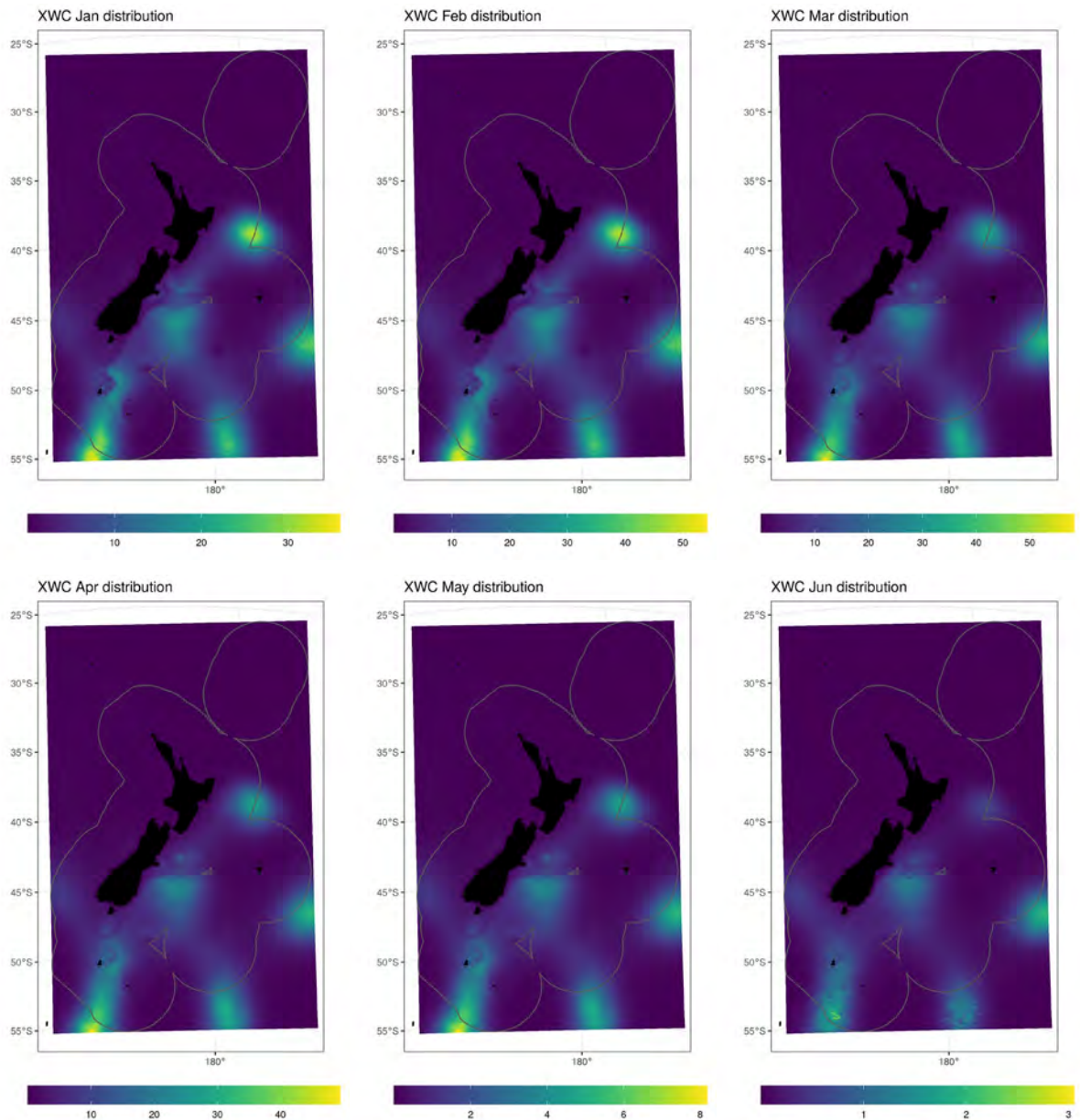


Figure F.11: Predicted relative spatial density of white-chinned petrel by month, for January-June. The colour scale for this figure is different for each month.

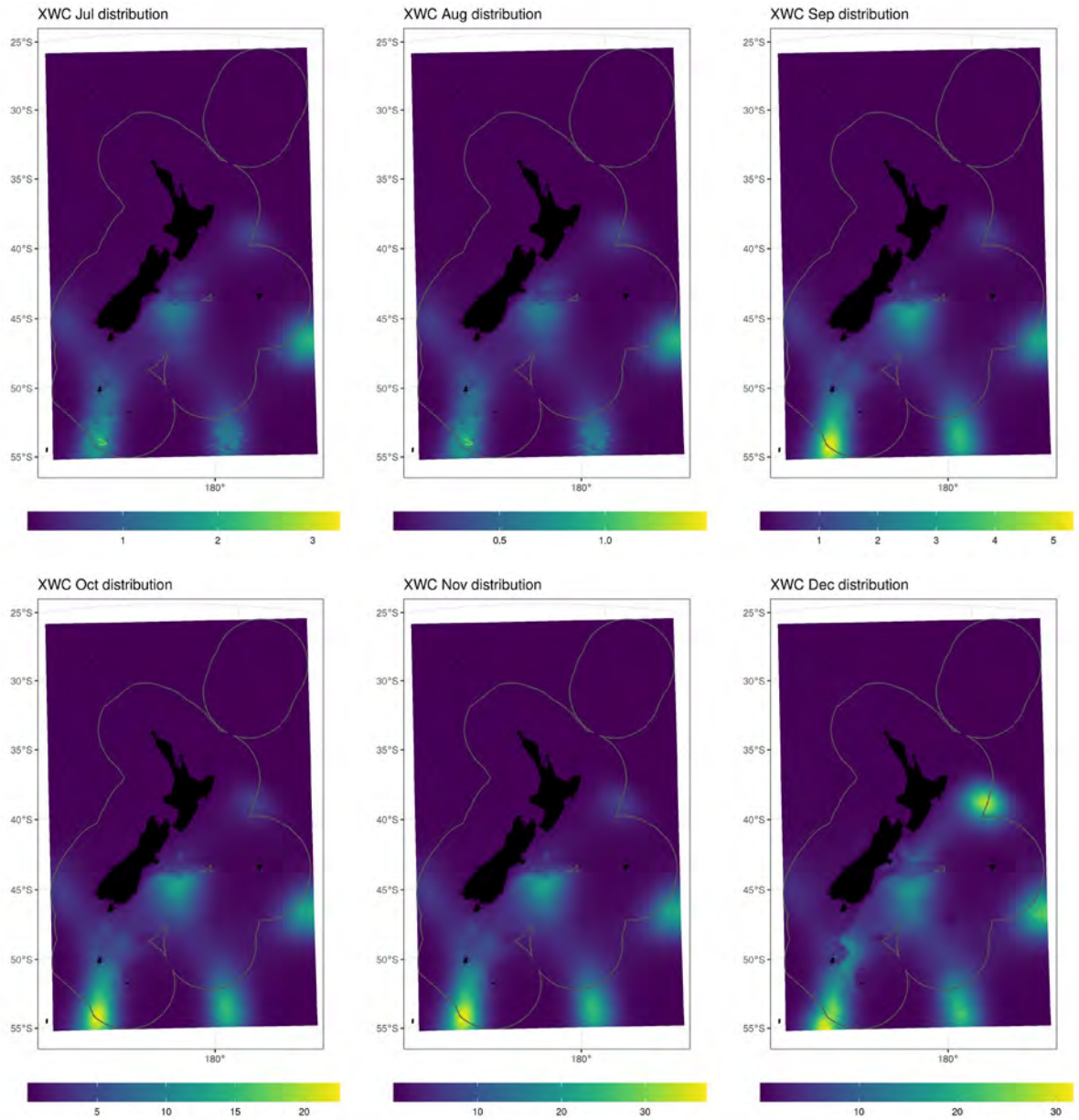


Figure F.12: Predicted relative spatial density of white-chinned petrel by month, for July-December. The colour scale for this figure is different for each month.

Northern and Southern Buller's albatross

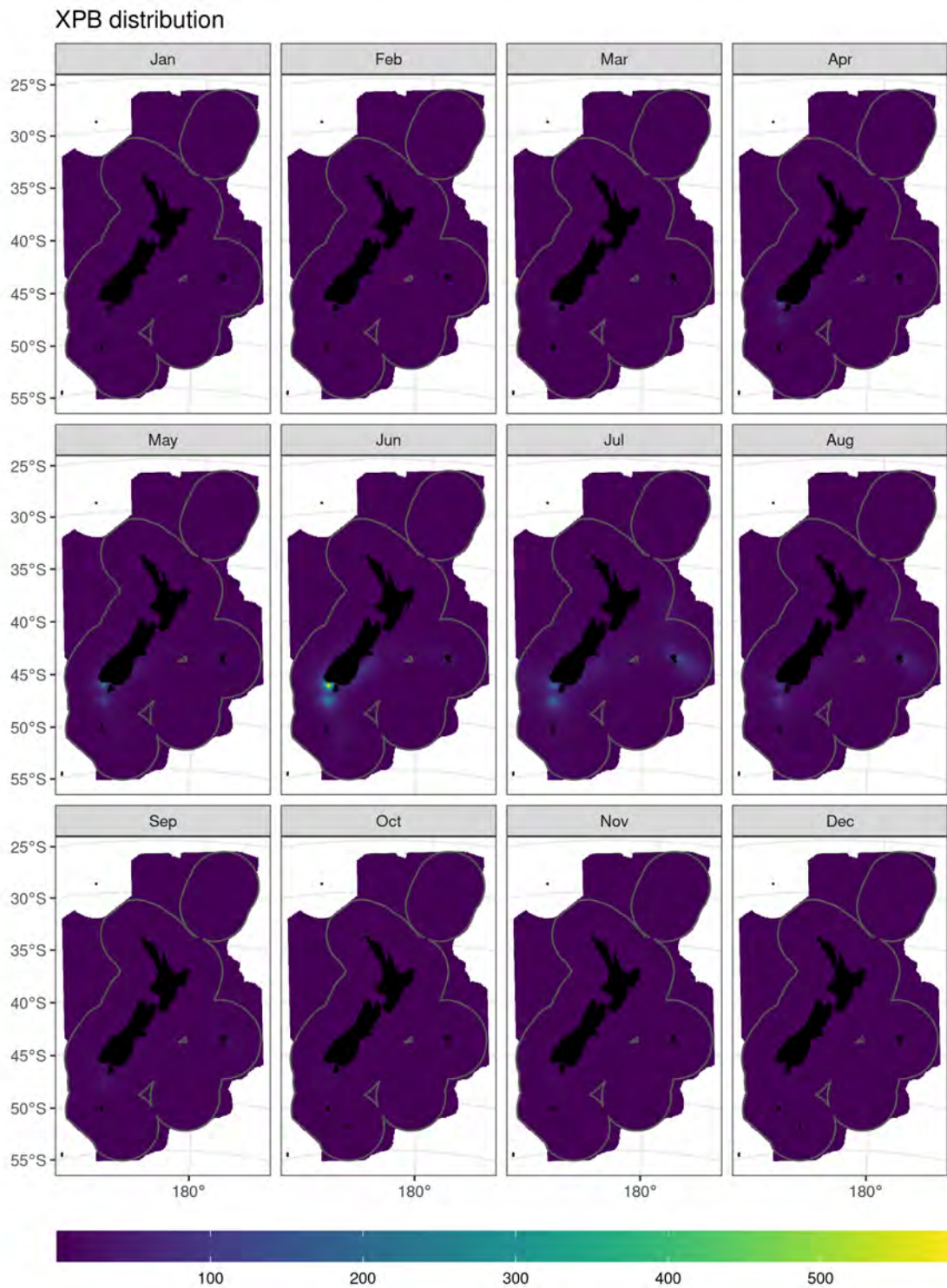


Figure F.13: Predicted relative spatial density of Northern and Southern Buller's albatross (combined) by month. The colour scale for this figure is shared across all months.

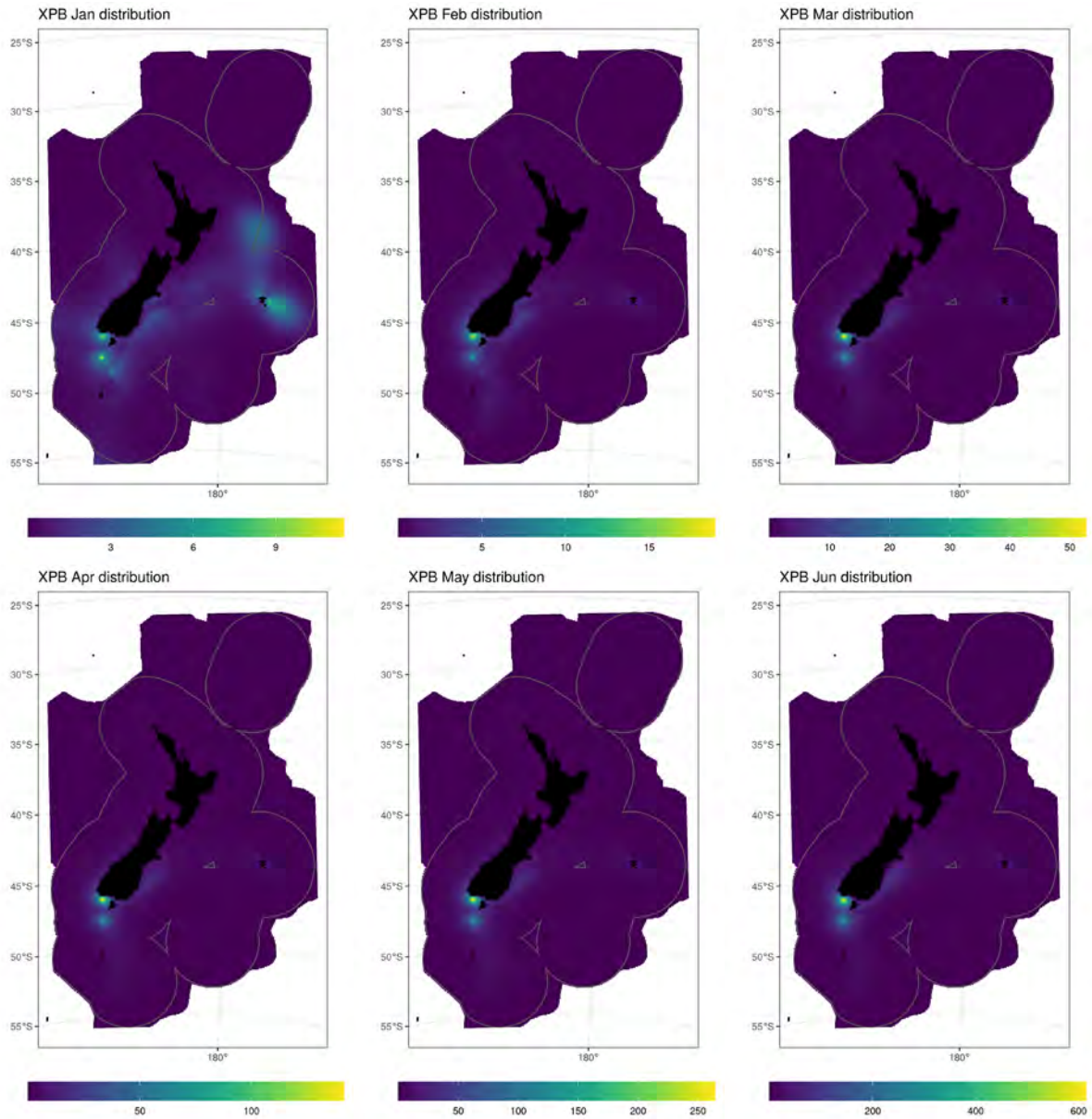


Figure F.14: Predicted relative spatial density of Northern and Southern Buller's albatross (combined) by month, for January-June. The colour scale for this figure is different for each month.

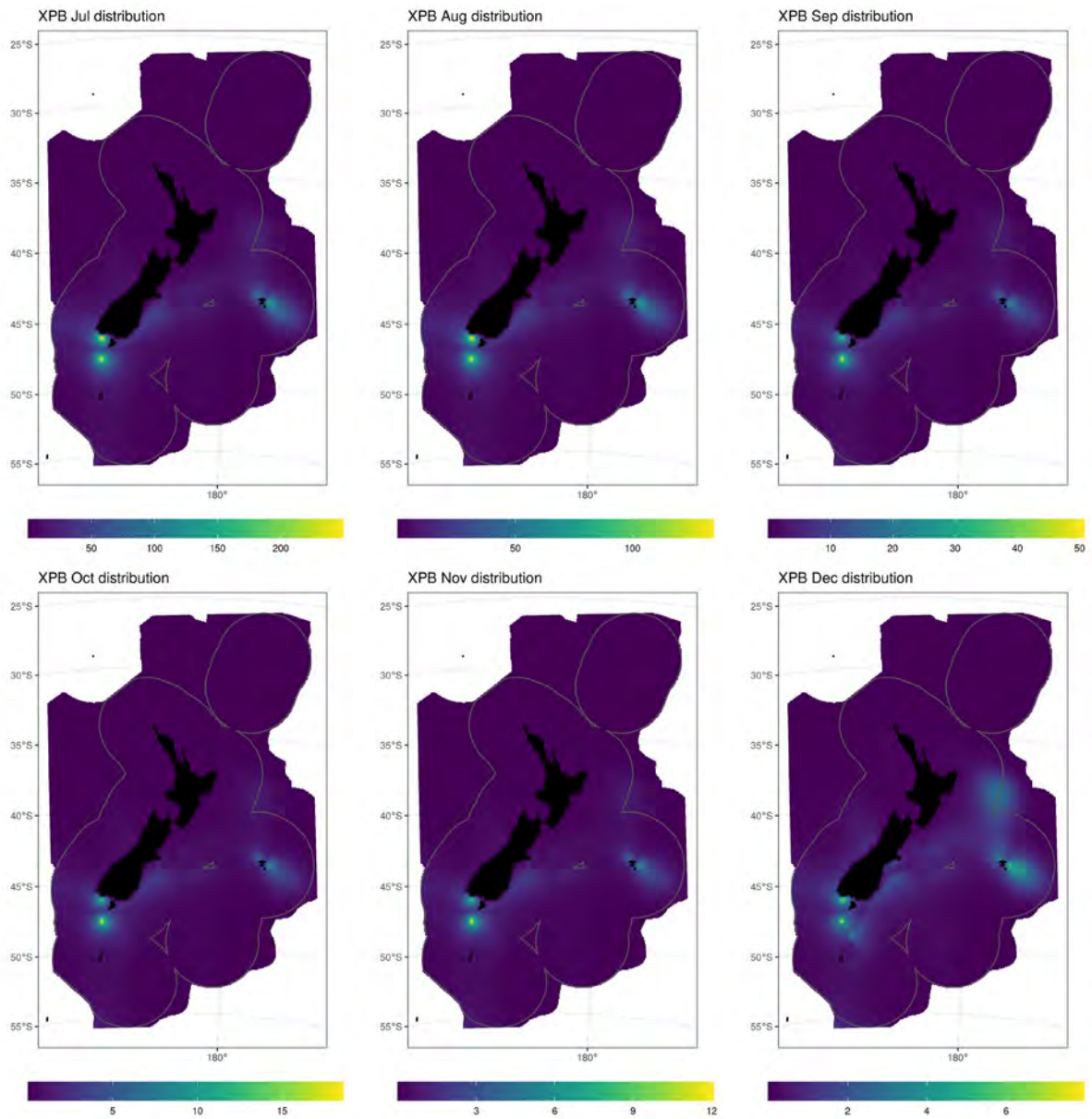


Figure F.15: Predicted relative spatial density of Northern and Southern Buller's albatross (combined) by month, for July-December. The colour scale for this figure is different for each month.

Northern Buller's albatross

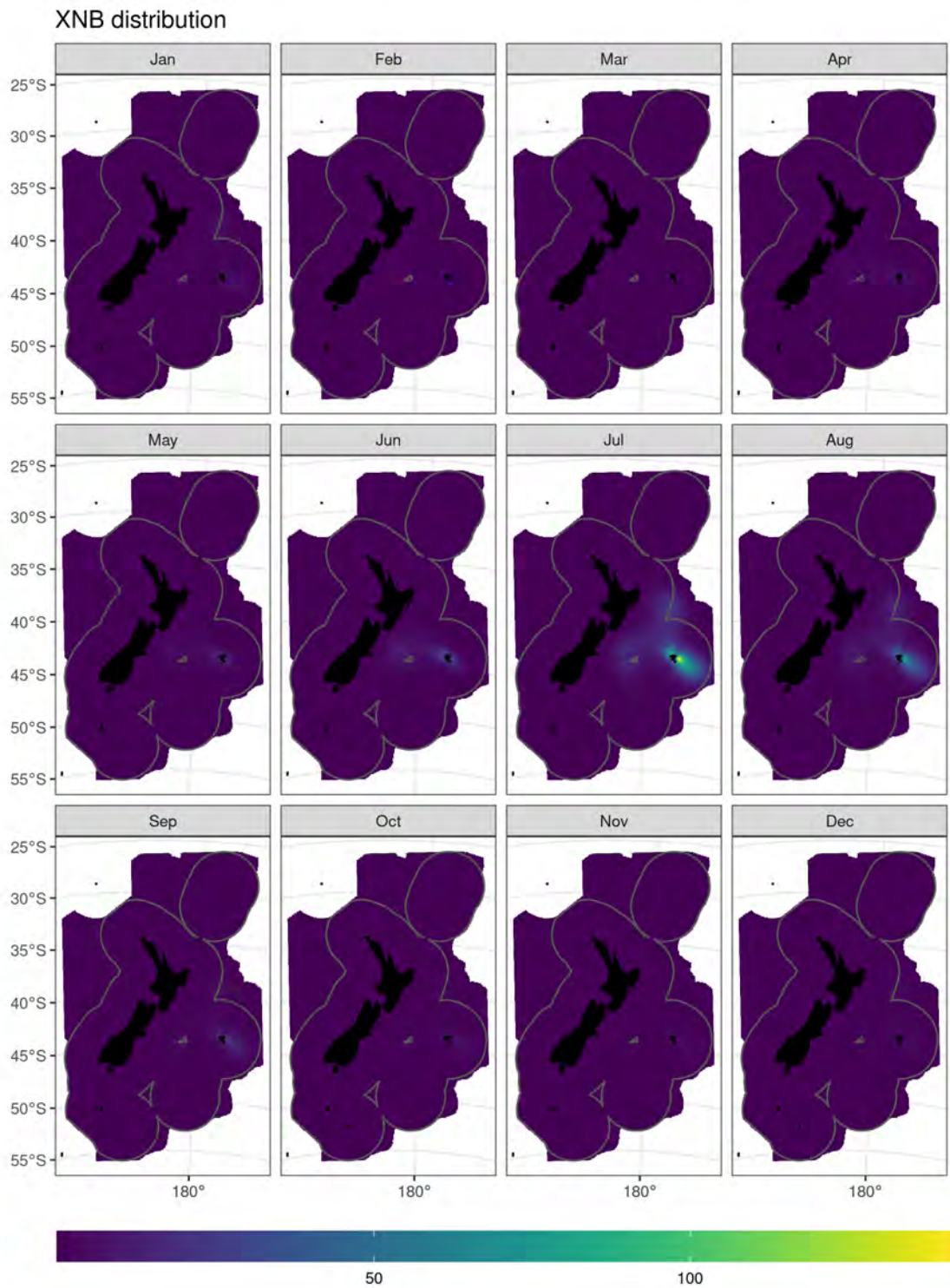


Figure F.16: Predicted relative spatial density of Northern Buller's albatross by month. The colour scale for this figure is shared across all months.

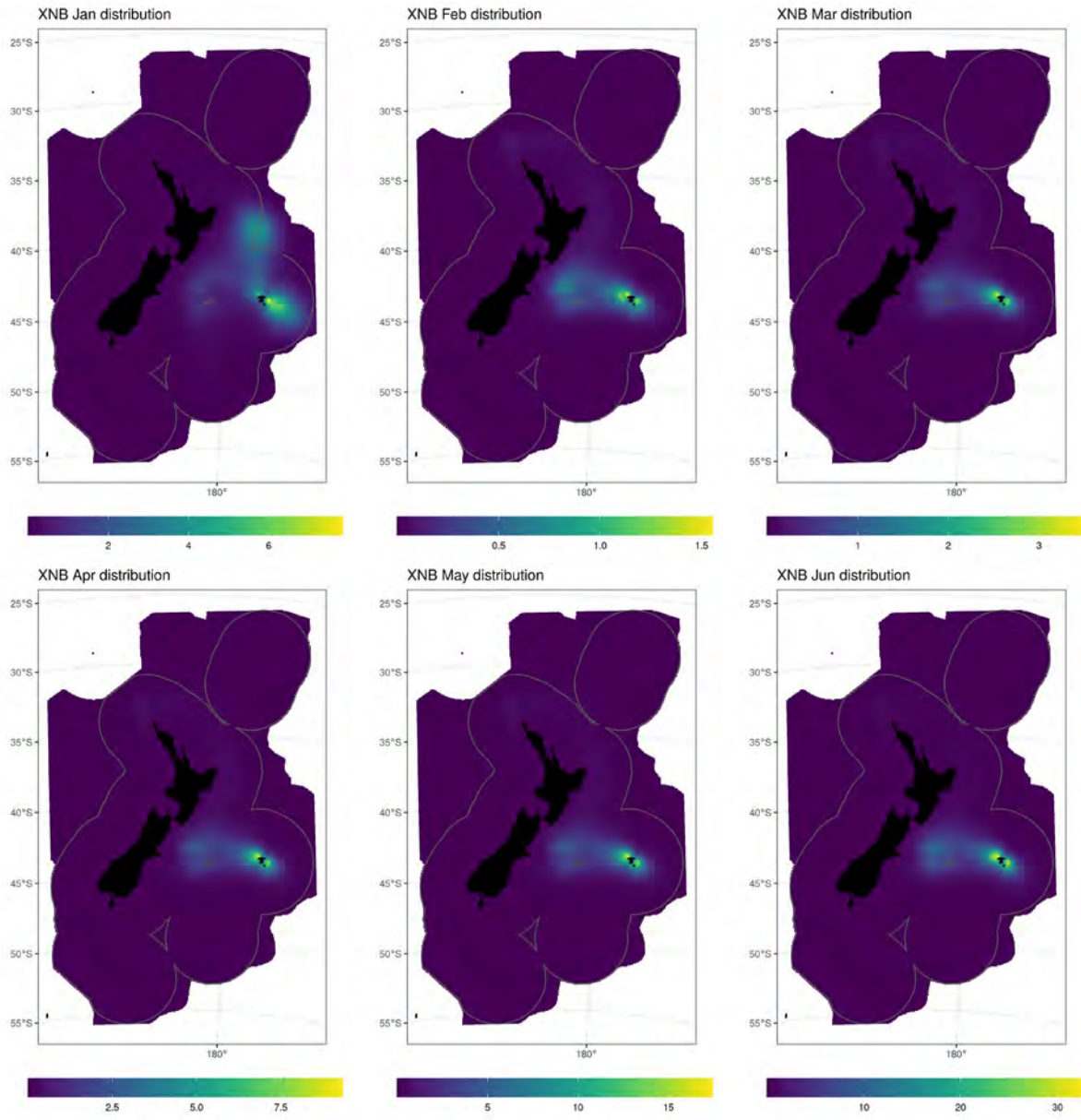


Figure F.17: Predicted relative spatial density of Northern Buller's albatross by month, for January-June. The colour scale for this figure is different for each month.

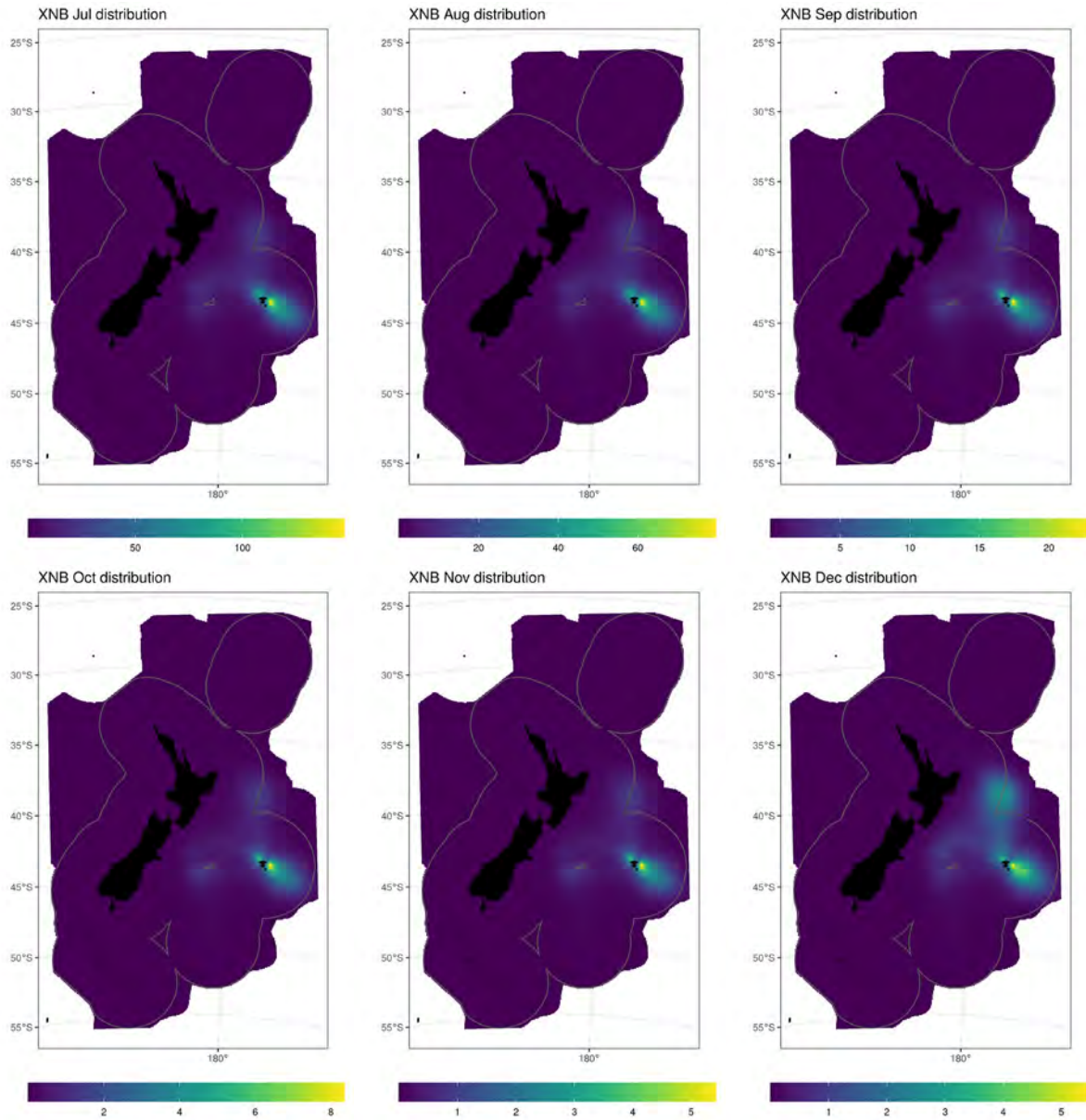


Figure F.18: Predicted relative spatial density of Northern Buller's albatross by month, for July-December. The colour scale for this figure is different for each month.

Southern Buller's albatross

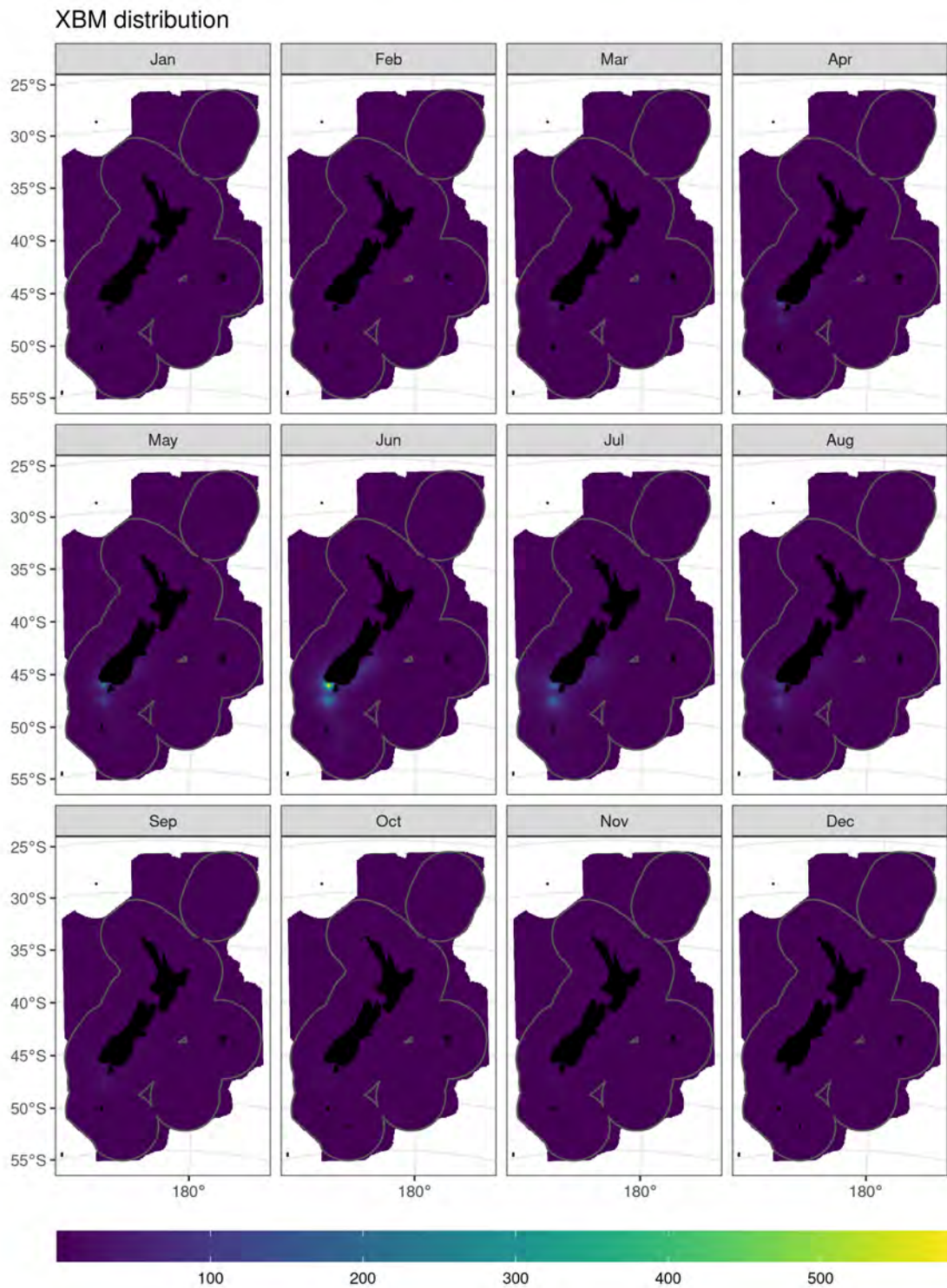


Figure F.19: Predicted relative spatial density of Southern Buller's albatross by month. The colour scale for this figure is shared across all months.

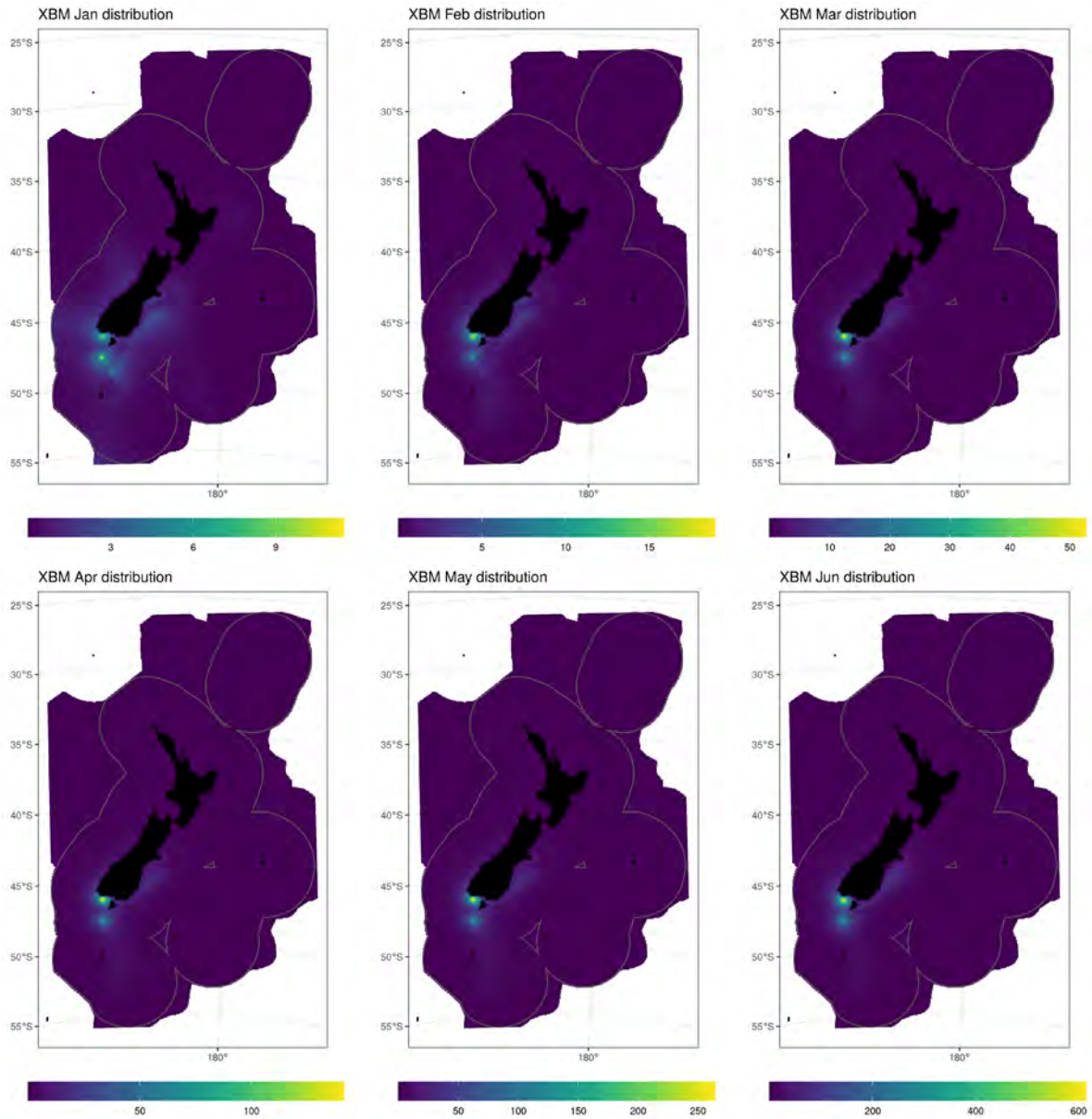


Figure F.20: Predicted relative spatial density of Southern Buller's albatross by month, for January-June. The colour scale for this figure is different for each month.

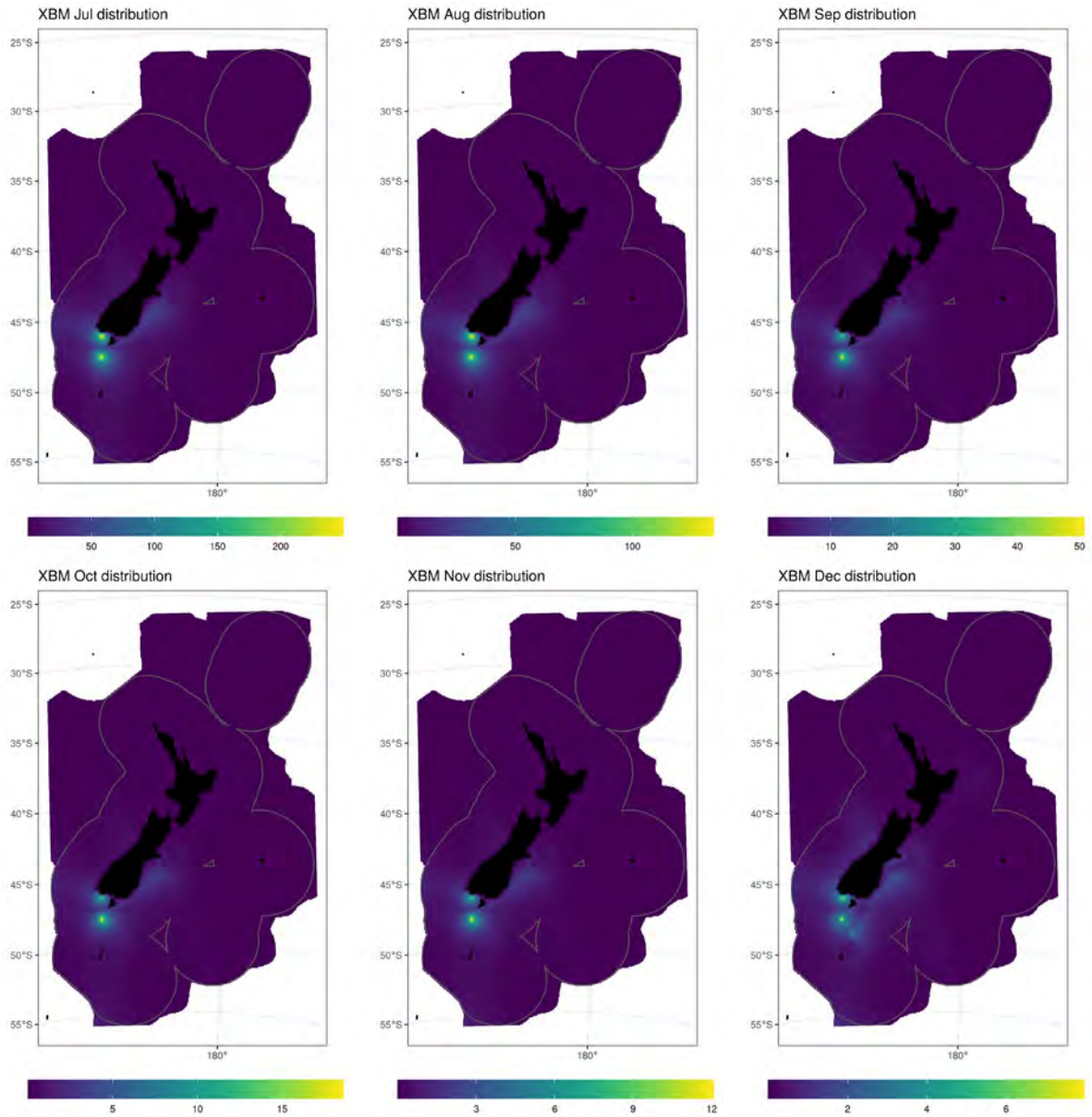


Figure F.21: Predicted relative spatial density of Southern Buller's albatross by month, for July-December. The colour scale for this figure is different for each month.

Chatham Island albatross

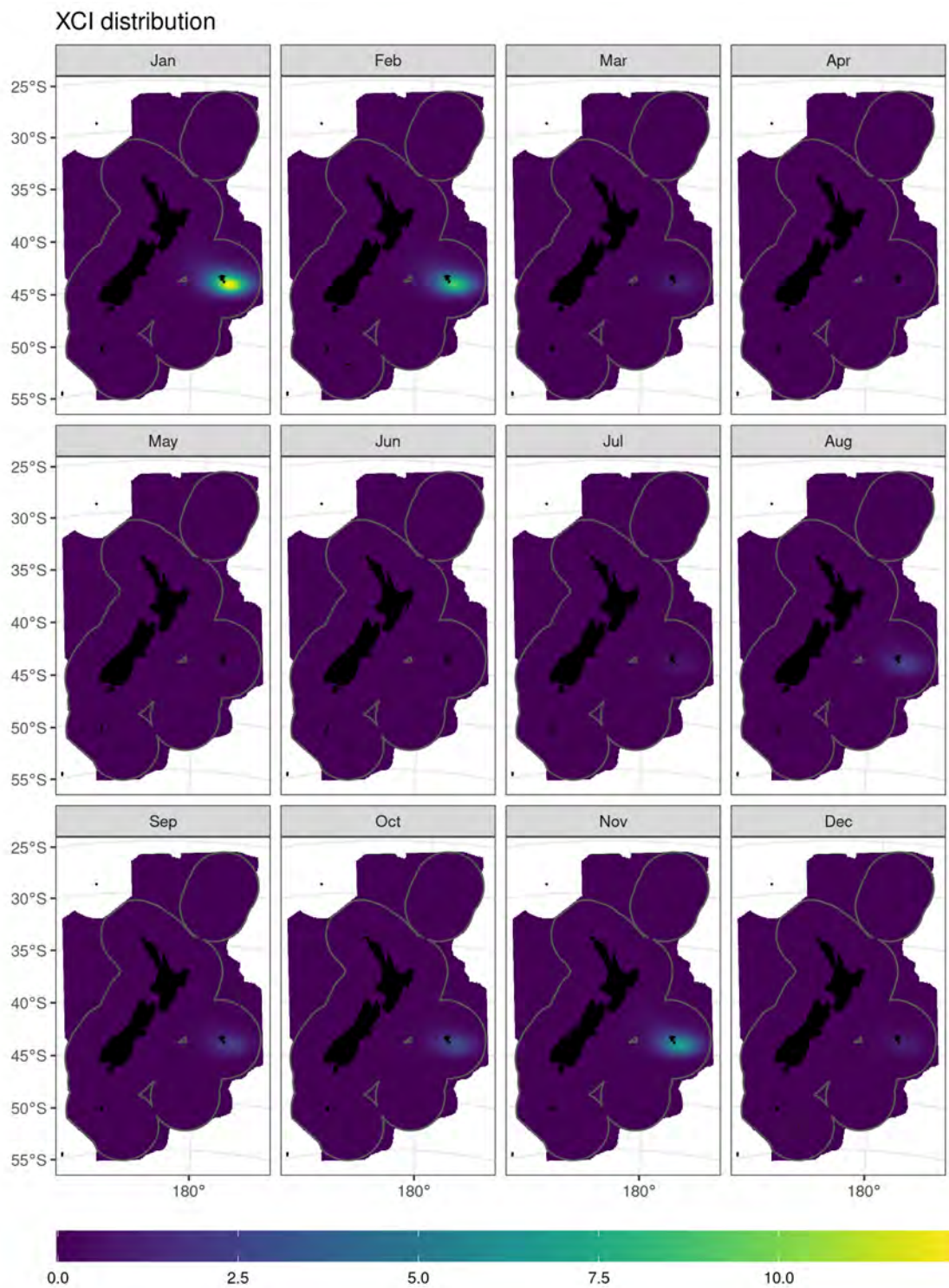


Figure F.22: Predicted relative spatial density of Chatham Island albatross by month. The colour scale for this figure is shared across all months.

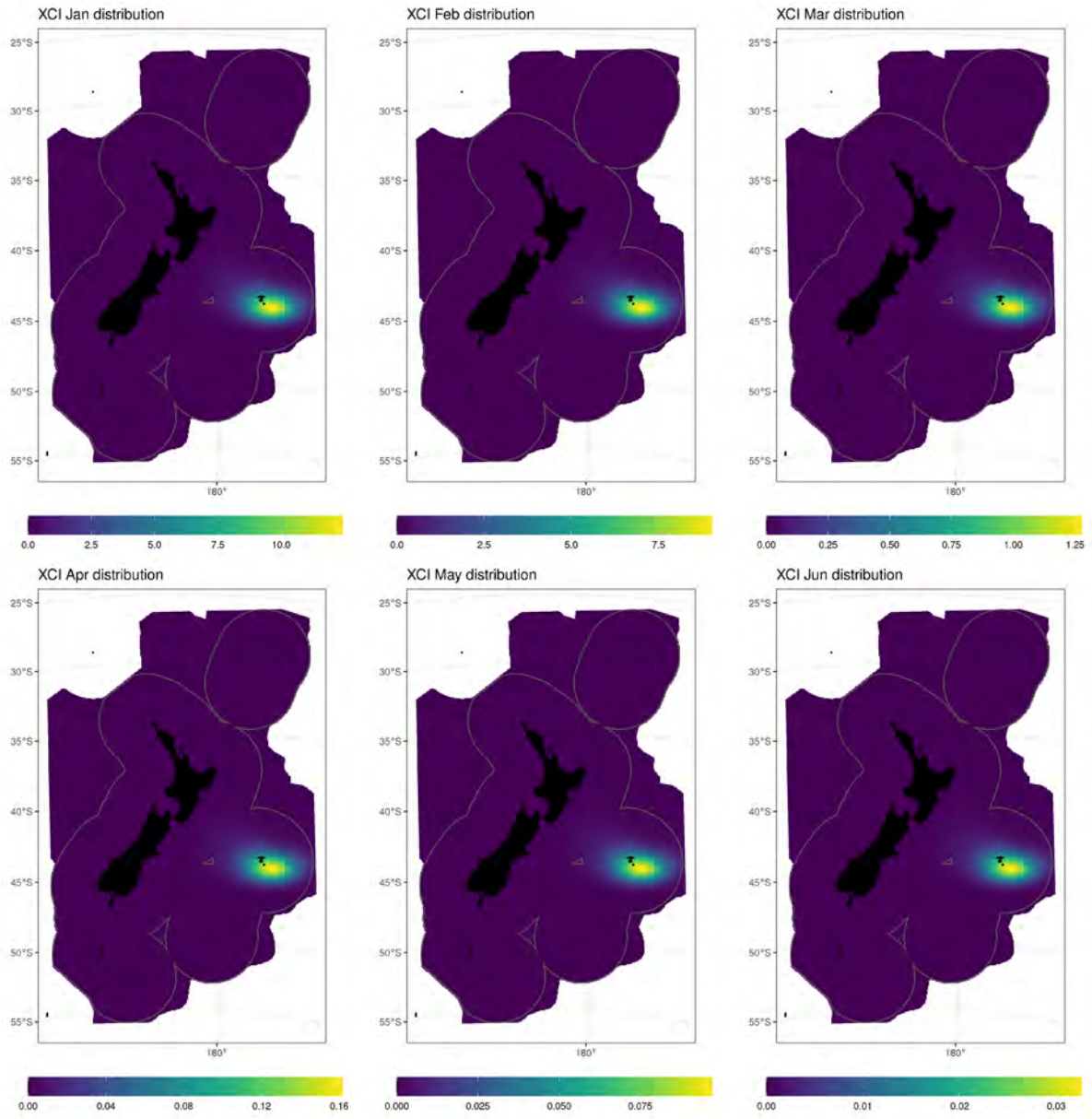


Figure F.23: Predicted relative spatial density of Chatham Island albatross by month, for January-June. The colour scale for this figure is different for each month.

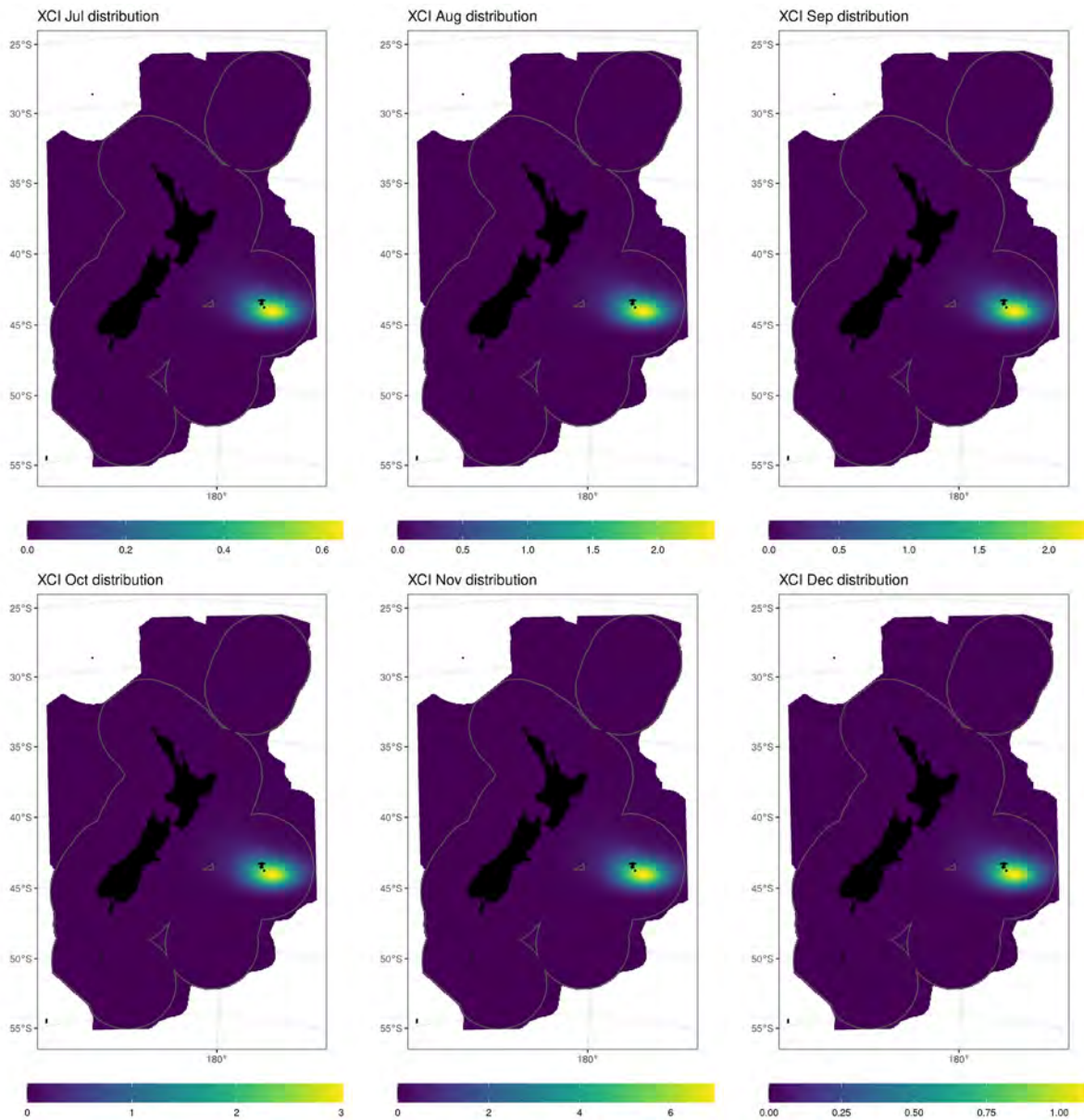


Figure F.24: Predicted relative spatial density of Chatham Island albatross by month, for July-December. The colour scale for this figure is different for each month.

Salvin's albatross

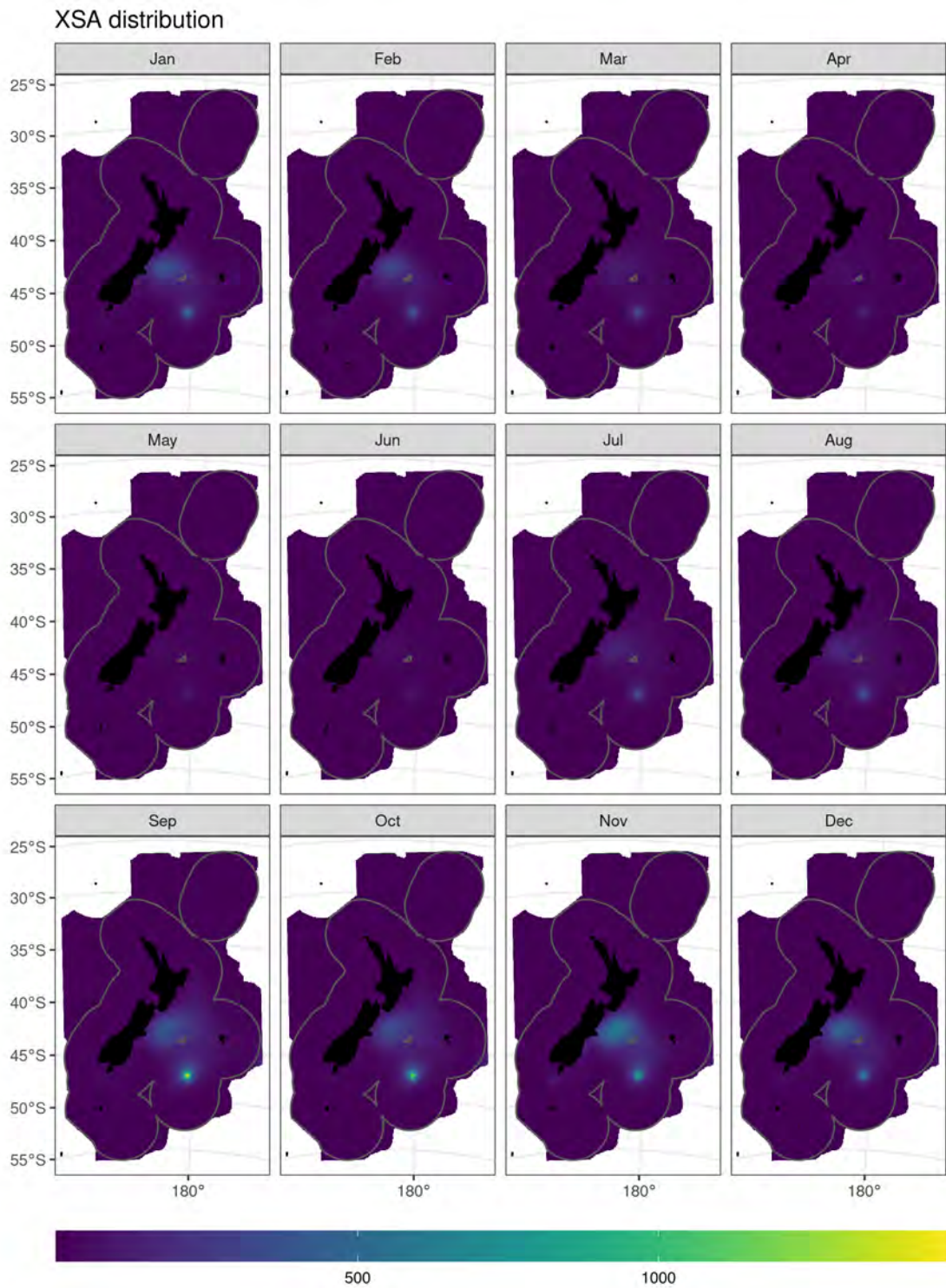


Figure F.25: Predicted relative spatial density of Salvin's albatross by month. The colour scale for this figure is shared across all months.

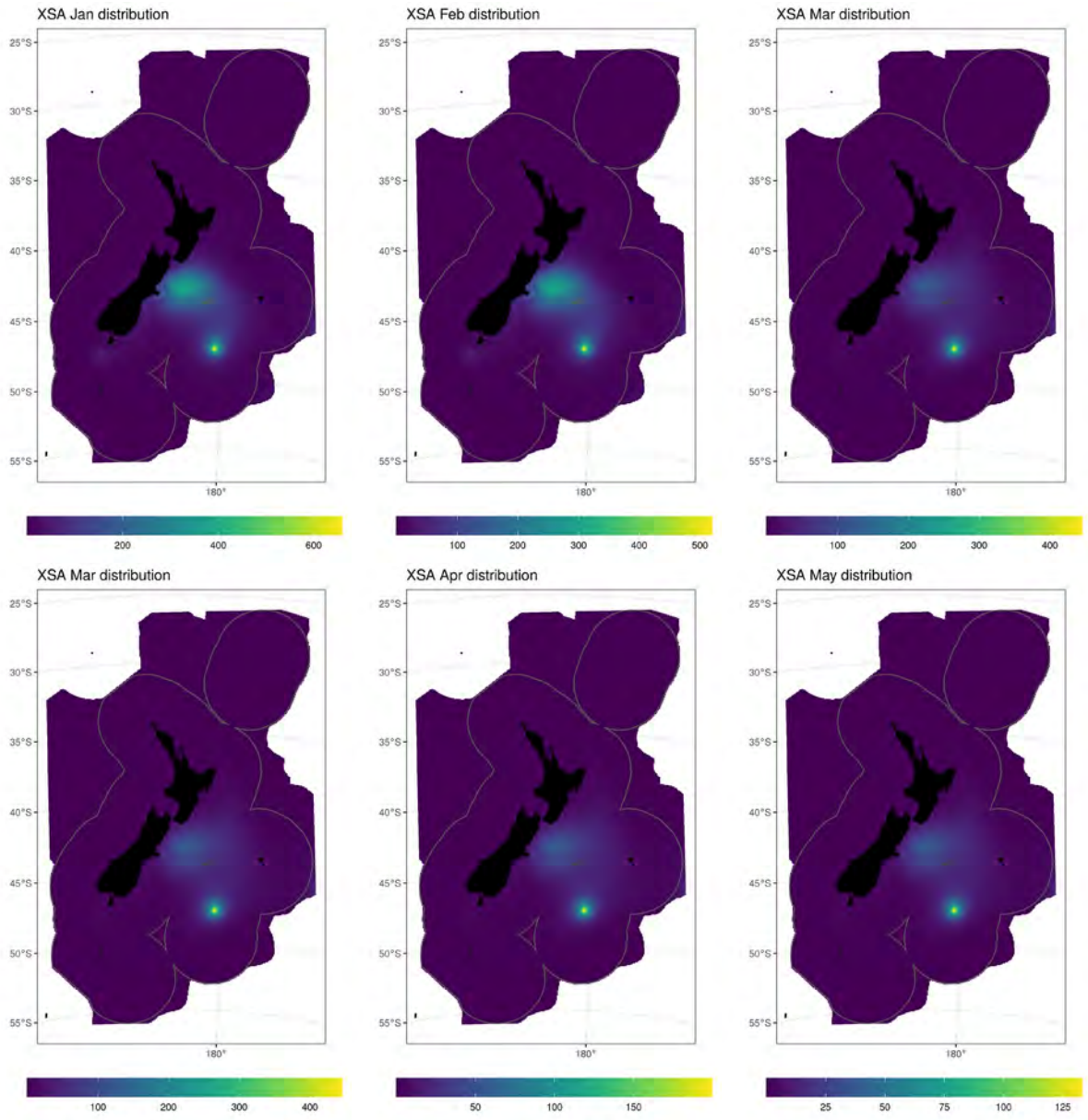


Figure F.26: Predicted relative spatial density of Salvin's albatross by month, for January-June. The colour scale for this figure is different for each month.

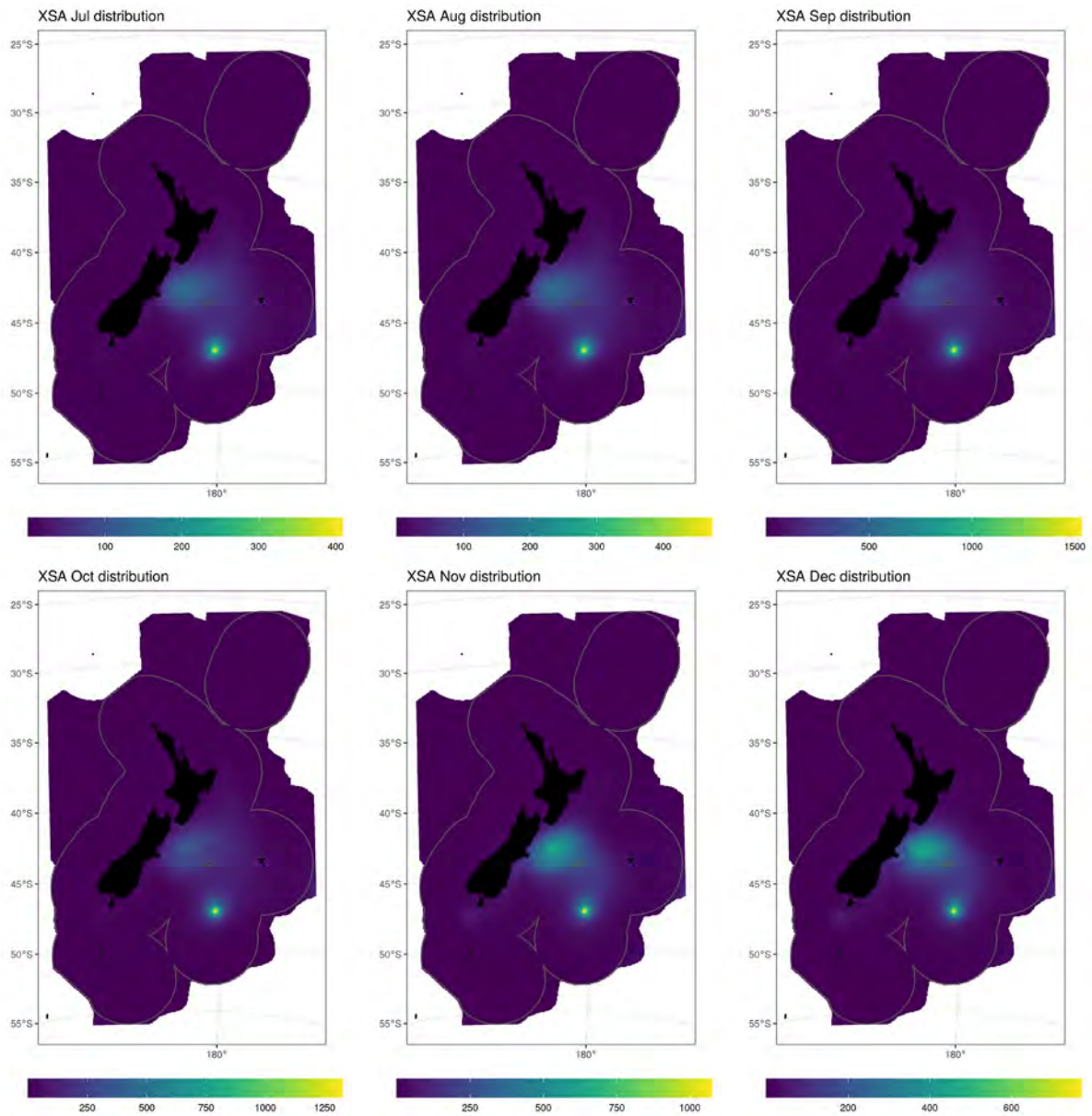


Figure F.27: Predicted relative spatial density of Salvin's albatross by month, for July-December. The colour scale for this figure is different for each month.

White-capped albatross

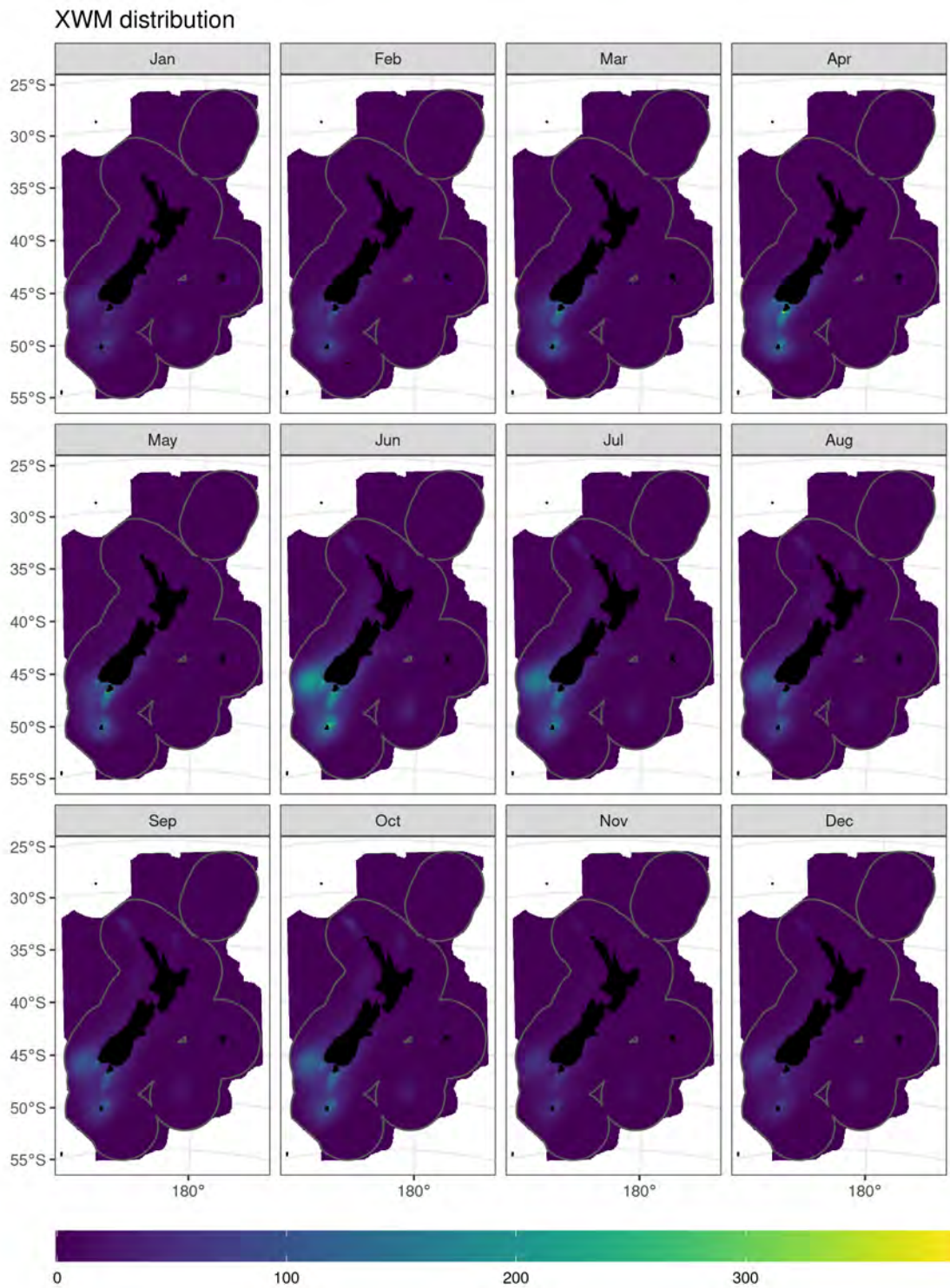


Figure F.28: Predicted relative spatial density of white-capped albatross by month. The colour scale for this figure is shared across all months.

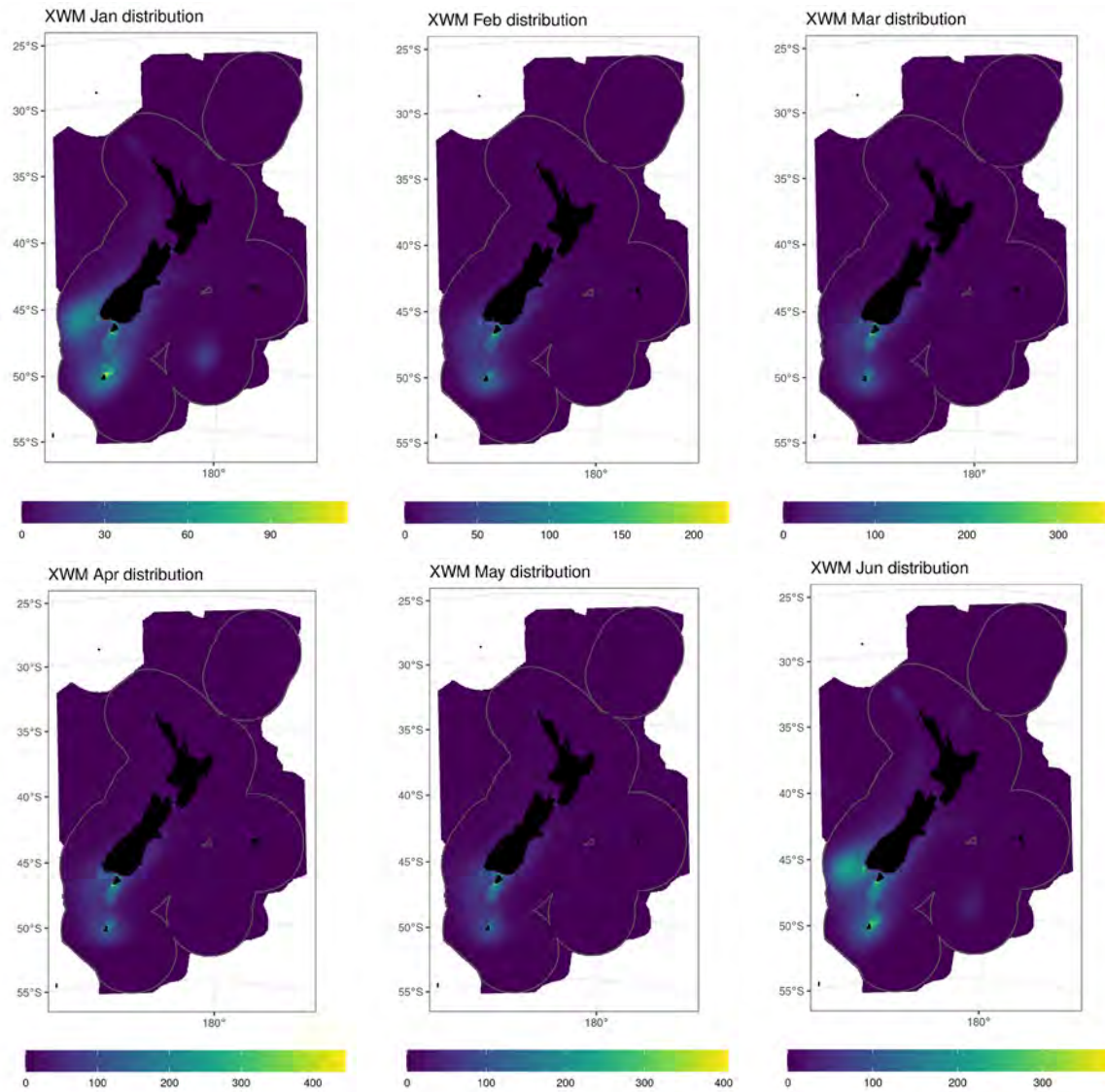


Figure F.29: Predicted relative spatial density of white-capped albatross by month, for January-June. The colour scale for this figure is different for each month.

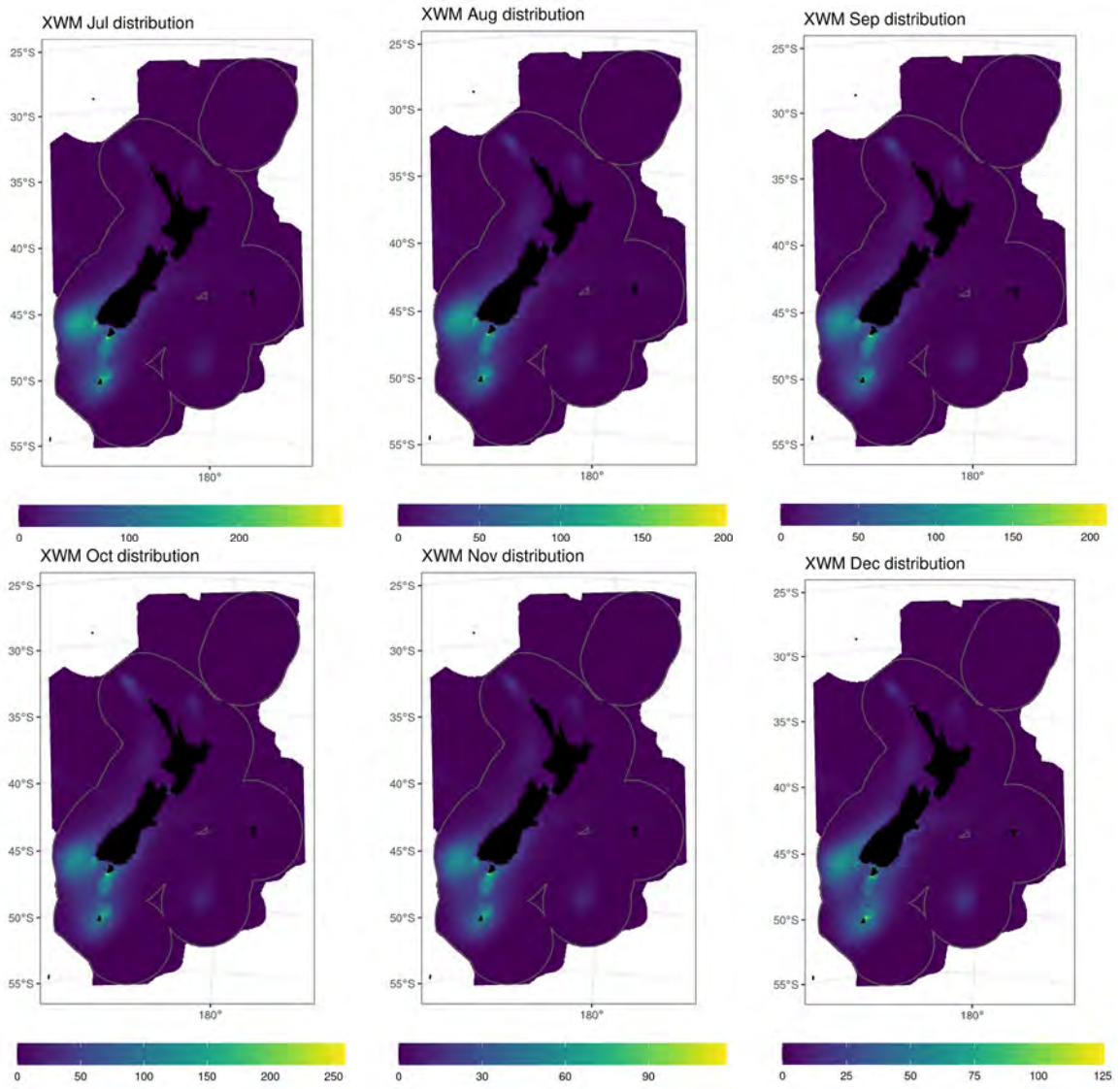


Figure F.30: Predicted relative spatial density of white-capped albatross by month, for July-December. The colour scale for this figure is different for each month.

Antipodean albatross

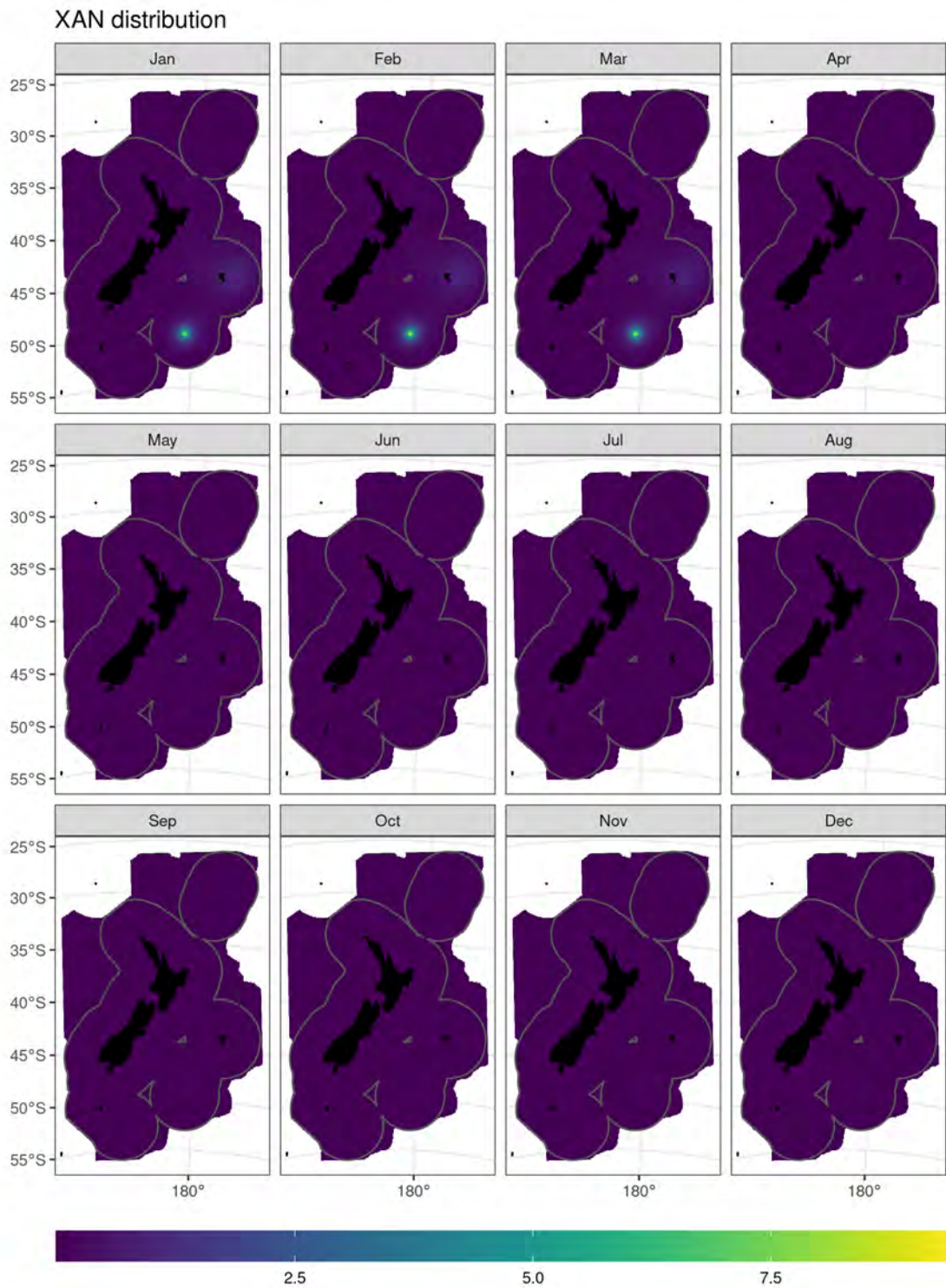


Figure F.31: Predicted relative spatial density of Antipodean albatross by month. The colour scale for this figure is shared across all months.

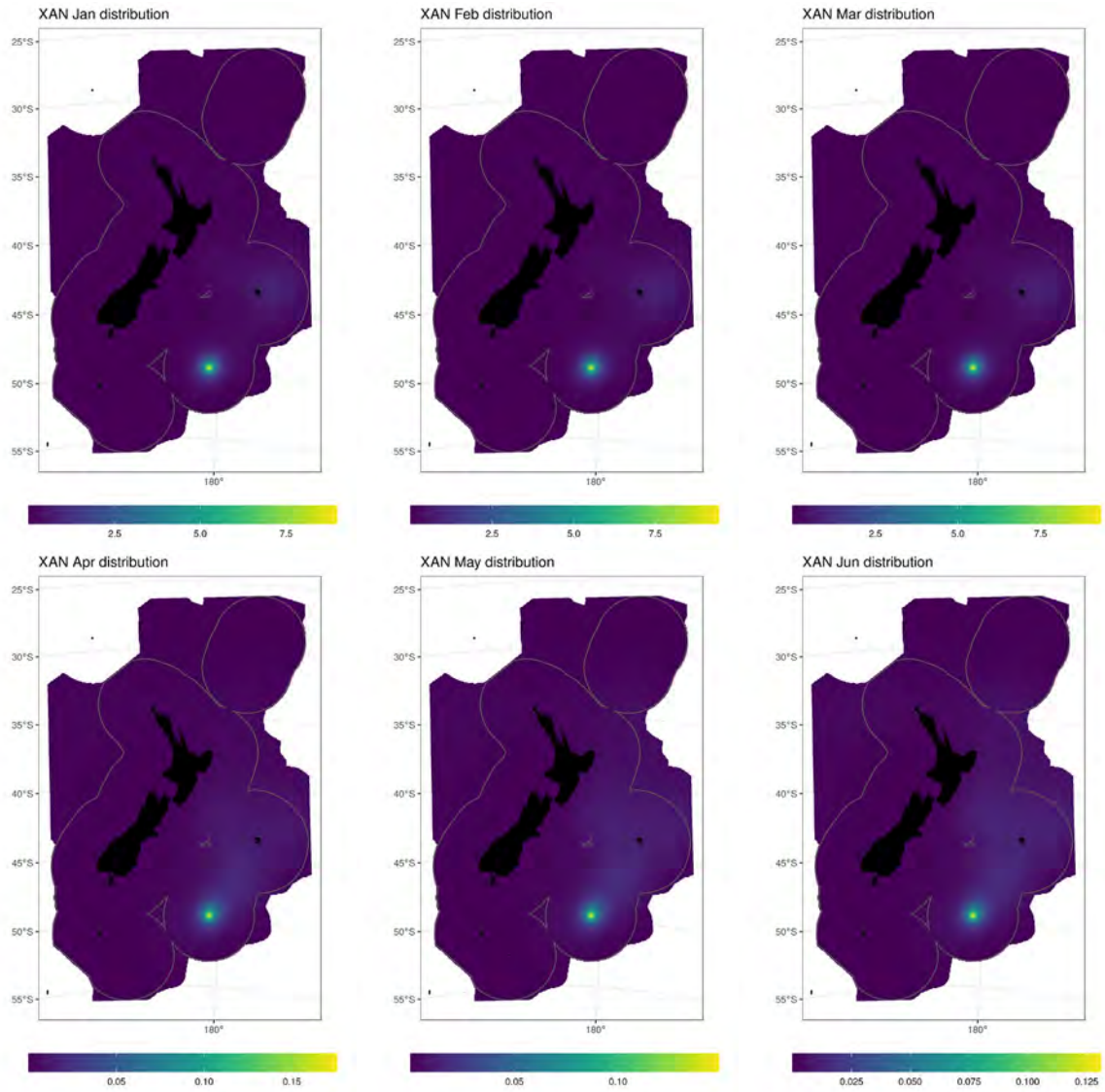


Figure F.32: Predicted relative spatial density of Antipodean albatross by month, for January-June. The colour scale for this figure is different for each month.

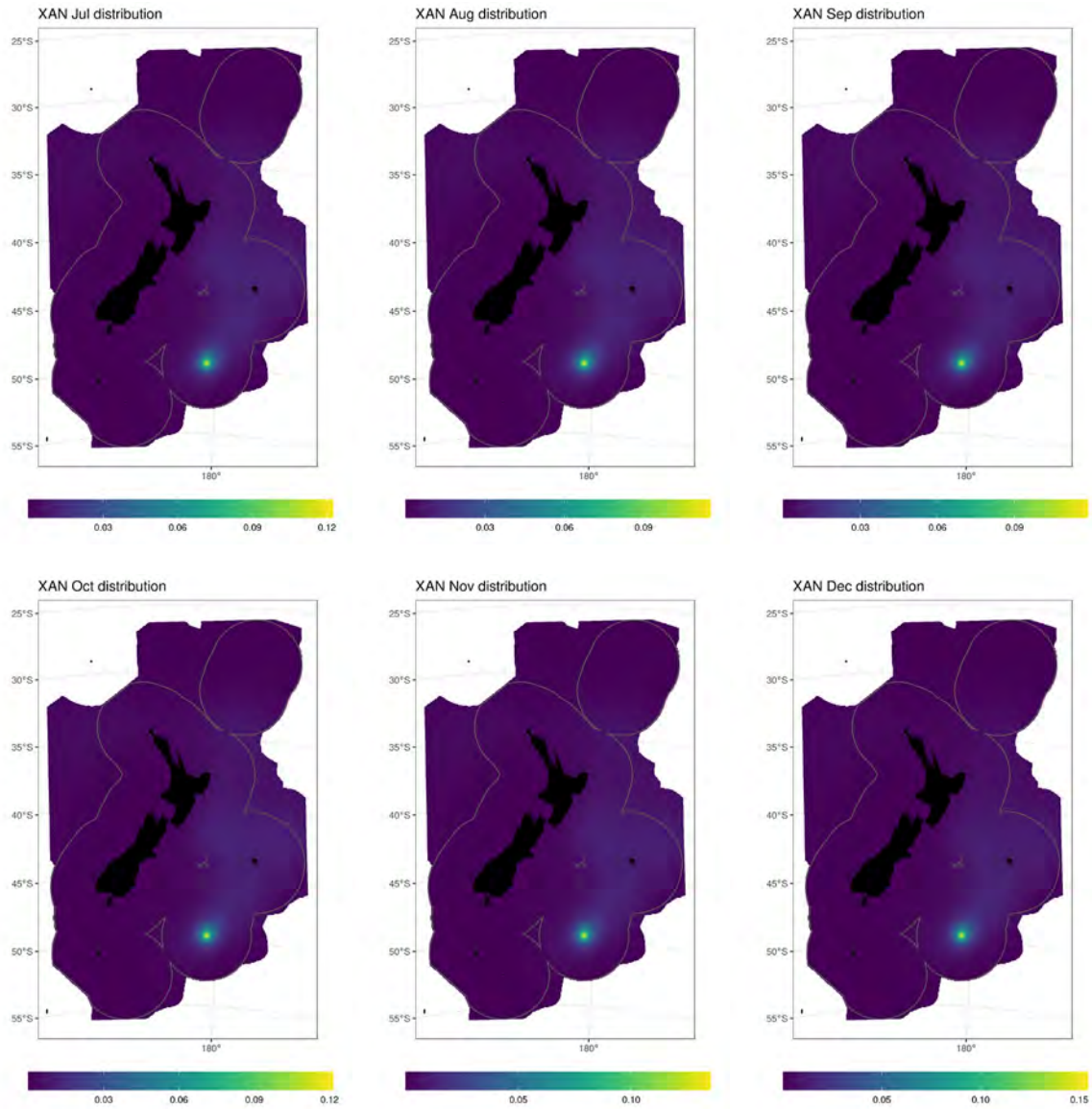


Figure F.33: Predicted relative spatial density of Antipodean albatross by month, for July-December. The colour scale for this figure is different for each month.

Gibson's albatross

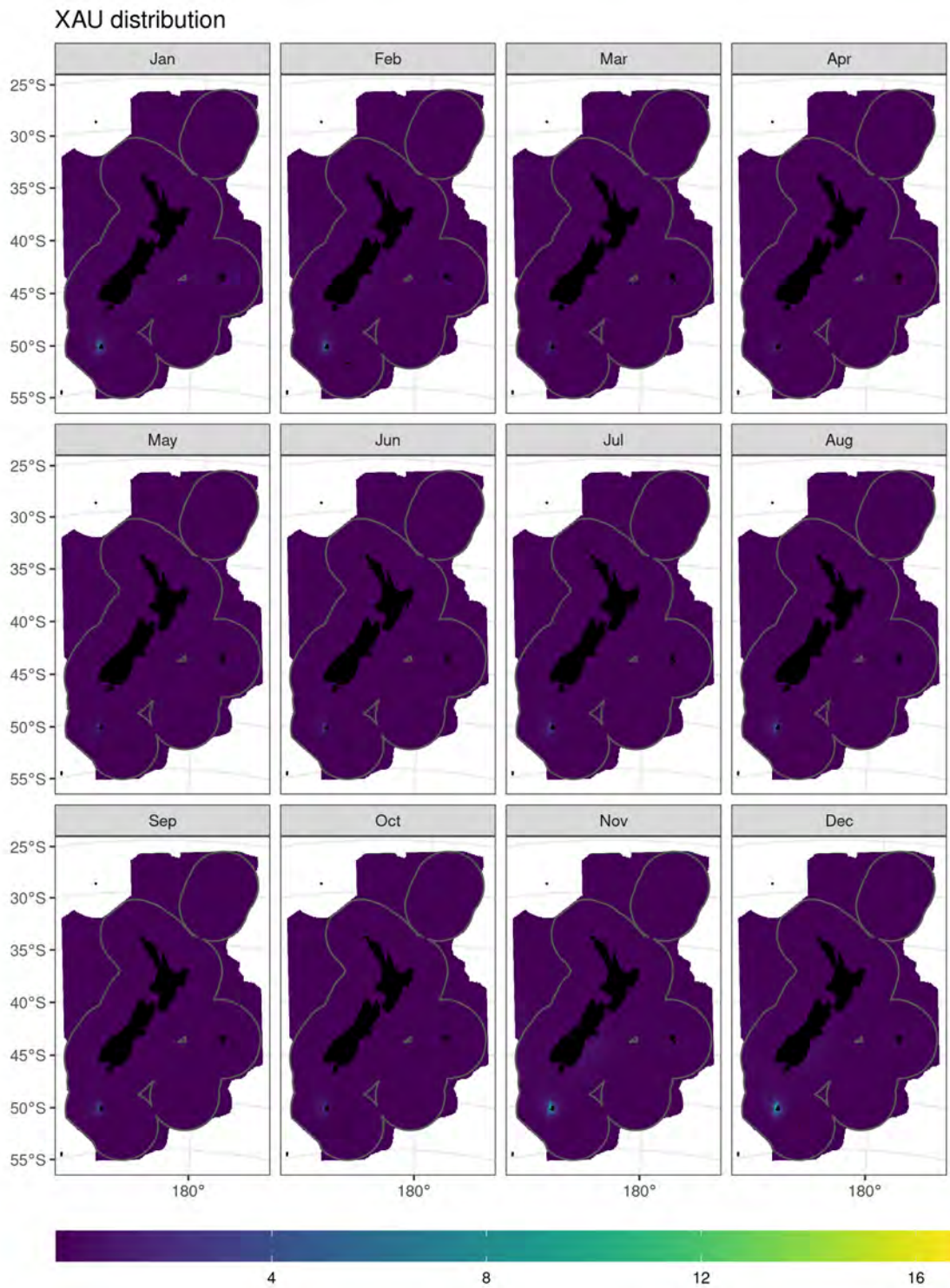


Figure F.34: Predicted relative spatial density of Gibson's albatross by month. The colour scale for this figure is shared across all months.

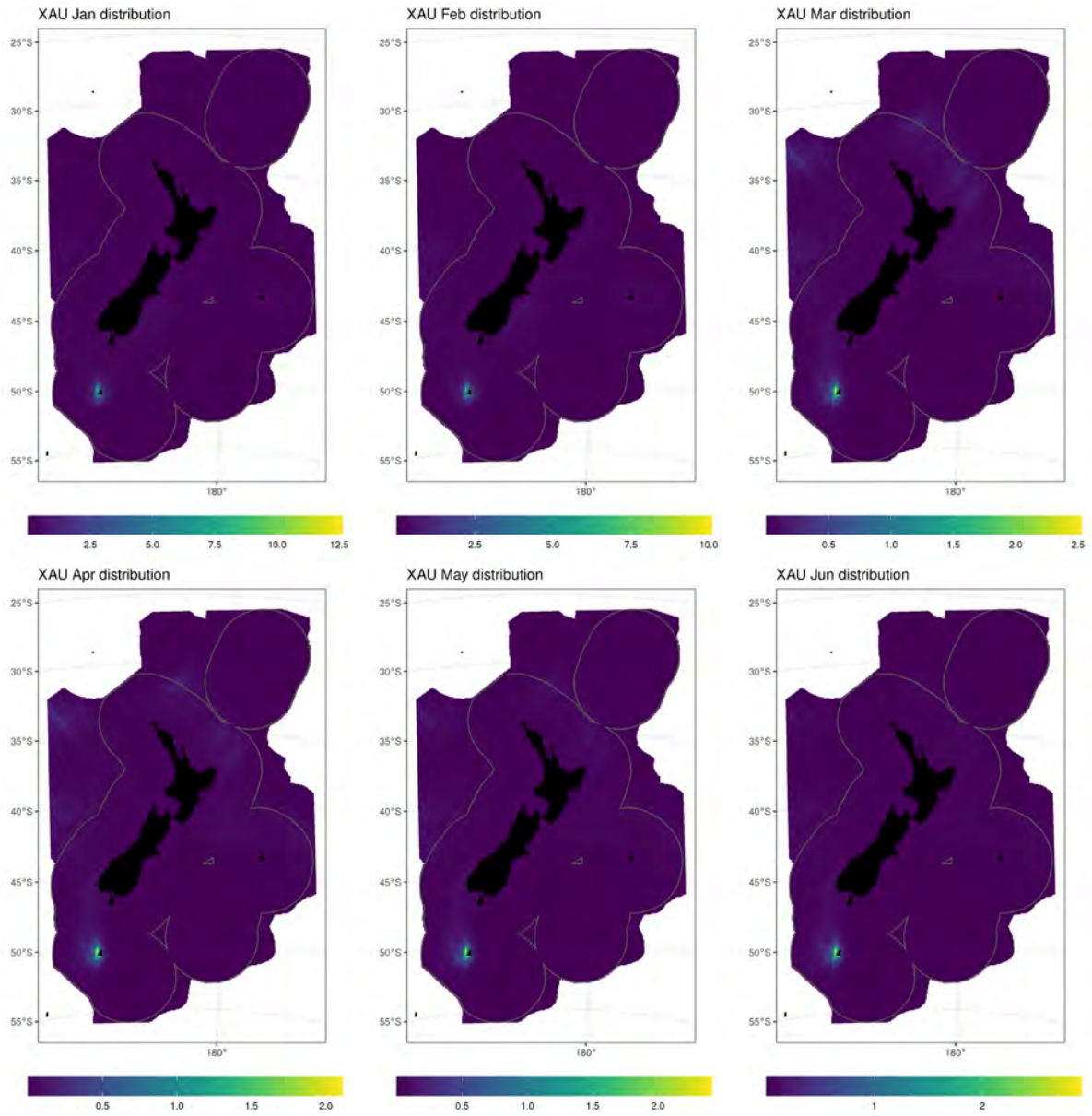


Figure F.35: Predicted relative spatial density of Gibson's albatross by month, for January-June. The colour scale for this figure is different for each month.

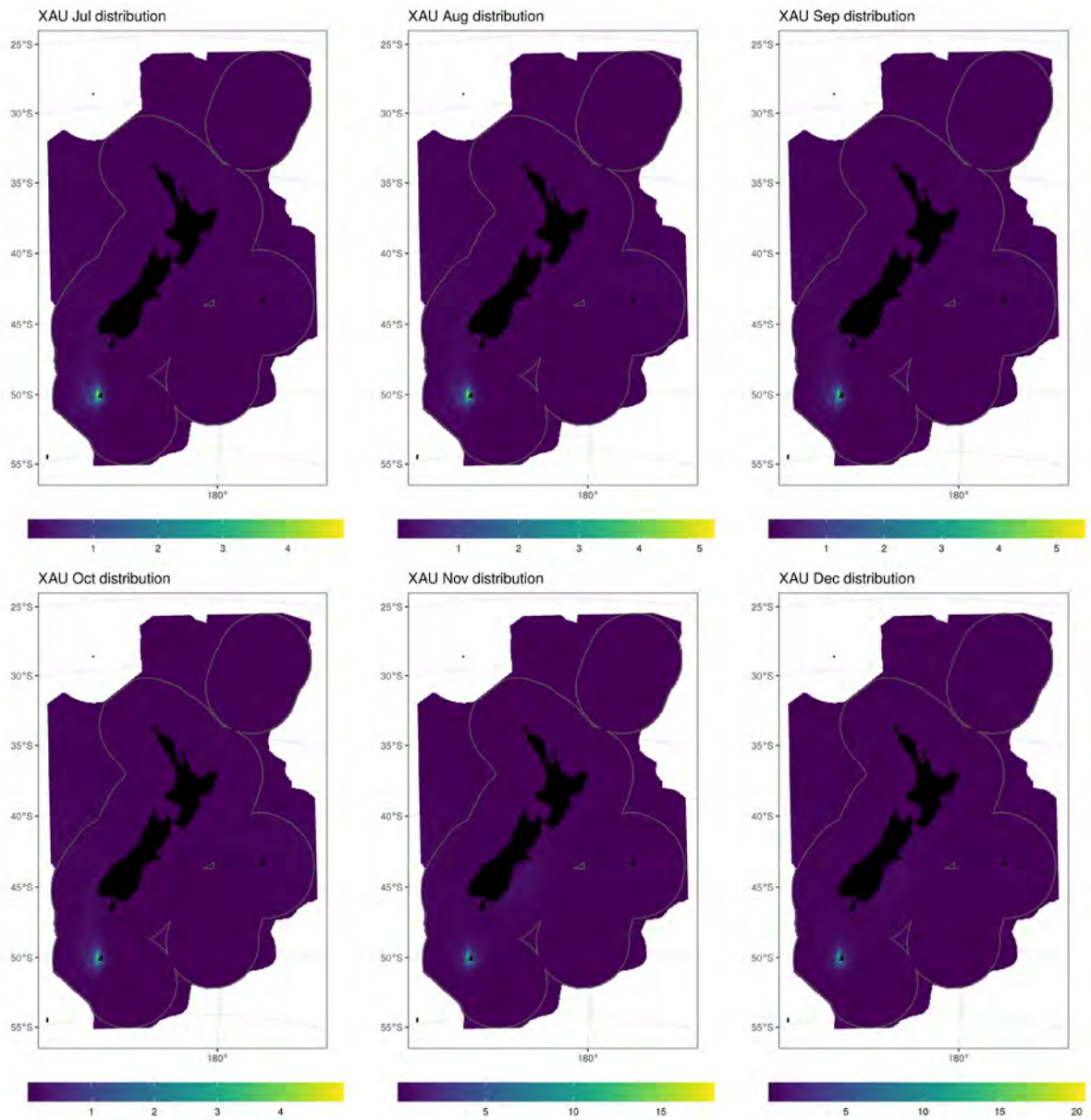


Figure F.36: Predicted relative spatial density of Gibson's albatross by month, for July-December. The colour scale for this figure is different for each month.

Yellow-eyed penguin

Fledglings

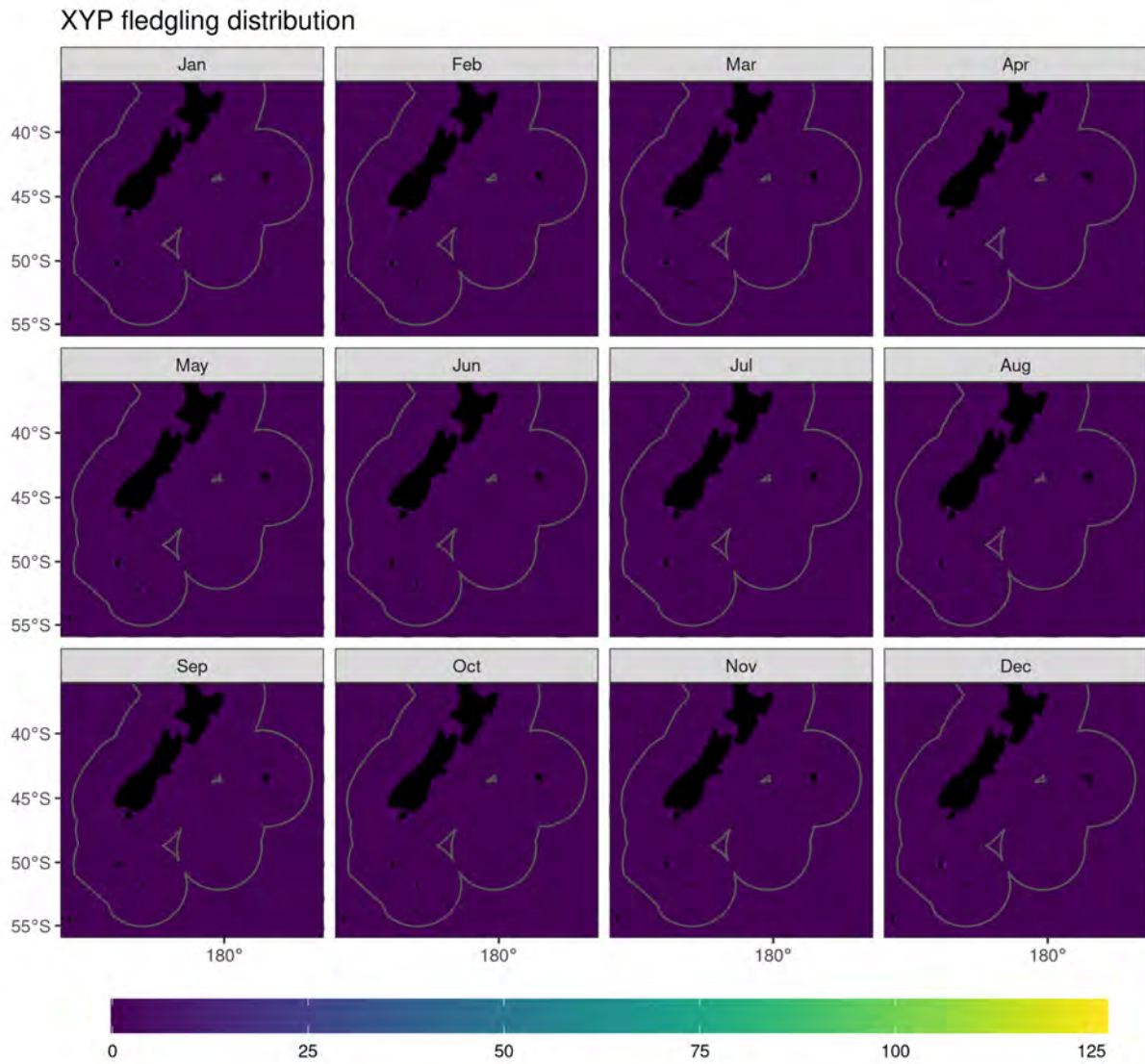


Figure F.37: Predicted relative spatial density of fledgling yellow-eyed penguin by month. The colour scale for this figure is shared across all months.

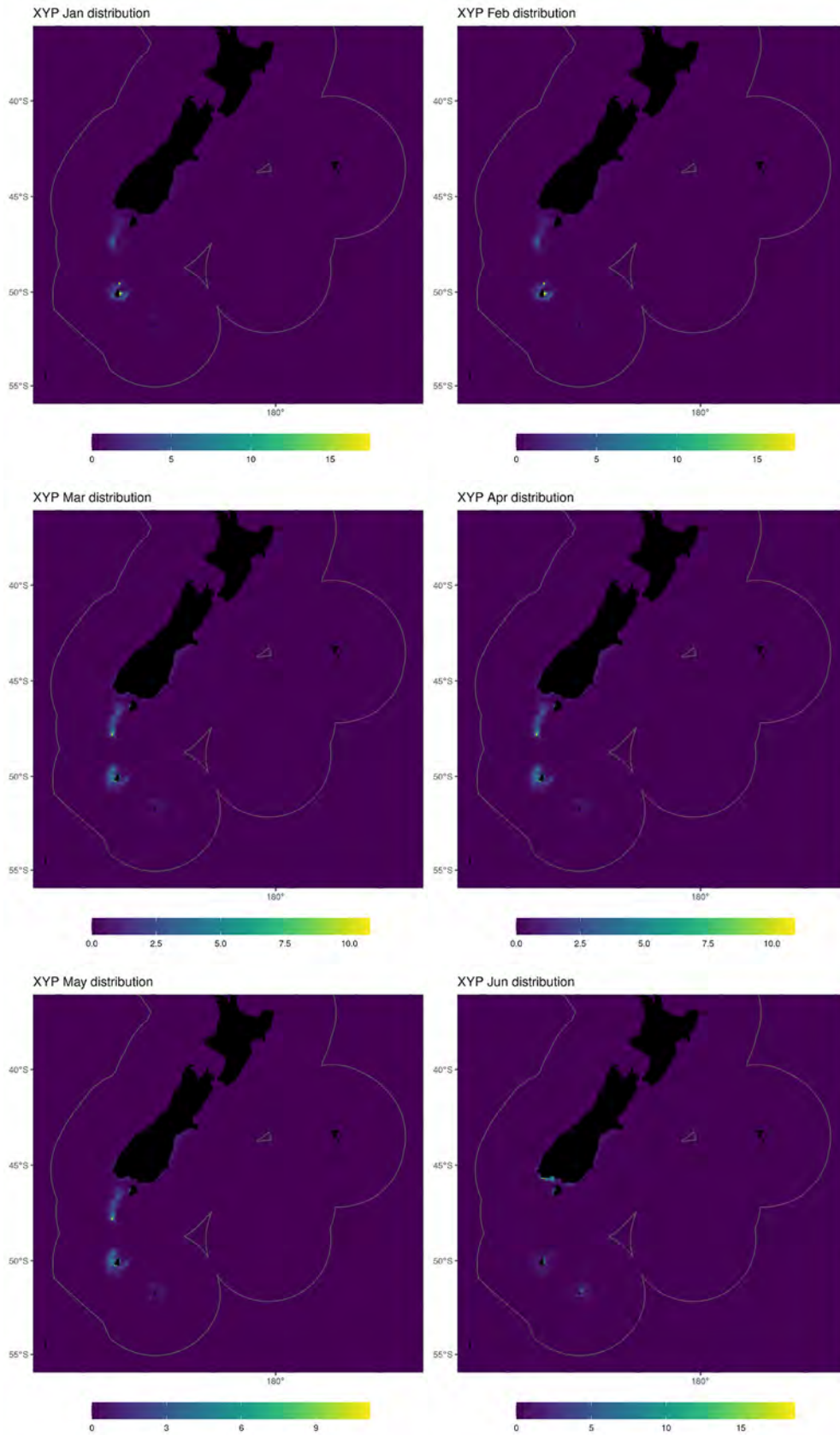


Figure F.38: Predicted relative spatial density of fledgling yellow-eyed penguin by month, for January-June. The colour scale for this figure is different for each month.

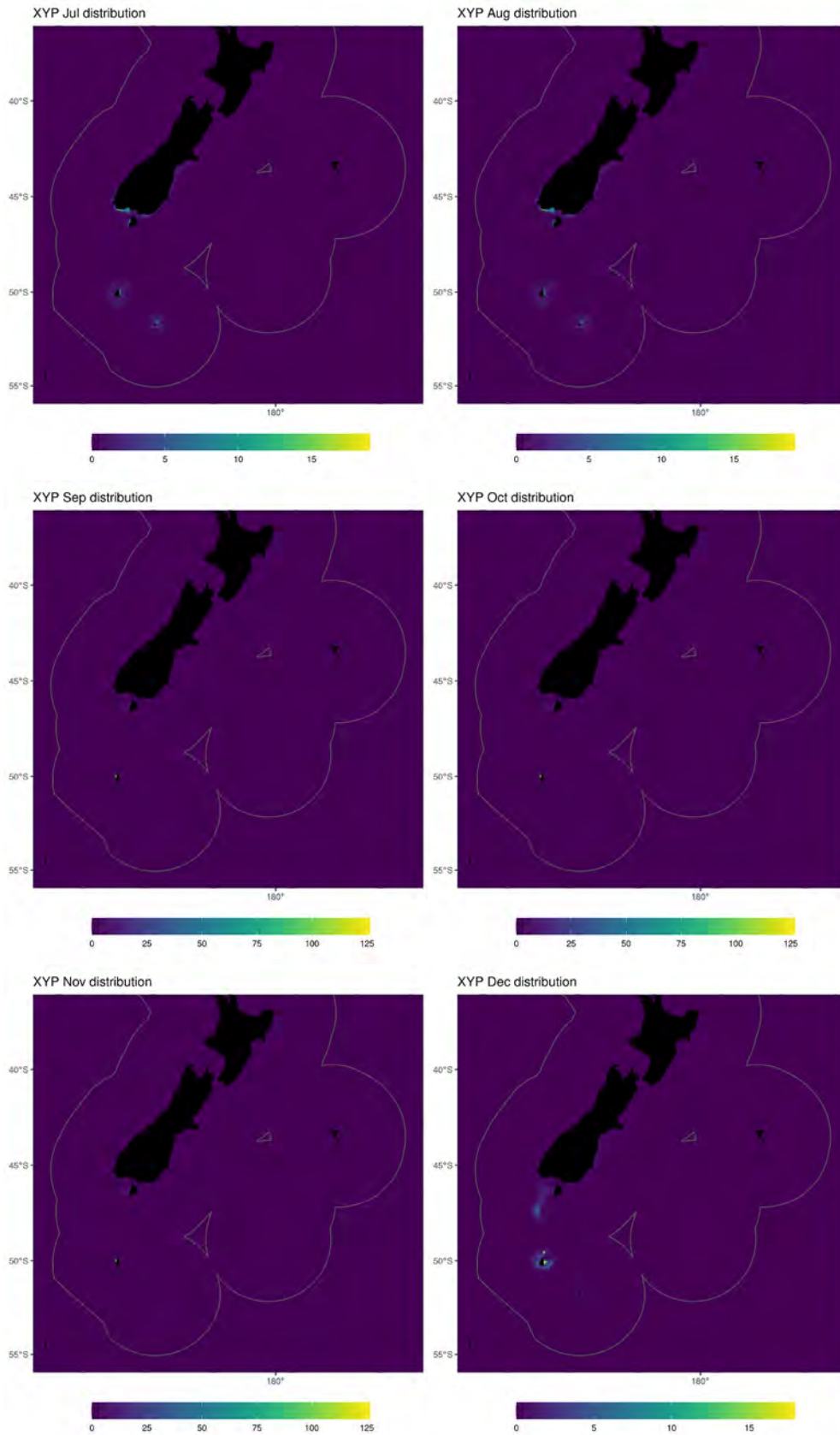


Figure F.39: Predicted relative spatial density of fledgling yellow-eyed penguin by month, for July-December. The colour scale for this figure is different for each month.

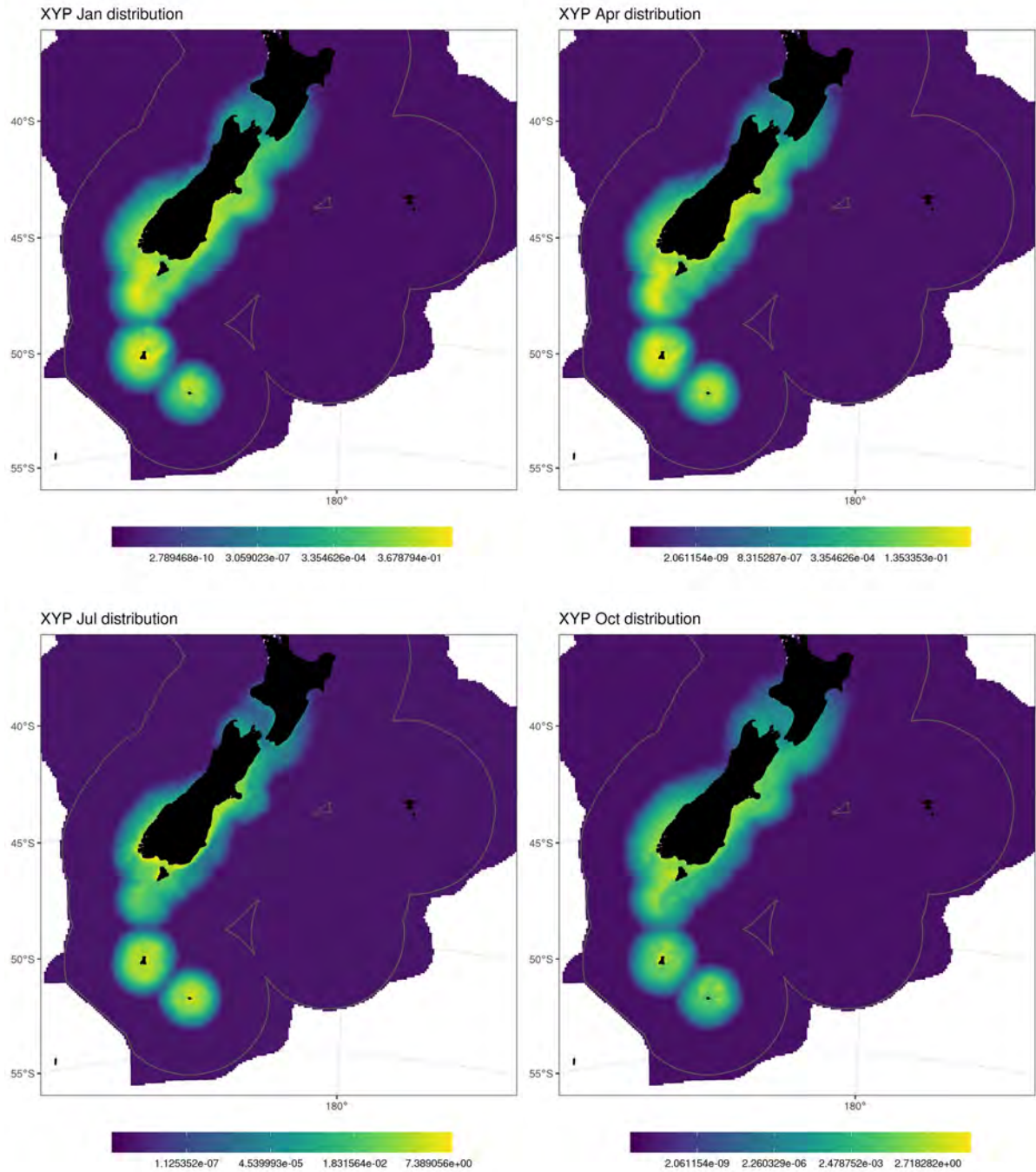


Figure F.40: Predicted relative spatial density of fledgling yellow-eyed penguin in log-space for four example months: January, April, July, and October.

Adults

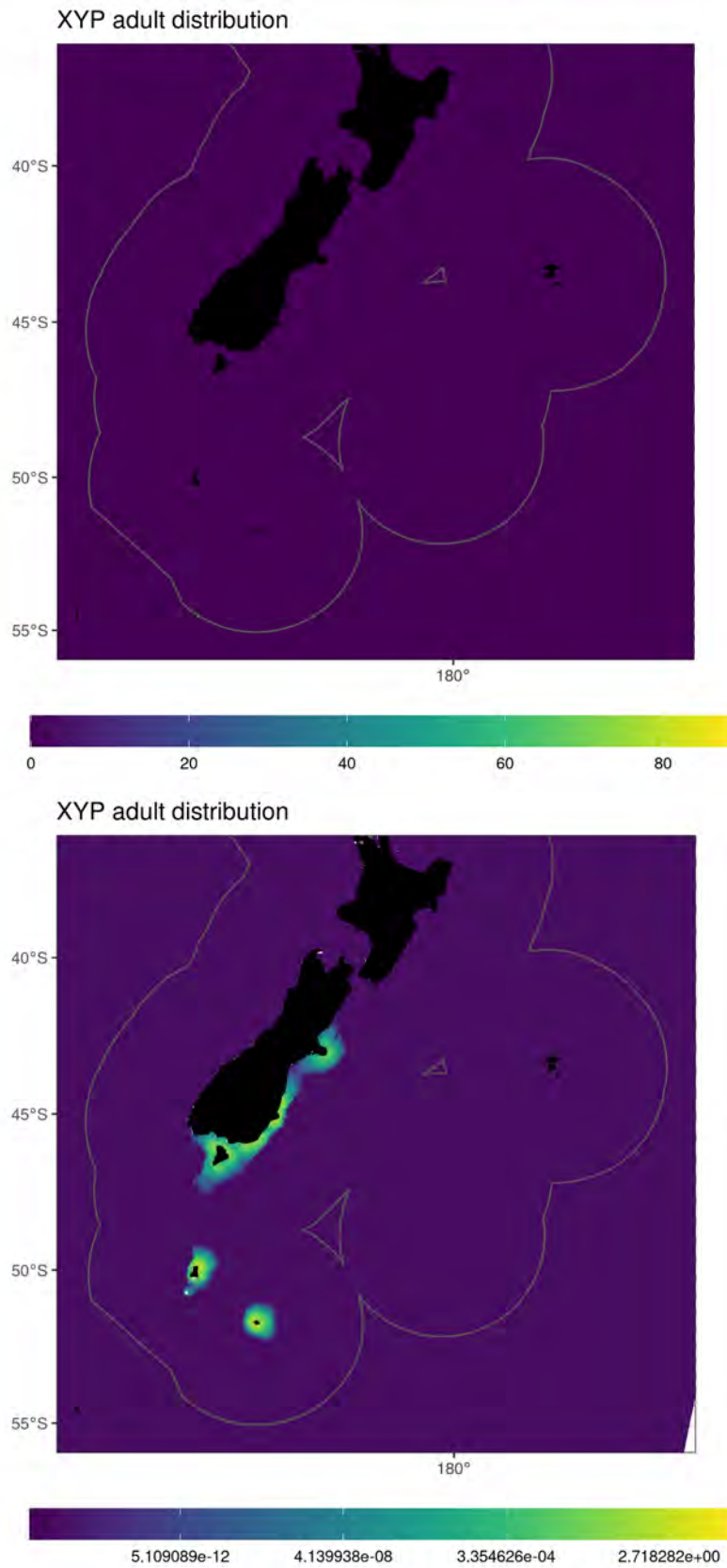


Figure F.41: Predicted relative spatial density of adult yellow-eyed penguin (for all months) in natural space [top] and log-space [bottom].